THESIS APPROVAL

The abstract and thesis of Darren L. Beckstrand for the Master of Science in Geology presented November 22, 2000, and accepted by the thesis committee and the Department.

COMMITTEE APPROVALS:

Curt D. Peterson, Chair

Errol C. Stock

Georg H. Grathoff

Virginia L. Butler
Representative of the Office of Graduate Studies

DEPARTMENTAL APPROVAL:

Ansel G. Johnson, Chair
Department of Geology

ABSTRACT

An abstract of the thesis of Darren L. Beckstrand for the Master of Science in Geology presented November 22, 2000

Title: Origin of the Coos Bay and Florence Dune Sheets, South Central Coast, Oregon

The Coos Bay and Florence dune sheets are situated on Oregon's south central coast, between Florence to the north and Coos Bay to the south. These two dune sheets comprise approximately 70 km of coastline; the largest coastal dune fields of Oregon. Heavy mineral analysis indicates a primary sand source from the Umpqua River, as evidenced by high hypersthene:augite ratios and a secondary source from streams to the south, yielding metamorphic amphiboles.

Complex directional emplacement trends indicate onshore transport of sand; however, different data suggest either a southern or a northern sand source. Dune lee-slope azimuth analyses suggest a northern sand source, whereas particle-size analysis indicates a southern source. Dune thickness and depth increase to the north. Accommodation space also increases to the north due to possible tectonic uplift to the south and incision by the paleo-Siuslaw River channel to the north.

Previously, these dune sheets were assumed to be Holocene features forced onshore during the latest de-glacial sea level rise. A Holocene age would require a high sea level stand emplacement model. Thermoluminescent (TL) dating of sand and C^{14} dating of organics suggest at least three pulses of sand supply. The oldest TL date

obtained is 70.2 ± 3.0 ka. Most of the eastern edge dune TL dates are between 30 and 40 ka. The westernmost sands are chiefly 1-3 ka. The earliest ages (70 and 30-40 ka) prohibit a high stand emplacement model. Rather, these ages suggest a sea level low stand model with sand transported across the exposed continental shelf to present dunal positions. Variable sea levels during the Pleistocene could have alternately encouraged sand transport alongshore (high-stand) and left the inner-continental shelf sands exposed to onshore eolian transport (low-stand), thereby episodically supplying the coastal dunes with the freshly available sand. Sand supply in the latest Holocene (1-3 ka) prograded a portion of the shoreline and covered some westernmost stabilized Pleistocene dune soils. However, late Holocene sand advances (hundreds of meters) are small compared to late Pleistocene advances (several kilometers). These results will impact previous interpretations of neotectonics, archaeology, and coastal sand supply in the south-central Oregon coastal zone.

ORIGIN OF THE COOS BAY AND FLORENCE DUNE SHEETS, SOUTH CENTRAL COAST, OREGON

by

DARREN L. BECKSTRAND

A thesis submitted in partial fulfillment of the
requirements for the degree of

MASTER OF SCIENCE
in
GEOLOGY

Portland State University
2001

Dedication

For Tiffany and Natalie

Acknowledgments

This thesis would not have been possible without the complete support of my wife, Tiffany. Her support and patience during the writing process, along with the love of my beautiful daughter Natalie, made this daunting task more worthwhile and fulfilling. My encouraging parents, Blaine and Marilyn Beckstrand, and in-laws Warren and Lynn Bevan, also provided the financial and emotional support that was needed. I lovingly thank my family for everything they have done for my education and, by extension, me.

Many thanks are given to Dr. Curt Peterson who, with much patience and after hours, has edited and revised this manuscript and provided insight and understanding when needed. Gratitude is in order for Dr. Georg Grathoff, who visited the coast with me and freely provided knowledge and interpretation to soil clay mineralogy. I also gratefully thank geologist Dr. Errol Stock, of Griffith University, Brisbane, Australia, for his support and much needed help throughout the steep learning curve of Oregon's coastal dunes. Geologist Courtney Cloyd of the Siuslaw National Forest provided the field expertise and immediate knowledge of the surrounding landscape, as well as the impetus for funding through the Forest Service. ODNRA Manager Ed Becker provided for access, ground logistics, and lodging for numerous researchers through the duration of this study.

The primary financial support for this thesis has been through U.S.D.A., U.S. Forest Service, Siuslaw National Forest Purchase Order numbers 43-04T0-9-0079 and 43-04T0-0009. Oregon Sea Grant also provided funding through grant number NSD-04.

Table of Contents

List of Tables

List of Figures

Introduction

A minimum of 45 percent, or 225 of the 500 kilometers, of the Oregon coast consists of active or partially stabilized dunes (Cooper, 1958; Peterson et al., 1991). Cooper recognized at least two periods of prehistoric dune advance, but lacked radiocarbon (C^{14}) and thermoluminesence (TL) dating techniques to establish dune advance ages. There are fundamental questions about the origins of these dunes, for example: 1) how old are the dunes? 2) where did the sand come from? and 3) what processes led to dune sheet emplacement? To date, there have been no comprehensive studies performed to address these concerns. Whereas researchers have speculated about the timing and origin of the dunes, the origin and stratigraphy of the dune fields have not previously been constrained (Cooper, 1958; Minor and Toepel, 1986).

Additionally, ponds, wetlands, and Snowy Plover nesting habitats exist in the dunal landscape (USDA Forest Service, 1981). These habitats vie for attention with human interests, which include extensive off-highway vehicle (OHV) use, residential and commercial development, and ground-water withdrawal (Hampton, 1963 and Robinson, 1973). The dunal resources are under increasing pressure from the variety of demands imposed by an increasing coastal population. With these increasing demands comes a need for increased understanding of how the dunal landscape can be utilized to cope with the provisions of each divergent use. More needs to be known about the dunal hydrology, vegetative stabilization, and soil properties for a long-term management of these resources (USDA Forest Service, 1996).

In 1995, Dr Errol Stock of Griffith University in Brisbane, Australia; my advisor, Dr. Curt Peterson; and Courtney Cloyd of the USDA Forest Service initiated a study of the Oregon Dunes National Recreation Area (ODNRA) dunes by means of air photo interpretation, field mapping, and soil and sand sampling. Over the following four years the Forest Service compiled a geographic information system (GIS) map from air photo interpretations of the Florence and Coos Bay dune sheets (Figure 1). This author processed dune sand and soil samples for grain size, pH, and Munsell color. Other fieldwork performed for this thesis will be detailed in the appropriate sections. Soil profiling and dating methods (TL and C^{14}) are the major tools used in this study to establish the age of dune sheet emplacement. The GIS database, including dune orientations (i.e.; paleowind directions), is used to constrain mechanisms of sand emplacement. Mineralogy of the dune sands is used to establish the ultimate and proximal sources of the dune sheet deposits.

The timing of the dune sheet's emplacement is uncertain, with most coastal researches speculating the last de-glacial period of 5-7 ka to be the major period of emplacement (Cooper, 1958; Erlandson et al., 1998; Peterson et al., 1993; Minor and Toefel, 1986; Nettleson et al., 1982). A major portion of this study is the investigation of sediment emplacement mechanism(s). Two chief ideas about the emplacement of the sand are tested, one involving a high sea level (near current elevation) model, the other being a low stand model. A commonly accepted, albeit unproven, high-stand model developed entails ocean waves forcing beach sand onshore during sea level

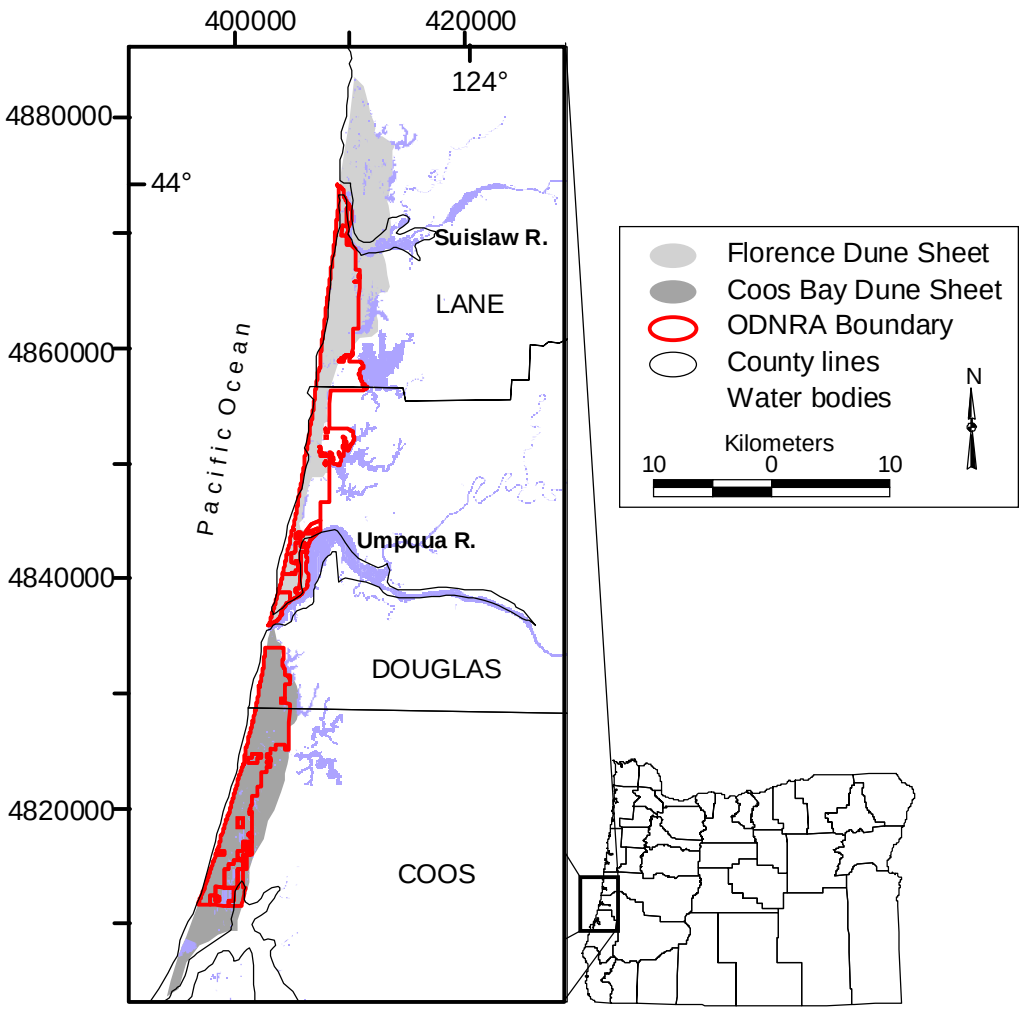

Figure 1: Location of the Florence/Coos Bay dune sheets. The Florence sheet runs from the north of the Umpqua River, while the Coos Bay dune sheet runs south of the Umpqua.

transgression and the subsequent high stand. Such a mechanism should lead to late Holocene and/or late Pleistocene dates (80-120 ka) for dune emplacement during marine high-stands (Figure 2). The resulting dune ages should then correspond to interglacial high sea levels. The low-stand model entails sand being blown in from the exposed continental shelf during sea level low-stands and building up against Coast Range foothills (Figure 3). This would require sand emplacement onto the Oregon Coast and subsequent ramping up to the Coast Range foothills during glacial periods.

The Florence/Coos Bay dune sheets are the largest and most active of the Pacific Northwest dune sheets. Findings about the dune sheet ages, mechanisms for emplacement, and periods of stabilization from this study should have application to other dune sheets on the West coast.

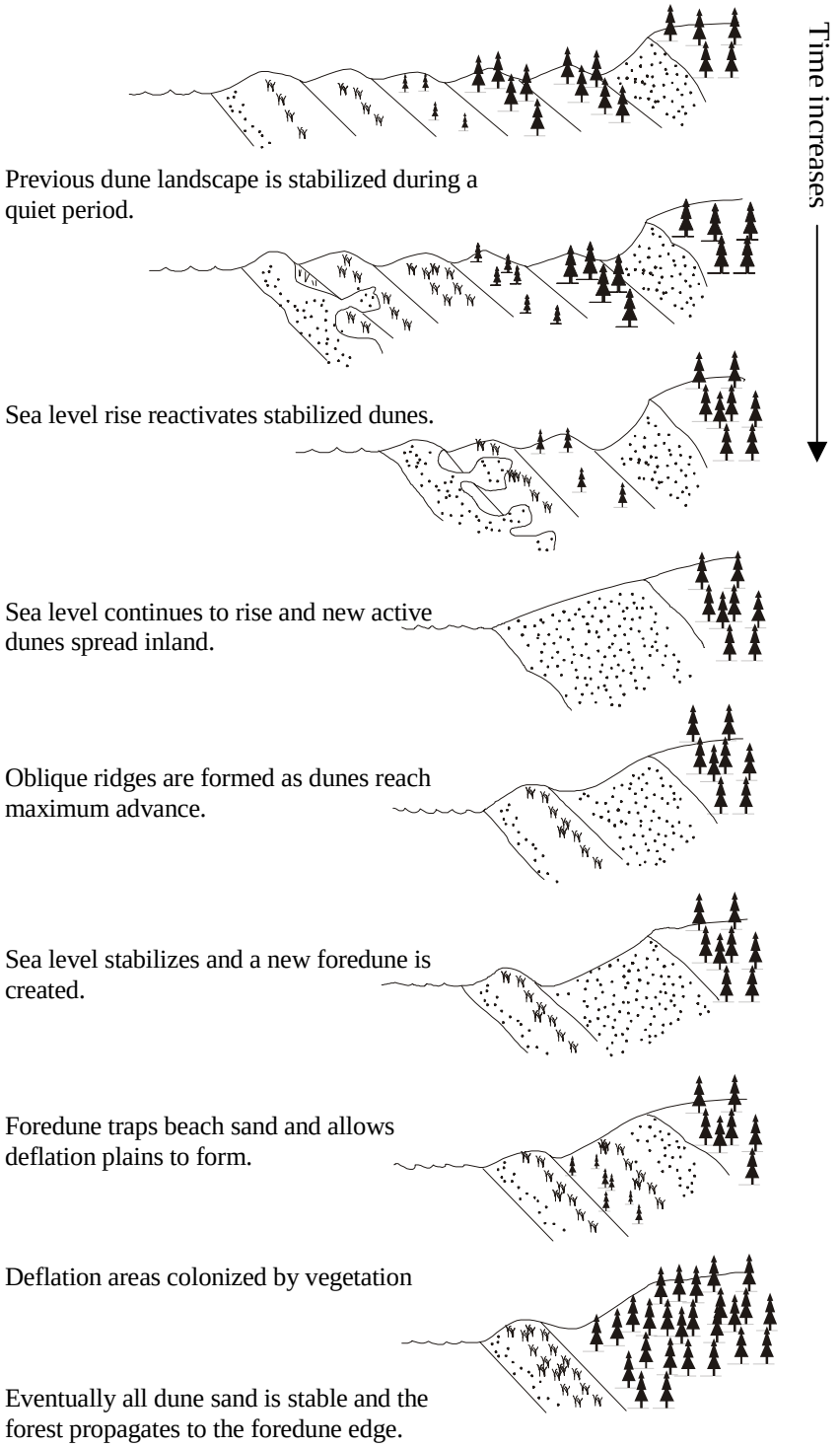

Figure 2: Schematic illustration of the high-stand emplacement model. Modified from Schultz, 1990.

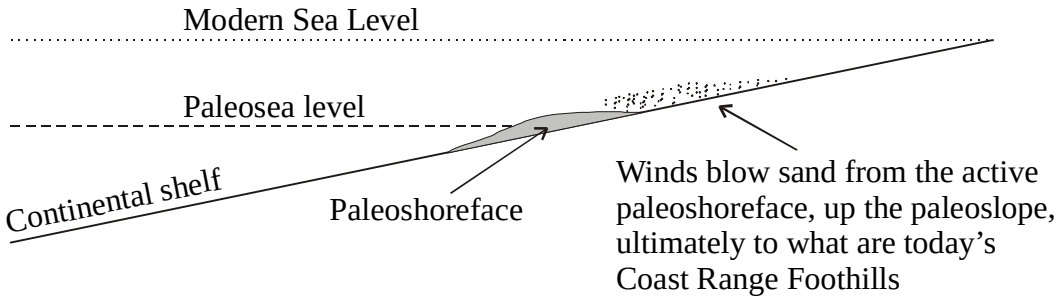

Figure 3: Schematic diagram of the low-stand emplacement model.

Background

Due to the broad character of this thesis, this background section is general in nature and some material and references regarding specific aspects are deferred to the discussion.

Study Area

The areas of study are the Florence and Coos Bay dune sheets, separated by the Umpqua River and its associated headland. The Florence dune sheet extends from Heceta Head (Sea Lion Point) north of Florence, south to the Umpqua River at Reedsport. The Coos Bay dune extends from the Umpqua River south, to north of Coos Bay (Figure 1). These two dune sheets occupies a large portion the Oregon Dunes National Recreation Area, managed by the U.S. Department of Agriculture's Forest Service.

Geography

The climate is moist and temperate. Winters are cool (average temperature of 7°C) and most of the precipitation falls during this time. Summers are dry and warm 15°C, with occasional rains (Beaulieu and Hughs, 1975). Between 1931 and 1997, an annual average of 160 cm of rain fell at the Coos Bay/North Bend Airport (Table 1 and Figure 4). Maximum rainfall, 45 – 55 cm per month, occurs between October and March (Table 1). Winds are seasonally bi-directional with winter winds from the southwest and summer winds from the northwest (Figure 5). The area is humid throughout the year, with clouds and fog occurring regularly.

Table 1: Average monthly and annual rainfall amount recorded at the Coos Bay/North Bend Airport between 1931 and 1997 (cm). Data provided by Jackson, personal communication, 1998.

	Jan	Feb	Mar	Apr	May	Jun	Jul	Aug	Sep	Oct	Nov	Dec	Annual
Mean	25.79	20.01	19.61	11.63	7.38	4.19	1.15	1.83	4.46	13.17	23.98	27.46	159.65
Max	55.25	45.36	44.45	28.27	18.31	14.53	7.09	13.94	14.48	45.69	57.63	56.79	237.59
Min	4.70	5.89	4.19	1.07	0.76	0.20	0.00	0.00	0.00	0.76	1.68	4.32	85.14

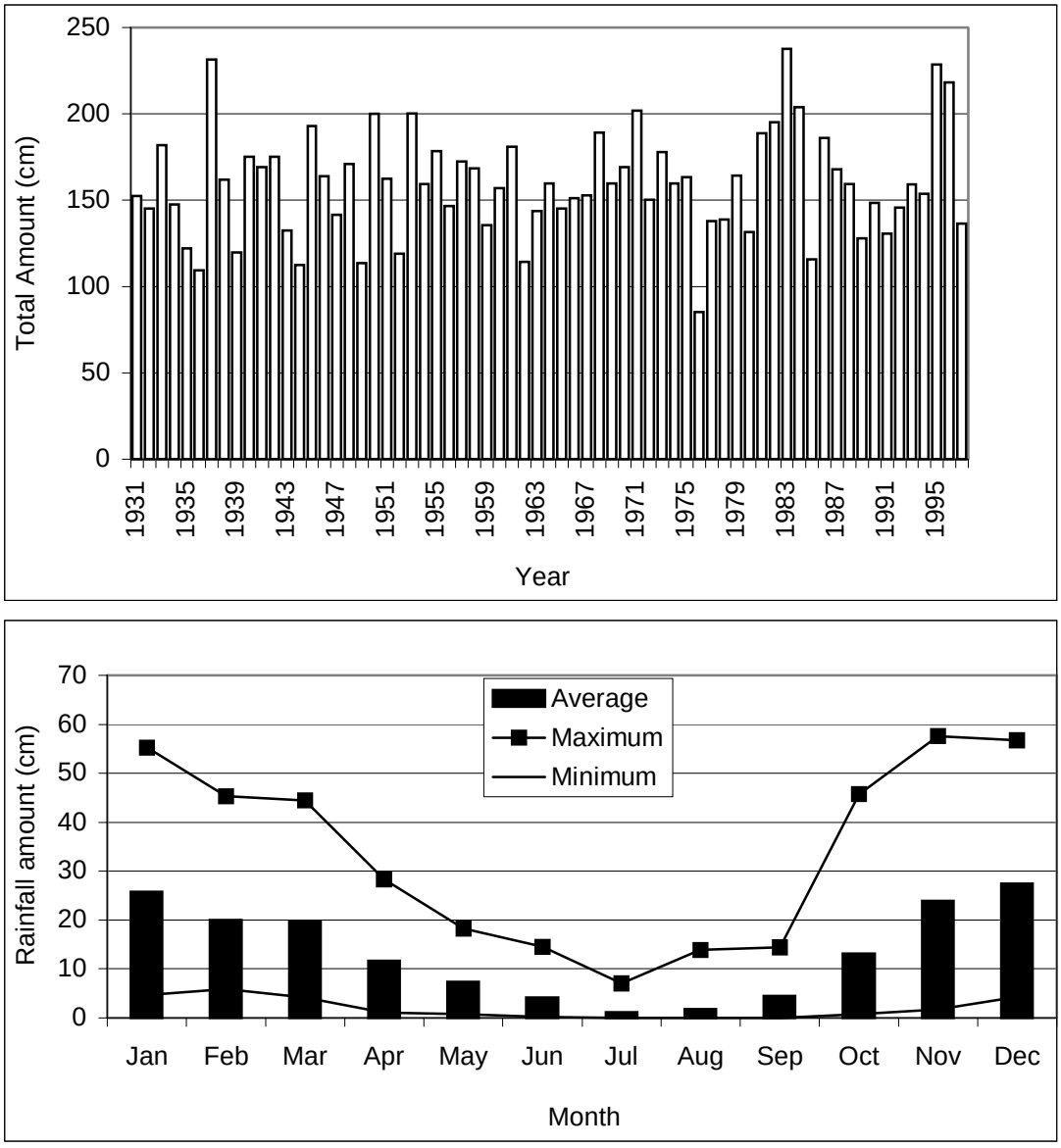

Figure 4: Histograms and line graphs showing annual and average monthly precipitation between years 1931 and 1997 at the Coos Bay/North Bend Airport. Data provided by Jackson, personal communication, 1998.

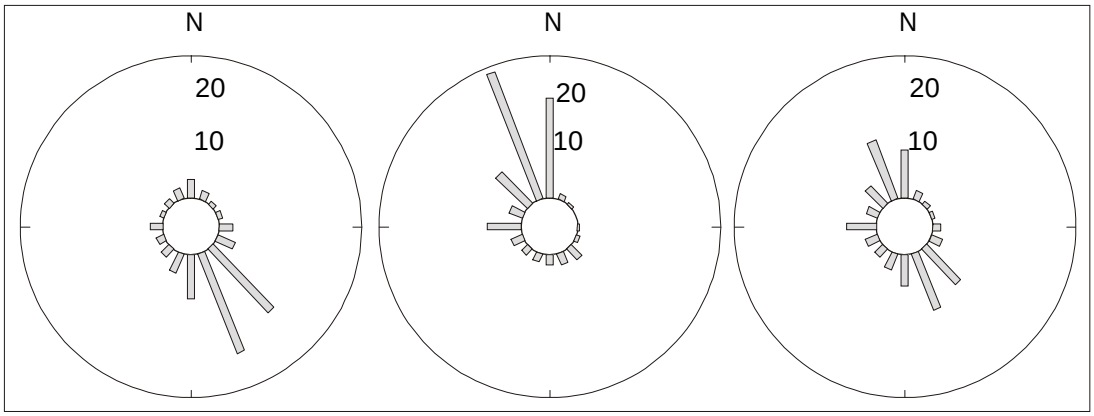

Figure 5: Wind-rose diagrams, from left to right, for January, July, and an yearly average between the years 1984 and 1989. Summer winds displayed are not completley representative due to local topography near the gaging station at the Coos Bay/North Bend airport. Axial values are in knots; north is true north. Modified from data provided by Jackson, personal communication, 1998.

These conditions lead to a complex seasonal interaction between wind, rain, dune-sand cohesion, and dune-sand mobility. During the summer months the persistent, but weak northwest winds blow dry sand toward the southeast. During the winter months, the brief but strong southwest winds blow sand to the northeast. Additionally, greater complexity of dune orientations result from wind convergence and divergence around local dune topography. A comparison between modern, active and prehistoric, stabilized dunes has yet to be performed in this area. Hunter et al. (1983) performed an analysis of migration rates of oblique dunes south of the Umpqua River. They found that the migration rate of these dunes is 3.8 m/y towards an azimuth of 126°. They also found that the migration primarily took place during strong winter storms, rather than during the dry summer months.

The bathymetry of the coast reveals a narrow shelf between 0 and –80 m, then increasing in width between –80 and –120 m. Note the wider continental shelf exposure in the northern portion (~25 km) versus the southern portion (~15 km) (Figure 6).

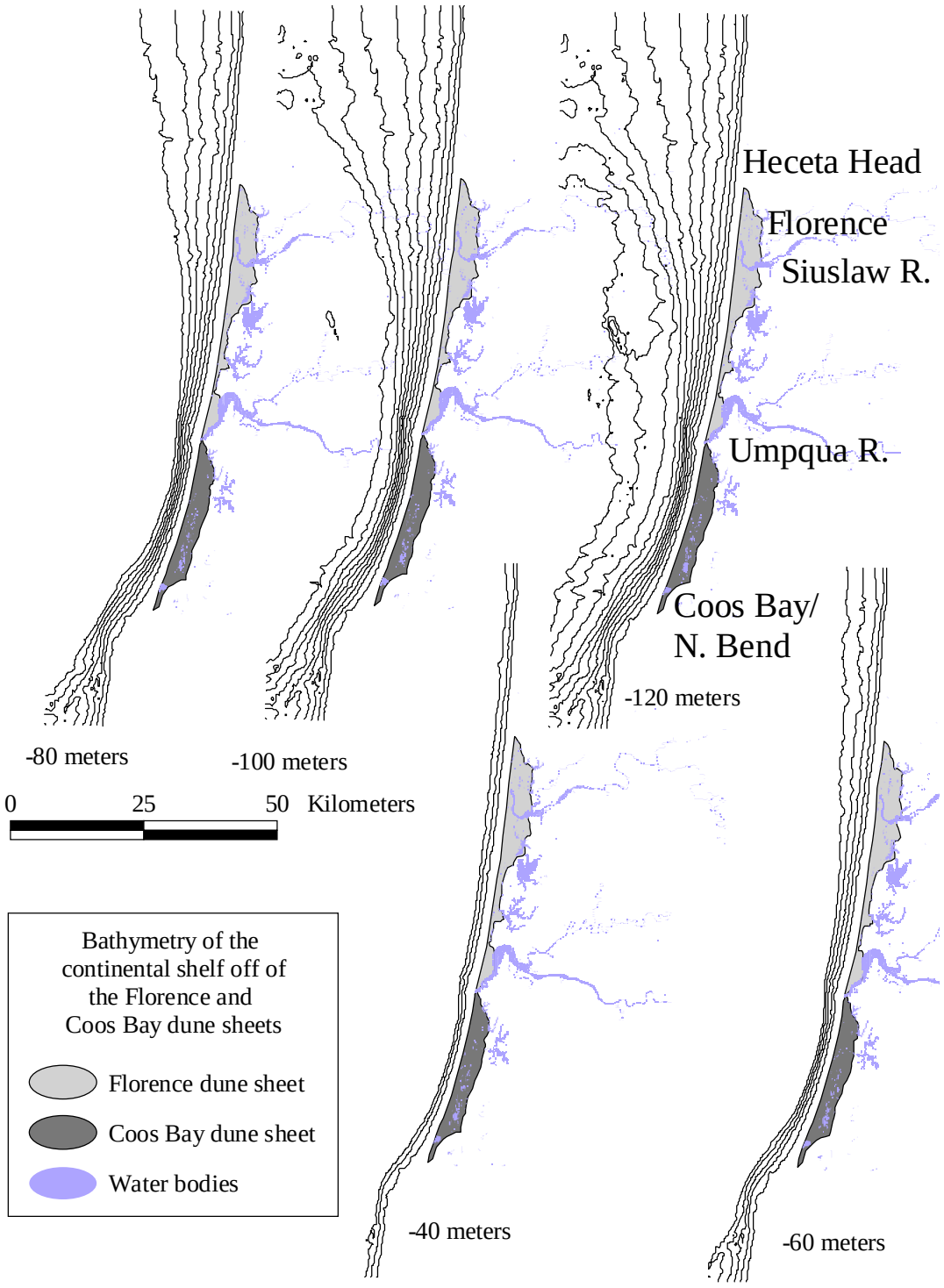

Figure 6: Nearshore bathymetry off of the Florence and Coos Bay dune sheets. Note the large increase of continental shelf exposure starting between –80 and –100 meters.

Local Geology

A brief, general geologic history of the area begins with the emplacement of Oregon's Coast Range-Siletzia terrain consisting primarily of oceanic basalts during the Eocene. During the emplacement of the Coast Range, the proto-Cascade volcanic arc became established and sediments spilled from it (as well as from the southwest and the southeast Kalamath terrain) into the forearc basin. These sediments became the bedrock units (consisting of mudstones, siltstones, and sandstones) in the study area (Beaulieu and Hughs, 1975). These formations are the Eocene marine interbedded siltstones and sandstones of the Tyee, Flournoy and Coaledo (Beaulieu and Hughs, 1975). These units outcrop at the west-facing front of the Coast Range, upon which the dune fields onlap from the west. Cooper (1958) and Orr et al. (1992) report that the dunes rest on marine cut terrace surfaces. However, these terraces are not exposed at the shoreline or at landward sites in the study area due to modest tectonic uplift (no terraces) and/or thick dune cover.

Sediment transport considerations

The research presented here is related to the aspects of sand source, emplacement timing, and mechanism(s) of sand supply. This last aspect involved consideration of sand transport. Theoretical entrainment velocities do not address all issues of transport. For example, sand masses moving across the continental slope during sea-level low-stands must move fast enough to outrun the transgressing sea and must be free to move (that is not stabilized by vegetation). The role that vegetation plays is quite significant in terms of critical entrainment velocities, dune forms, and rates of transport. Increased

vegetation limits the amount and velocity of transport, resulting in dune stabilization and loss of open dunes (Bressolier and Thomas, 1977).

The role of precipitation in eolian sand transport is important in two ways. When the climate is drier, cohesion due to moisture diminishes, and sand transport is more efficient. Additionally, precipitation promotes vegetative growth and dune stabilization. The presence of large areas of active dunes on the Coos Bay and Florence dune sheets testifies to the effectiveness of sand mobility under present-day conditions of precipitation and prevailing wind regimes (Table 2). However, there has been little net migration of the larger dune masses in historic time (Reckendorf, 1987). Therefore, different conditions of sand supply, wind strength, and vegetative growth must have prevailed in the past to account for the existing distribution of larger dune masses.

Origins of coastal dunes

The subject of coastal dune fields is a field of research that has been evolving in recent decades. Early researchers did not attempt to distinguish between inland and coastal dunes. Until the late 1980s, papers on dunes tended to rely on the landmark papers of Bagnold (1936, 1941) and widely cited papers such as Cooper (1958). In the early 1980s, a shift "towards exploring the morphodynamic status of dunes" began (Short and Hesp, 1982). As seen in Figure 7, large portions of the world's coasts complement dune formation with compatible physiographies (relatively low relief shoreline, adequate sand supply) (Carter et al., 1990).

Figure 7: Distribution of major dune coasts of the world. Modified from Carter et al. (1990).

An ideal definition of coastal dune occurrences is found in Carter, 1990, paraphrased here:

> Coastal dunes are found above the high water marks of sandy beaches. They occur on ocean, estuary and lake shorelines from the Arctic to the Equator…Coastal dunes find their greatest expression on windward coasts, especially where suitably textured sediment is abundant….The basic requirement is for particles with a hydraulic equivalence approximating well-rounded, sand sized (2 to 0.2mm) quartz grains with a specific gravity in air of 2.65 g cm^{-3}. Dunes occur on many types of shoreline, from low, gently sloping surfaces to cliffed coasts. Dune formation is a function of sediment grain size, the characteristics of the beach profiles, and the wind regime. Dunes form most readily on low angle shorelines under dissipative (spilling) wave domains, where the foreshore dries out at low water or where swash bars weld regularly onto the upper beach (Short and Hesp, 1982; Carter, 1986)… The deposition of sand

> is controlled by topography, the presence of obstructions (litter lines, tree trunks), obstacles, (buildings, seawalls) and above all vegetation. The role of vegetation in fixing, trapping and replenishing sediment sources and reworking the foredunes distinguish coastal dunes from the majority of active dunes in arid regions.

Oregon's dune systems

Twenhofel (1946) was the first researcher in the area to carefully study the actively mobile coastal sediments. He reported on the mineralogy and physical composition of beach sands, largely quartz and feldspars, from the Columbia River to Coos Bay. The small percentage of unstable lithic fragments (5-10 percent) and the sub-rounding of quartz indicated multicycle sediment supplies; i.e., a prolonged history of transport and abrasion along Oregon's high-energy coastline (Twenhofel, 1946).

The dunes of Oregon, as well as those in Washington and California, have been characterized and classified by the works of Cooper (1958, 1967). While there have been modifications and advancements of Cooper's work (Hunter, 1980; Hunter et al., 1983, Fryberger, 1991), his work is still widely respected and cited. Cooper (1958) separated the Washington and Oregon coasts into four regions based on morphologic features, with these regions further subdivided into distinct localities. The Coos Bay and Florence dune sheets are an entire region unto themselves (Table 2). Common dunal features define Cooper's regions, with all but Region 1 bearing features of retrogradation. (Cooper, 1958). The following is a brief summary of the mapping performed by Cooper (1958); for a complete discussion of dunal features see Cooper (1958). Localities are shown in Figure 8.

- Locality 19, Heceta Head and Siuslaw River. The majority of the dunes are stabilized. Numerous, disconnected areas of active sand exist throughout the stabilized central portion. These active areas of sand consist of transverse dunes or ~500 m long oblique ridges with transverse dune forms between ridges. Active slipfaces, also known as precipitation ridges, bound the eastern boundaries of active dunal areas. Approximately 20 percent of Locality 19 consists of these active sands.
- Locality 20, Siuslaw River to Siltcoos River. Majority of dunes are active. Transverse ridges dominate active areas, with eastern portions consisting of oblique ridges (~500-1500 m) with transverse dunes between ridges. Most of the eastern edge consists of precipitation ridges migrating into stabilized dunes or forest. Approximately 95 percent of the area is active.
- Locality 21, Siltcoos River to Umpqua River. Majority of the dunes are active. Transverse ridges dominate active areas, with eastern portions in the northern and central areas consisting of oblique ridges (~300-500 m) with transverse dunes between ridges. Approximately half of the eastern edge consists of precipitation ridges migrating into stabilized dunes or forest. Approximately 80 percent of the area is active.
- Locality 22, Umpqua River to Tenmile Creek. Majority of the dunes are active. Oblique ridges (~300-3000 m) with few transverse dunes and some partially stabilized dunes between ridges dominate the dune forms. Transverse ridges dominate the western portions of the locality. The majority of the eastern edge consists of precipitation ridges migrating into stabilized dunes or forest. Approximately 80 percent of the area is active.
- Locality 23, Tenmile Creek to Coos Bay. Ratio of active to stable dunes is nearly 1-to-1. Open, undifferentiated sand and oblique ridges (~300-1000 m) with few transverse dunes between ridges dominate active dune sands. These two classifications are nearly equal, with transverse ridges comprising approximately 10 percent of active sands. Approximately half of the eastern edge consists of precipitation ridges migrating into stabilized

dunes or forest. Numerous small lakes are interspersed throughout vegetated portions. Both active and stabilized dunes are discontinuous in the eastern half of the locality. Approximately 65 percent of the area is active.

Since Cooper's time of mapping (1936-1965), the coastal dunes have experienced aggressive vegetative stabilization by introduced European beachgrass (*Ammophila arenaria*). This species of beach grass was introduced in the 1930s to stabilize the dunes to facilitate development and reduce road obstructions (Reckendorf et al., 1987). The stiff, needle-like blades of European beachgrass prohibit sediment transport during high wind velocities. Unlike the American beachgrass species (*Ammophila breviligulata*) that bows over in high winds, the European grass is adept at trapping sand and then recovering from frequent burial.

Table 2: Cooper's (1958) division of Oregon and Washington's dune sheets based on geopraphical and morphological charateristics.

Region 1: Columbia River (Washington)	15. Yaquina Bay
1. Grays Harbor North	16. Alsea Bay
2. Grays Harbor South	17. Tenmile Creek
3. Willipa Bay	18. China Creek
4. Clatsop Plains (Oregon)	Region 3: Coos Bay Dune Sheet
Region 2: Northern Oregon	19. Siuslaw River North
5. Nehalem River	20. Siuslaw River South
6. Rockaway	21. Umpqua River North
7. Tillamook Bay	22. Umpqua River South
8. Netarts Bay	23. Coos Bay
9. Sand Lake	Region 4: Southern Oregon
10. Nestucca Bay	24. Coquille River North
11. Neskowin Creek	25. Coquille River South
12. Salmon River	26. Fourmile Creek
13. Devil's Lake	27. Sixes River
14. Siletz Bay	28. Elk River
	29. Euchre Creek
	30. Pistol River

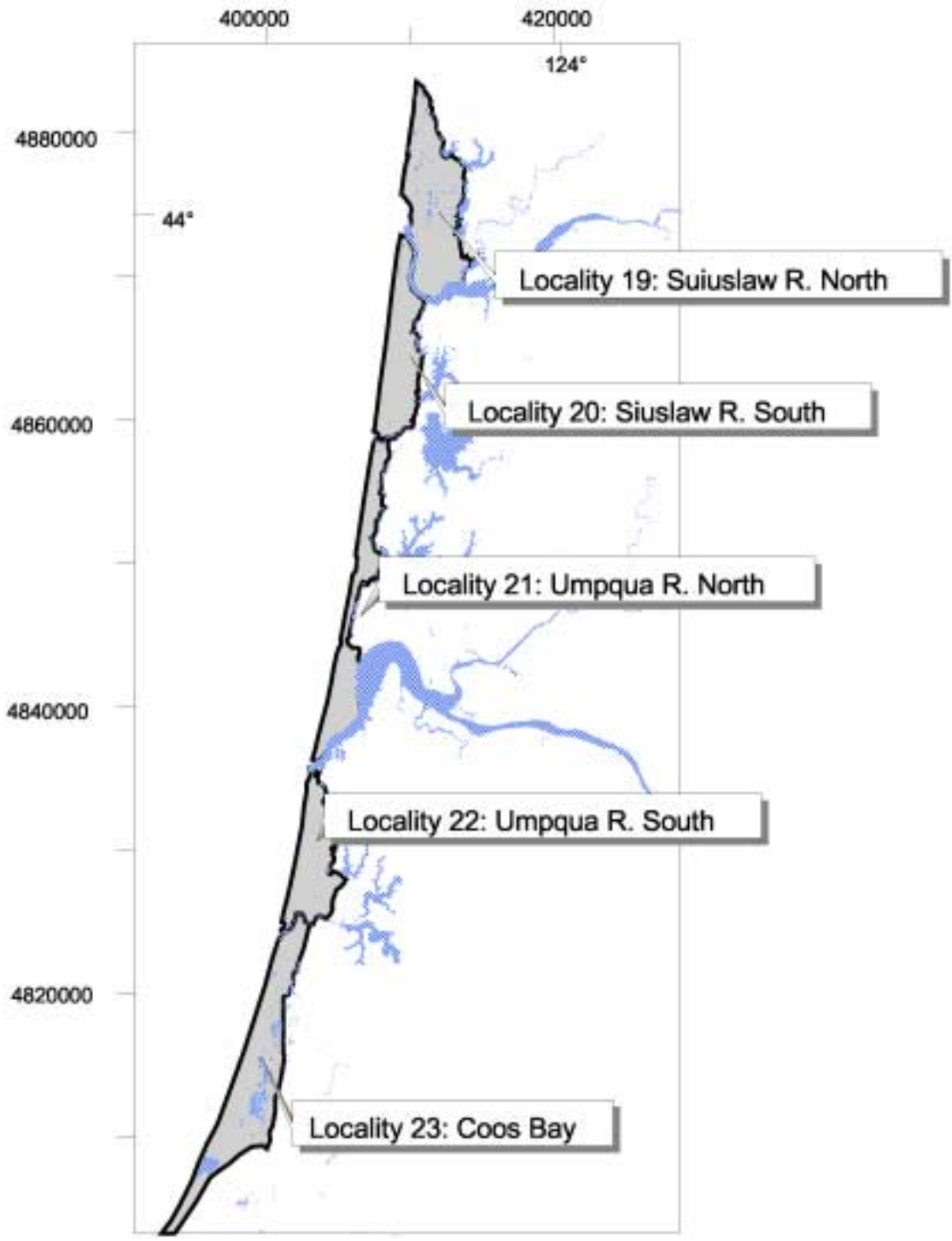

Figure 8: The five different localities of the Coos Bay dune sheet, modified from Cooper, 1958.

Dune/sediment mapping and descriptions

Cooper (1958) attributed the inland extent of the coastal dunes of the West Coast to a receptive shoreline, backed by low-relief terrain, for which dune migration is favorable. Cooper summarized the apparent histories of dune advancement and reactivation for each locality he studied. He proposed that the chief method of dune migration is/was precipitation ridges migrating into established vegetation. Precipitation ridges were defined as ridges of mobile sand moving over stabilized/forested areas. Whereas some precipitation ridges are still active (Figure 9), many prehistoric advances are now fully stabilized by forest cover.

Figure 9: Example of a precipitation ridge advancing over a forested area. The precipitation ridge is behind the storage units and is advancing over the forested area to the right. Eventually, the dune would likely advance into the established structures, forcing sand removal and mitigation. Note the buildings in the foreground are built on a preexisting dune sheet.

Hunter, et al. (1983) examined the active oblique dunes south of the Umpqua River. The authors conclude that the open dunes are not stationary or relict as thought by Cooper (1958). They found that the dunes migrated mainly in the winter months, despite the large amounts of rainfall. The north-northwesterly summer winds modify the dune forms, but do not alter the dune trend. These dunes were reported to migrate at an average of 3.8 m/yr toward an azimuth of N026°E (Hunter et al., 1983). If this rate had remained constant during the late Holocene (last 5,000 years), late Holocene dunes would be expected at least 4 km inland from today's coastline.

Previous interpretations of sediment source

There has been much speculation about the source of the dune sands, informal reports suggest that the sand originated from the Columbia River, Coast Range, Klamath, and/or Cascade drainages (ODNRA visitors booth, 1998). Cooper (1958) states that the ultimate source of dune sands could possibly be the Rocky Mountains of Canada, implying the Columbia River. In this instance, however, he is talking about the entire Oregon coastline, not specifying the Coos Bay/Florence dune sheets, and he left the ultimate source unconfirmed. In general, mobile dune sand has been assumed to be supplied from the beaches immediately in front of the dunes. This assumption has formed the basis of dune management in the ODNRA since its inception. If this hypothesis is true, then the major dune advances should coincide with sea level high stands, following marine transgressions during interglacial periods.

Local Paleoclimate

The paleoclimate of the region plays a large role in eolian transport in terms of precipitation and wind regimes. Based on pollen data from Little Lake, in the Coast

Range east of Florence, Worona and Whitlock (1995) infer that from approximately 17 to 25 ka, the coast range was 50 percent drier than today, and had a mean annual temperature of 7°C. This dryness would greatly increase the mobility of sand, due to less precipitation and reduced vegetative cover.

Wind patterns present in the NE Pacific at the last glacial maximum (LGM) were different than today, as evidenced by marine microfossil records offshore of the Pacific Northwest coast (Ortiz et al., 1997). Modeling of winter downwelling of ocean currents indicates levels much greater than those of today, demonstrating stronger southerly winds. Comparing the modern simulation value at 43° N latitude for offshore Ekman transport (~-45) to the simulated values at the LGM (~-145), the difference was 100 metric tons/sec/100 m of coastline, signifying much stronger winter downwelling, with stronger corresponding winds.

Eustatic sea level changes

During interglacial periods, such as at present, eustatic sea level reaches higher mean elevations. During times of continental glaciation, the accumulation of land-bound ice at the poles and high latitudes leads to lower eustatic mean sea levels. Milliman and Emery (1968) place the lowest elevation of the latest glacial maximum of 16 ka at an elevation of 130 meters below present sea level. Rapid Holocene transgression likely began 14,000 years ago and rapidly rose to near today's elevation by about 5-6,000 ybp.

Pirazzoli's (1993) summary of recent eustatic sea level work follows that of Milliman and Emery (1968). Pirazzoli's LGM low-stand occurred at approximately 17 ka, at an elevation 120 -130 meters below current sea level. Pirazzoli's work differs from that of Milliman and Emery (1968) by showing that there is much more

uncertainty in sea level before 30 ka. While the numerical values for mean sea level differ between data sets, what is consistent is that there are many fluctuations between 70 and 30 ka (Figure 10). There is much more agreement about the high stands of 80, 105, and 120 ka. These high-stands correlate, respectively, to oxygen-isotope stages of 5a, 5c, and 5e. During these stages, the eustatic sea level nearly reached the current sea level. Since then, the deposits associated with these high-stands have been uplifted along portions of the Oregon coast to produce distinctive marine terraces (Nettleson et al., 1982).

Attempts have been made to date the soils on the heavily dissected marine-cut terraces. The terrace surfaces of interest are the Tenmile terrace, with an elevation of 7-15 meters and C^{14} ages of 5,280 to 10,850 RCYBP, and the Whiskey Run terrace, at an elevation of about 30 meters (Nettleson et al., 1982). Eolian sand is present on the Pioneer and Seven Devils terraces, at 60 and 120 meters elevation at Cape Blanco, south of the study area (Nettleson et al., 1982).

Continental shelf sediment composition

Scheidegger et al., (1971) studied shelf sediment sources and dispersal patterns based on heavy mineral assemblages. The dispersal patterns of sand show that the net direction of littoral transport had been to the north, for at least the last 18,000 years. Longshore sand transport has been limited in the last 3,000 years due to natural obstacles such as resistant headlands. Based on heavy mineral analysis of the shelf sand fractions, Scheidegger et al., (1971) showed that the heavy minerals of the Umpqua River are the major source of heavy minerals to shelf sand located immediately offshore of the two dune sheets.

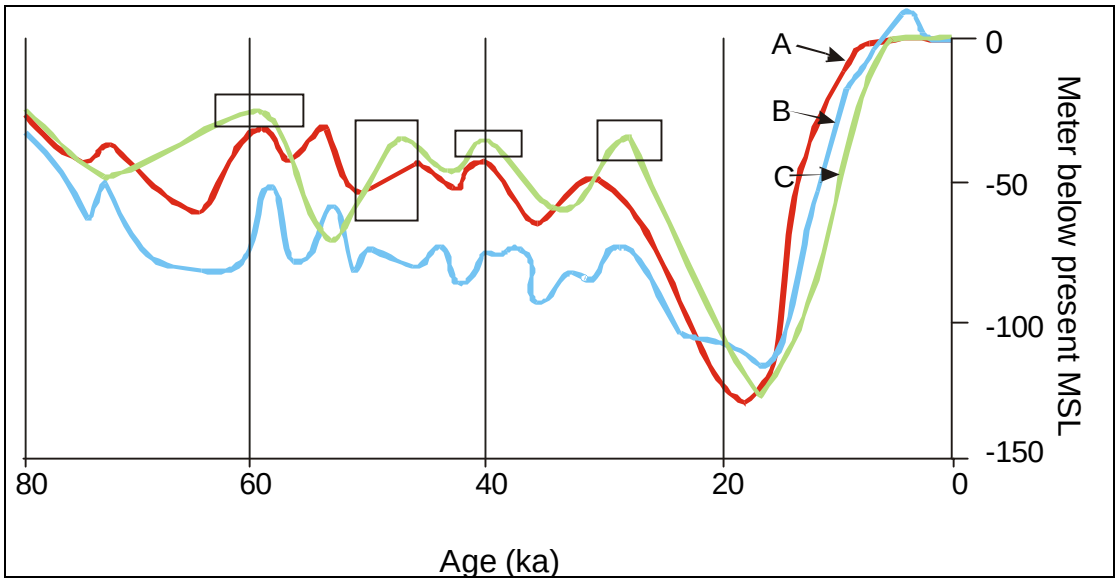

Figure 10: Eustatic sea level fluctuations and absolute elevations. Note the variation and uncertainty between 30 and 80 ka. The three lines are those of Chappell and Shackleton (1986) (A), Shackleton (1987) (B), and Bloom and Yonekura (1985) (C). Boxes indicated probable errors of age and heigth related to curve C. Modified from Pirazzoli (1993).

Karlin (1979, 1980) studied the sources of sediment and clay minerals on the continental shelf and slope off the Oregon Coast. His results indicate that chlorite is the most abundant mineral on the continental slope south of Coos Bay, accounting for over 50 percent of the clay minerals detected, by quantitative XRD analysis . From the Umpqua River south, chlorite ranges from 40-50 percent, and from the Umpqua River north to Heceta Head, chlorite ranges from 40-30 percent. Smectite (montmorillonite) increases northward, from 40 to 20 percent, while illite decreases northward, from 30 to 20 percent (Figure 11). Samples obtained on the continental shelf represent 43 percent (12 of 28) of the total number samples analyzed off of the southern Oregon coast.

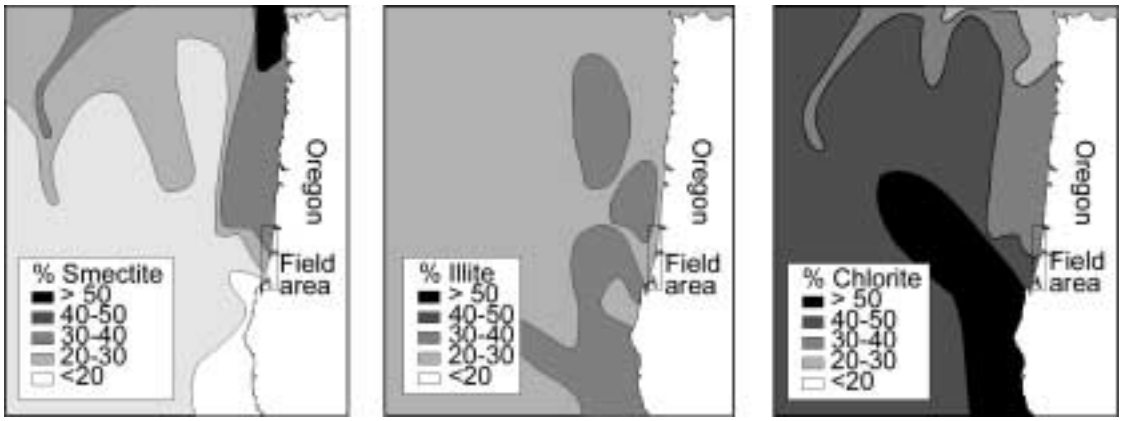

Figure 11: Relative abundances of smectite (montmorillionite), illite, and chlorite on the continental shelf and slope of Oregon. The boxed area is the field area. Modified from Karlin, 1980.

Soils

The definition of 'soil' for this study is that of Joffe (1949): a natural body consisting of soil layers (horizons) of mineral and/or organic components that differ from the parent material in their morphological, physical, chemical, and mineralogical properties (Figure 12). In general, horizons are unconsolidated, but some contain sufficient amounts of silica, carbonates, or iron oxides to be cemented. High rainfall, salt-water mist, acidic soils, and warm temperatures contribute to hasten the soil formation process on the coast (Birkeland, 1984).

Many of the soils in coastal southern Oregon have low pH, high organic carbon, and abundant Al in exchange sites (Bockheim et al., 1996). Nettleson et al. (1982) found that the marine terraces at Cape Blanco displayed sequentially more-developed (mature) soil profiles on the Tenmile (7-15 meters elevation), Whiskey Run (30 meters elevation), Pioneer (60 meters elevation), and Seven Devils terrace (120 meters elevation). The majority of these soils formed on the marine terraces in the area are

either Inceptisols or Spodosols (Nettleson et al., 1982). The terrace soils display developmental progression from Spodosols, to Spodosols with clay-rich horizons, to Ultisols (Bockheim et al., 1996). Spodic horizons are eventually masked by clay accumulation from in situ weathering, neoformation of clays, and clay translocation (Bockheim et al., 1996). The primary age- related trends include increases in relative abundances of silt and clay, ratio of quartz-to- feldspar in very fine sand fractions, and increasing amounts of dithionite-extracatble Fe and Al and crystalline forms of Fe in the profile with increasing duration of development (Bockheim et al., 1996). The moisture regime is udic and the temperature regime is isomesic (Langley-Turnbaugh and Bockheim, 1997).

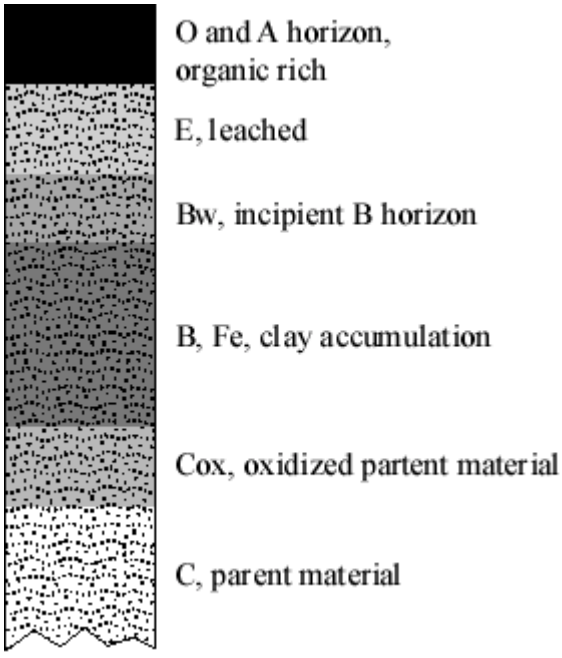

Figure 12: Soil horizon nomenclature used in this thesis.

If the more landward dunes are age correlative with these earlier and uplifted marine terraces at Cape Blanco, then their easternmost ages should correspond to the

older high stands of 80, 105, and 120 ka. Alternatively, the greater amount of soil development on the older and higher terraces might represent longer periods of exposure to soil-forming processes. That is to say, the more westward and younger dune soils on the lower terraces might represent less or degrees of soil development due to multiple dune sheet advances, thus resetting the "weathering clock" with each successive advance.

Anthropology

Accurate landscape reconstructions are essential for archaeological studies. First, they assist in predictions about site locations and expected ages of remains found on different surfaces. Second, accurate reconstructions promote the understanding of the environmental context in which past people lived and potential ways humans responded to environmental change. Minor and Toepel (1986) examined a midden site at western edge of Tahkenitch Lake (Figure 13). They found a record of inhabitation going back 8,000 RCYBP. The authors divided the site's deposits into three components. Table 3 summarizes the Minor and Toepel's interpretations based on marine species found in the midden. Their interpretation of why inhabitation ceased involved dune encroachment blocking an outlet of a pre-historic estuarine Tahkenitch Lake, limiting the number of marine species available at/near the midden site.

Table 3: Findings and interpretations of Minor and Toepel (1986) at an archaeological site on the western shore of Tahkenitch Lake.

Component	Inhabitation dates and findings
Component I	8000-5200 RCYBP Saline species; interpreted as estuary; inhabited as a fishing camp
Component II	5200-3000 RCYBP Abundant shallow-water saline species (molluscs), whale bone; village
Component III	3000-historic Occupation now sparse (historic canoe landing)…dunes blocked proposed esturine outlet creating current lake

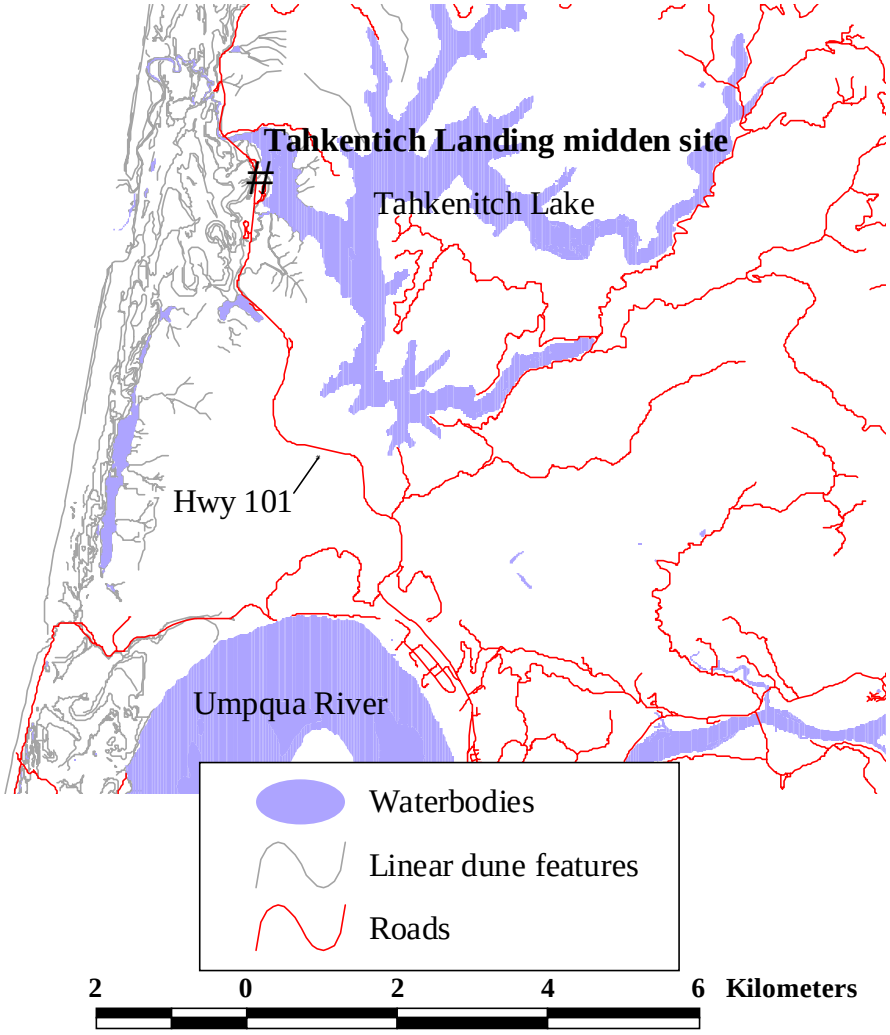

Figure 13: Location Map of the Tahkenitch Landing midden site.

Methodology

The Methodology section, as well as the results section, will deal with three subjects. In order, they are 1) surficial physical and geomorphologic dunal features, 2) dunal subsurface features, and 3) age dating techniques.

Sand source

The source of the dune sands, as stated earlier, has been hypothesized to be from the Columbia River, Coast Range, Klamath, and Cascade drainages (ODNRA visitors booth, 1998). To obtain constraint on the sand source, heavy mineral analysis and grain size analysis was performed on samples from the dunes and surrounding rivers.

Heavy mineralogy

Grab samples were taken and analyzed in 1995 by Dr. Curt Peterson from 13 sites in and around the Florence and Coos Bay dunes sheets (Table 4). They were analyzed by 300 random grain counts of mounted slides by means of a binocular petrologic microscope. The heavy minerals are separated by settling through Na- polytungstate (3.0 g/cm^3) and are within in the size range of 250-75μm. The minerals analyzed for were augite (Coast Range province), hypersthene (Umpqua River draining andesites of the Oregon High Cascades), common hornblende, and blue-green (metamorphic) hornblende (Umpqua River tributaries and other rivers south of the Umpqua draining high-grade metamorphic rocks of the Klamath) (Scheidegger et al., 1971). Normalizing heavy mineral quantities should group sands from sampled areas to the likely source river.

Table 4: Locations of samples obtained for heavy mineral analysis.

Sample Site and Location	Sample Site and Location	Sample Site and Location
Modern rivers	*Modern dunes, south of Florence*	*Dune paleosols*
Coos River	Foredune	Tree island 1, S of Florence
4801500 N 407000 E	4861600 N 407700 E	4862150 N 409400 E
Umpqua River	Deflation Plain	Tree island 3, S of Florence
4838700 N 416600 E	4861600 N 408100 E	4862000 N 410800 E
Siuslaw River		Tree island 4, S of Florence
4870300 N 416000 E		4862300 N 409950 E
		Tree island 10, S of Florence
		4861900 N 409600 E

Grain size analysis

Laboratory procedures

Dry-sieve analysis was performed on all samples, using the following procedures. A dried sample (50-100 g) was sieved through a W. S. Tyler RX-86 sediment shaker for five to seven minutes. These procedures were in general accordance with ASTM standards D1188-54 (quantities to be shaken) and D422 (time shaking). United States Standard Sieve sizes used included the 35, 45, 60, 120, and 230 (500, 355, 256, 125, and 63 μm opening sizes respectively). The sieved sample was then weighed to the nearest tenth of a gram for each sieve. Each sieve weight was then calculated as weight percent; subsequent cumulative percentages were plotted (Prothero and Schwab, 1996). The difference between start weight and summed sieve weight was recorded as loss and was negligible for all samples.

If the sample contained significant (>10 percent) silt and clay, hydrometer analysis was performed, using type 152H hydrometers. The weighed, oven-dried sample was wet sieved in the aforementioned sieves after sitting overnight in sodium

metahexaphosphate, $(NaPO_3)_6$. The material passing through the 230 sieve (63 μm) was then placed in a 1000 mL settling tube, mixed, and measured in general accordance with ASTM 422.

Data processing

The mean grain size for each sample was calculated by dividing the sum of the product of weight percent (wt percent) and size class (gz) by the sum of weight percents,

$$\text{mean} = \frac{\sum (wt\% \times gz)}{\sum wt\%} \qquad \text{Equation 1}$$

This is not the traditional graphical mean obtained from the cumulative percent charts in phi units as described by Prothero and Schwab (1996). Rather, this is a direct method of obtaining the mean.

Surficial and subsurface dune morphology

The information gathered for the morphology of the surface and subsurface was provided by surficial lee-slope azimuth analysis for dune migration analysis and subsurface information is provided by vibracoring and drilling via a solid stem auger in the deflation plain as discussed in the following sections.

Dune azimuth analysis (GIS based)

The U.S. Forest Service, Siuslaw District, provided all GIS data for this analysis. Dr. Errol Stock supplied air photo interpretation to the Forest Service, which then transferred the interpretations to the GIS database. Interpretations are from 1:12,000 USFS air photos taken in the summer of 1989. The raw azimuth data are shown in Appendix B.

Modern and prehistoric dunes display lee-slope morphology that can be interpreted and converted to transport trajectories (azimuths) (Figure 14). Azimuth data used for this thesis was entered into the database as fitting into one of 32 possible azimuth classes (012°). Azimuths are oriented to true north and are current (at time of photography) transport directions based on lee-slope interpretations. Original photos are available through the US Forest Service, Siuslaw District.

Dune azimuth analysis

The emplacement directions of the dunes play an important role in emplacement interpretation. Azimuths of generally active dunes (western section of the dune sheets) and generally stable dunes (eastern portion of the dune sheets) were compared, as well as trends indigenous to Coos Bay and Florence dune sheets.

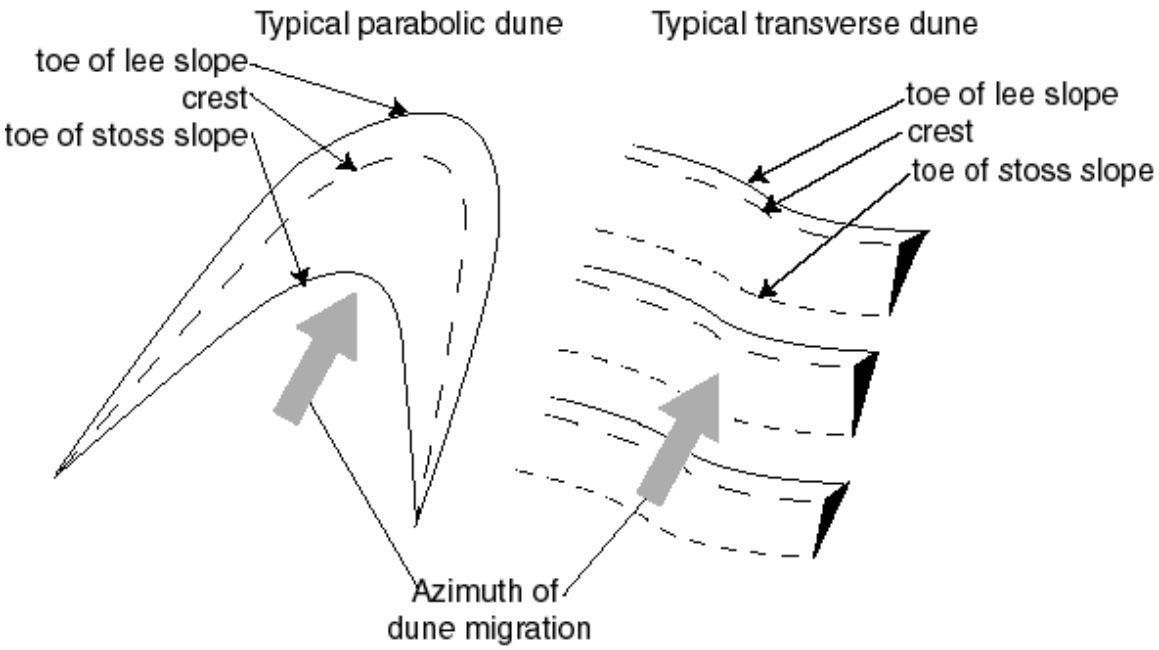

Figure 14: Schematic illustrating the interpretation of azimuths from lee-slope morphology.

The primary portion of the analysis utilizes a grid overlay. This was performed on the azimuth points of the ODNRA point data set. The grid data was then imported into to Microsoft Excel for statistical tests. More detailed descriptions of these procedures are discussed below.

Grid analysis

A one-kilometer by one-kilometer grid was generated and placed over the azimuth data. The average azimuth (true north) for each cell was calculated in ArcView 3.1, the GIS software package used for this analysis. The chief weakness of this analysis is that cells with only one data point were weighted equally as those with 25. This weakness was present in subsequent procedures performed on this derived data set. Considering this weakness, this method should be used in conjunction with other data and analyses, and not solely relied upon.

Statistical tests

The primary statistical test for directional data is Rayleigh's test (Davis, 1970; Swan and Sandilands, 1995). This test examines the presence of a preferred trend in the data. This test consists of finding $\overline{R}$, (the resultant mean length of vectors in the field) which is a measure of the relative strength, thus the significance of the mean derived azimuth. This test was performed on the average azimuth per one square kilometer data set, thus passing on its bias as discussed earlier. $\overline{R}$ is described as below:

$$\overline{R} = \frac{1}{n}\sqrt{\left(\sum_{i=1}^{n}\sin\theta_i\right)^2 + \left(\sum_{i=1}^{n}\cos\theta_i\right)^2} \qquad \text{Equation 2}$$

- where $\overline{R}$ is the test statistic
- *n* is the number of samples

- θ is the average azimuth of the cell, with respect to true north

Also calculated was the azimuth of the mean resultant vector,

$$\bar{\theta} = \tan^{-1}\left(\frac{\sum \sin\theta}{\sum \cos\theta}\right) \qquad \text{Equation 3}$$

and the azimuth confidence interval (95 percent), confidence $= \bar{\theta} \pm 1.96 s_e$

- where $s_e = \frac{1}{\sqrt{n\bar{R}\kappa}}$
- and κ is a concentration parameter related to $\bar{R}$ (Appendix 2.13, Swan and Sandilands, 1995).

Individual analyses were performed on the entire data set, cells of the eastern (stable) and western (active) portions, and on cells of the Coos Bay and Florence dune sheets.

Subsurface investigation

Vibracoring

Vibracoring of the deflation plain deposits between Goose Pasture and the Siltcoos River was performed to establish the origin of the deflation plain sand (Figure 27). Sedimentary structures, such as dune foresets or beach face laminae, were used to discriminate between eolian or beach progradation origins of the deflation plain sands. The vibracores were also examined for the wood or shell material to be used for later radio- carbon dating. Finally, the bottom sections of the vibracores were left sealed in darkness, for eventual submittal to a TL dating facility.

The sedimentary structure of the sediments underlying the deflation plain will reveal the sediment source of active dunes east of the deflation plain. This will assist in

the interpretation of source of the now-stable precipitation ridges and advances discussed by Cooper (1958). If beach sediments underlie the deflation plain, then the sediment source for dunes east of the deflation plain are likely derived from beach sands. However, if dune sands underlie the deflation plain, then the sediment source is likely recycled dune sand.

The vibracore unit is comprised of a concrete shaker bolted to aluminum irrigation pipe, mounted on a tripod. Portland State University, Geology Department's vibracore tripod is mounted onto a trailer suitable for highway, or off-highway use when attached to an OHV (Figure 15). The vibracore is suitable only for wet sand, since dry sand sedimentary structure would be destroyed by vibration, and the suction required to retrieve the core is not obtained in dry sand.

Vibracoring in the deflation plain of the Florence Dune took place in late fall/early winter 1998 due to the requirement of a high water table. The three sites were chosen based on accessibility and position in the deflation plain. They came from immediately behind the foredune, mid-portion of the plain, and one at the eastern edge of the deflation plain vegetation. All core logs are drafted using Adobe Illustrator v.7.0.

Figure 15: Vibracore setup on the deflation plain. A TL sample was extracted from this site (SD2).

Drilling

A solid-stem auger was utilized to drill to greater depths (3-10 m) in the deflation plain. The drilling was performed by Oregon Department of Transportation using a CME 75 rotary auger. Courtney Cloyd (USFS) and this author performed core logging by laying the auger threads on a plastic tarp for inspection. The auger materials were cut from the threads and laid on the plastic tarp for description, photographing, and sub-sampling. 10.7 meters (35 feet) was the maximum depth achievable due to available equipment.

Sand thickness and depth

Existing water well logs from representative sites in the Florence and Coos Bay dune sheets were examined to constrain dune sand depth and isopach thickness. The components of this study are 1) a well log search, 2) selection from State of Oregon archives well logs, and 3) the use of global positioning systems to pinpoint the location and elevation of the wells. The details of each are in the following sub-sections.

Well logs

The Oregon Water Resources Department's online database was used to search for relevant well logs. The methods used to select well logs in the area involved first consulting USGS topographic maps to find what townships were in the study area. The study area was defined geographically, with Heceta Head to the north and Coos Bay/North Bend to the south (Figure 1), with a 6-km inland width-restriction. These boundaries were chosen based on the expected extent of the dunes. The relevant township and range boundaries were then entered into Oregon Water Resources' online well log retrieval system (GRID) and abridged well details were then displayed. Downloading the well log was dependent on the depth, since information on the depth of the sand-bedrock contact and thickness was sought after.

131 well logs were retrieved in this manner. Time and funding restrictions disallowed all the wells to be entered into the GPS database, requiring the formulation of criteria for the proper narrowing down of the wells had to be formulated. Selection criteria included locatable (and legible) addresses printed on logs and well depths that could indicate the sand/bedrock contact. In order to attempt GPS control on the wellhead, selected well logs had to contain information that displayed significant patterns that would not have been observed otherwise. In areas sparsely populated with wells, some criteria were ignored. This reduced the number of wells to be located to about 50.

After locating the wells, a Trimble GeoExplorer II GPS unit was used to collect high-accuracy phase data for the required time interval of ten minutes. If possible, the

GPS unit was placed directly on the well. When this was not possible, it was placed as close to the well as possible and recorded in field notes.

The data were collected using GPS phase data and differentially corrected with the Trimble Pathfinder Office Phase Processor to obtain horizontal control to ± 1m and vertical control to an unspecified certainty, although all but one elevation was found to be accurate when compared to USGS topographic maps at a 40-foot contour interval. By the end of the survey, 21 of the selected 50 wells were surveyed with GPS equipment; all others (29) were not locatable (Figure 16).

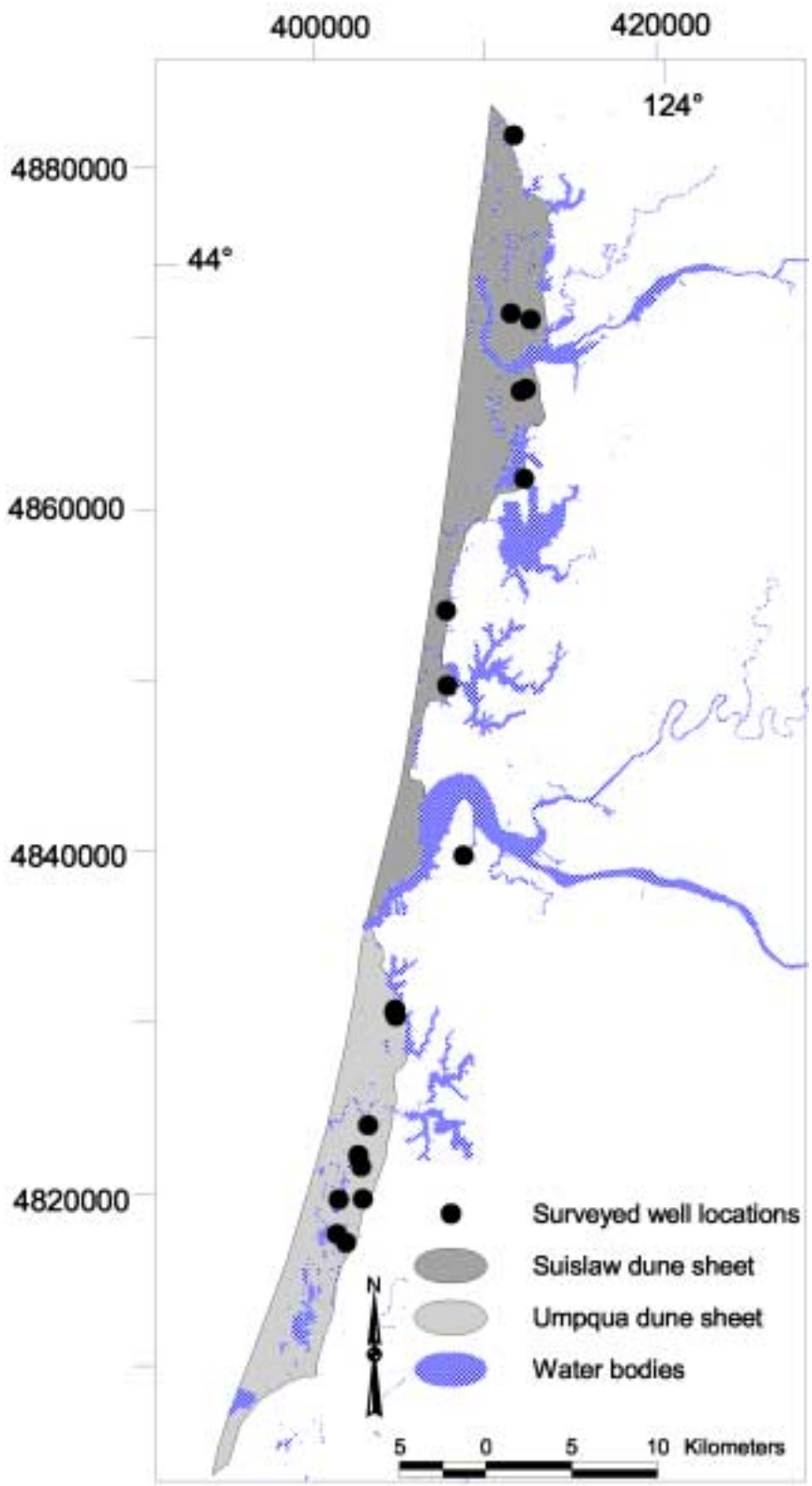

Figure 16: Location map of the 21 wells located with global positioning equipment. Horizontal datum is NAD27 and vertical datum is WGS84 international feet.

Age dating

Age dating of the dune deposits is accomplished with qualitative analysis of soil profiles (relative dating) and with TL and ^{14}C dating of sands and organic matter. Soil mineralogy is also considered for age dating and dune emplacement, in that particular weathering products are indicative of weathering sequences. Grain size work described above is also considered for the weathering of sand to silt/clay in the soil profiles. See the following sections for more detailed descriptions of these methods.

Soil characteristics

Soil profile samples collected from the reconnaissance mapping work (see Background) were analyzed for grain size, pH, and color. Characteristics of soil profiles relative to a particular field area are good indicators of relative soil development (Terhune et al., 1986). The development of soil profiles is useful in correlating soils of known ages to undated soils (Harden et al., 1988). There are many types soil of indices that can give qualitative and quantitative results from soil characteristics (Birkeland, 1984). Better indices rely on soil color changes resulting from the pedogenic development of the profile. There are three color indices commonly used today (Birkeland, 1984). They are the Buntley-Westin, Hurst, and rubification indices (Buntley and Westin, 1965; Hurst, 1977; Harden, 1982a; Harden, 1982b). All are similar in that the Munsell colors are converted into a single numerical value; however, the Buntley-Westin index only uses dry colors, while Rubification uses both wet and dry. Two indices, the Buntley-Westin index and the rubification index, are used in this project (see Background). They were selected because both still increase with increasing age (>5,000 years), while the Hurst index becomes asymptotic near 5,500 years (Figure

17) (Miller and Birkeland, 1974). The implications of using these types of analyses is further discussed in the Discussion section.

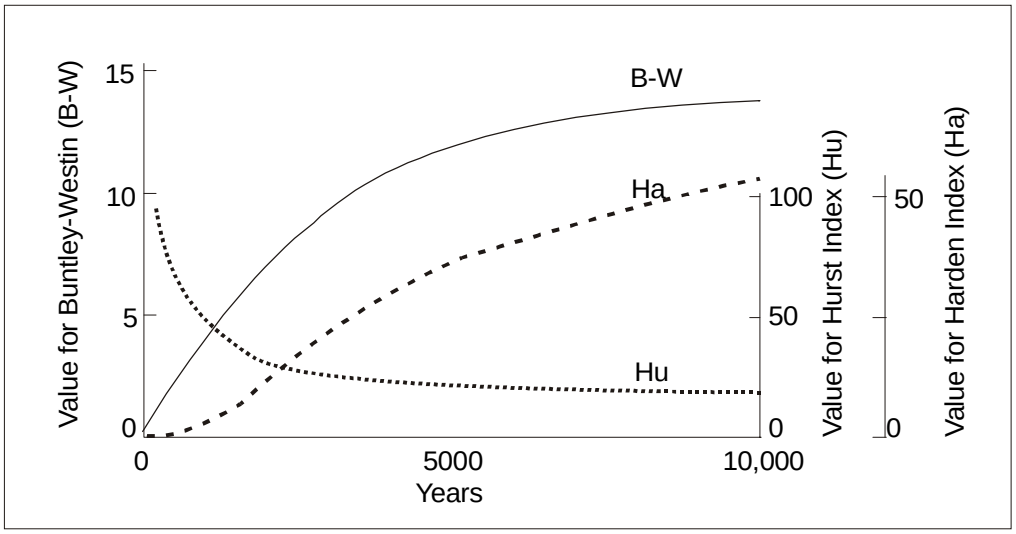

Figure 17: Examples of Hurst (Hu), Buntley-Westin (B-W), and rubification (Ha) values with time in Holocene soils. The soil sequence is from Wind River Mountains in Wyoming, USA. Modified from Birkeland, 1984.

Munsell soil colors

Dr. Errol Stock of Griffith University of Brisbane, Australia, identified Munsell soil colors for each sample from each core site. Two colors were taken from each sample, wet and oven dried. The wet color was taken from a sample that was wetted so that each grain was coated but the sample was not oversaturated such that water would not freely flow from the sample. The methods in which these colors were utilized are addressed below.

Harden's soil maturity index

The different analyses utilized in this thesis, as described by Harden (1982) were melanization (decrease in color value), total texture (maximum grain size change between samples within a soil profile), and rubification (increase in color chroma). With

this index, one can use a standard soil field description of a soil chronosequence and find relative ages of soils of the chronosequence. Jenny (1941) described a chronosequence as a series of related soils developed when all development factors, except time, are held relatively constant. While not every soil development factor in this study is held absolutely constant over the complete duration of pedogenic development, for the purposes of this thesis, it is assumed that the concept of a chronosequence is upheld.

Buntley-Westin color index

The Buntley-Westin color index is also used, which involves a hue with a numerical assignment multiplied by the chroma. This index is applied as described by Birkeland (1984) and Buntley and Westin (1965).

Penetrometer

A hand-held pocket penetrometer was used to estimate the unconfined compressive strength of the soil mass by resistance by the soil to the application of a direct force (Figure 18). Units are tons/ft^2 and range from 0.25 to 4.5. However, values given by this device are only approximates of the actual soil cohesion, and do not replace laboratory testing.

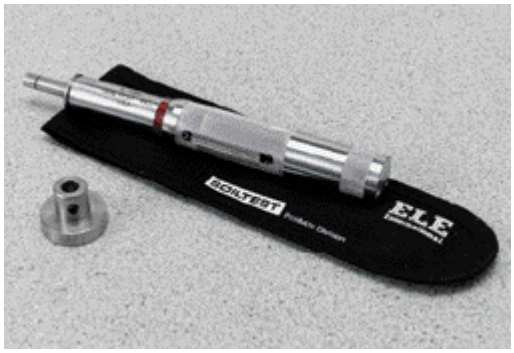

Figure 18: Photo of a pocket penetrometer.

Radiocarbon and Thermoluminesence dating

Timing of dune emplacement is the most important aspect of this study. Therefore, dating of the dunes plays a vital role. The criteria for choosing samples to be dated were based on location. Deflation plain sites were selected to test Holocene progradation. Most other samples were at the eastern extent of dune sheets. This provides an age for the easternmost advance of eolian sand, and consequently a maximum dune age in the locality.

TL dating

Thermoluminesence (TL) dating techniques provide an estimate of the last time that the quartz and feldspar grains were last illuminated by light. Therefore, this technique gives an age of long-term burial. Since a basal sand sample could not be obtained, TL dates represent an age that signifies long-term stability. This dating method is best suited for eolian environments, since the grains are sufficiently exposed to sunlight to nearly completely reset their luminescence signal prior to burial (Clarke et al., 1999).

A typical TL sample site from a road cut would be bored out with an auger near the bottom of the slope, then a TL sample would be extracted from a cored (auger or vibracore) sample from the bottom of the hole under black plastic sheets. The TL samples were protected from light at all times. The extraction of samples from the field has to be performed with caution, since any light contacting the sample could skew the dates. Therefore, a large, light-tight tarp was placed over the person extracting the sample (Figure 19). Ideally, the sample was located one or two meters from the surface both vertically and horizontally. The sample is then wrapped in aluminum foil, plastic

and sent to Wollagong University labs in Australia. If the sample was extracted using a vibracore unit (Figure 15), the sample (approximately 30 cm of pipe length) was cut from the bottom of the pipe, then both ends were wrapped in layers of aluminum foil and sent to the dating labs. Huntley et al. (1985) and Berger (1988) describe the TL dating process.

Radiocarbon dating

Carbon-14 dating was used at three sites (CG1, tree stump and TI1-1 and TI1-3, carbon). In the field, the sample for dating was double wrapped in plastic or aluminum foil and later frozen for preservation. After the sample was thawed, it was oven dried for 12 to 24 hours, and sent to Beta Analytic. At Beta Analytic, each sample was pretreated with an acid (HCl) and an alkali (NaOH) wash.

Figure 19: The extraction of samples to be TL dated involved this large tarp, which blocked light from reaching the sample. This is Dr. Errol Stock checking conditions before setting up to extract a sample.

Clay mineralogy

Mineralogy of clay minerals is an important source of information on the source of clay as either originating from pedogenesis or eolian transport. The identity of clay minerals in the soil profile will be identified from X-ray diffraction and microprobe analyses of clay coatings of grains. Samples were selected based on dated sites (HS1 and NW1) or on unrecognized morphological features (ME1) (i.e. clayey white nodules in dunal cross-beds).

Digital Photomicrographs

Soil and paleosol samples were photographed (at 24x magnification under direct light), washed under running water for 15 minutes, dried, and re-photographed (at 60x magnification under direct light). This was performed to display the underlying texture of sand grains in soil profiles.

X-ray diffraction methods

The summarized methods of deriving the clay-sized fraction from the bulk soil sample are as follows and are fully described in Moore and Reynolds (1997).

1. Soak the sample in distilled water overnight.
2. Sieve the sample to separate out the sand and root material.
3. Apply dispersant (sodium metahexaphosphate) to flocculating slurries.
4. Settle the undesired size fraction under the influence of gravity using Stokes Law.
5. Transfer desired size fraction (<2μm) to glass slides from sediment separated out by micro-pore filters and a vacuum pump. This will produce oriented slides.
6. Place under diffractometer and run the sample from 2° to 35° 2θ at 1°/minute. The diffractometer used is a Phillips X`Pert X-ray Diffractometer recording digital data. Settings for kV = 40, mA = 30.
7. Use visual analysis and the computer database to solve for which minerals are present and run additional analysis with glycolated and oven dried samples as needed.

Microprobe methods

Microprobe analyses of fresh, broken soil peds were performed at Oregon State University's College of Oceanography. The instrument utilized was a Camica SX50 four-spectrometer electron microprobe operated by Heather Petcovic under the direction of Dr. Roger Nielsen. The freshly broken soil peds were mounted on graphite tape and carbon coated. The reflective analyses were performed on ped surfaces from two different sample sites (ME1 and NW1). These samples were selected based on one having a TL age at the time (NW1) and the other displaying unrecognized morphological features (ME1).

Results

In the Results section of this thesis, I report on new work involving 1) dune sand sources, 2) dune sand morphology, 3) paleosol/soil development, and 4) dune sand age of emplacement. Due to the large scope of this thesis, this Results section includes brief interpretations of data. The Discussion section is restricted to specific aspects of source, transport, timing, and mechanics of dune sand emplacement.

Dune sand sources

Scheidegger et al. (1971) performed mineral analysis of continental shelf sands in 1971 (Background). He reported that the primary source of sand to the Florence inner shelf sand was sediment from the Umpqua River, while sand to the Coos Bay inner shelf is supplied from the Klamath and Coast Range terrains. The grain size and additional heavy mineral analyses performed for this project extends the coastal sand source analysis to the origin of the onshore dune sands.

Heavy mineral analysis

Heavy mineral separation and analyses were completed to establish the provenance(s) of the dune sands (see Methods). Samples were analyzed from the Coos, Umpqua, and Siuslaw Rivers and multiple sites in the dune fields (Figure 20, Table 5 and Table 6). Following the work of Scheidegger et al. (1971), the following minerals were counted to establish Coast Range (augite), High Cascades (hypersthene), and/or Klamath Terrain (metamorphic amphiboles, i.e., blue green hornblende, actinolite, and tremolite) sources. This analysis revealed that all but one of the dunal sites contained normalized hypersthene/ pyroxene ratios (1.1/1.0) similar to those of the Umpqua River (1.2/1.0), and not similar to those of the Siuslaw (0.1/1.0) or other minor rivers in the

area. The one exception is from a dunal site near the north end of Coos Bay. It is close to a 50/50 mix of the Coos River and Umpqua River sands, as seen in Figure 20 that illustrates normalized percentages of augite, hypersthene, and hornblende. A statistical analysis of the normalized hypersthene ratios of dunal samples yielded a 3 percent standard deviation about a mean of 39.6 percent. The Umpqua River sample fits within the 3 percent standard deviation of the dune samples. The largest range in normalized metamorphic ratios for the dune samples partly reflects the small number of grain counts. Larger sample grain counts are needed to establish any trends in this variable. In addition, nearly all of the dune sample sites were from the Florence dune sheet, north of the Umpqua River; therefore, the Coos Bay dune sheet is under-represented in this analysis. Finally, these samples reflect surficial deposits of either Holocene or late Pleistocene age (see Discussion). No samples from basal dune deposits (earliest dune advances) were analyzed in this study.

Grain size analyses of the dunes in the area

Grain size analyses of the dune sand samples were performed to establish potential trends in size across the dune fields and identify the presence of paleosols (see Methods). The samples were collected from road cuts and shallow auger borings (Figure 21). The results show dune-wide trends, as well as confirming paleosols in cores. Sand auger cores that displayed visual evidence of silt- and clay-rich layers contained corresponding intervals of decreased grain size per sample, mid-core for paleosols and the uppermost portion for modern soils (Figure 22). Appendix A contains all grain size separations used in this study.

Table 5: Results of grain counts (300 counts per sample) on grab samples of sands in and around the Florence and Coos Bay dune sheets.

Sample Site and Location	Augite	Hypersthene	Common Hornblende	Meta-amphiboles
Modern rivers				
Coos River 4801500 N 407000 E	60 **%**	5 **%**	25 **%**	10 **%**
Umpqua River 4838700 N 416600 E	35	41	19	5
Siuslaw River 4870300 N 416000 E	65	4	27	4
Modern dunes, south of Florence				
Foredune 4861600 N 407700 E	39	39	20	2
Deflation Plain 4861600 N 408100 E	38	35	23	4
Dune paleosols				
Tree island, S of Florence 1 4862150 N 409400 E	34	43	19	4
Tree island, S of Florence 3 4862000 N 410800 E	36	42	18	4
Tree island, S of Florence 4 4862300 N 409950 E	37	41	16	6
Tree island, S of Florence 10 4861900 N 409600 E	36	39	22	2
Coast Guard Station, Florence 4872750 N 409950 E	41	36	17	6
N. Woahink Road 4864900 N 414000 E	32	39	24	5
North Beach Siltcoos Lake 4860500 N 410400 E	35	40	23	1
Dunes near Coos Bay 4812400 N 400600 E	51	21	21	7

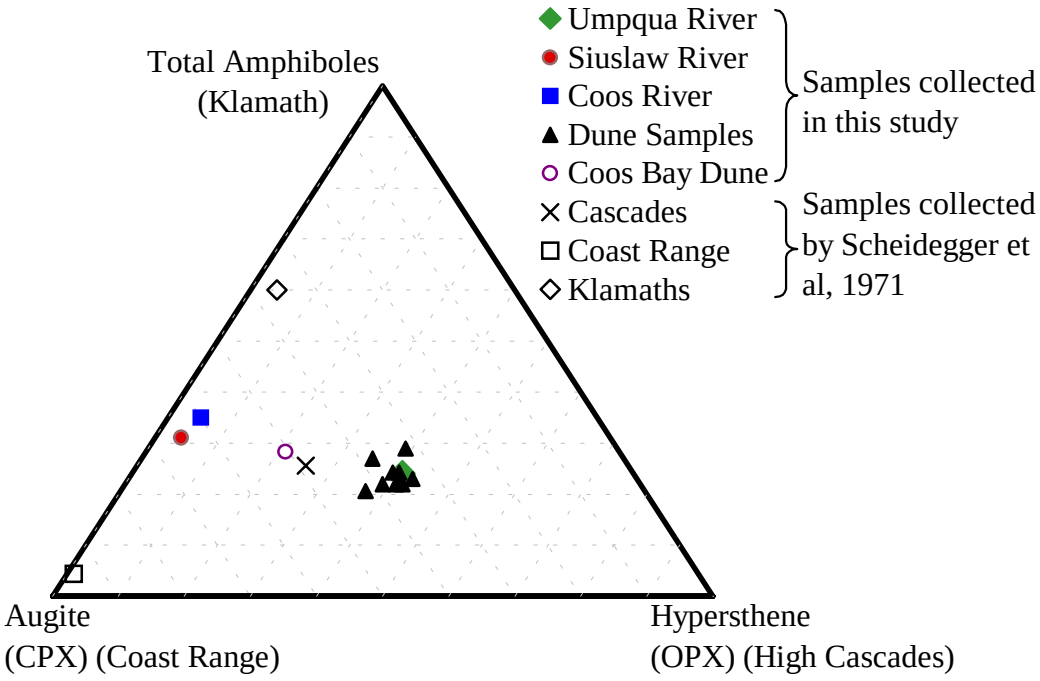

Figure 20: Ternary diagram with normalized heavy mineral percentages and end members of the distictive mineralogical signatures discussed in the text. Note the grouping of dune sands around the Umpqua River sands. Some data as indicated above from Scheidegger et al, 1971.

Table 6: Normalized heavy mineral ratios.

Sample Site	Augite	Hypersthene	Total Hornblende
Modern rivers			
Coos River	60 **%**	5 **%**	35 **%**
Umpqua River	35	41	24
Siuslaw River	65	4	31
Modern Dunes just south of Florence			
Foredune	39	39	22
Deflation Plain	38	35	27
Dune paleosols			
Tree island, S of Florence 1	34	43	23
Tree island, S of Florence 3	36	42	22
Tree island, S of Florence 4	37	41	22
Tree island, S of Florence 10	36	39	24
Coast Guard Station, Florence	42	37	21
N. Woahink Road	32	39	29
North Beach Siltcoos Lake	35	40	24
Dunes near Coos Bay	51	21	28

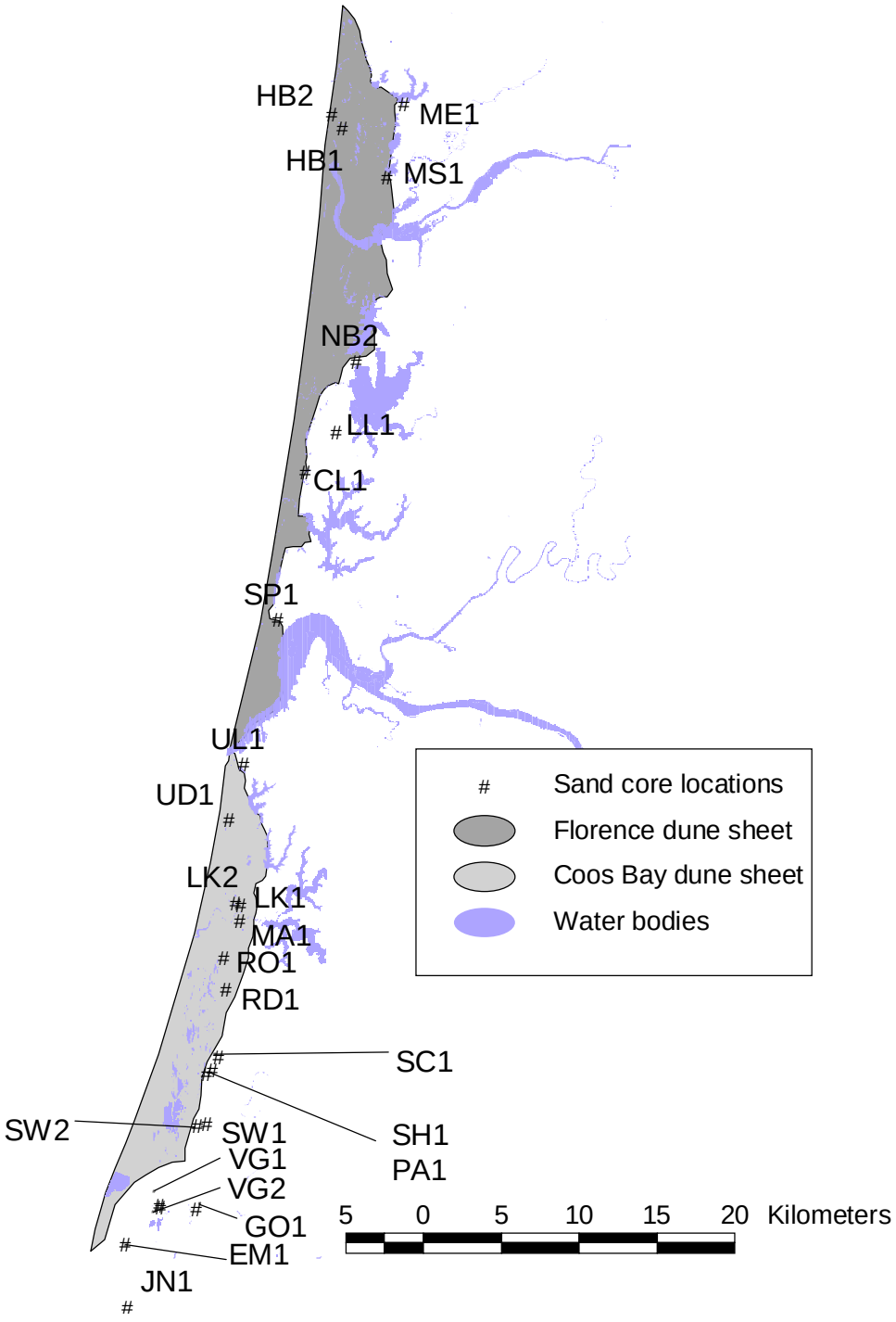

Figure 21: Location map of shallow core and road cut sites used in grain size analysis.

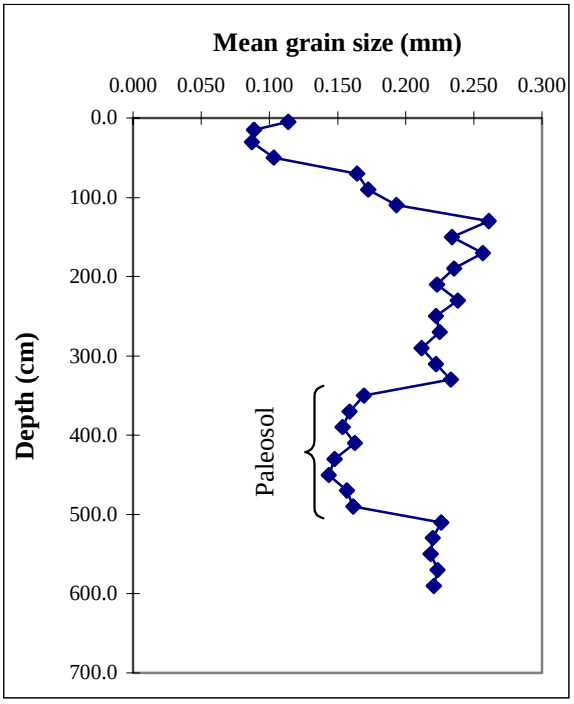

Figure 22: Mean grain size per sample decreases down the depth of the sand auger cores. The decrease in grain-size correspondes to silt- and clay-rich paleosols. Auger core GO1.

Trend surface analysis of mean grain size per core, with data layers for soils and paleosols removed, revealed a statistically significant trend of grain sizes becoming finer to the north (Figure 23). The coastline and associated dune fields are subparallel to the UTM coordinates used. To remove this bias, the trends analysis was also performed with the coastline angle removed. This further trend surface analysis also demonstrates a statistically significant trend of fining of grain sizes to the north (Figure 23). Trend surface analyses for the two individual dune sheets are also presented in Figure 23. When separated into two individual dune sheets, the Coos Bay sheet shows a strong trend of fining to the north, but the Florence sheet shows no net fining to the north. Results for ANOVA tests of all four scenarios are presented as Table 7. The overall trend of fining to the northwest is likely biased by the small variation in E-W location

sites versus the large variation in the N-S location sites. Additional work is needed to establish any significant E-W trends in grain size in the ODNRA. Interpretations of the decrease in sand size to the north, both in the overall trend and in the Coos Bay dune sheet, are presented in the Discussion section.

Surficial and subsurface dune morphology

Geospatial analyses

Modern and prehistoric dunes display lee-slope morphology can be interpreted and converted to transport azimuths (see Methodology) (Figure 16). Dominant transport azimuths should reflect dominant wind directions. Transport directions might change between interglacial and glacial time or between modern and recent times. The potential variance of dune transport azimuths between modern, active dunes, and vegetated or stabilized dunes needed to be established. Additionally, these results are highly dependent on the 32 classes used to record azimuth data to the GIS database. To test these possibilities, a geospatial analysis of dune azimuths with the aid of a GIS system was utilized. This analysis incorporated aforementioned air photo interpretations by Dr. Errol Stock as presented in GIS coverages provided by the USDA Forest Service (see Background and Methods).

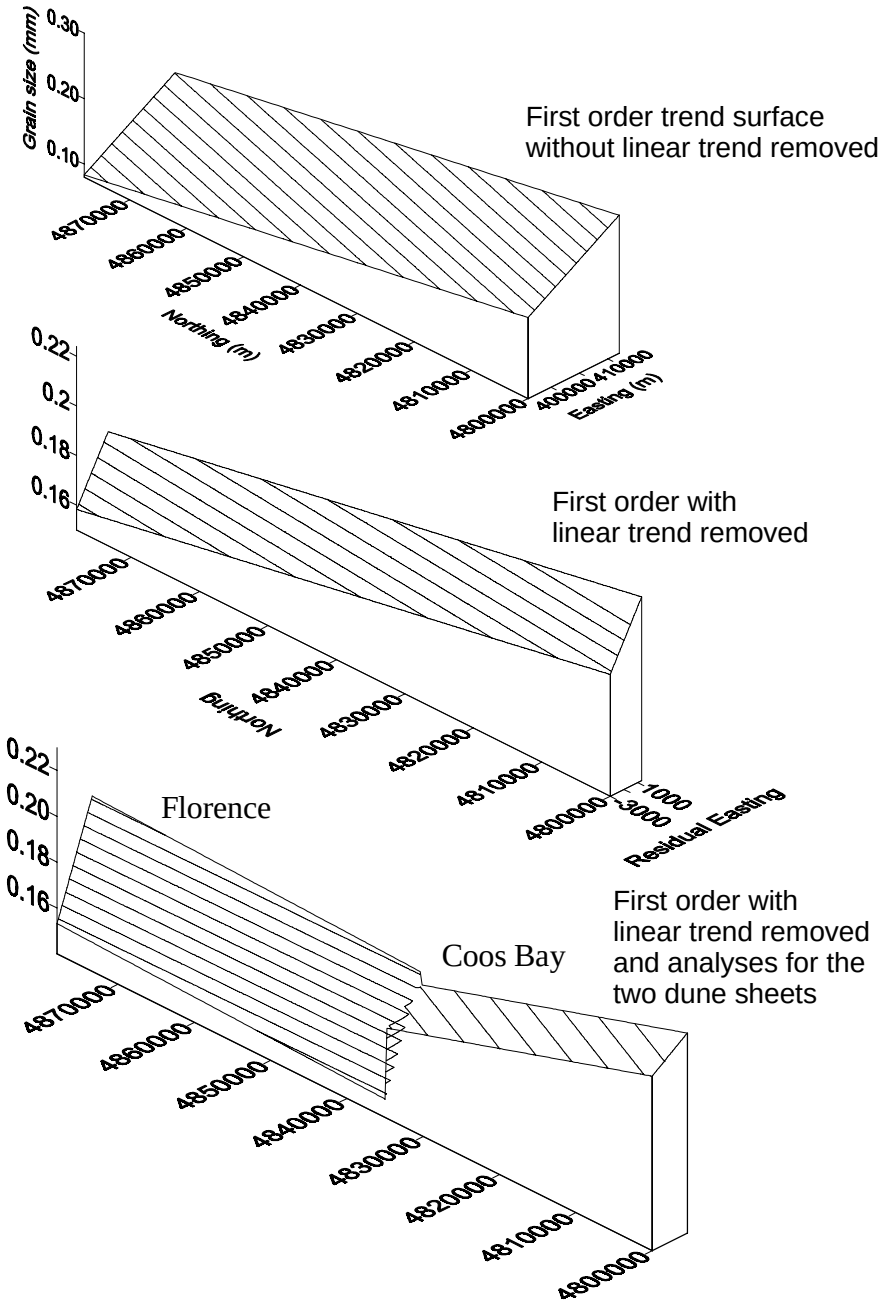

Figure 23: Trend surface analyses for first-order trend surface analyses on core mean grain size for original coordinates (top), coastline linear trend removal (middle), and each individual dune sheet with liner trend removed (bottom). Data contours are shown in 0.01 mm intervals. Mean grain size drops from greater than 0.23 mm in the southeast sites to less than 0.14 mm in the northwestern sites. Mean grain size decreases to the west and to the north.

Table 7: Results of ANOVA test for statisitcal significance of the first order trend surface. H_0 = the trend displayed is not statitically significant. Level of confidence is 95 percent.

Trend surface	F – statistic	Critical F	H_0 accepted or rejected?
First order trend surface	9.29	2.02	Rejected
First order trend surface with linear trend removed	9.29	2.02	Rejected
Florence dune sheet w/o linear trend	0.41	3.73	Fail to reject
Coos Bay dune sheet w/o linear trend	15.16	2.79	Rejected

The grid analysis of current dune migration azimuths per one square-kilometer grid cells is presented in Figure 24. Preliminary results reveal the plotted lee-slope azimuths show a) strong east-southeast transport, b) secondary localized trends of northeast of south east transport in the modern (active) dunes and, c) very localized corridors of north or south transport in the modern (active) dunes. The variable azimuths suggest strong topographic/vegetative control of dune advance rather than simple dominance by northwest summer winds (transport to the southeast) or southwest winter winds (transport to the northeast). The bi-directional seasonal wind patterns likely add to the transport complexity. To establish whether prehistoric (stabilized dunes) and historic (active dunes) conditions differed from one another, some additional statistical tests were performed on the azimuth data. These test were also used to test whether lee-slope azimuths varied between the Florence dune sheet (north or the Umpqua River) and the Coos Bay dune sheet (south of the Umpqua River).

Rayleigh's test results indicate that in all cases, the null hypothesis of the $\kappa > \kappa$-critical was rejected where κ, the concentration parameter, is a measure of how clustered the data is (see Methodology). Clustered data sets indicate significant trends in the

directional parameter measured. Higher κ's correspond to a smaller spread about the mean (greater clustering around the mean resultant azimuth). All sample subsets (north/south of visual break point, stable versus active areas) displayed a significant trend at a high 99 percent confidence level. As shown in Table 8, the mean azimuths, as well as most other parameters, were nearly the same. When examining the rose diagram (Figure 25) of azimuth data, one would expect that even if the resultant azimuths were nearly the same, then surely the mean resultant length ($\overline{R}$) would differ. Nonetheless, the only findings that changed were the critical $\overline{R}$ value and the azimuth confidence interval, both of which are affected strongly by *n*. In summary, the entire combined data, as well as all sample subsets, displayed statistically significant lee-slope azimuth trends, with small differences between subsets.

It should be noted that the bi-directional wind patterns for this section of coast (Figure 5) would skew this data depending on the time of year the air photo base maps were photographed. These photos were taken in summer of 1989 and therefore could display a bias (on the western, active edge) to the southeast.

In summary, the dune transport azimuths from the air photo GIS data demonstrate very complex transport directions, likely based on local topography, not on regional wind regimes. At the regional scale there are no net differences between modern and prehistoric or between northern and southern dune lee-slope azimuths. These results appear to contradict a trend of net northward transport as indicated by a decrease in sand size to the north (see previous Results section). This possible contradiction is addressed in the Discussion section of this thesis.

Table 8: Summary of results for the GIS azimuth analysis for 1-km^2 grid cells for all azimuth data, and separated based on dune sheet (Florence and Coos Bay), and east-west placement.

Statistical test parameters	All azimuth data	Florence sheet	Coos Bay sheet	Western cells	Eastern cells
n	181	113	68	116	65
$\overline{R}$	0.78	0.55	0.57	0.61	0.62
99 percent confidence level for $\overline{R}$	0.16	0.22	0.28	0.22	0.28
H_0 rejected or accepted?	Rejected	Rejected	Rejected	Rejected	Rejected
κ	2.65	1.29	1.36	1.56	1.60
Azimuth of mean	135°	134°	137°	141°	146°
Azimuth confidence interval (95 percent)	5.8°	12.5°	15.5°	10.7°	13.9°
Azimuth Range	129.5-141.1°	121.8-146.8°	121.5-152.5°	130.6-152.0°	132.0-159.9°

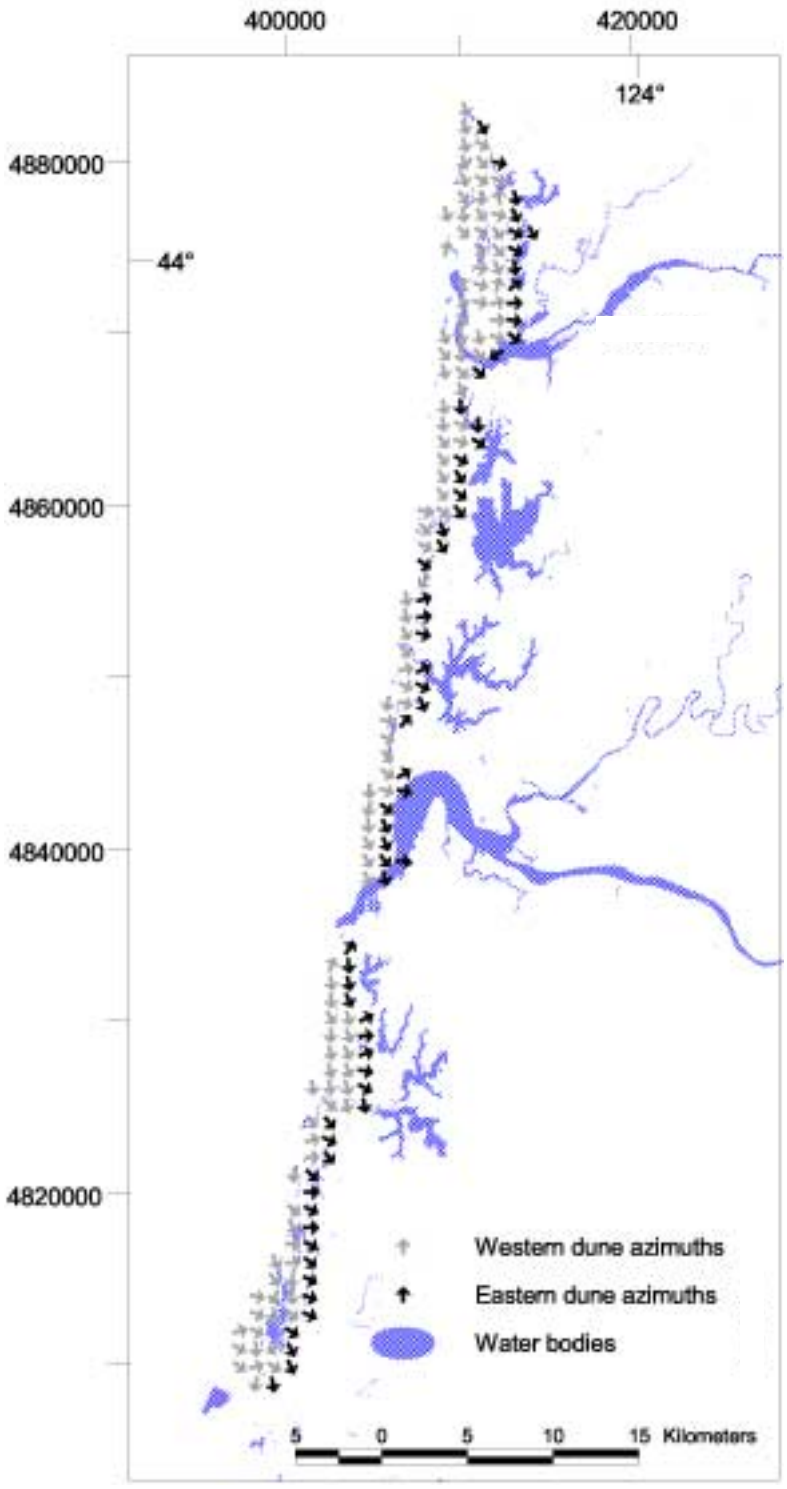

Figure 24: Mean dune azimuth per one sqaure-kilometer grid cell. The azimuths represent the direction of present or past dune migration. The eastern-most edge of the grid is representative of stabilized dunes, since few dunes are active that far inland. The stablized dunes' directions of transport are shown by bold arrows. Mean dune transport azimuths along the western edge are shown by the lighly shaded arrows.

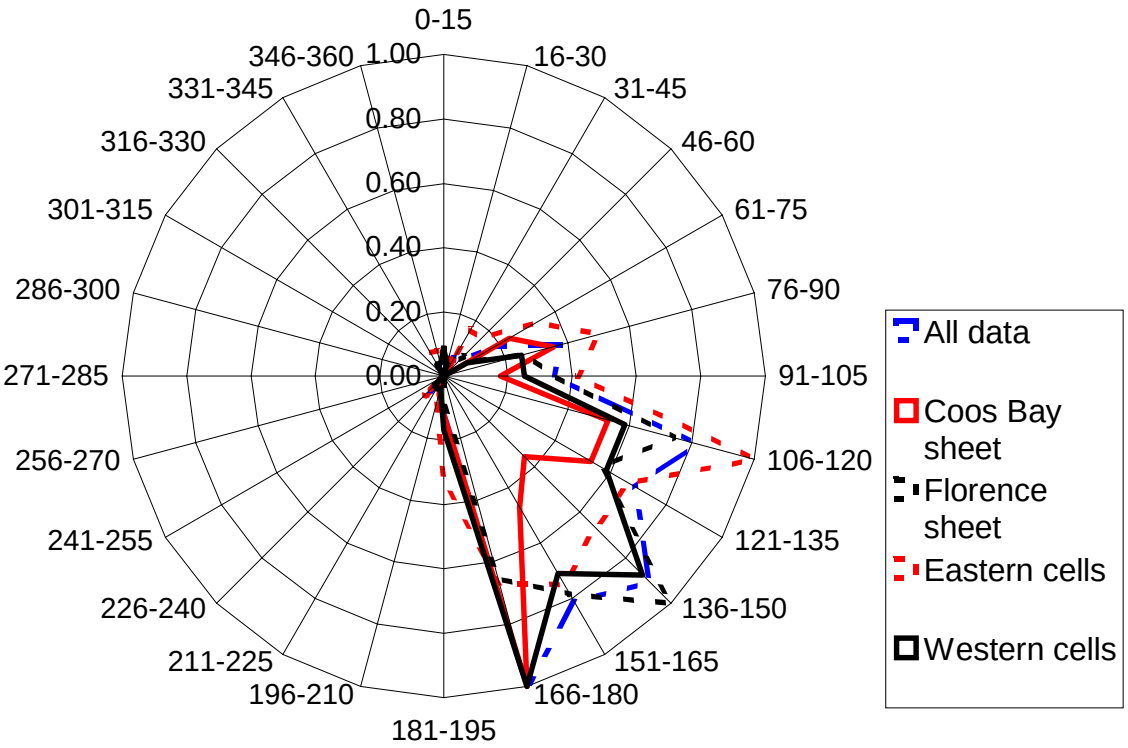

Figure 25: Rose diagram for dune azimuth analysis. Note the dominance of southern transport direction in the Coos Bay sheet and the western cells, and the more easterly direction of transport for the eastern (stabilized) cells and the Florence sheet.

Vibracore

Vibracoring was performed to determine what units the deflation plain is founded upon. The nature of these units should provide insight into the origin(s) of the active sand belt. Specifically, does the sediment upon which the deflation plain is founded represent progradation or deflation of previous dune sand? The vibracore sub-surface sampling of the deflation plain (Figure 27) revealed that it is founded upon cross-bedded, fine-grained, well-sorted sand to depths of ~3 meters (Appendix C). There were multiple foreset beds displayed in the cores. All but one of the cores had nearly the same grain size in the top as the bottom, and all with the same apparent mineralogy from top

to bottom. See Table 9 for a summary of the vibracore results. Figure 27 displays photos of the vibracore sites. Appendix C contains the grain-size separations and the core logs. The western-most site (SD1) contained shells, likely beach overwash materials, at the bottom of the core. A larger mean grain-size in GP1 suggests that this portion of the deflation plain rests upon beach sands. Therefore, the modern fordune appears to overlie Holocene beach deposits. TL dating of deflation plain subsurface deposits is discussed in a later Results section of this thesis.

Figure 26: Photos of vibracore sites. Clockwise from top left: SD1, SD2, and SD3. SD1 taken immediately behind the foredune, SD2 from the eastern edge of the deflation plain, and SD3 from the approximate mid-section of the deflation plain.

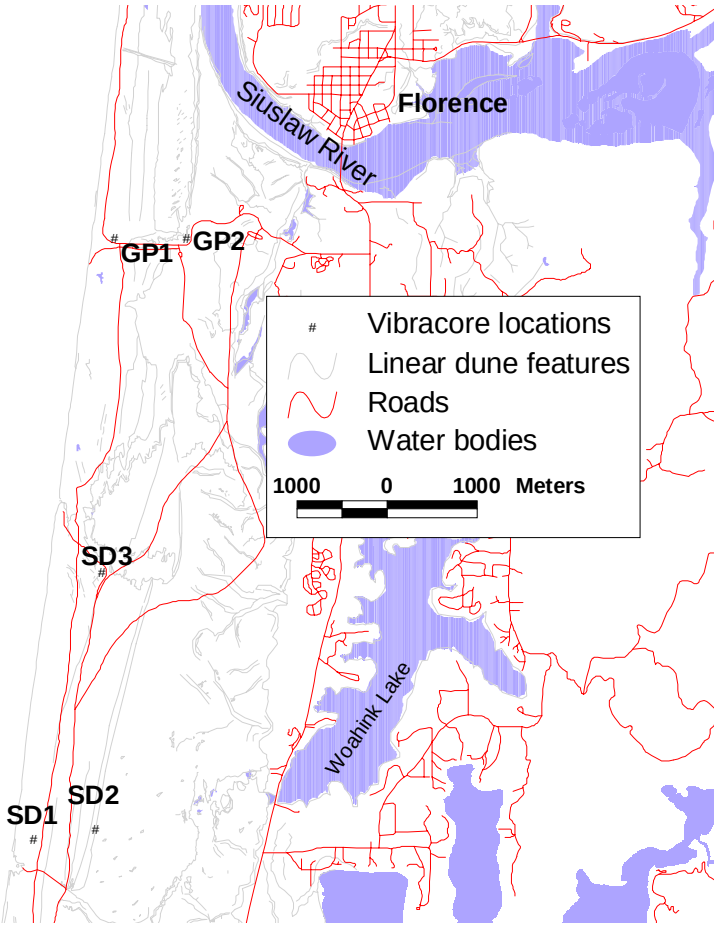

Figure 27: Location map for vibracore sites.

Table 9: Summary of vibracore results. Italicized data from USGS topographic maps, rather than GPS equipment.

Core	Morphostratigraphic position	Northing (m)	Easting (m)	Mean grain size top (mm)	Mean grain size bottom (mm)
SD1	Immediately behind foredune	4860803	407746	0.12	0.15
SD2	At the eastern edge of vegetated deflation plain	4860915	408418	0.12	0.12
SD3	Mid-section of the deflation plain	4863772	408488	0.12	0.13
GP1	Western portion of the deflation plain	*4867450*	*408650*	0.13	0.25
GP2	Eastern deflation	*4867450*	*409450*	0.12	0.12

plain

Drilling

Drilling via a solid stem auger was needed to extend the depth of the vibracore borings. Specifically, deeper borings were needed to establish whether the apparently "young" shallow sub-surface dunes overlaid Pleistocene marine terraces or Holocene progradational beach deposits. Drilling in the deflation plain south of the Siuslaw River and south of the Umpqua River yielded penetration depths of 10.6 meters (35 feet). The Siuslaw River sites were at the Goose Pasture ATV staging area on the South Jetty Road and at the sand access road at the northward turning bend behind the foredune (Figure 28). The Umpqua River site is at the northeastern edge of the ODNRA Umpqua dune #3 parking lot (Figure 28). While no thick paleosols were found in any cores, small paleosols were present in two cores (Figure 29). UD2 contained clay starting at 9.2 meters (30 feet) of depth and increased in relative percentage with depth. The clay was a gray color and cohesive. Core GP3-b contained brown silt and clay rich sediments and organics between 9.8 and 10.4 meters (32 and 34 feet) depth, which was archived for potential future C^{14} and XRD analysis. Core GP4 contained fine sand to 7 meters (23 feet) of depth where the sand was then much coarser, well packed, and contained rounded shell fragments to the end of core, 10.7 meters. This seaward-most site is interpreted as a progradational beach deposit.

In summary, the modern deflation plain appears to be composed of a relatively thick (10 m) deposit of Holocene dunes, based on the lack of well-developed paleosols (see later Results section of this thesis). Unfortunately, the drilling on the eastern side of the modern deflation plain stopped short of establishing the nature of the "platform"

units underlying the Holocene dune deposits. Deeper borings, located further inland, are reported in the next Results section of this thesis.

Table 10: Morphostratigraphic position and UTM locations for solid stem auger drilling sites.

Core	Morphostratigraphic position	Northing (m)	Easting (m)
GP4	~150 m behind foredune	4867340	408690
GP3-b	At the eastern edge of deflation plain	4867240	409410
UD2	~100 m behind foredune	4831680	402410

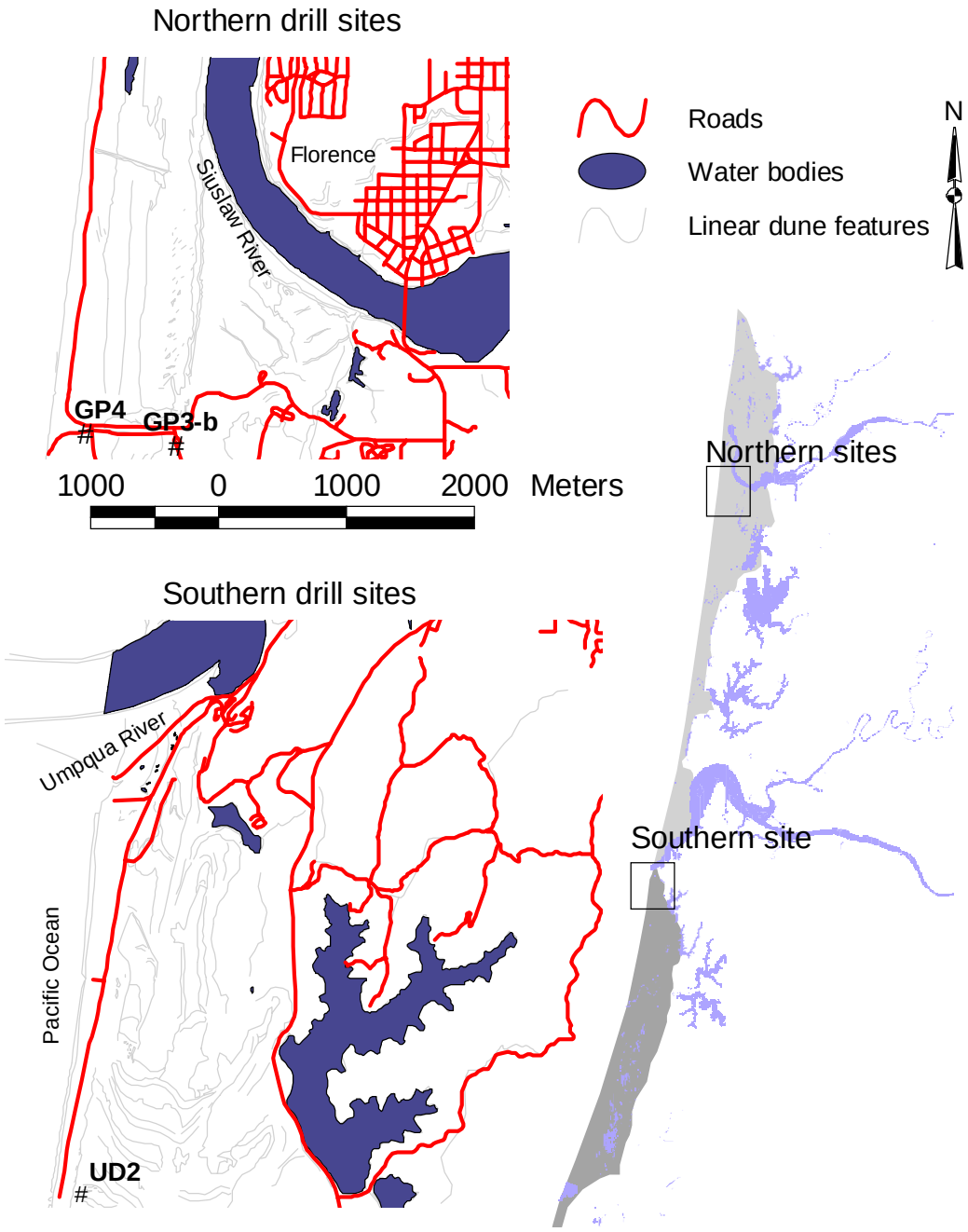

Figure 28: Location map of drill sites. Drill sites are labeled GP4 and GP3-b. GP4 is approximatly 120 meters east of the foredune backedge and GP3-b is approximatley 1100 meters east of the foredune, and west of the eastern dune ridge. Both GP4 and GP3-b are northern drill sites. The southern site, UD2, is south of the Umpqua River. The site is about 100 meters from the lee side of the foredune.

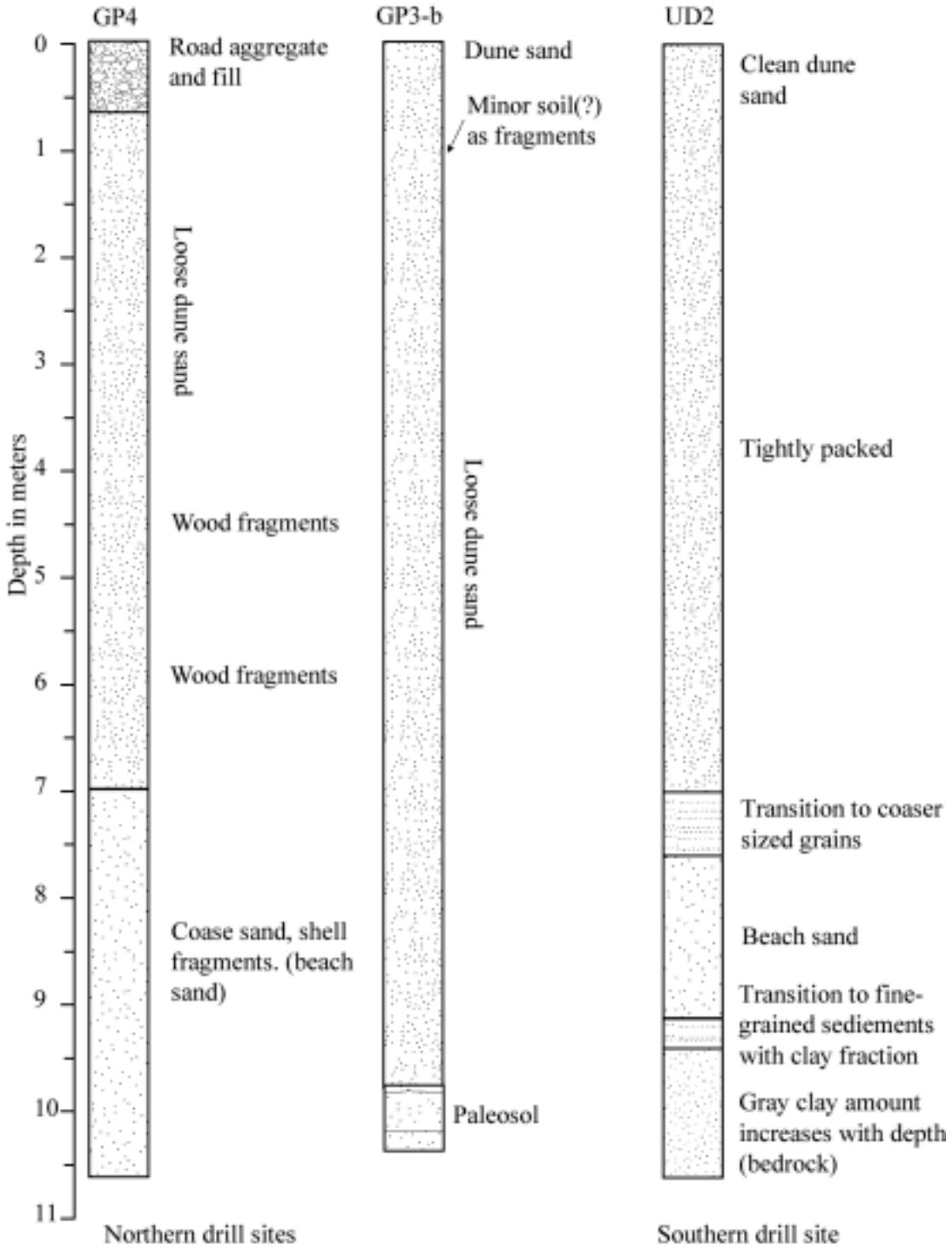

Figure 29: Summary boring logs from the solid stem auger drilling of the deflation plain. Note the paleosol in GP3-b and the beach sand in GP4 and UD2, and the likely contact with bedrock in UD2. Modified from Cloyd, unpublished data, 2000.

Sand thickness and depth

Well logs were examined to establish the total thickness of the dunes and elevation of basal contacts. Water well records were used due to the relative abundance of wells in the area and the coverage they provide, particularly around Florence and Coos Bay. The coordinates of the wells are shown in Table 11, with map in Figure 30. Dune sand thickness and depths display trends relative to their northing coordinates. In general, the dune sands are thicker and deeper to the north (Figure 31). The variability of bottom contact elevations in the north reflects the channel/mouth of the Siuslaw River meandering through time on the late Pleistocene/Holocene coastal plain. If the basal contacts are on marine wave-cut platforms, then higher elevations of the sand bedrock contact to the south could imply tectonic uplift to the south. Supplementary data on the wells, including state well log number and street addresses are presented in Appendix D. Some sand-bedrock contact depths are minimum depths, since the well did not reach bedrock. A modified fence diagram displaying the sand-bedrock contacts is shown in Figure 32. The stratigraphic layers in the modified fence diagram represent interpretations from the drillers' description of the lithology down core. For example, many logs contained descriptions of "blue sand" or "coarse sand." These sediments are interpreted to be beach or estuarine sand. Descriptions of "fine sand" are interpreted as dune sands. Discrete clay layers within sands in the well log are interpreted as paleosols. ANOVA analysis on the linear regression of sand depth and sand thickness concluded that both linear trends of increasing sand thickness and increasing sand contact depth to the north are significant at a confidence interval of 95 percent (Table 12).

Table 11: UTM coordinates for wells in the ODNRA (NAD 27, Zone 10). Due to GPS errors or incomplete data, italicized items are not from GPS equipment, but from USGS topographic maps.

Easting	Northing	Elevation (m)	Depth of sand (m)	Elevation of contact (m)	Distance to the shoreline (km)
411511	4881792	21	0	21	1.6
411364	4871405	21	38	-17	2.6
412496	4871024	14	42	-27	3.8
412224	4867010	*~60*	28	31	4.0
411942	4866851	51	29	22	3.7
412120	4861751	38	12	26	4.5
407589	4854029	41	48	-7	1.0
407647	4849686	11	13	-2	1.7
408585	4839751	16	0	16	4.7
404642	4830770	83	29	54	2.6
404573	4830622	74	0	74	2.5
404661	4830354	66	5	62	2.6
403046	4824001	45	2	43	2.4
402488	4822270	37	>29	<8	2.3
402465	4822211	37	0	36	2.3
402629	4821573	*~79*	1	79	2.7
402735	4819699	94	4	91	3.3
401348	4819666	32	>16	<16	1.9
401236	4817657	32	31	1	2.5

Table 12: ANOVA results for sand thickness' and elevation of sand-bedrock contacts versus UTM northing. H_0 = Slope of sand tickness and depth trend line is not significantly different from zero. F distribution at 95 percent confidence.

Data set	t statistic	t-crit	H_0 results
Sand thickness	1.89	1.72	Rejected
Sand bedrock contact elevation	4.51	1.72	Rejected

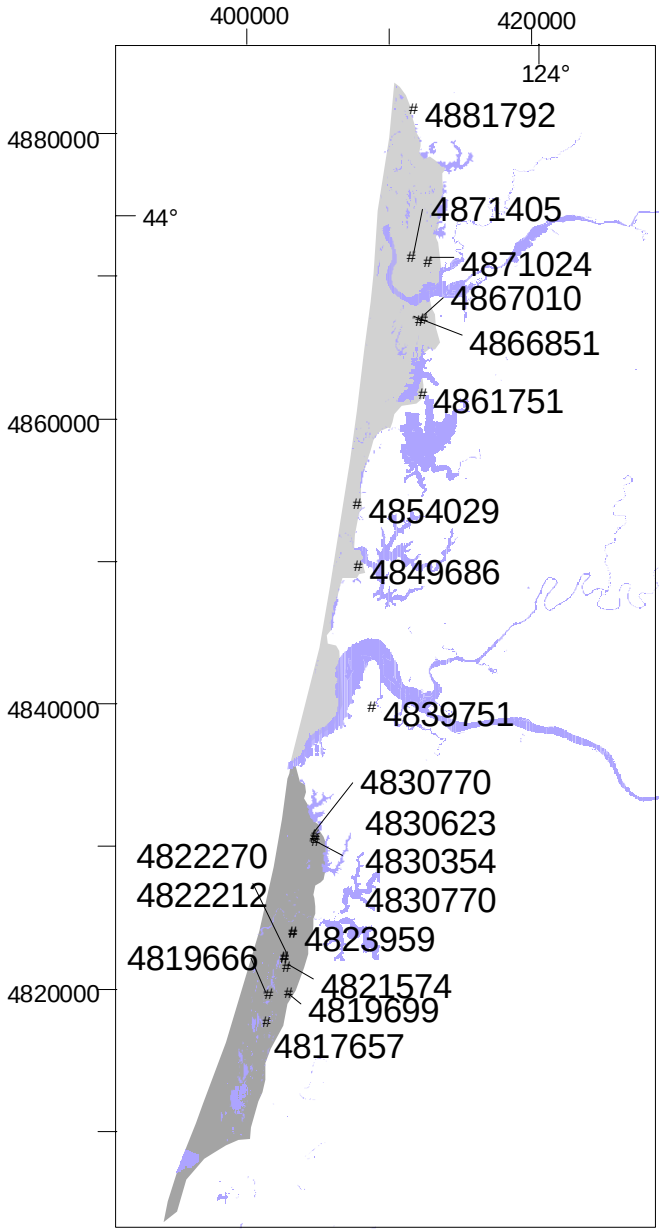

Figure 30: Map showing locations of surveyed well logs. Northing coordinate is labeled to index well log to other figures.

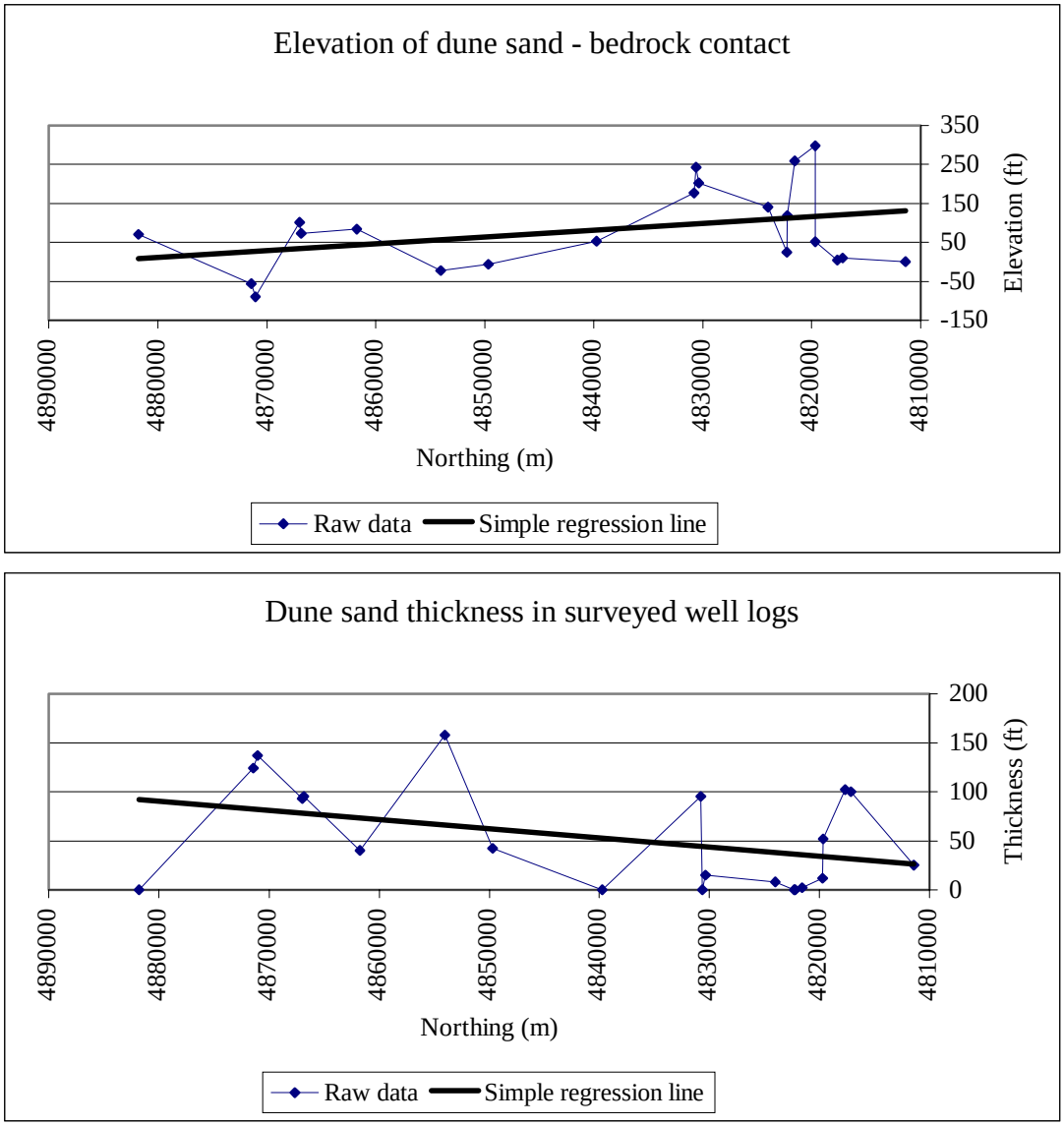

Figure 31: Graph of sand thickness and depths in wells on the Coos Bay/Florence dune sheets as a function of the wells' northing coordinate. Variability shown by the elevation of the bottom contact in the north is affected by the Siuslaw River and higher elevations in the south could indicate relative tectonic uplift.

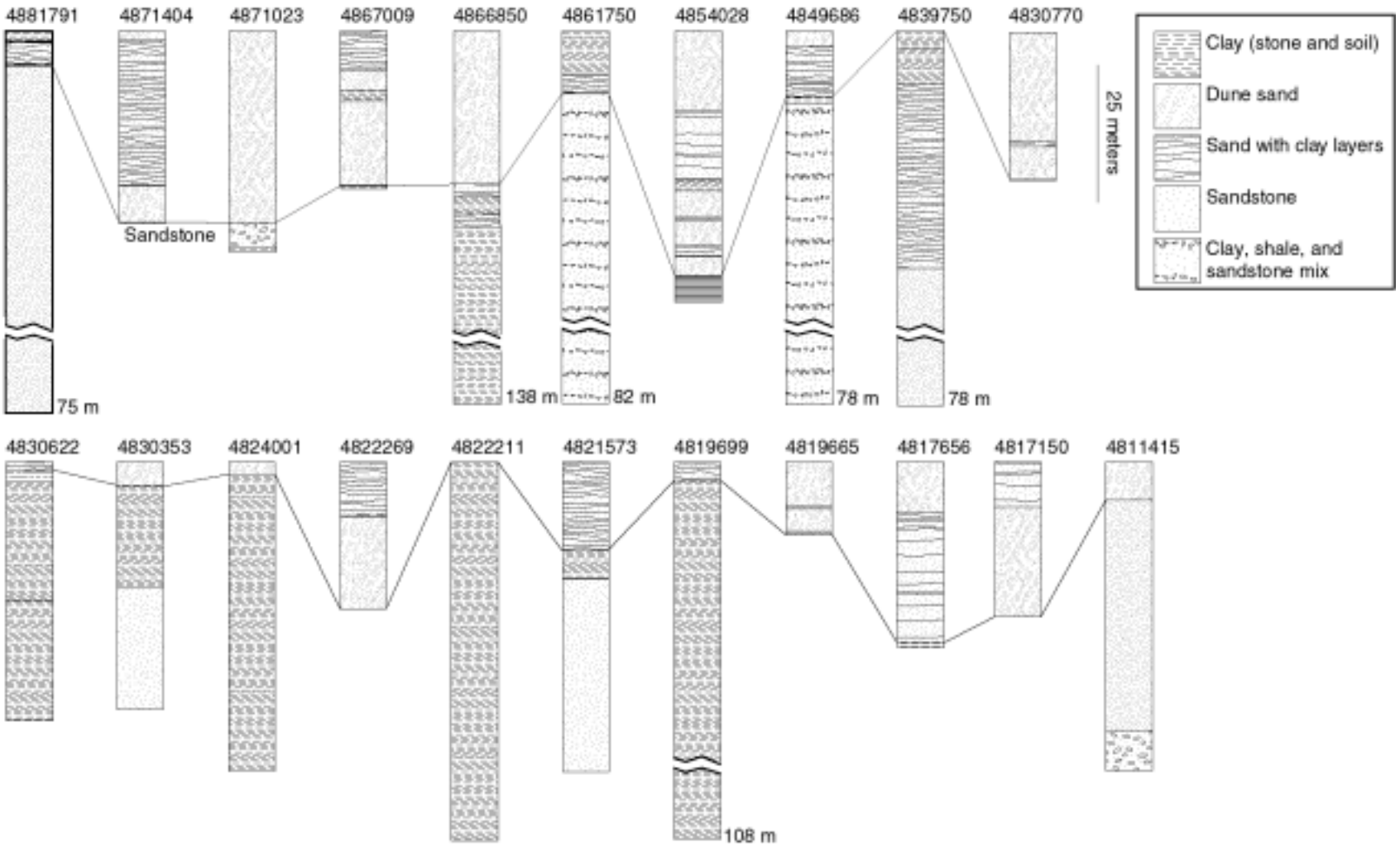

Figure 32: Modified fence diagram for the 21 survey wells of the field area. The line represents the sand/bedrock contact.

Soil/Paleosol development

Relative soil development is an important aspect of this study, because the development of pedologic horizons is related to development duration (see Background) (Harden, 1982; Birkeland, 1984). Four methods of detailing soil characteristics that are used in this thesis are soil development indices, X-ray diffraction, electron microprobe analysis, and binocular optical microscope.

Optical microscope

Figure 33 presents digital photomicrographs of soil and sand samples. Soil and paleosol samples were photographed, washed, and re-photographed. This was done to show the underlying texture of sand grains in soil profiles. Washed sand grains displayed surface pitting with clay in fractures to a greater degree than fresh sand samples (Figure 33). This suggests that clay is at least partially weathering directly from the less stable minerals in the sand (Quartz was relatively unpitted), in addition to loess and/or airborne clays.

Soil development indices

The soil development indices of rubification, Buntley-Westin, and maximum grain size decrease were calculated and compared. Appendix G displays the correlation that the indices had with one another, and with the normalized values also found in Appendix H. A correlation matrix of the data (Table 13) suggests that the indices of rubification and Buntley-Westin are somewhat correlated. Core EM1 ranked the highest in all indices, except in the Buntley-Westin index, where a normalized score of 0.75 was established.

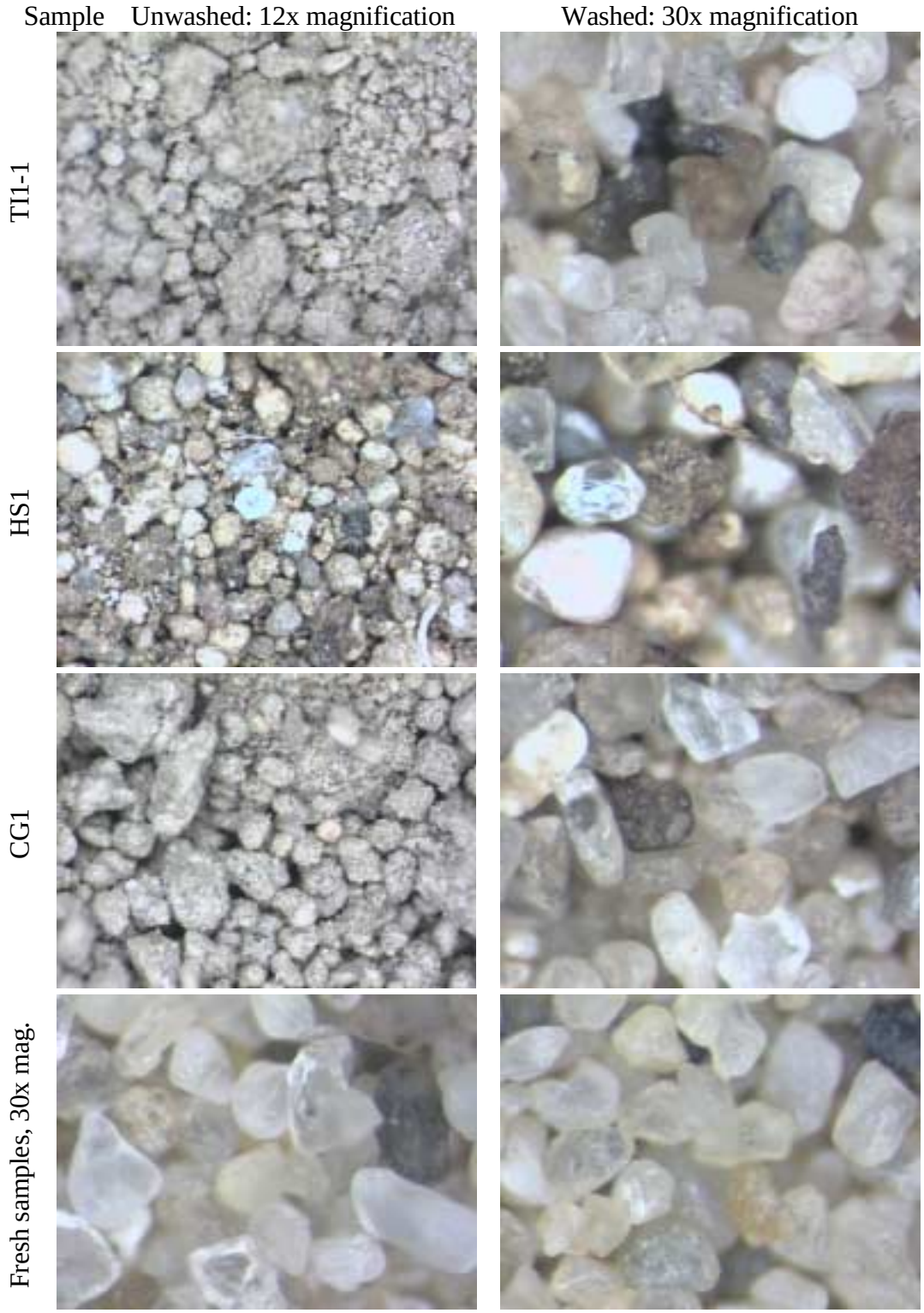

Figure 33: Photomicrographs displaying weathered grains from paleosols and soils. Two samples of fresh sand are included for comparison. Note that the grains in the washed samples are pitted to a greater degree than fresh samples.

Table 13: Correlation coefficient, variance, and covariance for soil indices. Calculations based on normalized data. Correlation coefficent above the diagonal (**Bold**), varience on the diagonal (no emphasis), and covarience below the diagonal (***Bold Italics***).

	BW	Rubification	Grain Size
BW	0.04	**0.64**	**0.62**
Rubification	***0.03***	0.05	**0.42**
Grain Size	***0.03***	***0.02***	0.07

Table 14: Soil properties compared of dated cores. For TL dates, age is TLYBP; for ^{14}C dates, age is in RCYPB.

Core	Age (ka)	Dating method	Modern or buried	Color Field	Color Dry	Color Wet	Structure	Thick-ness (m)	Penetro-meter	Buntley-Westin	Rubi-fication
TI1	>46.5	^{14}C	Buried	7.5YR 4/4	10YR 4.5/6	7.5YR 3/4	Blocky	>0.3	2.7	18	40
TI1	32.4	TL	Buried	7.5YR 4/4	10YR 4.5/6	7.5YR 3/4	Blocky	>0.3	2.7	18	40
TI1	0.7	^{14}C	Buried	**No longer exposed**							
CG1	24.6	^{14}C	Buried	7.5YR 3/4	10YR 5.5/4	7.5YR 3/3	Blocky	0.6	>4.5	12	10
RD1	32.9	TL	Modern	7.5YR 3/4	10YR 4/6	7.5YR 3/4	Blocky	1.2	2.4	18	40
HS1	30.5	TL	Modern	10YR 3/6	10YR 5/6	10YR 3/4	Massive	1.6	1.75	18	60
WW1	6.9	TL	Modern	10YR 4/6	10YR 5/5	10YR 3/6	Granluar	0.2	0.2	15	70
NW1	37.2	TL	Modern	7.5YR 3/3	7.5YR 3/4	7.5YR 3/2	Blocky	1.2	0.7	16	10
ME1	70.2	TL	Modern	7.5YR 3/3	7.5YR 4/4	7.5YR 3/3	Blocky	1.0	4.5	16	20
SD1	2.9	TL	Modern	10YR 5/2	10YR 6/2	10YR 4/2	Granular	0.0	0.0	6	0
SD2	1.5	TL	Modern	10YR 5/2	10YR 6/2	10YR 4/2	Granular	0.0	0.0	6	0
Parent	-	-	Modern	10YR 6/2	10YR 6/2	10YR 4/2	Granular	0.0	0.0	6	0

In an effort to correlate soil development parameters with dated cores, rubification, Buntley-Westin, thickness, and hand penetrometer readings were performed on dated cores (Table 14). Use of the hand penetrometer appeared to give the most reliable correlation to age (Figure 34).

The soils ranged in thickness from 10 cm to ~2 m. Soil colors in the B-horizons are typically near 10YR4/2. Minimum mean grain size in the B-horizons is 0.02 mm, well into the silt size fraction. The average B-horizon grain size was 0.10 mm with a standard deviation of 0.04 mm.

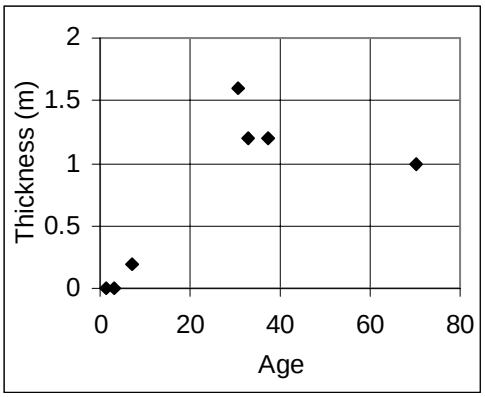

Correlation Coefficient: 0.71

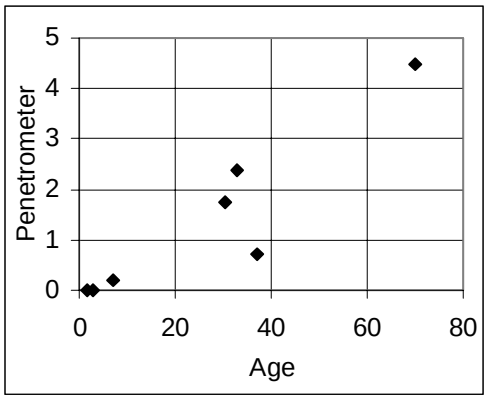

Correlation Coefficient: 0.94

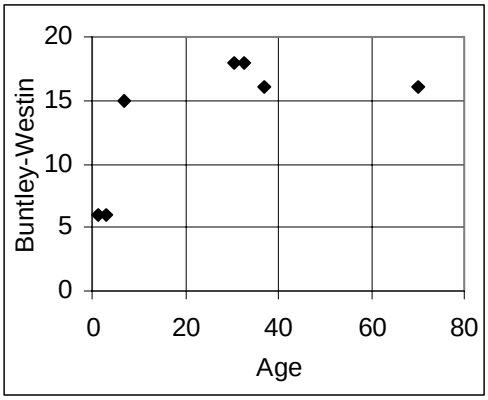

Correlation Coefficient: 0.66

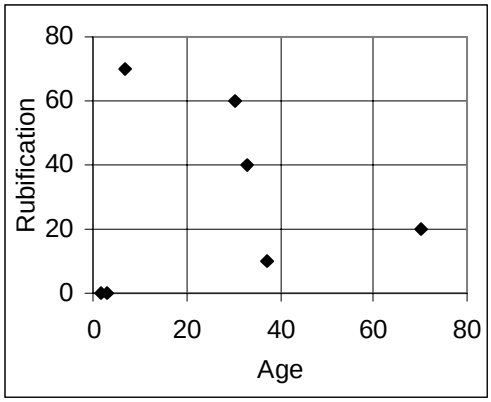

Correlation Coefficient: 0.05

Figure 34: Scatter plots of correlation between different soil indicies and age. Use of the hand penetrometer appears to give the most reliable correlation to age. For TL dates, age is TLYBP; for ^{14}C dates, age is in RCYPB. All ages are in thousands of years.

Based on field visits, the overall trend is that the surficial soils in the eastern portion of the two dune sheets are more developed than those in the western portions. The eastern dune surfaces have apparently been vegitatively stabilized for longer periods than the western portions of the dune sheets (see upcoming Results section). Direct quantitative comparison between surface soils and paleosols is not possible, since the paleosols are not in the same pedogenic environment than the surface soils, which is a key factor in relative soil comparisons. However, qualitative comparison is still

possible. Upon burial, the soil is no longer receiving organic matter and the associated acids, a condition inhibiting further development. Additionally, burial alters the environment of soil development, and thus changes the physical characteristics of the buried soils. Less developed surface soils to the west suggest more recent dunal advances from the oceanward side. The most developed paleosols appear to represent shorter periods of stability than the most developed, eastern dune surfaces.

X-ray diffraction results

X-ray diffraction analysis was performed on representative surface soils to establish mineralogy of the clay fraction (<2μm). Full scans of the x-ray diffraction (XRD) patterns can be found in Appendix E. The mineralogy of the less than 2μm size fractions are interpreted from the XRD scans, and with the utilization of a search-match database. The minerals identified in the samples examined are vermiculite ($(Mg,Fe^{2+},Al)_2(Al,Si)_4O_{10}(OH)_2 \cdot 4(H_2O)$), kaolinite ($Al_2Si_2O_5(OH)_4$), and gibbsite ($Al(OH)_3$) or a combination of the three. Vermiculites dominate the weathered profiles, such as in NW1. Vermiculite is determined by the 6.2 °2θ (14.3Å) peak, and tests that showed no peak shifts upon heating and only very slight shifts upon glycolation (Figure 35). It should be noted that the mineral identified as vermiculite in this thesis could also be a poorly ordered chloritic-smectite intergrade. Additionally, soil vermiculites are morphologically different from metamorphic vermiculites. However, for purposes for this thesis it is referred to as vermiculite. In addition to paleosols, some interstratial weathering products are also apparent in the parent material. For example, at sample location ME1, south of Mercer Lake, as well as other locations, gibbsite has been found in discrete balls in unweathered dune cross-beds (Appendix E and Figure 36). Clay

sized particles (<2μm) in sample ME1 are nearly 100 percent gibbsite. Gibbsite also occurs in weathered soil profiles. Soil core JN1 (sample depth 80 cm) also contained large amounts of gibbsite (Appendix E). The peak of highest intensity in gibbsite is the 4.82 Å peak.

In summary, the presence of gibbsite in the soils indicates high levels of leaching occurring either in the soil horizons or in the interstitial layers associated with groundwater movement (Deer et al., 1992). Vermiculite is possibly the initial clay mineral being formed from the weathering of sand grains, with kaolinite possibly being an intermediary or accessory mineral.

Table 15: Summary of results of X-ray diffraction.

Core name	Depth (cm)	Geographic and UTM Position (NAD27, Zone 10)	Core age, if available	Clay minerals present
JN1	80	4800020 N 396390 E		Gibbsite, vermiculite, kaolinite.
NW1	60	E-NE of Woahink lake 4864850 N 413990 E	37.2 ± 4.8 ka	Primarily vermiculite, small amounts of gibbsite and kaolinite.
SP1	150	4844150 N 406080 E		Vermiculite with smaller amounts of kaolinite.
ME1	In road cut, ~3m from surface	On the south east banks of Mercer Lake 4872550 N 413090 E	70.2 ± 3.0 ka	Gibbsite (one unidentified peak).

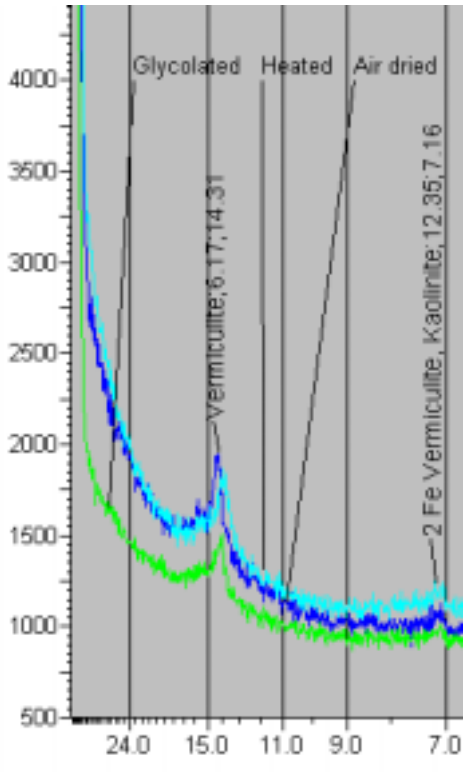

Figure 35: Vermiculite x-ray diffraction pattern. The core location is SP1, with the full scan available in Appendix E.

Figure 36: Photo to the left is of gibbsite nodules found dunal sands. The sample site is ME1, on the southeastern banks of Mercer Lake northeast of Florence.

Microprobe

Microprobe analyses were performed to distinguish individual elemental components to help verify mineral constituents. Electron microprobe analysis was performed on gibbsite nodules from Mercer Lake (ME1) (Figure 36) and soil samples from North Woahink (NW1). More detailed analyses, complete with photos, are presented in Appendix F. A characteristic gibbsite nodule contained nearly 95 weight percent Al_2O_3, while the soil profile at NW1 showed gibbsite ranging from 8 percent to 32 percent. Silica (SiO_2) values at NW1 ranged from 42 percent to 81 percent; at ME1, values were lower. Iron (Fe_2O_3) at NW1 was near 7 percent; at ME1, values are bimodal, with one group at 1 percent and the other near 15 percent. This distribution is consistent with the signature expected from the probe scanning a gibbsite nodule containing gibbsite-coated quartz, feldspar, or silicate fragment.

In summary, microprobe results confirm that the gibbsite likely formed in-situ by precipitation into nodules, by the absence of elements other than those found in gibbsite. This precipitation likely reflects in-situ geochemistry of interstitial fluids (groundwater geochemistry) that is over-saturated in Al. Presumably, the more mobile Fe, Ca, and Si have been lost to groundwater discharge. The fates of those dissolved elements are not addressed in this study.

Table 16: Charateristic normalized Microprobe results for samples from Mercer Lake (ME1) and North Woahink (NW1). The listed concentrations are normalized as oxide weight percentages. Complete tabular results and scans for all analyses are available in Appendix F.

	Na	Mg	Al	Si	P	S	Cl	K	Ca	Ti	Cr	Mn	Fe
ME1.gibbsite2	0.01	0.06	94.59	4.11	0.20	0.07	0.05	0.03	0.04	0.12	0.08	0.00	0.63
NW1.40.1	0.20	0.32	8.28	80.95	0.09	0.10	0.09	0.30	0.06	1.34	0.02	0.06	8.18
NW1.60.1	0.02	0.01	25.76	65.91	0.00	0.02	0.02	0.12	0.07	0.68	0.00	0.00	7.39
NW1.60.2	0.12	0.28	10.55	81.07	0.10	0.38	0.11	0.24	0.57	0.38	0.00	0.00	6.19
NW1.60.3	0.10	0.35	32.22	41.68	0.41	0.19	0.08	0.21	15.59	0.37	0.01	0.07	8.70

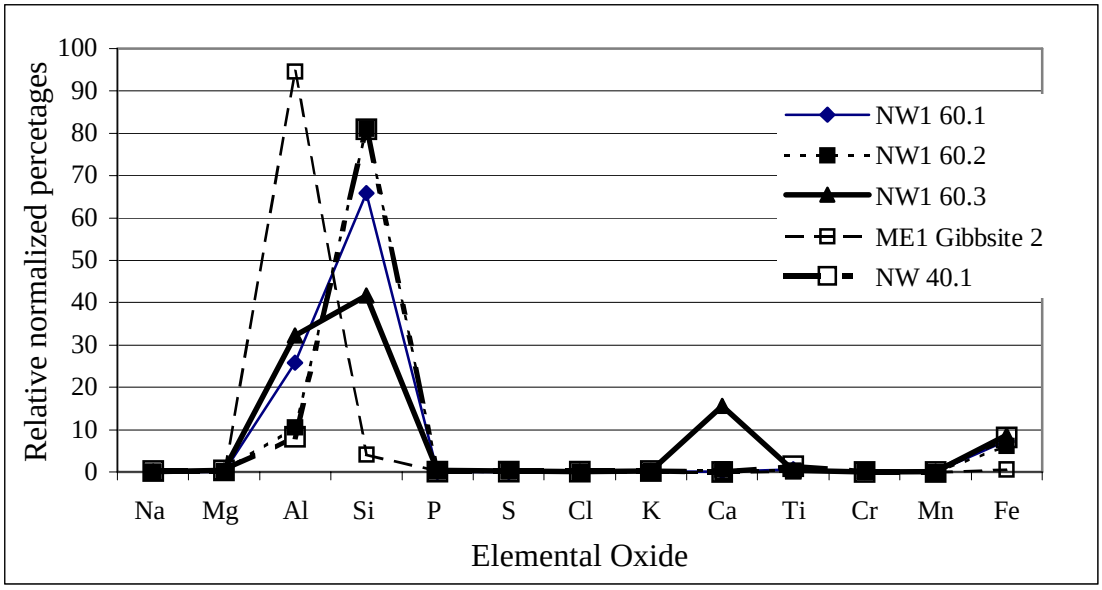

Figure 37: Graph of charateristic normailzed element percetages for samples from Mercer Lake (ME1) and North Woahink (NW1) at depths of 40 and 60 cm.

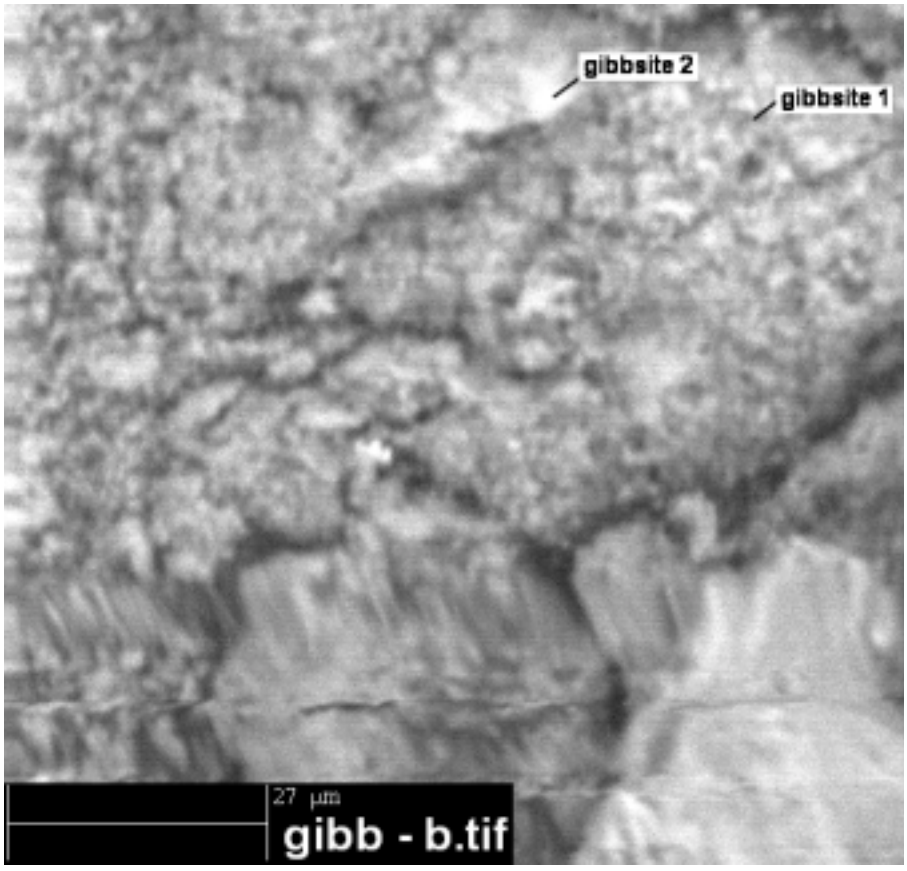

a

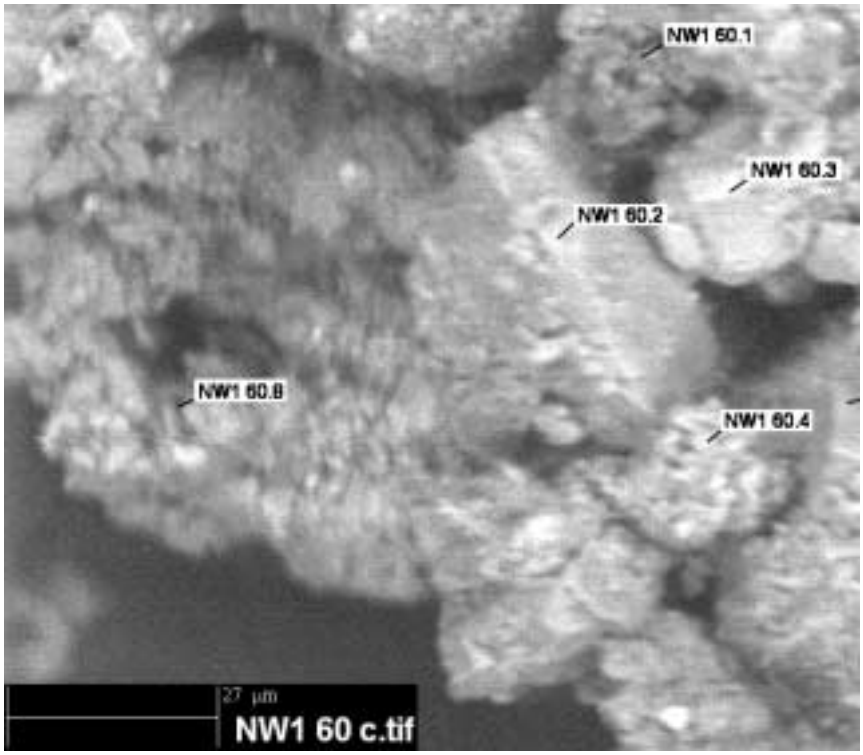

b

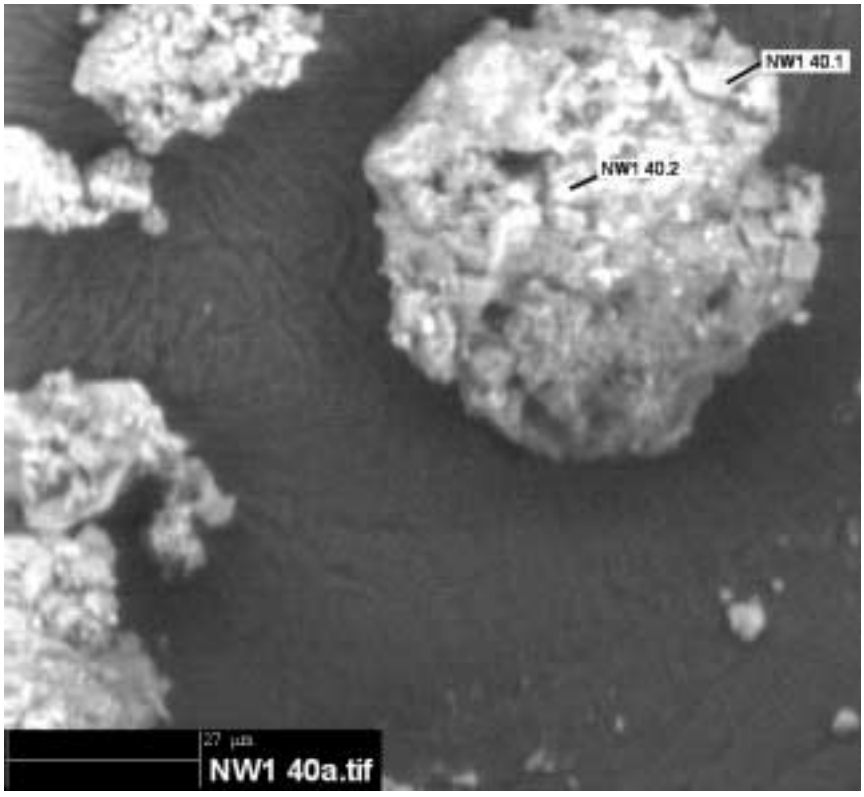

c

Figure 38: Microprobe photographs of the samples analysed and specific places were analysis was completed. Samples from Mercer Lake (ME1) gibbsite is labeled *a*; samples from North Woahink (NW1) at depths of 40 and 60 cm are labeled *b* and *c*.

Radiocarbon and thermoluminesence dating

Paleosols in well logs and differing relative soil development in shallow core samples suggest different ages of dune emplacement and/or durations of vegetative stabilization in the ODNRA field area. Both ^{14}C and TL dating (see Methods) were used to constrain the ages of dune sand emplacement. These ages of emplacement should also provide insight to periods and mechanisms of dune sand supply. Complete results of the TL analyses are shown in Appendix H.

Twelve sites have been dated on the Coos Bay and Florence dune sheets (Figure 39 and Table 17). The oldest date is 70.2 ± 3.0 TLYBP, which represents an age nearly twice as old as the next youngest at 37.2 ka, with the exception of the TI1 ^{14}C date (which was radiocarbon dead at 46.5 RCYBP). Other dates group near 30,000 YBP, while the remaining dates are entirely Holocene (Figure 39 and Table 17). The youngest dates are near reactivated areas (WW1, CG1, TI1, CG2 SD1, SD2-1), while the older dates are from sites generally further east (ME1, NW1, RD1, TI1, HS1, CG1), representing earlier advances and subsequent stabilization. The only eastern-edge date that is "young" is WW1 (4.7 TLYBP). This young date is likely due to a Holocene advance eastward, or to late Holocene dune reactivation. Currently, active dunes do exist ~5 km inland northeast of Florence. Therefore, these types of reactivated eastern dunes are seen in the field area. Additional work is needed to establish the factors that lead to this localized dune reactivation along the eastern margin.

Potential errors in TL dating could result from in-situ or external radiation sources, as well as incomplete re-zeroing by sunlight during transport (Berger, 1988). Specifically, cosmic radiation can partially reset the TL signal, as can radiogenic

elemental components in the soil. Such effects would result in younger than actual dates. Incomplete re-zeroing of the TL signal can occur by sediment that is not completely exposed to sunlight during transport, resulting in artificially old dates. However, as stated in the Methodology section, TL dating is ideal for eolian sediments due to the sub-aerial nature of transport (Clarke et al., 1999). Some evidence exists for radiation affecting the dates of these ODNRA deposits. For example, both a TL and C^{14} date was taken at the Tree Island site on adjacent exhumed paleosols dated at 32.4 ± 8.2 ka and >46.5 ka, respectively. These two dates are at least 6,000 years from one another, based on the TL date showing a ± 25 percent error range. It is possible that sample quality had been degraded due to a partial resetting of the TL signal. Another possibility is that the adjacent paleosols of the same period of origin. Additional testing of the same sediments by both C^{14} and TL is warranted to establish the similarity of these two dating techniques in the ODNRA.

No basal dates (bottom of the dune sheets) were obtained for this thesis project. However, the shallow subsurface dates indicate at least two and possibly three periods of dune advance. An early advance, rarely exposed at the surface, is represented by indurated deposits (semi-consolidated) dated to 72 ka at Mercer Lake. Further dating of basal dune deposits are needed to confirm this earliest dune advance. A widespread younger advance in indicated by a suite of dates (37-24 ka), as indicated by western paleosols or from eastern surface soils.

Table 17: Summary of TL and C^{14} dates found on the Coos Bay/Florence dune sheets.

Age	Geographic and UTM position	Core	Dating method
70.2 ± 3.0 ka	Eastern edge, 4877280 N 414120 E	ME1	TL
4.7 ± 0.4 ka	Eastern edge, 4830050 N 404480 E	WW1	TL
37.2 ± 4.8 ka	Eastern edge, 4864850 N 413990 E	NW1	TL
32.9 ± 3.6 ka	Eastern edge, 4820420 N 402720 E	RD1	TL
0.7 ± .06 ka (Beta #89164)	Tree island behind deflation plain, ~4860940 N 410020 E	TI1-3	^{14}C
32.4 ± 8.2 ka	Tree island behind deflation plain, 4862130 N 409390 E	TI1-2	TL
>46.5 ka (Beta #84374)	Tree island behind deflation plain, 4862115 N 409410 E	TI1-1	^{14}C
30.5 ± 5.9 ka	Eastern edge, 4816060 N 402260 E	HS1	TL
24.6 ± 3.1 ka	Coastal site under paleosols, 4872730 N 409940 E	CG1	TL
6.9 ± 0.07 ka (Beta #84373)	Coastal site above paleosols, 4872730 N 409940 E	CG1	^{14}C
2.9 ± 0.3 ka	Immediately behind beach foredune, 4860803 N 407746 E	SD1	TL
1.5 ± 0.3ka	Eastern edge of deflation plain, 4860915 N 408418 E	SD2-1	TL

Finally, the western side of the dune sheet, both on the deflation plain and in surface deposits of the larger dune ramps (Tree Island), contains late Holocene dune dates. Figure 40 exhibits a cross section of a traverse of dates for the Tree Island and related sites. Note the Holocene dates in the deflation plain and in the upper portion of the tree island, which indicates Holocene activity in the western portion of the dune fields. Late Pleistocene dates are at the bottom of the Tree Island and further inland at site NW1. Additionally, Figure 41 displays the error range relative to each site dated. These periods of dune advance/activity are interpreted in terms of dune field origins under the Discussion section of this thesis.

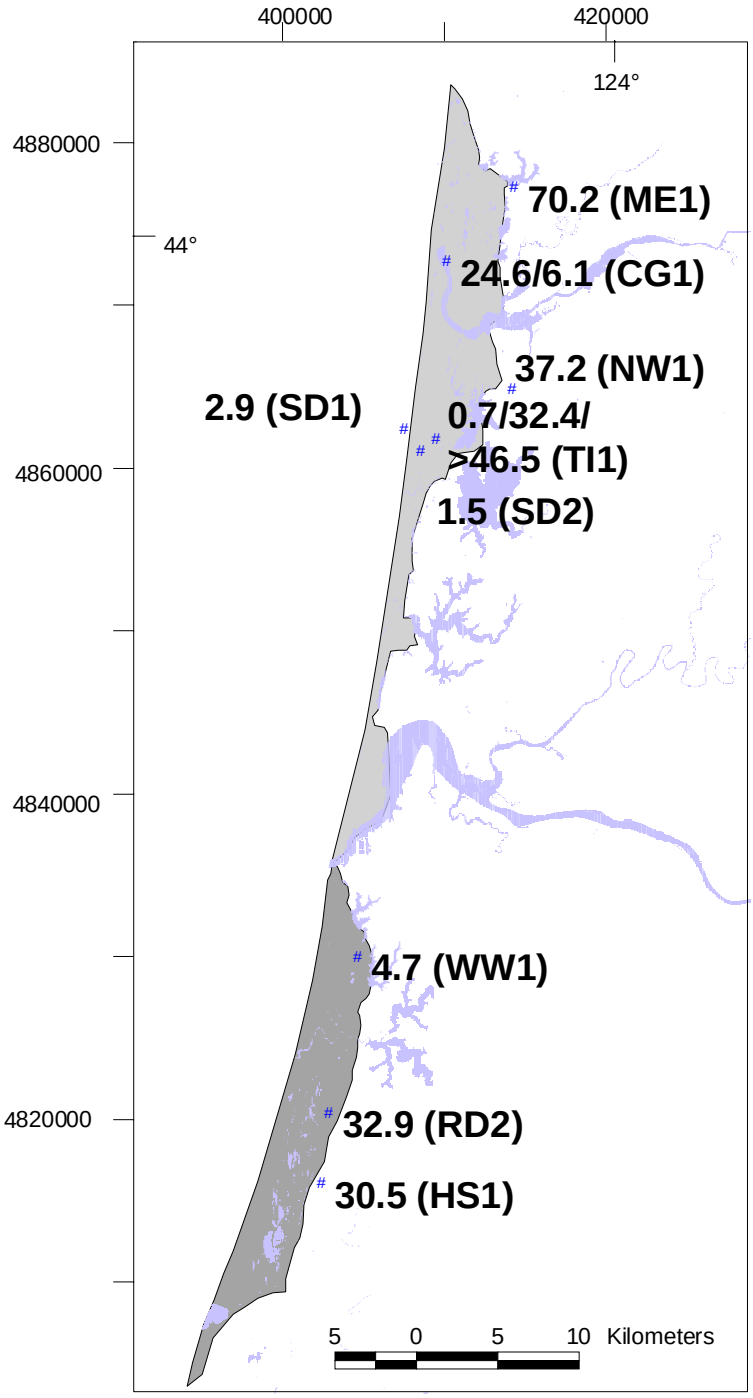

Figure 39: Map of TL and ^{14}C dates. Core names are in parentheses. Site CG1 and two dates taken below and above a paleosol, and site TI1 had three dates taken at different possitions in the island profile. Radiocarbon dates are 6.1, 0.7, and >46.5 at sites CG1, TI1-3, and TI1-1, respectievly. All other dates are in TLYBP.

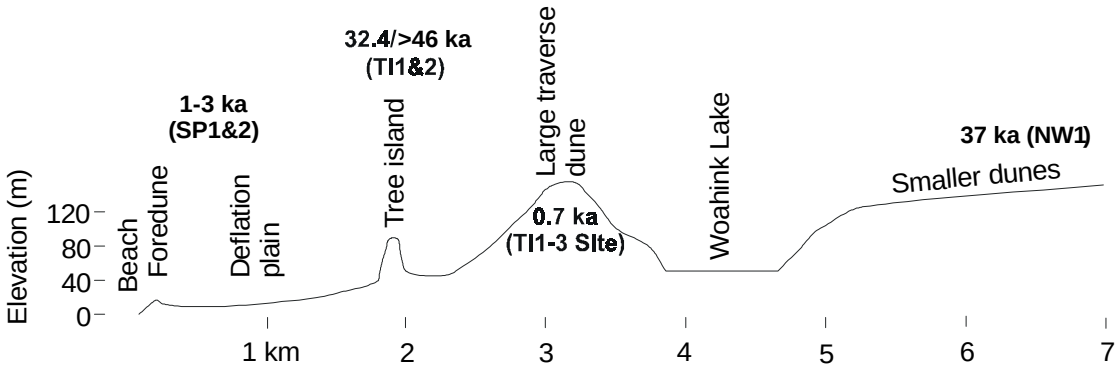

Figure 40: Representaive cross-section of a traverse crossing numerous dated sites. Note the younger ages on the western side, a tree island in the middle with late Pleistocene to late Holocene dates, and a date of 37,000 TLYBP near the eastern extent of the dune sheet. TI1-1 and TI1-2 are from the same surface, at the northern base of the tree island. See Table 17 for complete results, including standard errors and dating technique.

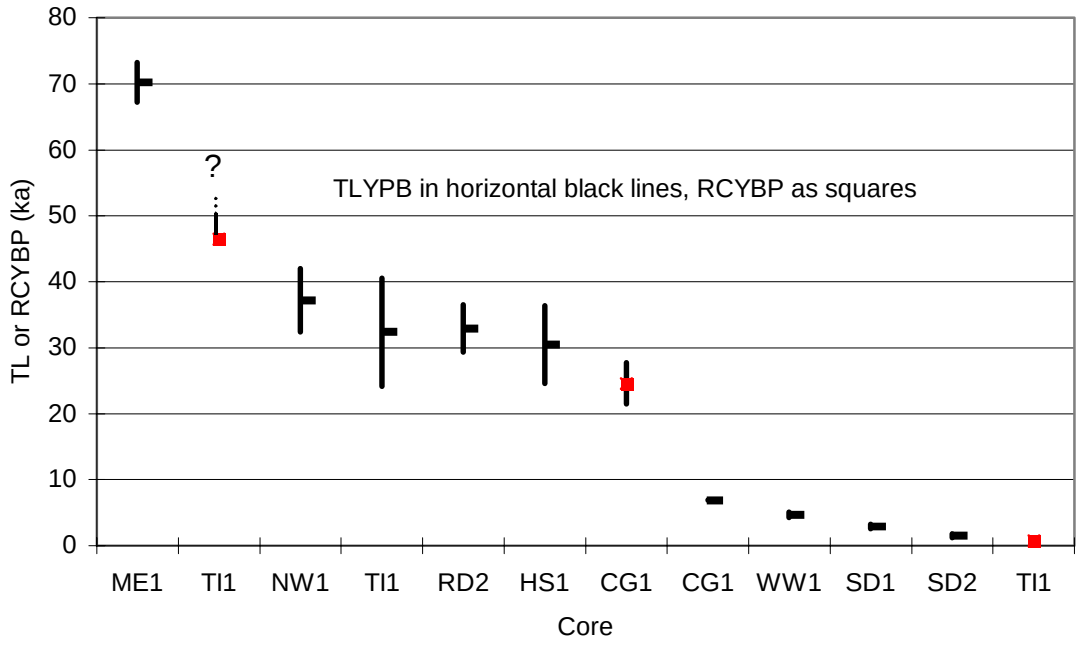

Figure 41: Chart displaying the error range for all dated cores relative to each other. Three periods of advance are apparent.

Discussion

Interpretation of data

The data gathered for this project are used for investigating the source, age(s), and emplacement mechanisms of the ODNRA dune sheets. The information regarding the inferred sand source of the dunes is provided by grain size and heavy mineral analysis. Grain-size trends also help with the interpretation of possible emplacement mechanisms. Surficial morphology is analyzed based on orientations of dune form. Subsurface stratigraphy is interpreted from vibracore and solid-stem auger sampling, and water well log interpretations. Sedimentary structures determined from vibracoring provided the necessary information to determine the origin of sand deposits immediately beneath the deflation plain. Solid-stem augering of the deflation plain extended the stratigraphic information of late-Holocene development of the underlying deflation plain deposits. Soil profiling and interpretation of well logs for presence of paleosols provide relative age estimates for dune/advances and periods of vegetative stabilization. Clay mineralogy provided insight into pedogenic processes on stabilized sands, as well as sources for possible loess in the soil profile. Dating techniques provide ages of dune emplacement and periods of stabilization. These data sets are integrated with published sea level curves and shelf bathymetric data to propose a sea-level low stand condition for eolian supply of coastal sand deposits.

Inferred sand source

The ultimate source of the dune sand is the High Cascades and, to a lesser extent, the Klamath provenance as drained by the Umpqua River and the Coos River, respectively (Figure 42). These sources are identified on the basis of high-hypersthene

abundances and moderate abundances of metamorphic amphiboles (Scheidegger et al., 1971). Minor sand constituents are certainly added by small rivers draining the Coast Range, such as the Tahkenitch River. However, the addition of characteristic minerals (augite) by these rivers was not sufficient to discriminate this source based on the heavy mineral analyses. The potential mechanisms by which the sand arrived to form the coastal dunes are discussed below.

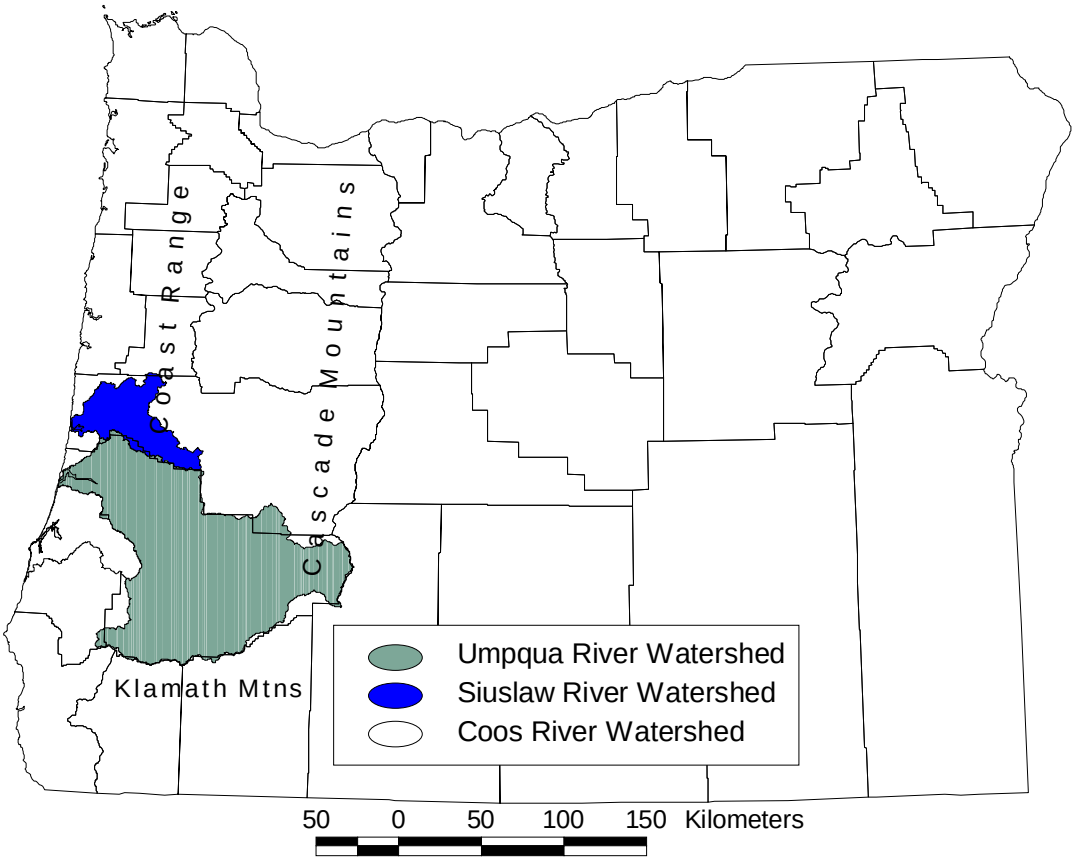

Figure 42: Drainage basins for the Siuslaw, Umpqua, and Coos Rivers, the two largest rivers in or near the Florence or Coos Bay dune sheets.

Shelf mineralogy by Scheidegger et al. (1971) is plotted on a map with bathymetric data and possible emplacement azimuth trends based on corresponding

mineralogical attributes. (Figure 43). Note in this figure the evidence pointing to differing emplacement azimuth trends, even though all the data points to the onshore movement of sand. However, it is important to note that the Coos Bay dune sheet is under-represented in the heavy mineral analyses and that the grain size trends can be interpreted in two separate ways. Nevertheless, all evidence points to onshore movement of sand. It is also important to realize that the mineralogy defined by Scheidegger et al.(1971) reflects Holocene placement of sand offshore, not mineralogy trends of the late Pleistocene. Heavy mineral analysis of deeper cores offshore would be needed to recognize the trends in the late Pleistocene shelf deposits.

Emplacement mechanisms and controls

The way in which the sand came onshore is tied closely with its associated timing. The earliest dune emplacement dated in this study is about 70,000 TLYBP. If this age represents a major period of sand transport eastward, then the sediment could have blown off the continental shelf following the last major interglacial at 83 ka. At 70,000 TLYBP, global sea levels were approximately 50 meters below the current level (Figure 10). This would equate to a shelf width of 5-9 kilometers greater than today.

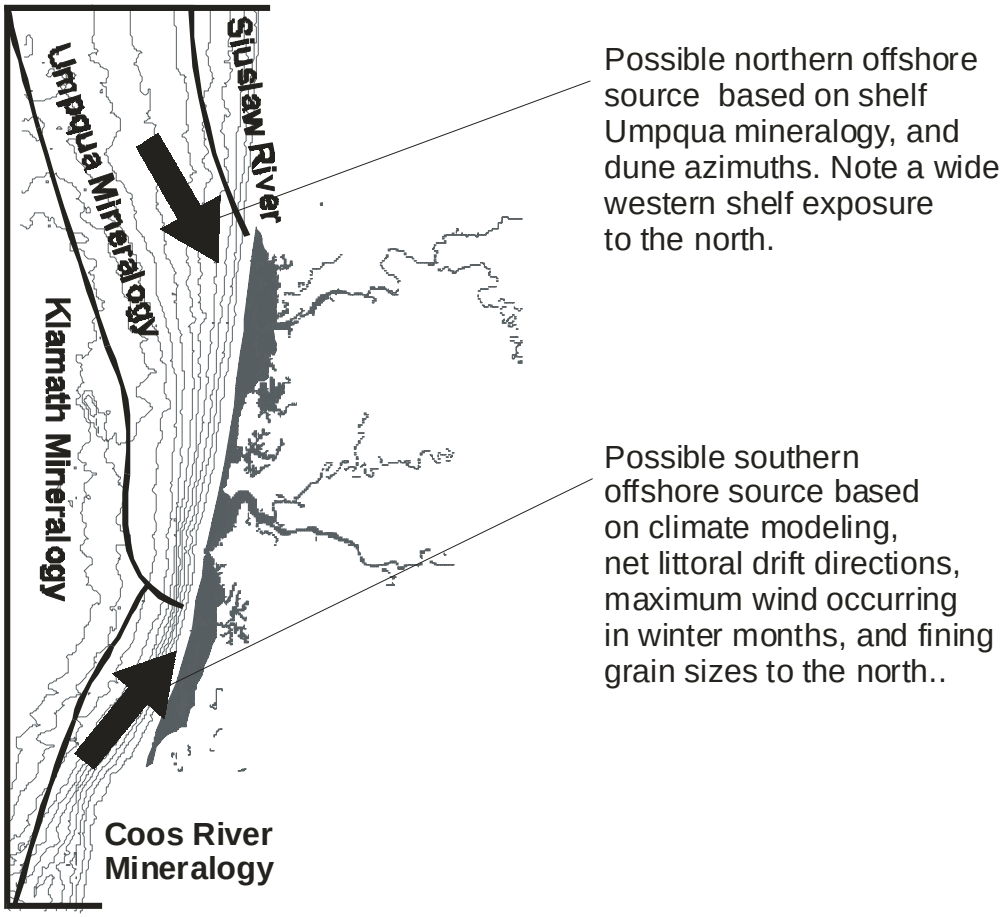

Figure 43: Composite diagram of shelf bathymetry to a depth of 120 m, with 10 meter contour intervals, shelf mineralogical data modified from Scheidegger et al. (1971), and possible transport directions based on multiple data sets.

Dune migration rates

Hunter et al. (1983) found that the modern oblique dunes just south of the Umpqua River migrated at an average rate of 3.8 m per year. At this rate, the eastward progression of Pleistocene dunes (70 ka) over a 5-9 km shelf distance would take approximately 1,300 to 2,400 years. However, this rate does not reflect the long-term rate of dune sheet advance, i.e., under late Holocene conditions at the foot of the Coast Range. At a rate of 3.8 m/yr, the eastern edge of the ODNRA dunes would be mid to late Holocene in age. However, nearly all of the eastern edge dates are greater than 30

ka, i.e., late Pleistocene in age. Whereas some active dunes are moving at the high rate, the gross dune sheet advance must be much slower. For example, under late Holocene conditions, the overriding dunes progress along the length of a stabilized dune mass until they reach the eastern edge, where they encounter steeper slopes and more mature vegetation (Cooper, 1958). Sand transport is much less favorable when encountering uphill slopes and stabilizing vegetation (see Background). The net result could lead to active dunes with progression rates of ~3.8 m/yr, but overall dune sheet advance at rates on an order of magnitude lower. For example, Figure 44 displays periods of dune advance, with each active dune advancing at a rate of 3.8 m/yr. The second dune pulse needs to cover the same length as the first dune, plus that of its own advance into virgin vegetation. In a hypothetical situation, the first dune covered 300 m with its first advance, and then 150 years passed until conditions allowed for a second dune advance. The second dune advance will now cover the original 300 m, plus an arbitrary 75 m advance past the eastern limits of the first dune advance. Following this scenario, the gross rate of progression is 1.1 m/yr. If longer episodic stabilization periods are used, e.g., 500 years or more, then the net advance is reduced to about a decimeter per year, which is closer to the estimated long-term migration rate of the late Holocene dune advance on the order of 1.0-0.1 m/yr.

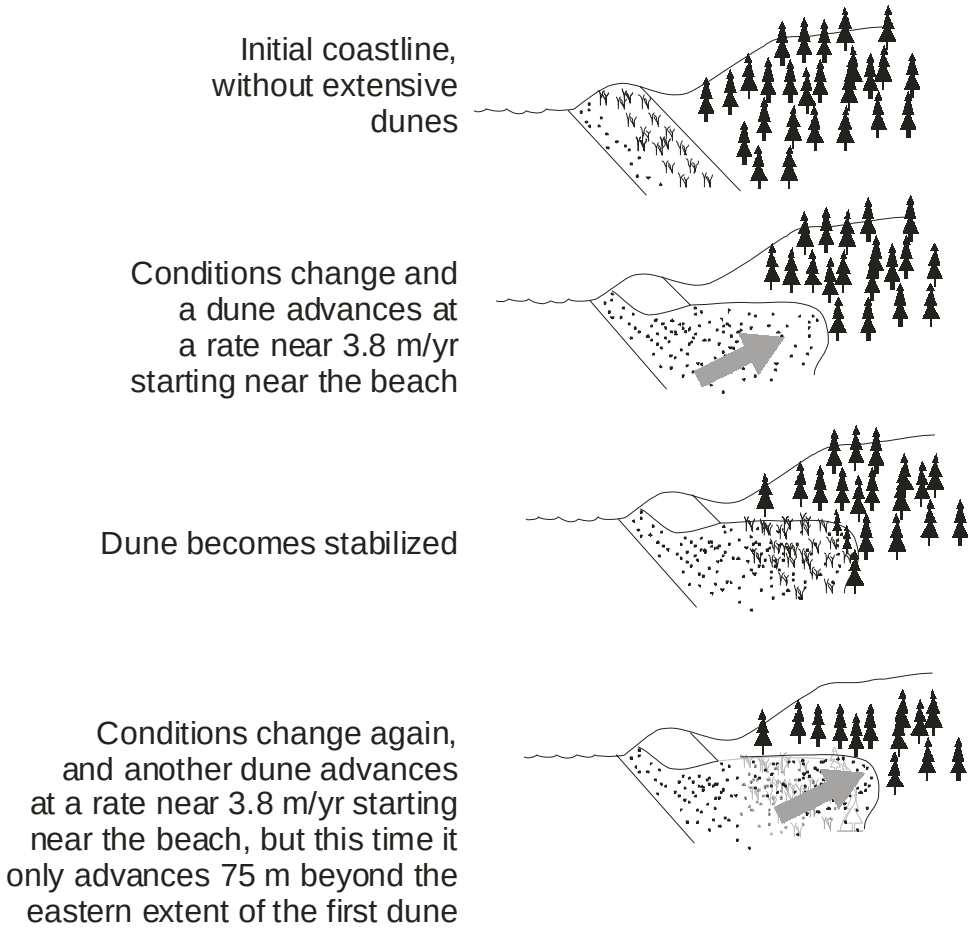

Figure 44: Schematic of a series of dune advances over stablized surfaces. Note the that the gross eastern advance rate of the dunes would be much less than 3.8 m/yr.

The conditions of the late Pleistocene glacial periods were likely much different than those of the Holocene interglacial periods (Worona and Whitlock, 1995; Ortiz et al., 1997). For example, lower sea levels could support a much larger eolian sand supply due to 1) wide continental shelf exposure, 2) lower base level for eroding rivers to supply sediment to the coast, 3) drier climate, and 4) differing wind conditions (see Background). Under those conditions the dunes should have been able to advance rapidly across the 10-15 km of shelf and shoreline. When the climatic conditions changed, due to rising sea level and increased precipitation (Worona and Whitlock,

1995), the intervals of rapid, gross dune sheet advance should have ceased. Using Hunter's rates of dune advance on the order of meters per year, the eastern edge of the ODNRA dunes might be expected to have dates a few thousand years younger than the last low stand at 17 ka, when sea level was 120 m below modern sea level (Figure 10). Furthermore, Worona and Whitlock (1995) found that the climate was 50 percent drier and a mean annual temperature of 7°C at 17-25 ka (see Background). This dryness would have aided in the mobility of sand. In addition to this, modeled Ekman transport and associated winter downwelling at the LGM was three times stronger then that it is now, indicating stronger winter winds, coming onshore from the southwest (Ortiz et al., 1997). Furthermore, summer Ekman transport for the LGM indicated nearly neutral downwelling/upwelling rates, signifying onshore summer wind directions nearly perpendicular to the shoreline (Ortiz et al., 1997) (see Background). Stronger winter winds combined with a drier climate and onshore summer winds should have increased the annual sand transport rate. However, the eastern-edge dates are actually closer to 35 ka. This contradiction is addressed in a later section of the Discussion.

Discrepancy between grain size trends and lee-slope azimuths

First-order trend surfacing of average sand grain size indicates that sand becomes finer to the north in the Coos Bay dune sheet (Figure 23). Following the logic of sand becoming finer the further it is transported, this analysis suggests the source of eolian sand is offshore and to the south. By comparison, the Florence dune sheet shows a statistically insignificant slight fining to the south. The trend surfacing of the grain sizes does not agree with the azimuth analysis of the dunes in either of the dune sheets. The azimuth analyses point to a transport direction toward 136° (true north) for the

combined dune sheets, whereas the trend surface analysis points to a more northerly or directly onshore direction. A possible resolution to this discrepancy is in that the surface dunes reflect waning transport conditions from northwest summer winds. This possible scenario would lead to the conclusion that the geospatial GIS analysis reflects the bi-directional annual wind regimes, while the northward trend of finer grain sizes is the result of southerly winds. Perhaps the northern fining trend in the Coos Bay dune sheet resulted from pre-existing conditions of more northward transport by previously dominant southwest winter winds. The eastern, stabilized dunes are less affected by seasonal wind patterns, due to their vegetative cover. Their transport directions are likely dominated by the localized topography of the Coast Range foothills during their time of deposition. In contrast to the Coos Bay dune sheet, the Florence dune sheet presents less of a conflict between the grain size trend analysis and lee-slope azimuths. It is not fully understood how these two similar dune sheets can show the different trends in mean grain size distribution.

Timing of sand emplacement

Relative dating

The soils and paleosols in the dune sheets are the primary markers used for relative dating. Paleosols are indicated by decreasing grain size in shallow cores, and by clay layers in well logs (Figure 45). The thickness of the soil/paleosol layer is an indicator of the duration of stability, since greater clay accumulation (both thickness and percentage) indicate longer time intervals for pedogenic processes to break down the parent material (Harden, 1982, Brikeland, 1984).

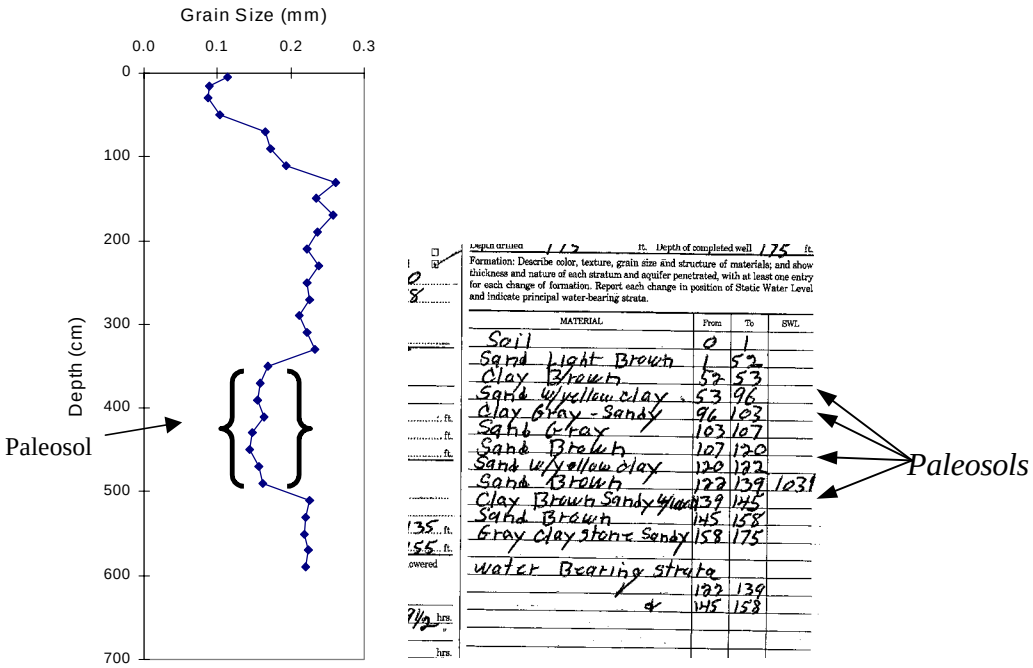

Figure 45: Two independent indicators of the presence of paleosols. On the left, finer overall grain sizes down the core indicate paleosols (from Figure 22). On the right, thin clay layers within sand indicated in well logs signify paleosols, along with color and thickness. This well log is from the Oregon Dunes Overlook water supply well.

The primary interpretation from well log paleosols is that there were multiple periods of stability throughout the dune sheets. Whereas, the number of paleosols in the boreholes is not equal, the periods of stabilization are not interpreted to be widespread over the entire dune sheet(s). Twelve of the surveyed wells had no apparent paleosols, five had one paleosol, two had two paleosols, and two had four paleosols. The durations of various periods of stability are also shown to differ between boreholes, based on the variable thickness of clay rich layers. It is possible that some of the thicker silt- and clay-rich soils might reflect the addition of chlorite-rich loess, a possible precursor to digenetic vermiculite (Douglas, 1977; Grim, 1962; Calle and Susquet, 1988; Moore and Reynolds, 1997). Chlorite is present on the continental shelf and slope (Karlin, 1978,

1980). Additional fine-scale stratigraphic analysis of the thicker paleosols is needed to discriminate between an alteration-source (weathering in-situ) versus an eolian-source (eolian chlorite-rich silts) of the clay precursor materials.

Significance of gibbsite nodules

Nodules of gibbsite, $Al(OH)_3$, were found at Mercer Lake (ME1), the oldest (TL) dated site in the study area (Table 17 and Figure 36). The nodules were also found, although in relatively lower abundance and purity, at the Houser Slough site (HS1). Microprobe analysis and X-ray diffraction of the North Woahink soil site (NW1) did not show the high Al characteristic of gibbsite (Table 16, Figure 37, Figure 38, Appendix E, and Appendix F). The presence of gibbsite in ME1 and HS1 could be explained by at least three models: 1) dissolution and precipitation of hydrous Al by acidic soils, 2) dissolution and precipitation from tephra deposits, or 3) gibbsite being the end-product of weathering in the sequence vermiculite $\Rightarrow$ kaolinite $\Rightarrow$ gibbsite.

It is possible that the gibbsite represents weathering of tephra deposits. The gibbsite balls of MS1 could have been eolian pumice fragments blown into cross-beds and fully weathered to gibbsite. Taylor and Lasaga (1997) found weathering of volcanic glass and plagioclase could form gibbsite by precipitation and re-dissolution in inceptisol soils. If the Mercer Lake site was younger, this could explain the rapid gibbsite development required for young soils. Additionally, no ash layers in the cross sections or pumice fragments under petrographic microscopes were observed in cursory investigations.

Keller (1958) proposed that the formation of gibbsite in soils is a precipitation reaction, and that it is controlled by pH and the concentration of Al and Si in solution.

The formation of gibbsite can be very rapid once the Al is separated from the Si. If groundwater transport is slow, the concentration of Si may gradually increase and recombine with Al to form kaolinite. However, the dunes are highly permeable, therefore the Si is unlikely to accumulate to form kaolinite. The controlling factors, which determine whether or not gibbsite will form directly from the primary aluminum silicates or through a kaolinite intermediary, are rainfall, temperature, parent rocks, topography, groundwater table, time, and groundwater chemistry (Dixon and Weed, 1989). Environmental factors that contribute to in-situ gibbsite precipitation in soils (including C horizons) are high rainfall, tropical or subtropical temperatures, mafic or intermediate rocks, and upland topography. These contributing factors all support good drainage (Abbott, 1958; Young and Stephen, 1965; Sherman et al., 1967). The ODNRA dunes are characterized by high rainfall, moderately high levels of unstable minerals, (Twenhofel, 1946; Scheidegger et al., 1971), and high permeability.

The pH of the soil also plays an important role in the formation of gibbsite. The formation of gibbsite is commonly associated with a low pH (Dixon and Weed, 1989). Capillary waters under pH 4 can readily carry 100 μM Al in solution, but most of this will be precipitated at pH of 5, leaving only about 4 μM Al in solution (Paterson et al., 1991). As shown by many soil pH profiles (Appendix A), the pH in dunal soils was commonly between 4.5 and 5.0 in the upper portions of the soils. The pH of core ME1 containing the most abundant gibbsite in the Cox horizon varied between 5.0 and 5.3. Although the pH in the upper portion of the soil profile might have changed over time, the current pH should not mobilize Al. One proposed scenario is when the pH of this Al enriched solution became more basic lower in the section, as is typical in the dunes, the

Al precipitated out of solution, forming gibbsite in the more porous material of the crossbeds (Figure 36).

Another possible explanation is that gibbsite is the end product of a weathering sequence of clay minerals precipitated in the sequence: vermiculite ⇒ kaolinite ⇒ gibbsite. The promise that this model has is that gibbsite is the end product of a series of steps, all taking some time. The well-developed and pure nodules were at the Mercer Lake (ME1) site with a TL age around 70.2 ka (Table 17). The poorly developed nodules at the Hauser Slough (HS1) site are in sand about half the age of the Mercer Lake site. The drawback to this model is that similar nodules were rarely observed at the other core sites (which had a similar age of the Houser Slough site). The lack of uniformity in the dune sheets creates a conflict regarding the proposed process. Furthermore, the kaolinite identified in the XRD scans is neither well-ordered nor abundant. It is possible that the vermiculite is weathering directly to gibbsite, bypassing the kaolinite intermediate step (Abbott, 1958; Keller, 1958; Young and Stephen, 1965; Sherman et al., 1967).

Yet another possibility is that the gibbsite nodules were developed during previous conditions of climate or vegetation. This possibility would require that climate and/or vegetation (and associated pH levels) had changed enough between 40 and 70.2 ka to no longer support the *formation* of gibbsite in the soil profile, but had not changed enough to promote the *destruction* of the gibbsite nodules already formed. If this scenario is correct, then the presence of gibbsite nodules in some dune sands of the Oregon coast could prove to be an indicator of paleoclimate and/or paleovegetation, and by extension, relative age of the sand dune.

Vermiculite dominance of clay minerals in soils

Vermiculite dominates the clay mineralogy of the dunal soils (see Results). Literature reports on vermiculite originating primarily from the alteration of micaceous minerals, chiefly biotite, phlogopite, and chlorite (Douglas, 1977; Grim, 1962; Calle and Susquet, 1988; Moore and Reynolds, 1997). There is little to no micaceous material present in the dune sands, whereas the presence of chlorite offshore (Figure 11) to the southwest is a possible source of the abundant vermiculite. Ross and Kodama (1974) suggest that there are two ways to achieve the chlorite to vermiculite transformation, one of which is applicable to dunal soils (the other being part of metamorphism). The applicable scenario involves acidic weathering giving rise to the transition. The pH of modern dunal soil profiles is sometimes quite low in the A-horizon, sometimes in the 4.0-4.5 range. However, sand grains from soil samples indicate that some clay is likely weathering in-situ, rather than from loess (Figure 33).

Further investigations are required to fully explain the dominance of vermiculite of the soil clay minerals. However, the weathering products (gibbsite and vermiculite) observed in the dune soils are likely to reflect extreme alteration by acidic meteoric waters leaching through very porous sand.

Application of soil indices

The use of the rubification and Buntley-Westin quantitative soil indices provided inconsistent results. As stated in Table 13, the correlation coefficient between the two indices is 0.64, with graphs in Appendix G displaying the considerable scatter. Furthermore, neither index shows a strong correlation with decreased grain size, which can be a direct mechanical measure of soil development.

A possible cause of this problem's occurrence stems from the concept of a chronosequence, where the only variable in comparing soils is time, with all other soil forming factors assumed constant between sites. As stated in the Background section, a soil chronosequence is required for the application of the soil indices to provide reliable results. Many soils are on slopes of differing angles, which would lead to differing groundwater conditions and corresponding weathering rates based on the amount of water passing through the soil. Slope failures could have also led to unpredictable soil attributes. At the Mercer Lake site (ME1), which had the oldest TL date (70.2 TLYBP), the soil was not the most developed, based on any soil index or physical indication. However, the slope directly under the core site leads to Mercer Lake, which could have possibly undermined the slope and caused a slope failure leading to deceptive soil characteristics. Finally, the two measures did not agree in the relative development on a same-sample basis regardless of age. For example, dated core RD1 (32.9 TLYBP) yielded a value of 0.08 in the normalized Buntley-Westin index, while a value of 0.56 was obtained in the rubification index (Appendix H). Additionally, cores RD1 (32.9 TLYBP) and ME1 (70.2 TLYBP) had identical scores (0.56) in the Rubification index. In the future, care must be taken to identify these potential chronosequence issues and choose sites accordingly.

Although the correlations are weakly positive, and in conjunction with field observations, the results were not favorable enough to continue with the development of a relative dating scheme based solely on soil development. Periodically mobilized dunes, with differing slope and groundwater characteristics over a large area, such as in the ODNRA, are not the best candidates for high-resolution relative dating via soil

indices. Additionally, the use of soil properties for relative dating on Pleistocene dunal soils of the east coast of the USA has not been successful (Phillips et al., 1996).

When comparing soil properties between dated cores exclusively, the ideal method of relative dating is use of a hand-held pocket penetrometer (Figure 34). Unfortunately, the majority of the dunal soils sampled in the initial field effort did not have this test performed. Future work in dunal soils should utilize and formulate a relative dating scheme involving the pocket penetrometer in addition to the field methods established in those areas. It should also be noted that each region in which this method is utilized should have a database of dates and corresponding penetrometer readings in order to formulate a local relation between estimated strength and age.

Even though the use of soil properties in interpreting dunal emplacement times was useful in determining Pleistocene versus Holocene dune forms, a TL or ^{14}C dating technique was required to discriminate late-Pleistocene ages of dunal emplacement.

Radiocarbon and thermoluminesence dating

The timing of the dunal emplacements is complex, as revealed by three age-date distributions, i.e., 1) 70 ka, 2) ~30-38 ka, and 3) 1-5 ka (Table 17, Figure 39, and Figure 41). There appears to be an early advance at about 70 ka, although additional dates are needed to confirm this single sample. However, the degrees of weathering, consolidation, and gibbsite precipitation all attest to a relatively long period of post-emplacement weathering/alteration for this site. Some late-Pleistocene dates group around 33 ka. These dates are clearly from a pre-Holocene period of sand supply. Glacial and interglacial changes in mean sea level have occurred well into the Pleistocene. Dune advances that could be greater than 70 ka in age might be recorded in

basal dune sections not dated in this study. Nevertheless, it is interesting that the oldest eastern-edge date to be recorded (70 ka) is relatively young compared to some coastal sequences such as in Australia (100 ka to ~1 ma) (Thom et al., 1994; Lees et al., 1990; Pye and Rhodes, 1983). Specifically, the question arises as to whether dunes advanced onshore during glacial intervals prior to 80 ka. The dating of basal dune deposits in the ODNRA might address this question.

Holocene dune ages

Nearshore stratigraphic relations are interpreted from borings of the deflation plain and from late-Holocene dates in the deflation plain. The lack of well-developed paleosols, lack of gibbsite, and the Holocene TL dates all imply that the underlying deposits are late Holocene. Dune stratigraphy in the deflation plain as revealed by vibracoring indicated that in addition to Holocene progradation, the deflation occurring on the deflation plain is scouring out dune sand. Additionally, it is believed that the wave cut terrace was encountered at drilling site UD2 (gray, weathered claystone rather than sandy, brown or red paleosol deposits) at a depth of ~11 m, just south of the Umpqua River. This signifies thinner, Holocene advances, since the wave cut terrace is near current sea level and is now covered by beach and eolian sand (Figure 28 and Appendix C). Additionally, drilling site GP2 contained shell fragments and coarser sand grains, indicating a vertical sequence of dune sand over beach sand in the immediate nearshore environment. These two sites, closest to the modern shoreface, indicated a minor Holocene event that ended about 3 ka (Figure 29, Figure 39, Figure 41, and Table 17). In addition, the deflation plain sites show little to no soil/paleosol development with at least two late-Holocene dates near 1-3 ka. Therefore, some high stand sand supply

certainly occurred in late-Holocene times and lead to shoreline progradation. To assist in interpretation of dune timing and source, Figure 6 shows the shelf exposures corresponding to past and present sea level positions. The bathymetry reveals a large increase in area susceptible to eolian transport starting at depths between –80 and –100 meters. Therefore, when sea levels fell to these depths, sediment available to eolian transport increased.

General dune emplacement, timing, and source

As stated earlier, the timing of the dunal emplacements is complex, as revealed by three general age date distributions i.e. 1) 70 ka, 2) ~30-38 ka, and 3) 1-5 ka (Table 17, Figure 39 and Figure 41). The oldest (70 ka) date is the eastern- and northern-most site to be dated in this study. The younger dates, from 38 to 30 ka, are all close to the eastern boundaries of the dunes in the local area, about 5-7 km inland. The expected trend is the dates becoming younger to the west. Two significant departures from this trend are sites TI1 (32.4 ± 8.2 ka) and CG1 (24.6 ± 3.1 ka), which are within 1 km of the modern shoreline (Table 17). TI1 was taken under a paleosol at the base of a tree island under 750 meters from the modern surfzone. CG1 came from the banks of the Siuslaw River under a paleosol at sea level less than 900 meters from the modern surfzone. Additionally, this site (CG1) does not fit within the aforementioned three distributions; it is possible that this date signifies not a dune advance, but a reactivation of pre-existing dunes.

The first two date distributions (70 and 30-38 ka) represent separate dune advances of the late Pleistocene. However, it would be preferred that the earliest (70 ka) date be supported by additional dates to confine the age and extent of this earliest dated

advance. The 30-38 ka grouping is geographically widespread, and usually represents the eastern extent of dunes in the local area in which the cores were taken (Figure 39). The TI1 and CG1 sites represent western remnants of this date grouping. The paleosols of these two sites (TI1 and CG1) also both have Holocene dated sediments (~0.6-6.9 ka) overriding the exhumed paleosols, which represent a dunal advance or widespread reactivation (Figure 46). This Holocene date grouping is also represented in the deflation plain sediments, which indicates that this Holocene dune activity also lead to shoreline progradation on the order of 500-1000 meters. It is likely that the CG1 Holocene date of 6.9 ka, the oldest of the Holocene dates, denotes the initiation of the mid- to late-Holocene dune advance.

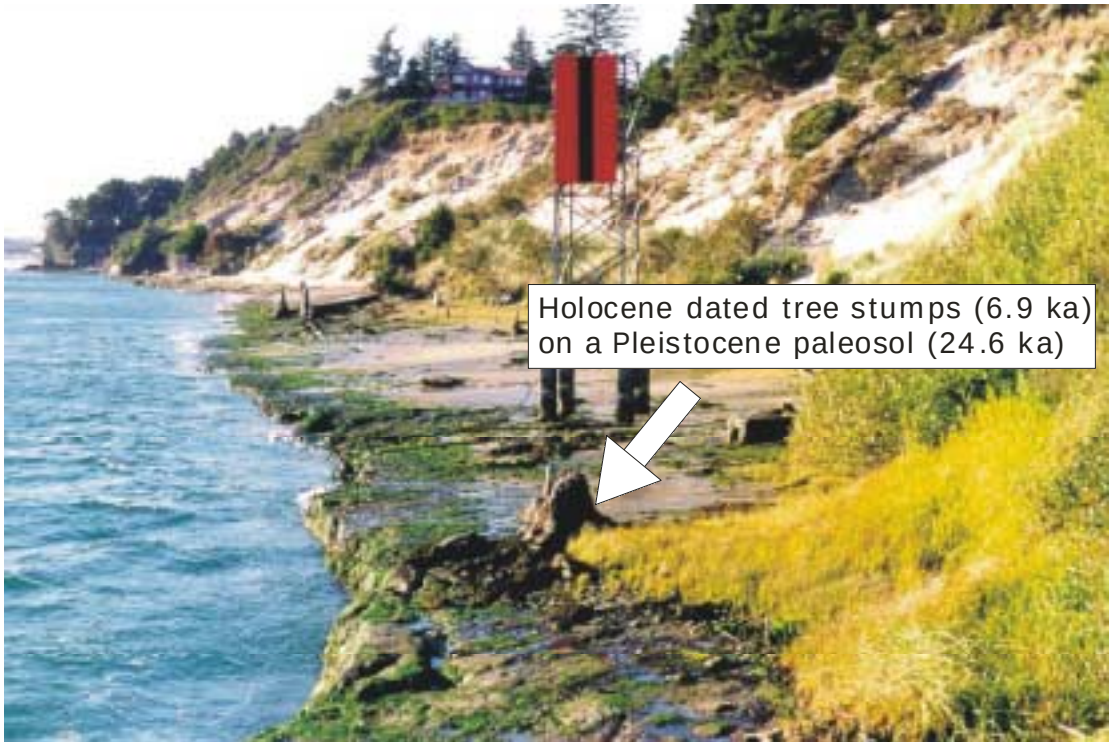

Figure 46: Site CG1, on the banks of the Siuslaw River, contains a paleosol which has Holocene dated tree stumps atop a Pleistocene soil. The Holocene date signifies when the soil was buried by a dune advance.

The preferred interpretation is that during fluctuations of sea level in the late Pleistocene (Figure 47), multiple shorefaces were created and abandoned by the rising and falling sea level (Figure 48). These abandoned shorefaces were then exposed to strong winds, which could then blow the shoreface sands inland (Figure 49). The strong winds of the Last Glacial Maximum (LGM), and presumably during the more brief interglacial periods before that, would be sufficient enough to blow the sand inland. These sands would have then traveled across the shelf, to the Coast Range foothills (Figure 43).

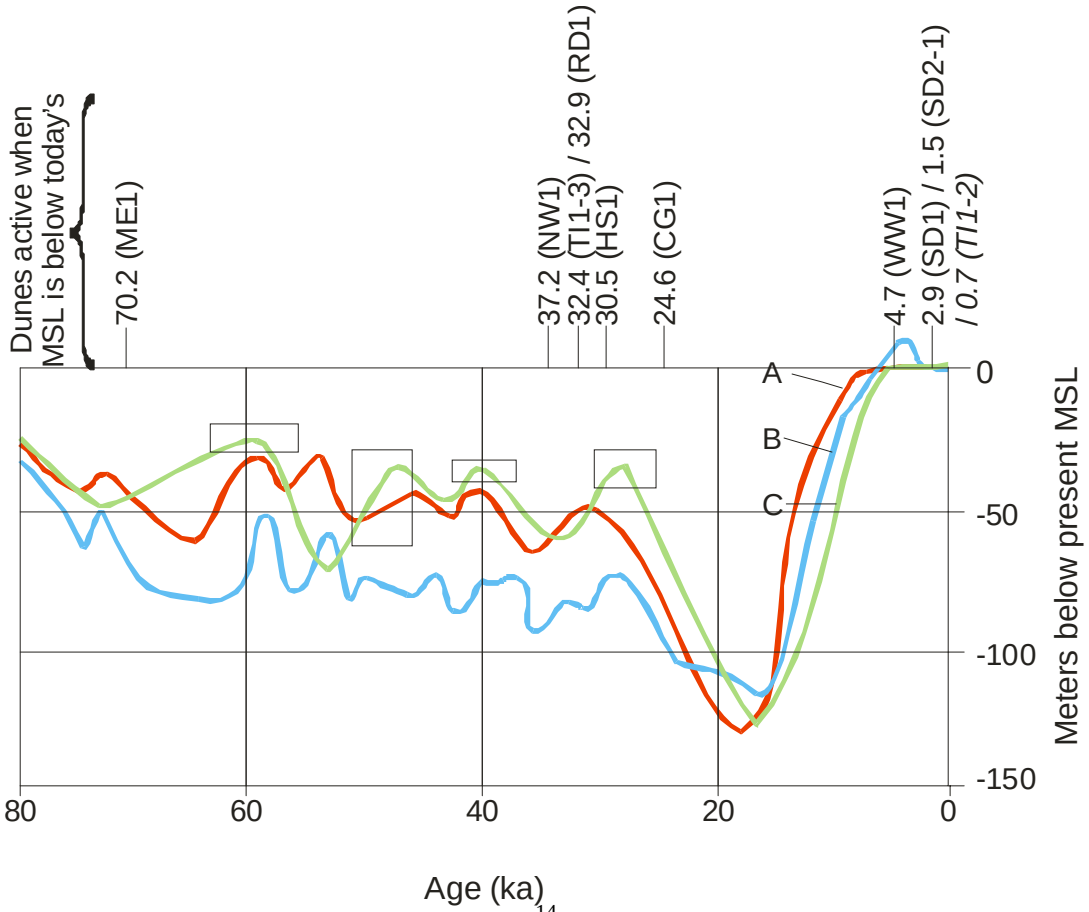

Figure 47: Sea level curve with TL and C^{14} (*italics*) dates added. For an explanation of the sea level curves, see Figure 10.

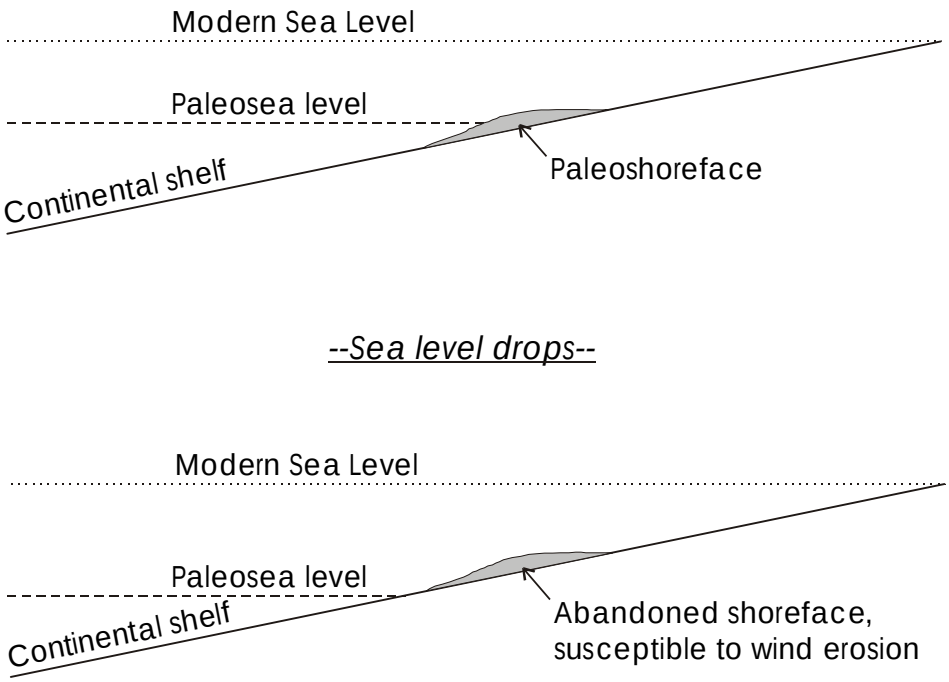

Figure 48: Creation and abandonment of shorefaces relative to rise and fall of sea level in a combination model of high stand forcing of sand up the shelf and the low stand model of sand being blown in by an active shoreface west of the modern shoreface.

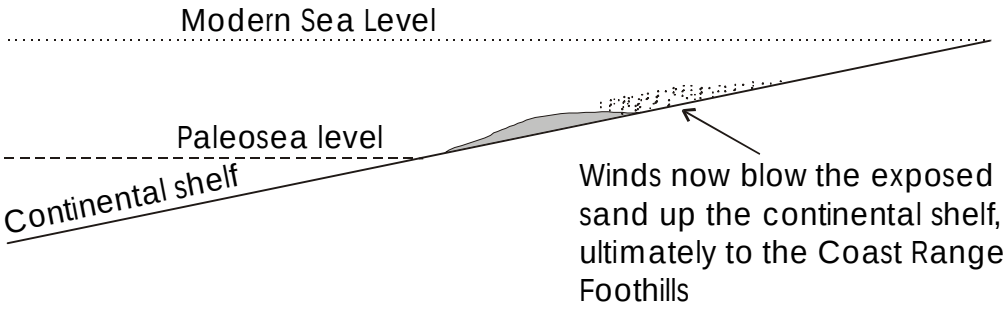

Figure 49: Abandoned shoreface sands were exposed to winds after a fall in sea level. The sand consequently blew inland to the Coast Range foothills.

Three possible emplacement directions are possible based on the data gathered for this thesis: 1) the sand was transported from the southwest; 2) the sand was transported from the north; or 3) the sand came directly onshore (Figure 43). General dune emplacement from the southwest would require large volumes of sand sourcing from the

most narrow portion of the continental shelf, i.e, south of the Umpqua River (Figure 6). The thicker dunes of the Florence dune sheet have a more gradual slope from the continental shelf to the modern shoreface and backing dunes than the Coos Bay sheet. This, coupled with the filling of the Siuslaw paleochannel, results in the Florence dune sheet being the deeper and thicker of the two. The relatively narrow strip of continental shelf just south of the Umpqua River might have resulted in the thinner and shallower dunes of the Coos Bay dune sheet. However, a northeast transport direction would require significant quantities of sand to be forced northward into the Florence dune sheet across the offshore extent of the Umpqua River, possibly being captured in the river flow. This issue raises the possibility that significant quantities were transported seaward by the Umpqua River. It should be noted that the sand carried offshore by the Umpqua River could eventually return to the shore by eolian transport. The Umpqua River could have provided a significant barrier to northern cross-shelf transport.

Another possible scenario is that the sand was transported to the southeast from the broader exposed shelf to the north of the Umpqua River. The significantly longer transport distance over the exposed continental shelf northwestward of the Florence dune sheet could account for the greater winnowing and fining of the sand there, relative to the Coos Bay dune sheet. This is contrary to the hypothesis of sand winnowing due to transport near parallel to the coastline as is required for a northeastern direction of transport. A southeastern transport direction would also support the evidence presented by the lee-slope azimuth data, which displays significant trends to the southeast or east for all ages of dunes. While no volumetric calculations were made, measurements of area, depth, and thickness of sand are generally greater in the Florence dune sheet

compared to those of the Coos Bay sheet. These facts and interpretations support the hypothesis of an offshore sand source from the northwest.

The important point is that both models involve *onshore* sand movement. To resolve the issue of southern versus northern sand source, additional investigations are required. Investigations should include heavy mineral analysis of additional dunal sites and deeper offshore borings to identify late Pleistocene basal sand deposit mineralogy of the continental shelf.

Local, regional and global perspectives

In this section, several coastal dune localities of the U.S. and overseas are compared in terms of age and extent of dune sheet advance to the ODNRA study area, as well as interpretations previously made within the dune sheets.

Within the study area, geologic interpretations based on anthropologic findings have been made in the past (Minor and Toepel, 1986). Table 3 summarizes the interpretations of Minor and Toepel (1986), while Table 18 summarizes potential new interpretations in light of this thesis. Component I could now be interpreted as an inland food preparation site due to the nature of the shoreline being further west at that time as a result of lower sea levels. Component II could be interpreted as it was before (village), but with the perspective of the shoreline being closer due to the lack of Holocene dunal progradation. Component III could be interpreted with this change: while the Holocene dunal progradation occurred, food transport became difficult and the inhabitants moved to a site that better suited their needs. The position of the shoreline further to the west challenges Minor and Toepel's (1986) estuary model. The model proposed by this thesis makes their model less likely since the dunes were largely in place at the beginning of

human occupation, with only a relatively small amount of Holocene dune progradation. However, these interpretations need further support by means of coring and dating dunes west of the landing site and lake bottom sediments, which were not addressed by this study.

Table 18: Potential new interpretations of settlement history of the Tahkenitch Lake midden site.

Component	Inhabitation dates and possible new interpretations
Component I	8000-5200 RCYBP
	Inland food preparation site
Component II	5200-3000 RCYBP
	Now closer to shore; before full Holocene progradation
Component III	3000-historic
	Holocene dunal progradation made food transport difficult

The Morro dune field in southern California possesses late Pleistocene dune fields comprising over 50 percent of the dune field (Orme, 1990). One ^{14}C date of the youngest paleodune is ~27 ka, with most paleodunes resting upon a marine terrace formed about 130 ka. This study concluded that the Holocene dunes rest upon a framework set in motion by Pleistocene events, such as tectonic deformation creating a receptive shoreline, which in turn allowed the dune advance. Research on Pleistocene and Holocene dunes of coastal Georgia and the Carolinas suggest that dunes on the southern U.S. Atlantic seaboard formed during periods of low rainfall in bi-directional wind regimes, and were probably emplaced during the sea-level low stands of glacial maxima (Markewich et al., 1994).

Coastal dunes of the eastern Atlantic (on the island of Madeira) began to be emplaced between 200,000-300,000 ybp (Goodfriend et al., 1996). This dunal sequence

includes clay deposits up to 2 m thick and black volcanic sands. It has been found that the black volcanic sands were deposited during sea-level low stands, while the clay rich deposits were found to be deposited during the lowest sea level stands. The authors suggest that fine marine sediments exposed during lowest sea-level low stands may be the dominant source of the silty and clayey units of other coastal eolian deposits of the Atlantic and Mediterranean.

Episodic dune advances have also been found in Australian dunes fields (Shulmeister, 1996; Thom et al., 1994; Lees et al., 1993; Shulmeister and Lees, 1992; Lees et al., 1990; Pye and Rhodes, 1985; Pye, 1983; Thompson; 1983). TL dates from some Australian dunes indicate that the dunes become stabilized as loose groupings, as shown by dates which cluster around specific periods (Thom et al., 1994; Lees et al., 1993; Shulmeister and Lees, 1992; Lees et al., 1990). While most of the dates are Holocene, many sites have TL ages dating as far back as 171 ka, with groupings also at 81 ka and 25-30 ka (Lees et al., 1990). At least one researcher reported on dune fields going as far back 250, 400, 760, and 1,000 ka, (Ward and Little, 1975; Ward, 1977). However, these dates were brought into question (Pye, 1983). Eolian sands at 30 m below current sea level are also reported from Australian coasts. The offshore dune deposits have ^{14}C dates indicating that these dunes were active 9.5-6 ka (Pye, 1983). These dates and stratigraphic positions clearly support the idea of a sea-level low-stand model. This is due to the fact that the current position of sea level is at its highest point since the Pleistocene, which would require that sands be blown inland off of an exposed continental shelf, prior to Holocene transgression.

Directions for further research

The research for this thesis covered many aspects of the origin of the Coos Bay and Florence dune sheets. Due to the reconnaissance nature of this study, not all aspects could be fully explored. The processes of soil development and the interpretation of these processes, initially thought to be straightforward, proved to be an inconsistent measure of relative profile age. In addition, clay mineralogy of dunal soils and other alteration products in dune sand were unexpected and are not yet understood in terms of alteration sequences and rate(s) of formation. Perhaps the most promising research direction resulting from this thesis is the application of the dune origin models upon other dune sheet localities in Oregon and California by additional TL and ^{14}C dating (Cooper, 1958; Cooper, 1967).

Future work in the ODNRA should focus on obtaining/developing 1) accurate relative soil dating, 2) further heavy mineral analysis, and 3) additional TL dates of basal dune sheet deposits.

Work should specifically focus on the factors involved in the soil-forming processes that result in poor relative dating results of Pleistocene soils. However, the traditional reductionist view (variability can be explained with more and better measurements) might not be reconciled with the nonlinear dynamics view (variability may be an irresolvable outcome of complex system dynamics) (Phillips et al., 1996). Ultimately, more dating by TL and ^{14}C techniques are required.

Additional heavy mineral analyses of the Coos Bay and southern Florence dune sheet are required to fully constrain and resolve sand supply and source between the two dune sheets. Vertical heavy mineral sequencing would be particularly helpful in

determining possible changing sources of dune sands; however, this should be completed in conjunction with additional heavy mineral analyses of offshore borings. This offshore work would be required due to the fact that the offshore surficial mineralogical analyses of Scheidegger et al., (1971) are likely biased by mineral dispersal from the Holocene transgression.

Obtaining additional dates within the dune sheets is needed to further constrain the periods of emplacement. Drilling to the bedrock in order to obtain basal TL dates in at least three positions within the dune sheets (north, central, and southern) should be a high priority for this direction of research. Without these data, a maximum age of dune sheet emplacement cannot be predicted. These basal dates could also tie the ODNRA into a global model of coastal dune advance, i.e., comparison to widely dated dunes of Australia and Europe.

The proposed low-stand supply model of the ONDRA dune fields signifies a change in interpretation of the dune sheet origins. The commonly accepted notion of recent late-Holocene dune advance from the current shoreface is not supported by the late-Pleistocene TL ages. Theses results should impact neotectonic studies (marine terrace dating), archeology (searches for pre-Holocene occupation sites), and nearshore sedimentology (source of modern beach sand) in the ONDRA study area.

Conclusions

The ultimate source of sand for the Florence and Coos Bay dune sheets, as evidenced by sand heavy mineral analysis and trends in grain size, is the High Cascades and, to a lesser extent, the Klamath Mountains, both drained by the Umpqua River. Differences between ratios of hypersthene (a Cascade tracer mineral) to total pyroxenes of the dune sands from the Umpqua River have a standard deviation of 3 percent, indicating a well-matched source. Trend surfacing of the dune sheets revealed sand generally became finer to the north, indicating an emplacement vector from the south or from the north, depending on the interpretation of the fining northward pattern. The southern source emplacement direction agrees with previous research of paleowind indicators (Ortiz et al., 1997). The northern emplacement source does agree with dune migration azimuths for the two dune sheets and with the Holocene shelf mineralogy of Scheidegger et al., (1971). Northwestern summer winds are influencing the dunes to migrate in a southeastern direction. Topography of the Coast Range could be influencing the wind and thus impacting the eastern stabilized dunes in a localized manner, leading to complex transport directions.

The Coos Bay and Florence dune sheets are not features emplaced during entirely during the Holocene. Rather, they were largely emplaced during the late Pleistocene. A thermoluminesence date at 70.2 TLYBP clearly indicates the Pleistocene origins of at least the Florence dune sheet. The timing of emplacement is complex, with at least one early advance at ~70 ka (TLYBP), many dunes becoming stable at the eastern edge of the dune sheet, and some within 1000 meters of the current shoreline, between 38-30 ka (TLYBP). Finally, younger dates at the Siuslaw Coast Guard Station (6 ka) and at the

Tree Island site (0.7 ka) and the deflation plain dates all point to a late Holocene sand supply event. Although minor by comparison to the late Pleistocene dune advance, it was significant on the western side of the dune complex.

Rise and fall of sea level during these times forced shorelines to advance and retreat over the continental shelf multiple times. Once sea level dropped and these shorefaces were abandoned, the sand associated with it would be exposed to eolian action, which would transport the sand onshore. This model of sand being blown onshore during a low stand of sea level is contrary to previous assumptions of dune emplacement. Formerly, common thought was that the dunes were Holocene features emplaced during the last 6,000 years. This age corresponds with completion of the rapid rise of sea level following the last glacial maximum at approximately 18,000 ka. This rise is believed to have forced the sand to elevations previously not reached by the shoreline. Subsequently, the sand would then blow inland to terrains without any previous eolian dunes.

This low stand model presented here entails the highly variable sea level forcing sand inland, then retreating relatively rapidly. The sand that was forced inland has now been abandoned by wave action and is left on a relatively flat continental shelf. This sand is now exposed to wind, which then drives the sand inland in a northeasterly direction. This sand will be blown until it encounters a resistant feature, in which case it will accumulate until sand supply is exhausted, or the feature is buried and the dune continue. This model at least partially explains the thick, deep, and wide portion of the northern Florence dune sheet.

The dunes of the ODNRA are Pleistocene features that could be indicative of coastal dunes across western North America. The numerous coastal dunes could signify a major advance of sand that is related not only to local sand supply, but more importantly, to large-scale regional effects of sea level on the emplacement, timing, and extent of coastal dunes.

References

Abbott, A. T., 1958, Occurrence of gibbsite on the island of Kauai, Hawaiian Islands: Economic Geology and the Bulletin of the Society of Economic Geologists, v. 53, no. 7, p. 842-853.

Bagnold, R. A., 1936, The Movement of Desert Sand: Proc. Royal Society of London, v. A157, p. 594-620.

Bagnold, R. A., 1941, The Physics of Blown Sand and Desert Dunes: New York, Morrow, 265 p.

Beaulieu, J. D., and Hughs, P. W., 1975, Environmental Geology of Western Coos and Douglas Counties, Oregon: Oregon Department of Geology and Mineral Industries, Bulletin 87.

Berger, G. W., 1988, Dating Quaternary events by luminescence: Geological Society of America, v. Special Paper 227, p. 13-50.

Bloom, A. L., and Yonekura, N., 1985, Coastal terraces generated by sea-level change and tectonic uplift, *in* Woldenberg, M. J., ed., Models in Geomorphology: Boston, Allen and Unwin, p. 139-154.

Bokheim, J. G., Marshall, J. G., and Kelsey, H. M., 1996, Soil-forming processes and rates on uplifted marine terraces in southwestern Oregon, USA: Geoderma, v. 73, p. 39-63.

Bressolier, C., and Thomas, Y.-F., 1977, Studies on wind and plant interactions on French Atlantic coastal dunes: Journal of Sedimentary Petrology, v. 47, no. 1, p. 331-338.

Birkeland, P. W., 1984, Soils and Geomorphology: New York, Oxford University Press, 372 p.

Buntley, G. J., and Westin, F. C., 1965, A comparative study of developmental color in a Chestnut-Cherozem-Brunizem soil climosequence: Soil Science Society American Proceedings, v. 29, p. 579-582.

Calle, C. de la, Susquet, H., 1988, Vermiculite: in Baliey, S. W., editor, *Hydrous Phyllosilicates (exclusive of micas),* Vol. 19 in Reviews *in* Mineralogy, Mineralogical Society of America, Washington D.C., 455-496

Carlson, J., Reckendorf, F., and Ternyik, W., 1991, Stabilizing Coastal Sand Dunes in the Pacific Northwest: United States Department of Agriculture: Soil Conservation Service, Agriculture Handbook 687.

Carter, R. W. G., 1986, The morphodynamics of beach ridge development, Magilligan, Northern Ireland: Marine Geology, v. 73, p. 191-214.

Carter, R. W. G., Hesp, P. A., and Nordstrom, K. F., 1990, Erosional landforms in coastal dunes, *in* Nordstrom, K. F., and Psuty, N., eds., Coastal Dunes: Form and Process: New York, John Wiley and Sons, p. 217-250.

Carter, R. W. G., Nordstrom, K. F., and Psuty, N. P., 1990, The study of coastal dunes, *in* Nordstrom, K. F., and Psuty, N. P., eds., Coastal Dunes: Forms and Process: New York, John Wiley and Sons, p. 1-14.

Chappell, J., and Shackleton, N. J., 1986, Oxygen isotopes and sea level: Nature, v. 324, p. 137-140.

Clarke, M. L., Rendell, H. M., and Wintle, A. G., 1999, Quality assurance in luminescence dating: Geomorphology, v. 29, no. 1-2, p. 173-185.
Cooper, W., 1958, Coastal sand dunes of Oregon and Washington, Geological Society of America. Memoir 72: New York, Geological Society of America, 169 p.
Cooper, W. S., 1967, Coastal Dunes of California, The Geological Society of America Memoir: Boulder, CO, The Geological Society of America, 131 p.
Davis, J. C., 1970, Statistics and data analysis in geology: New York, John Wiley & Sons, 646 p.
Deer, W. A., Zussman, J., and Howie, R. A., 1992, An Introduction to the Rock-Forming Minerals: New York, Addison-Wesley Pub Co., 720 p.
Dixon, J. B., and Weed, S. B., 1989, Minerals in soil environments, Soil Science Society of America Book Series: Madison, WI, Soil Science Society of America, p. 1244.
Douglas, L. A., 1965, Clay mineralogy of a Sassafras soil in New Jersey: Soil Science Society of America Proceedings, v. 29, p. 163-167
Erlandson, J. M., Tveskov, M. A., and Byram, S., 1998, The development of maritime adaptation on the southern Northwest Coast: Arctic Anthropology, v. 35, p. 6-22.
Fitzgerald, J. I., 1996, The application of Harden soil profile development indices to soils of the eastern Piedmont of Mount Olympus, Pieria, Greece, Ohio University, Athens, Athens, OH, United States, 116 p.
Fryberger, S. G., and Seely, M. E., 1991, Unusual sedimentary structures in the Oregon coastal dunes: DUNES '89 meeting on the Geomorphology and ecology of desert and coastal sand dunes, v. 21, no. 2, p. 131-150.
Goodfriend, G. A., Cameron, R. A. D., Cook, L. M., Courty, M. A., Fedoroff, N., Livett, E., and Tallis, J., 1996, The Quaternary eolian sequence of Madeira: stratigraphy, chronology, and paleoenvironmental interpretation: Palaeogeography, Palaeoclimatology, Palaeoecology, v. 120, no. 3, p. 195-234.
Grim, R. E., 1962, *Applied Clay Mineralogy*: McGraw-Hill, New York, 442 pp.
Hampton, E. R., 1963, Ground Water in the Coastal Dune Area Near Florence, Oregon: United States Geological Survey, 1539-K.
Harden, J. W., 1982a, A quantitative index of soil development from field descriptions; examples from a chronosequence in central California: Geoderma, v. 28, no. 1, p. 1-28.
Harden, J. W., 1982, A study of soil development using the geochronology of Merced River deposits, California [Doctoral thesis]: University of California, Berkeley, Berkeley, CA, United States, 247 p.
Harden, J. W., 1988, Genetic interpretations of elemental and chemical differences in a soil chronosequence, California: Geoderma, v. 43, no. 2-3, p. 179-193.
Hunter, R. E., 1980, Depositional environments of some Pleistocene coastal terrace deposits, southwestern Oregon; case history of a progradational beach and dune sequence: Sedimentary Geology, v. 27, no. 4, p. 241-262.
Hunter, R. E., Richmond, B. M., and Alpha, T. R., 1983, Storm-controlled oblique dunes of the Oregon coast: Geological Society of America Bulletin, v. 94, no. 12, p. 1450-1465.

Huntley, D. J., Godfrey-Smith, D. I., and Thewalt, M. L. W., 1985, Optical dating of sediments: Nature, v. 313, no. 5998, p. 105-107.
Hurst, V. J., 1977, Visual estimation of iron in saprolite: Geological Society of America Bulletin, v. 88, no. 2, p. 174-176.
Jenny, H., 1941, Factors of soil formation: New York, McGraw-Hill.
Joffe, J. S., 1949, Pedology: New Bruniswick, N.J., Pedology Publications, 662 p.
Karlin, R., 1979, Sediment sources and clay mineral distributions off the Oregon coast; evidence for a poleward slope undercurrent, Oregon State University, Corvallis, OR, United States, 88 p.
Karlin, R., 1980, Sediment sources and clay mineral distributions off the Oregon coast: Journal of Sedimentary Petrology, v. 50, no. 2, p. 543-559.
Keller, W. D., 1958, Argillation and direct bauxitization in terms of concentrations of hydrogen and metal cations at surface of hydrolyzing aluminum silicates: Bulletin of the American Association of Petroleum Geologists, v. 42, no. 2, p. 233-245.
Langley-Turnbaugh, S. J., and Bockheim, J. G., 1997, Time-Dependent Changes in Pedogenic Processes on Marine Terraces in Coastal Oregon: Soil Science Society of America Journal, v. 61, p. 1428-1440.
Lees, B. G., Hayne, M., and Price, D., 1993, Marine transgression and dune initiation on western Cape York, northern Australia: Marine Geology, v. 114, no. 1-2, p. 81-89.
Lees, B. G., Yanchou, L., and Head, J., 1990, Reconnaissance thermoluminesence dating of northern Australian coastal dune systems: Quaternary Research, v. 34, no. 2, p. 169-185.
Lund, D. C., and Mix, A. C., 1998, Millenial-scale deep water oscillations: Reflections of the North Atlantic in the deep Pacific from 10 to 60 ka: Paleoceanography, v. 13, no. 1, p. 10-19.
Markewich, W. H., 1994, An overview of Pleistocene and Holocene inland dune in Georgia and the Carolinas; morphology, distribution, age, and paleoclimate, U. S. Geological Survey Bulletin: Reston, VA, U. S. Geological Survey, 32 p.
Miller, C. D., and Birkeland, P. W., 1974, Probable pre-Neoglacial age of the type Temple Lake Moraine, Wyoming; discussion and additional relative-age data: Arctic and Alpine Research, v. 6, no. 3, p. 301-306.
Milliman, J. D., and Emery, K. O., 1968, Sea levels during the past 35,000 years: Science, v. 162, p. 1121-1123.
Minor, R., and Toepel, K. A., 1986, The Archaeology of the Tahkenitch landing site: early prehistoric occupation on the Oregon coast: Heritage Research Associates.
Moore, D. M., and Reynolds, R. C., Jr., 1997, X-ray diffraction and the identification and analysis of clay minerals: United Kingdom, Oxford, Oxford University Press, United Kingdom, 378 p.
Nettleson, W. D., Parsons, R. B., Ness, A. O., and Gelderman, F. W., 1982, Spodosols Along the Southwest Oregon Coast: Soil Science Society of America Journal, v. 46, no. 3, p. 593-599.

Orme, A. R., 1990, The instability of Holocene coastal dunes: the case of the Morro dunes, California, *in* Nordstrom, K., Psuty, N., and Carter, B., eds., Coastal Dunes: Form and Process: New York, John Wiley and Sons, p. 315-336.

Orr, E. L., Orr, W. N., and Baldwin, E. M., 1992, Geology of Oregon: Dubuque, Iowa, Kendall/Hunt Publishing Co., 254 p.

Ortiz, J., Mix, A., Hostetler, S., and Kashgarian, M., 1997, The California Current of the last glacial maximum; reconstruction at 42 degrees N based on multiple proxies: Paleoceanography, v. 12, no. 2, p. 191-205.

Paterson, E., Goodman, B. A., and Farmer, V. C., 1991, The Chemistry of Aluminum, Iron and Manganese Oxides in Acid Soils, *in* Ulrich, B., and Sumner, M. E., eds., Soil Acidity: New York, Springer-Verlag, p. 224.

Peterson, C., Darienzo, M., Pettit, D. J., Jackson, P., and Rosenfeld, C., 1991, Littoral Cell Development in the Convergent Cascadia Margin of the Pacific Northwest, USA, *in* Osborne, R., ed., From Shoreline to Abyss, Contributions in Marine Geology in Honor of F. P. Shepard: SEPM Special Publication, SEPM, p. 17-34.

Peterson, C. D., Darienzo, M. E., Burns, S. F., and Burris, W. K., 1993, Field trip guide to Cascadia paleoseismic evidence along the northern Oregon Coast; evidence of subduction zone seismicity in the central Cascadia Margin: Oregon Geology, v. 55, no. 5, p. 99-114.

Phillips, J. D., Perry, D., Garbee, A. R., Carey, K., Stein, D., Morde, M. B., and Sheehy, J. A., 1996, Deterministic uncertainty and complex pedogenesis in some Pleistocene dune soils: Geoderma, v. 73, no. 3-4, p. 147-164.

Pirazzoli, P. A., 1993, Global sea-level changes and their measurement: Global and Planetary Change, v. 8, p. 135-148.

Prothero, D. R., and Schwab, F., 1996, Sedimentary Geology: An Introduction to Sedimentary Rocks and Stratigraphy: New York, W. H. Freeman and Company, 575 p.

Pye, K., and Rhodes, E. G., 1985, Holocene development of an episodic transgressive dune barrier, Ramsay Bay, North Queensland, Australia: Marine Geology, v. 64, no. 3-4, p. 189-202.

Pye, K., 1983, Dune formation on the humid tropical sector of the North Queensland coast, Australia: Earth Surface Processes and Landforms, v. 8, no. 4, p. 371-381.

Reckendorf, F., Leach, D., Baum, R., and Carlson, J., 1987, Stabilization of West Coast sand dunes, Coastal Zone '87 - Proceedings of the Symposium on Coastal and Ocean Management: Seattle, WA, p. 1328-1342.

Robinson, J. H., 1973, Hydrology of the dunes area north of Coos Bay, Oregon: United States Geological Survey.

Ross, G. J., and Kodama, H., 1974, Experimental transformation of a chlorite into a vermiculite: Clays and Clay Minerals, v. 22, p. 205-211.

Scheidegger, K. F., Kulm, L. D., and Runge, E. J., 1971, Sediment sources and dispersal patterns of Oregon continental shelf sands: Journal of Sedimentary Petrology, v. 41, no. 4, p. 1112-1120.

USDA Forest Service, 1996, Overlook Dunes Restoration Project, Environmental Assessment: USDA Forest Service, Siuslaw National Forest, Oregon Dunes National Recreation Area.

USDA Forest Service, 1981, Pacific Coast Ecological Inventory: Coos Bay, Oregon: United States Geological Survey, scale 1:250,000.
Shackleton, N. J., 1987, Oxygen isotopes, ice volume, and sea level: Quaternary Science Review, v. 6, p. 183-190.
Sherman, G. D., Cady, J. D., Ikawa, H., and Blumsburg, N. E., 1967, Genesis of bauxitic Hailu soils: Hawaii Agricultural Experimental Station Technical Bulletin, 56.
Shoji, S., Suzuki, Y., and Saigusa, M., 1987, Clay Mineralogical and Chemical Properties of Nonallophanic Andepts (Andisols) from Oregon, USA: Soil Science Society of America Journal, v. 51, p. 985-988.
Short, A. D., and Hesp, P. A., 1982, Wave, beach and dune interaction in southeast Australia: Marine Geology, v. 48, p. 259-284.
Shulmeister, J., and Lees, B. G., 1992, Morphology and chronostraigraphy of a coastal dunefield; Groote Eylandt, northern Australia: Geomorphology, v. 5, no. 6, p. 521-534.
Shulmeister, J., and Kirk, R. M., 1996, Holocene history and a thermoluminescence based chronology of coastal dune ridges near Leithfield, North Canterbury, New Zealand: New Zealand Journal of Geology and Geophysics, v. 39, no. 1, p. 25-32.
Shultz, S. T., 1990, The Northwest Coast: A Natural History: Portland, OR, Timber Press.
Swan, A. R. H., and Sandilands, M., 1995, Introduction to geological data analysis: United Kingdom, Blackwell Science, 446 p.
Taylor, A., and Lasaga, A., 1997, Flood basalts and the global Sr isotope budget: Geological Society of America, 1997 annual meeting, Abstracts with Programs, v. 29, no. 6, p. 87.
Terhune, C. L., Harden, J. W., and Matti, J. C., 1986, Application of a quantified field index of soil development to distinguish relative ages of geomorphic surfaces for regional geological mapping: The Geological Society of America, Cordilleran Section, 82nd annual meeting, v. 18, no. 2, p. 192.
Thom, B., Hesp, P., and Bryant, E., 1994, Last glacial "coastal" dunes in eastern Australia and implications for landscape stability during the Last Glacial Maximum: Palaeogeography, Palaeoclimatology, Palaeoecology, v. 111, no. 3-4, p. 229-248.
Thompson, C. H., 1983, Development and weathering of large parabolic dune systems along the subtropical coast of eastern Australia, *in* Jennings, J., and Hagedorn, H., eds., Dunes: Continental and Coastal: Berlin, Gebruder Borntraeger, p. 205-226.
Twenhofel, W. H., 1946, Mineralogical and physical composition of the sands of Oregon Coast from Coos Bay to the mouth of the Columbia River, *in* Bulletin - Oregon, Department of Geology and Mineral Industries, p. 64.
Velde, B., 1985, Clay Minerals: A Physiso-Chemical Explanation of their Occurrence, Developments in Sedimentology: New York, Elsevier.
Vidic, N. J., and Lobnik, F., 1997, Rates of soil development of the chronosequence in the Ljubljana Basin, Slovenia: Geoderma, v. 76, no. 1-2, p. 35-64.

Ward, W. T., 1977, Sand Movement on Fraser Island: A response to changing climates: Occasional Papers in Anthropology, v. 8, p. 113-126.
Ward, W. T., and Little, I. P., 1975, Times of coastal sand accumulation in southeast Queensland: Proceedings of the Ecological Society of Australia , v. 9, p. 313-317.
Worona, M. A., and Whitlock, C., 1995, Late Quaternary vegetation and climate history near Little Lake, central Coast Range, Oregon: GSA Bulletin, v. 107, no. 7, p. 867-876.
Young, A., and Stephan, I., 1965, Rock weathering and soil formation of high-altitude plateaux of Malawi: Journal of Soil Science, v. 16, p. 803-809.

Appendix A: Grain size, pH, and soil color analyses

Core: **JN1**	Date Collected: **12-Dec-96**	UTM Zone 10: **396390 E 4800020 N**		Elevation (m): **90**	
Sample Depth	*pH*	*Mean size (mm)*	*St Dev (mm)*	*Dry Color*	*Moist color*
5	5.03	0.03	0.00	7.5YR6/8	5YR4/6
15	4.98	0.02	0.00	2.5Y6/4	10YR5/4
80	5.08	0.03	0.00	2.5Y7/4	10YR5/4
120	5.08	0.07	0.01	2.5Y6/4-7/4	10YR5/6
180	5.13	0.09	0.01	10YR6/6 some 10YR6/8	7.5YR4/6 some 10YR5/8
230	5.18	0.16	0.04	2.5Y7/6	10YR5/4
250	5.10	0.17	0.04	2.5Y7/4	2.5Y5/4
280	5.55	0.16	0.04	2.5Y7/6	2.5Y5/4

Core: **HB1**	Date Collected: **13-Dec-96**	UTM Zone 10: **410200 E 4875670 N**		Elevation (m): **25**	
Sample Depth	pH	Mean size (mm)	St Dev (mm)	Dry Color	Moist color
0	5.25	Leaf matter (clumped)			
5	4.68	0.12	0.02	10YR7/1 - mainly humus	10YR5/1
15	5.40	0.12	0.02	10YR7/2	10YR4/1
30	5.65	0.14	0.04	2.5Y6/4	2.5Y5/4
50	5.18	0.14	0.04	2.5Y7/4	2.5Y5/3
70	5.73	0.14	0.04	2.5Y7/3	2.5Y5/3
90	5.40	0.13	0.04	2.5Y7/3	2.5Y5/3
110	5.65	0.13	0.04	2.5Y7/3	2.5Y5/3
130	5.78	0.15	0.04	2.5Y7/2	2.5Y5/2
150	5.75	0.13	0.04	2.5Y7/2	2.5Y5/2

Core: **NA1**	Date Collected: **10-Dec-96**	UTM Zone 10: **Not recorded**		Elevation (m): **Not recorded**	
Sample Depth	*pH*	*Mean size (mm)*	*St Dev (mm)*	*Dry Color*	*Moist color*
2	5.13	0.17	0.04	10YR7/1	10YR5/1
5	5.30	0.17	0.04	10YR7/2	10YR5/3
15	5.15	0.18	0.05	10YR7/2	10YR5/3
25	5.23	0.18	0.05	2.5Y7/3	2.5Y5/3
35	5.15	0.19	0.05	2.5Y7/3	2.5Y5/3
45	5.28	0.19	0.05	2.5Y7/3	2.5Y5/3

Core: **NA2**	Date Collected: **10-Dec-96**	UTM Zone 10: **Not recorded**		Elevation (m): **Not recorded**	
Sample Depth	*pH*	*Mean size (mm)*	*St Dev (mm)*	*Dry Color*	*Moist color*
5	4.38	0.17	0.04	2.5Y7/2 - humus material	2.5Y5/2
2	5.98	0.18	0.04	2.5Y7/3	2.5Y5/3
6	6.00	0.19	0.05	2.5Y7/3	2.5Y5/3
15	5.85	0.18	0.04	2.5Y7/4	2.5Y5/4
30	6.00	0.17	0.04	2.5Y7/4	2.5Y5/4
50	6.00	0.20	0.05	2.5Y7/3	2.5Y6/3

Core: **NA4**	Date Collected: **10-Dec-96**	UTM Zone 10: **Not recorded**		Elevation (m): **Not recorded**	
Sample Depth	*pH*	*Mean size (mm)*	*St Dev (mm)*	*Dry Color*	*Moist color*
-15	5.73	0.18	0.05	2.5Y7/2	2.5Y6/3
-5	5.90	0.15	0.04	2.5Y7/2	2.5Y6/3
1	5.93			10YR6/1 - 7/1	2.5Y4/1
3	6.03			2.5Y7/1	2.5Y5/1
7	5.70	0.16	0.04	2.5Y7/2	2.5Y6/2
15	5.45	0.17	0.04	2.5Y7/4	2.5Y5/4
30	5.70	0.18	0.05	2.5Y7/6	2.5Y5/4
50	5.80	0.17	0.04	2.5Y7/6 - 6/6	2.5Y5/4
70	6.20	0.18	0.04	2.5Y7/6 - 6/6	2.5Y5/4 - 5/6
90	6.08	0.19	0.05	2.5Y7/4	2.5Y5/4
110	6.00	0.18	0.05	2.5Y7/3	2.5Y5/4

Core: **G01**	Date Collected: **11-Dec-96**	UTM Zone 10: **400830 E 4806340 N**		Elevation (m): **30**	
Sample Depth	*pH*	*Mean size (mm)*	*St Dev (mm)*	*Dry Color*	*Moist color*
0	5.05				
5	5.05	0.11	0.02	10YR5/4 - 5/6	10YR4/4
15	5.08	0.09	0.02	10YR6/6	10YR4/4
30	5.00	0.09	0.02	10YR6/6	10YR4/4
50	5.23	0.10	0.02	10YR6/6	10YR4/4
70	5.30	0.16	0.04	10YR7/6	10YR5/6
90	5.38	0.17	0.04	10YR7/6	10YR5/6
110	5.35	0.19	0.04	10YR7/6	10YR5/6
130	5.35	0.26	0.07	2.5Y7/6	2.5Y6/6
150	5.50	0.23	0.07	2.5Y7/4	2.5Y5/4
170	5.43	0.26	0.06	2.5Y7/4	2.5Y5/4
190	5.20	0.24	0.07	2.5Y7/4	2.5Y5/4
210	5.18	0.22	0.06	2.5Y7/4	2.5Y5/4
230	5.18	0.24	0.06	2.5Y7/4	2.5Y5/4
250	5.40	0.22	0.07	2.5Y7/4	2.5Y5/4
270	5.45	0.22	0.07	2.5Y7/4	2.5Y5/4
290	5.20	0.21	0.06	2.5Y7/4	2.5Y5/4
310	5.13	0.22	0.07	2.5Y7/4	2.5Y5/4
330	5.20	0.23	0.06	*2.5Y7/4*	*2.5Y5/4*
350	5.28	0.17	0.03	2.5Y7/4	2.5Y5/4
370	5.23	0.16	0.03	2.5Y7/4	2.5Y5/4
390	5.28	0.15	0.03	2.5Y7/3	2.5Y5/4
410	5.38	0.16	0.03	2.5Y7/3	2.5Y5/4
430	5.33	0.15	0.03	2.5Y7/3	2.5Y5/4
450	5.30	0.14	0.03	2.5Y7/4	2.5Y5/4 - 5/6
470	5.35	0.16	0.03	2.5Y7/4	2.5Y5/6
490	5.50	0.16	0.03	2.5Y7/4	2.5Y5/6
510	5.50	0.23	0.06	2.5Y7/4	2.5Y5/6
530	5.55	0.22	0.06	2.5Y7/3	2.5Y5/4
550	5.55	0.22	0.06	2.5Y7/3	2.5Y6/4
570	5.43	0.22	0.07	2.5Y7/3	2.5Y6/4
590	5.35	0.22	0.06	2.5Y7/3	2.5Y6/4

Core: **EM1**	Date Collected: **12-Dec-96**	UTM Zone 10: **396250 E 4804060 N**		Elevation (m): **12**	
Sample Depth	*pH*	*Mean size (mm)*	*St Dev (mm)*	*Dry Color*	*Moist color*
0	4.85	leaf litter			
5	4.65	0.07	0.01	10YR4/2 + humus material	10YR2/2
15	4.63	0.09	0.01	10YR4/2	10YR2/2
30	5.20	0.14	0.03	10YR4/3	10YR3/3
50	5.23	0.06	0.01	10YR4/3	10YR3/3
70	4.88	0.07	0.01	10YR5/4	10YR4/4
90	5.53	0.16	0.03	10YR5/4 and 7/8	10YR4/4 and 5/8
110	5.55	0.18	0.04	10YR7/8	10YR5/8
130	5.50	0.19	0.03	2.5Y7/6	2.5Y5/4
150	5.28	0.23	0.05	2.5Y7/4	2.5Y5/4
170	5.23	0.26	0.04	2.5Y7/3	2.5Y5/4
190	5.23	0.30	0.04	2.5Y7/2	2.5Y6/3
210	4.95	0.29	0.04	10YR6/4 and some humus material	10YR4/3
230	5.00	0.32	0.04	2.5Y7/3 and some 10YR6/4	2.5Y5/3
265	5.13	0.22	0.05	*2.5Y7/3*	*2.5Y6/3*
275	5.45	0.17	0.03	2.5Y7/2	2.5Y6/3
250	5.10	0.25	0.04	2.5Y7/3	2.5Y6/3

Core: **NA3**	Date Collected: **10-Dec-96**	UTM Zone 10: **Not Recorded**		Elevation (m): **Not Recorded**	
Sample Depth	*pH*	*Mean size (mm)*	*St Dev (mm)*	*Dry Color*	*Moist color*
1	5.60	0.15	0.04	10YR7/2	2.5Y6/3
6	6.30	0.19	0.05	2.5Y7/3	2.5Y5/3
15	6.23	0.19	0.05	2.5Y7/3	2.5Y5/3
30	6.28	0.21	0.06	2.5Y7/4	2.5Y5/4
50	5.93	0.21	0.06	10YR6/6	10YR5/4
70	5.75	0.21	0.06	10YR5/6 - some 10YR4/6 and 2.5Y7/4	10YR5/4
90	5.90	0.21	0.06	2.5Y7/4	2.5Y5/4
110	6.08	0.21	0.06	2.5Y7/2	2.5Y5/3
130	6.15	0.23	0.06	2.5Y7/2	2.5Y5/3
150	6.23	0.22	0.06	2.5Y7/2	2.5Y5/3
250	6.00	0.22	0.06	*2.5Y7/2*	*2.5Y5/3*

Core: **RD1**	Date Collected: **10-Dec-96**	UTM Zone 10: **402720 E 4820420 N**		Elevation (m): **134**	
Sample Depth	*pH*	*Mean size (mm)*	*St Dev (mm)*	*Dry Color*	*Moist color*
40	4.93	0.07	0.01	10YR5/4	10YR4/4
80	5.28	0.07	0.01	10YR5/6	10YR4/4
150	5.18	0.07	0.01	10YR5/4	10YR4/4
160	5.18	0.08	0.01	10YR6/6	10YR4/4 - 5/6
200	5.03	0.14	0.03	10YR6/6	10YR5/6
250	4.88	0.17	0.03	2.5Y7/6	10YR5/6
300	5.10	0.19	0.04	2.5Y7/6	10YR5/6
350	5.75	0.23	0.05	2.5Y7/4	2.5Y5/4

Core: **NB2**	Date Collected: **23-Nov-96**	UTM Zone 10: **411110 E 4860770 N**		Elevation (m): **36**	
Sample Depth	*pH*	*Mean size (mm)*	*St Dev (mm)*	*Dry Color*	*Moist color*
5	4.20	0.05	0.01	10YR5/3	10YR3/3
15	4.43	0.06	0.01	10YR5/3	10YR3/3
30	4.50	0.04	0.00	10YR5/4	10YR4/3
50	4.53	0.07	0.01	10YR6/4	10YR4/3
70	4.78	0.15	0.03	2.5Y7/4	2.5Y5/4
90	5.10	0.20	0.05	2.5Y7/6	2.5Y5/4
110	5.20	0.18	0.04	2.5Y7/6	2.5Y5/4
130	5.33	0.18	0.04	2.5Y7/4	2.5Y5/4
150	5.35	0.17	0.04	2.5Y7/6	2.5Y5/4
170	5.43	0.20	0.05	2.5Y7/4	2.5Y5/4
190	5.70	0.20	0.04	2.5Y7/4	2.5Y5/4
210	5.38	0.22	0.04	2.5Y7/4	2.5Y5/4
230	5.38	0.24	0.05	2.5Y7/3	2.5Y5/4
250	5.35	0.23	0.05	*2.5Y7/3*	*2.5Y5/4*

Core: **HB2**	Date Collected: **3-Dec-96**	UTM Zone 10: **409530 E 4876600 N**		Elevation (m): **18**	
Sample Depth	*pH*	*Mean size (mm)*	*St Dev (mm)*	*Dry Color*	*Moist color*
0	4.90	leaf litter			
5	5.70	0.18	0.03	2.5Y6/2	2.5Y5/2
15	5.95	0.16	0.04	2.5Y7/2	2.5Y5/3
30	5.73	0.18	0.04	2.5Y7/2	2.5Y5/3
50	5.90	0.18	0.04	2.5Y7/2	2.5Y5/3
70	6.08	0.17	0.04	2.5Y7/2	2.5Y5/3
90	5.98	0.17	0.04	2.5Y7/2	2.5Y5/3
110	6.15	0.16	0.04	2.5Y7/2	2.5Y5/3
130	6.15	0.17	0.04	2.5Y7/2	2.5Y5/3
150	6.30	0.19	0.05	2.5Y7/2	2.5Y5/3
170	6.10	0.18	0.05	2.5Y7/2	2.5Y5/3
190	6.08	0.16	0.04	2.5Y7/2	2.5Y5/3
230	6.15	0.16	0.04	2.5Y7/2	2.5Y5/3
250	5.90	0.16	0.04	2.5Y7/2	2.5Y5/3

Core: **LL1**	Date Collected: **5-Dec-96**	UTM Zone 10: **407810 E 4853640 N**		Elevation (m): **49**	
Sample Depth	*pH*	*Mean size (mm)*	*St Dev (mm)*	*Dry Color*	*Moist color*
0	4.60	litter - leaf and humus material			
5	4.38	0.14	0.02	10YR7/1 some humus material	too much humus to tell
15	4.50	0.14	0.02	10YR6/1 some roots	10YR4/1
25	4.73	0.18	0.03	10YR 6/6 some 6/1 and 7/6	10YR4/2 - 4/3
35	4.95	0.18	0.05	2.5Y5/4 10YR6/6 and 7/6	10YR3/4
50	4.85	0.18	0.05	2.5Y6/4 - 7/4	2.5Y4/4
70	5.28	0.18	0.04	2.5Y7/4	2.5Y4/4
90	5.45	0.18	0.05	2.5Y7/4-7/3	2.5Y5/4
110	5.50	0.18	0.05	2.5Y7/3	2.5Y5/4 - 5/3
130	5.60	0.19	0.05	2.5Y7/2	2.5Y5/4 - 5/3
150	5.75	0.19	0.05	2.5Y7/2	2.5Y5/3
170	5.65	0.20	0.06	2.5Y7/2	2.5Y5/3
190	5.85	0.23	0.06	2.5Y7/2	2.5Y5/3
210	5.85	0.20	0.05	2.5Y7/2	2.5Y5/3
230	5.85	0.20	0.05	2.5Y7/2	2.5Y5/3
250	5.85	0.20	0.05	2.5Y7/2	2.5Y5/3
270	6.00	0.18	0.05	2.5Y7/2	2.5Y5/3
290	6.00	0.18	0.04	2.5Y7/2	2.5Y5/3
310	5.95	0.17	0.04	2.5Y7/2	2.5Y5/3
330	5.90	0.18	0.05	2.5Y7/2	2.5Y5/3
350	5.90	0.17	0.04	2.5Y7/2	2.5Y5/3
370	5.85	0.17	0.04	2.5Y7/2	2.5Y5/3
390	5.95	0.17	0.04	2.5Y7/2	2.5Y5/3
410	5.90	0.18	0.04	2.5Y7/2	2.5Y5/3
430	5.85	0.17	0.04	2.5Y7/2	2.5Y5/3
450	5.70	0.18	0.04	2.5Y7/2	2.5Y5/3
470	5.80	0.17	0.04	2.5Y7/2	2.5Y5/3
510	5.80	0.19	0.05	2.5Y7/2	2.5Y5/3

Core: **UL1**	Date Collected: **3-Dec-96**	UTM Zone 10: **403880 E 4834890 N**		Elevation (m): **67**	
Sample Depth	*pH*	*Mean size (mm)*	*St Dev (mm)*	*Dry Color*	*Moist color*
0	3.83	leaf litter			
5	4.40	0.07	0.01	10YR4/2 some 6/2	10YR2/2
15	4.35	0.07	0.01	10YR5/3 some 5/4	10YR3/3
30	4.68	0.07	0.01	10YR5/4	10YR3/3
50	4.78	0.06	0.01	10YR5/4	10YR3/4
70	5.30	0.06	0.01	10YR6/4	10YR3/4
90	5.38	0.07	0.01	10YR6/4	10YR3/3
110	5.60	0.18	0.04	2.5Y6/4	2.5Y4/4
130	5.55	0.19	0.04	2.5Y6/4	2.5Y4/4
150	5.60	0.19	0.04	10YR7/6 and 2.5Y7/4	10YR5/6
170	5.55	0.23	0.05	2.5Y7/4	2.5Y5/4
185	5.50	0.23	0.06	*2.5Y7/6*	*2.5Y5/6*
195	5.58	0.08	0.01	2.5Y7/4	10YR5/4
210	5.45	0.10	0.02	2.5Y6/4	2.5Y5/4
230	5.53	0.12	0.02	2.5Y6/4 - 6/6	10YR5/4
250	5.38	0.16	0.03	2.5Y6/6	2.5Y5/6
270	5.18	0.19	0.05	2.5Y7/6	2.5Y5/4 and 10YR5/6
290	5.18	0.20	0.05	2.5Y7/6	2.5Y5/4
310	5.15	0.17	0.04	2.5Y7/6	2.5Y5/4
330	5.25	0.18	0.04	2.5Y7/4	2.5Y5/4
350	5.25	0.18	0.04	2.5Y7/4	2.5Y5/4
370	5.10	0.19	0.04	2.5Y7/4	2.5Y5/4
390	5.20	0.18	0.04	2.5Y7/4	2.5Y5/4

Core: **CL1**	Date Collected: **5-Dec-96**	UTM Zone 10: **409830 E 4856200 N**		Elevation (m): **25**	
Sample Depth	*pH*	*Mean size (mm)*	*St Dev (mm)*	*Dry Color*	*Moist color*
0	6.00	leaf litter			
5	4.90	0.12	0.02	10YR5/3 nodules	10YR4/3
15	4.78	0.12	0.02	10YR5/3 nodules	10YR4/3
25	4.48	0.10	0.02	10YR5/3 nodules	10YR4/3
35	4.38	0.10	0.02	10YR5/3 nodules of 4/3 & 6/3 mixed	10YR4/3 nodules of 2/2 & 4/3
45	5.38	0.11	0.02	10YR6/4	10YR4/3
55	5.45	0.11	0.02	10YR6/4	10YR4/3
70	5.43	0.11	0.02	10YR6/4	10YR4/3
90	5.30	0.11	0.02	10YR6/4	10YR4/3
110	5.28	0.14	0.02	10YR7/4	10YR4/4
130	5.38	0.18	0.05	2.5Y7/6	2.5Y5/4
150	5.35	0.19	0.05	2.5Y7/6	2.5Y5/4
170	5.50	0.19	0.05	2.5Y7/6	2.5Y5/4
190	5.45	0.22	0.04	2.5Y7/6	2.5Y5/4
210	5.45	0.17	0.04	2.5Y6/4	2.5Y5/4
230	5.60	0.18	0.04	*2.5Y6/4*	*2.5Y5/4*

Core: **VG1**	Date Collected: **12-Dec-96**	UTM Zone 10: **398410 E 4806560 N**		Elevation (m): **49**	
Sample Depth	*pH*	*Mean size (mm)*	*St Dev (mm)*	*Dry Color*	*Moist color*
5	5.25	0.14	0.03	10YR6/3 nodules of 6/2 & 7/3	10YR5/3 nodules of 5/2 & 5/4
15	5.20	0.14	0.03	10YR6/3 - 6/4 nodules of 6/2, 7/3 & 6/6	10YR5/3 nodules of 5/2, 5/4 & 5/6
30	5.08	0.19	0.04	10YR6/6	10YR4/4
50	5.23	0.24	0.06	2.5Y6/6 - 7/6	10YR5/6
70	5.35	0.23	0.05	2.5Y7/4	2.5Y5/4
90	5.30	0.24	0.05	2.5Y7/4	2.5Y5/4
110	5.25	0.24	0.05	2.5Y7/4	2.5Y5/4
130	5.15	0.23	0.05	2.5Y7/4	2.5Y5/4
150	5.00	0.22	0.05	*2.5Y7/4*	*2.5Y5/4*

Core: **VG2**	Date Collected: **12-Dec-96**	UTM Zone 10: **398490 E 4806490 N**		Elevation (m): **49**	
Sample Depth	*pH*	*Mean size (mm)*	*St Dev (mm)*	*Dry Color*	*Moist color*
3	4.03	0.13	0.02	10YR6/1	10YR4/1
9	4.73	0.13	0.02	10YR6/1 - 7/1 nodules	10YR5/1
8	4.73	0.14	0.02	10YR6/2 nodules	10YR5/2
15	4.43	0.15	0.03	10YR6/3 nodules	10YR5/3
30	4.70	0.16	0.04	10YR6/4 nodules	10YR5/4
50	5.45	0.18	0.05	2.5Y7/4	2.5Y5/4
70	5.53	0.16	0.04	2.5Y7/3	2.5Y5/4
90	5.58	0.16	0.04	2.5Y7/2	2.5Y5/3
110	5.53	0.16	0.04	2.5Y7/2	2.5Y5/3
130	5.48	0.16	0.04	2.5Y7/2	2.5Y5/3
150	5.65	0.16	0.04	2.5Y7/2	2.5Y6/3

Core: **MS1**	Date Collected: **Not Recorded**	UTM Zone 10: **413090 E 4872550 N**		Elevation (m): **55**	
Sample Depth	*pH*	*Mean size (mm)*	*St Dev (mm)*	*Dry Color*	*Moist color*
0	4.85	leaf litter			
5	4.63	0.17	0.04	2.5Y6/3 with litter	2.5Y5/3
15	5.25	0.16	0.04	2.5Y6/4 with roots, nodules 10YR6/6	2.5Y5/4, nodules of 2.5Y5/6 & 10YR5/6
30	5.68	0.16	0.04	2.5Y7/4	2.5Y5/4
50	5.78	0.16	0.04	2.5Y7/2	2.5Y6/3
70	6.03	0.16	0.04	2.5Y7/2	2.5Y6/3
90	5.90	0.15	0.04	2.5Y7/2	2.5Y6/3
110	5.88	0.16	0.04	2.5Y7/2	2.5Y6/3
130	6.10	0.16	0.04	2.5Y7/2	2.5Y6/3
150	6.20	0.15	0.04	2.5Y7/2	2.5Y6/3
170	6.13	0.15	0.04	2.5Y7/2	2.5Y6/3
190	6.03	0.15	0.04	2.5Y7/2	2.5Y6/3
210	6.10	0.15	0.04	2.5Y7/2	2.5Y5/3
230	6.13	0.17	0.04	2.5Y7/2	2.5Y5/3
248	6.00	0.17	0.04	2.5Y7/2	2.5Y5/3
263	5.85	0.17	0.04	2.5Y7/3	2.5Y5/3
275	5.90	0.17	0.04	2.5Y7/2	2.5Y5/3
290	6.05	0.17	0.04	2.5Y7/2	2.5Y5/3
310	6.08	0.17	0.04	2.5Y7/2	2.5Y5/3
330	6.10	0.16	0.04	2.5Y7/2	2.5Y5/3
350	6.23	0.18	0.04	2.5Y7/2	2.5Y5/3
370	6.08	0.17	0.04	2.5Y7/2	2.5Y5/3
390	6.10	0.16	0.04	2.5Y7/2	2.5Y5/3
410	6.18	0.18	0.04	2.5Y7/2	2.5Y5/3
430	6.10	0.17	0.04	2.5Y7/2	2.5Y5/3
450	6.13	0.17	0.04	2.5Y7/2	2.5Y5/3
470	6.00	0.17	0.04	Missing	Missing
490	6.10	0.16	0.04	2.5Y7/2	2.5Y5/3

Core: **SP1**	Date Collected: **1-Dec-96**	UTM Zone 10: **406080 E 4844150 N**		Elevation (m): **6**	
Sample Depth	*pH*	*Mean size (mm)*	*St Dev (mm)*	*Dry Color*	*Moist color*
5	5.20	0.10	0.02	10YR5/3	10YR4/3
15	4.93	0.11	0.02	10YR6/3	10YR5/3
30	5.43	0.10	0.02	10YR6/4 - 6/3	10YR5/3
50	5.58	0.10	0.02	10YR5/3 charcoal	10YR3/2
70	5.50	0.10	0.02	10YR5/3	10YR4/2
90	5.40	0.08	0.01	10YR5/4	10YR4/4
110	5.18	0.09	0.01	10YR4/2 & 5/4	10YR2/1 & 4/4
130	5.38	0.08	0.01	10YR6/4	10YR4/3
150	5.33	0.05	0.01	10YR6/4	10YR4/4
170	5.30	0.07	0.01	10YR5/4	10YR3/3
190	5.50	0.07	0.01	10YR6/4	10YR4/4
210	5.43	0.09	0.01	10YR6/4	10YR4/4
230	5.58	0.07	0.01	2.5Y7/4	2.5Y5/4
255	5.50	0.09	0.01	2.5Y7/4	10YR5/4
275	5.40	0.10	0.02	10YR7/6	10YR5/6
290	5.30	0.18	0.05	10YR7/6 - 2.5YR7/6	10YR5/6
310	5.10	0.19	0.05	10YR7/6	10YR5/6
330	5.08	0.18	0.04	2.5Y6/4	2.5Y5/4
390	5.63	0.16	0.04	2.5Y6/4	2.5Y5/4

Core: **RO1**	Date Collected: **24-Nov-96**	UTM Zone 10: **403620 E 4824850 N**		Elevation (m): **6**	
Sample Depth	*pH*	*Mean size (mm)*	*St Dev (mm)*	*Dry Color*	*Moist color*
30	4.78	0.07	0.01	10YR5/4	10YR3/4
60	4.95	0.08	0.01	10YR6/4&5/4	10YR3/3
100	5.48	0.16	0.04	2.5Y7/4&10YR7/6	2.5Y5/4
150	5.30	0.21	0.06	2.5Y7/6 & 10YR7/6	2.5Y5/4
200	5.53	0.17	0.04	2.5Y7/6 & 10YR7/6	2.5Y5/4
250	5.65	0.18	0.04	2.5Y7/4 & 10YR7/4	2.5Y5/4
300	5.55	0.18	0.04	2.5Y7/4 & 10YR7/4	2.5Y5/4

Core: **MA1**	Date Collected: **27-Nov-96**	UTM Zone 10: **402600 E 4822420 N**		Elevation (m): **37**	
Sample Depth	*pH*	*Mean size (mm)*	*St Dev (mm)*	*Dry Color*	*Moist color*
0	6.20	Leaf litter			
0	4.95	0.05	0.01	10YR5/4	10YR3/4
10	5.80	0.06	0.01	10YR5/4	10YR3/4
30	5.43	0.05	0.01	10YR5/6	10YR3/3
50	5.63	0.05	0.01	10YR5/4	10YR4/4
70	5.45	0.06	0.01	10YR5/4	10YR4/4
90	5.53	0.06	0.01	10YR6/4	10YR4/4
105	5.25	0.08	0.01	10YR6/4	10YR4/4
115	5.10	0.16	0.03	10YR6/4 & 6/6	10YR4/6 - 4/4
130	4.85	0.22	0.08	10YR6/6	10YR4/6
150	4.88	0.22	0.07	2.5Y7/6	2.5Y5/6
170	4.80	0.25	0.06	2.5Y7/4	2.5Y5/4
190	4.73	0.24	0.06	2.5Y7/4	2.5Y5/4
210	4.75	0.23	0.05	2.5Y7/3	2.5Y5/3
230	4.70	0.24	0.06	2.5Y7/3	2.5Y6/3
250	4.73	0.24	0.06	2.5Y7/3	2.5Y6/3
270	5.10	0.25	0.06	2.5Y7/3	2.5Y6/3
290	4.98	0.26	0.06	2.5Y7/3	2.5Y6/3
310	4.95	0.26	0.06	2.5Y7/3	2.5Y6/3
330	5.43	0.22	0.05	2.5Y7/3	2.5Y6/3
350	5.70	0.17	0.03	2.5Y7/4	2.5Y6/6
370	5.68	0.17	0.03	2.5Y7/4	2.5Y6/6
390	5.30	0.04	0.00	2.5Y6/4	2.5Y6/4
410	5.25	0.02	0.00	2.5Y 8/3, 7/3, 7/6 & some hard 6/3	2.5Y6/6

Core: **LK1**	Date Collected: **24-Nov-96**	UTM Zone 10: **403690 E 4825870 N**		Elevation (m): **25**	
Sample Depth	*pH*	*Mean size (mm)*	*St Dev (mm)*	*Dry Color*	*Moist color*
0	4.33	Leaf litter			
0	3.75	litter and humus			
10	4.88	0.18	0.03	2.5Y7/2	10YR5/2
15	5.40	0.17	0.04	2.5Y7/4 & 10YR7/2	2.5Y5/4
30	5.08	0.16	0.04	2.5Y7/4 & 10YR6/4	2.5Y5/4
50	5.43	0.16	0.04	2.5Y7/4 & 10YR6/4	2.5Y5/4
70	5.73	0.15	0.04	2.5Y7/4	2.5Y5/4
90	6.00	0.15	0.04	2.5Y7/3	2.5Y5/3
110	6.05	0.16	0.04	2.5Y7/3	2.5Y5/3 - 6/3
130	6.10	0.14	0.04	2.5Y7/2	2.5Y6/3
150	6.18	0.14	0.04	2.5Y7/2	2.5Y6/3
170	6.00	0.15	0.04	2.5Y7/2	2.5Y6/3
190	6.15	0.13	0.05	2.5Y7/2	2.5Y6/3
210	6.15	0.13	0.05	2.5Y7/2	2.5Y6/3
230	6.18	0.15	0.04	2.5Y7/2	2.5Y6/3
250	6.18	0.14	0.04	2.5Y7/2	2.5Y6/3
270	6.18	0.14	0.04	2.5Y7/2	2.5Y6/3
290	6.10	0.17	0.04	2.5Y7/2	2.5Y6/3
310	6.20	0.18	0.05	2.5Y7/2	2.5Y6/3
330	6.00	0.19	0.05	2.5Y7/2	2.5Y6/3
350	6.10	0.21	0.05	2.5Y7/2	2.5Y6/3
370	6.03	0.19	0.05	2.5Y7/2	2.5Y6/3
390	6.08	0.17	0.04	2.5Y7/2	2.5Y6/3
410	6.18	0.17	0.04	2.5Y7/2	2.5Y6/3
430	6.13	0.17	0.04	2.5Y7/2	2.5Y6/3
450	6.28	0.17	0.04	2.5Y7/2	2.5Y6/3
470	6.30	0.17	0.04	2.5Y7/2	2.5Y6/3
510	6.30	0.17	0.04	2.5Y7/2	2.5Y6/3

Core: **LK2**	Date Collected: **25-Nov-96**	UTM Zone 10: **403370 E 4826000 N**		Elevation (m): **25**	
Sample Depth	*pH*	*Mean size (mm)*	*St Dev (mm)*	*Dry Color*	*Moist color*
0	4.13	litter and humus			
5	4.23	0.15	0.04	2.5Y7/1 - 7/2	2.5Y5/2
15	4.93	0.16	0.04	2.5Y6/3	2.5Y5/3
30	5.80	0.17	0.04	2.5Y6/4	2.5Y5/4
50	6.00	0.17	0.04	2.5Y6/4	2.5Y5/4
70	5.85	0.17	0.04	2.5Y7/3	2.5Y5/4
90	5.58	0.15	0.04	2.5Y7/3	2.5Y5/3
110	5.65	0.15	0.04	2.5Y7/3	2.5Y5/3
130	5.55	0.17	0.04	2.5Y7/2	2.5Y6/3
150	6.28	0.18	0.04	2.5Y7/2	2.5Y6/3
170	6.23	0.19	0.05	2.5Y7/2	2.5Y6/3
190	6.18	0.19	0.05	2.5Y7/2	2.5Y6/3
210	6.03	0.18	0.05	2.5Y7/2	2.5Y6/3
230	5.63	0.19	0.05	2.5Y7/2	2.5Y6/3
250	6.15	0.19	0.05	2.5Y7/2	2.5Y6/3
270	6.00	0.19	0.05	2.5Y7/2	2.5Y6/3
290	5.93	0.19	0.05	2.5Y7/2	2.5Y6/3
310	5.83	0.18	0.05	2.5Y7/2	2.5Y6/3
330	5.70	0.19	0.05	2.5Y7/2	2.5Y6/3
350	5.90	0.18	0.05	2.5Y7/2	2.5Y6/3
370	5.85	0.17	0.05	2.5Y7/2	2.5Y6/3
390	5.85	0.18	0.05	2.5Y7/2	2.5Y6/3
410	5.90	0.18	0.05	2.5Y7/2	2.5Y6/3
430	5.58	0.19	0.05	2.5Y7/2	2.5Y6/3
450	6.18	0.19	0.05	2.5Y7/2	2.5Y6/3
470	6.08	0.17	0.05	2.5Y7/2	2.5Y6/3
510	5.70	0.18	0.05	2.5Y7/2	2.5Y6/3

Core: **PA1**	Date Collected: **23-Nov-96**	UTM Zone 10: **401470 E 4815050 N**		Elevation (m): **43**	
Sample Depth	*pH*	*Mean size (mm)*	*St Dev (mm)*	*Dry Color*	*Moist color*
10	3.85	0.04	0.00	10YR4/3	10YR3/3
40	4.23	0.05	0.01	10YR5/4	10YR4/4
80	4.85	0.08	0.01	10YR6/4	10YR5/4
100	5.00	0.13	0.02	10YR6/4	10YR5/4
130	5.15	0.18	0.04	2.5Y7/4	2.5Y5/4

Core: **SHS**	Date Collected: **22-Nov-96**	UTM Zone 10: **401860 E 4815250 N**		Elevation (m): **37**	
Sample Depth	*pH*	*Mean size (mm)*	*St Dev (mm)*	*Dry Color*	*Moist color*
35	4.88	0.04	0.00	10YR5/3	10YR4/3
65	4.80	0.04	0.00	10YR5/3	10YR4/3
105	5.05	0.12	0.02	2.5Y6/3 some 10YR6/8	2.5Y5/4 & 10YR5/8
155	5.05	0.19	0.05	2.5Y7/6 & 10YR7/8	2.5Y5/6
205	5.23	0.19	0.05	2.5Y7/4 & 7.5YR5/8	2.5Y6/4 & 3/4
240	5.50	0.04	0.01	2.5Y7/2	2.5Y5/3
310	5.58	0.08	0.01	2.5Y7/4 & 10YR6/8	2.5Y5/4 & 7.5YR5/8

Core: **SC1**	Date Collected: **23-Nov-96**	UTM Zone 10: **402260 E 4816060 N**		Elevation (m): **12**	
Sample Depth	*pH*	*Mean size (mm)*	*St Dev (mm)*	*Dry Color*	*Moist color*
25	5.20	0.09	0.01	10YR5/4	10YR4/4
45	5.10	0.10	0.02	10YR6/4	10YR4/4
70	4.85	0.10	0.02	10YR5/3	10YR4/4
90	5.40	0.11	0.02	2.5Y7/1	2.5Y5/2
115	5.23	0.31	0.06	2.5Y7/3	2.5Y5/4
140	5.25	0.25	0.05	2.5Y7/4	2.5Y6/4
180	5.30	0.21	0.06	2.5Y7/4	2.5Y5/4

Core: **SW1**	Date Collected: **23-Nov-96**	UTM Zone 10: **401470 E 4811770 N**		Elevation (m): **25**	
Sample Depth	*pH*	*Mean size (mm)*	*St Dev (mm)*	*Dry Color*	*Moist color*
5	5.35	0.19	0.05	2.5Y7/4	2.5Y5/4
35	4.50	0.10	0.02	10YR5/4	10YR3/4
60	4.98	0.11	0.02	10YR6/4	10YR4/4
95	5.30	0.24	0.06	2.5Y7/6	2.5Y5/6
140	5.40	0.09	0.02	2.5Y7/4	2.5Y5/4
180	5.35	0.22	0.06	10YR7/8	10YR5/8
270	5.25	0.25	0.07	2.5Y7/6	2.5Y5/4

Core: **ME1**	Date Collected: **9-Dec-96**	UTM Zone 10: **414120 E 4877280 N**		Elevation (m): **12**	
Sample Depth	*pH*	*Mean size (mm)*	*St Dev (mm)*	*Dry Color*	*Moist color*
0	5.10	leaf litter			
5	5.15	0.13	0.02	10YR5/3	10YR3/3
15	5.00	0.10	0.02	10YR5/3	10YR3/3
25	5.25	0.14	0.02	10YR5/3	10YR3/3
35	5.18	0.14	0.02	10YR5/3	10YR3/3
50	5.05	0.15	0.03	10YR5/3	10YR3/3
70	4.95	0.23	0.05	10YR6/6	10YR5/6
90	5.15	0.22	0.05	2.5Y6/4	10YR5/4
110	4.93	0.22	0.05	2.5Y6/4	2.5Y5/4
130	4.98	0.21	0.05	2.5Y7/4	2.5Y5/4
150	4.90	0.22	0.05	2.5Y7/4	2.5Y5/4
170	4.93	0.22	0.05	2.5Y7/4	2.5Y5/4
190	5.35	0.21	0.04	*2.5Y7/4*	*2.5Y5/4*
210	5.30	0.22	0.05	2.5Y7/4	2.5Y5/4
230	5.23	0.24	0.06	2.5Y7/3	2.5Y5/3
250	5.25	0.21	0.05	2.5Y7/3	2.5Y5/3
270	5.25	0.20	0.05	2.5Y7/3	2.5Y5/3
290	5.55	0.25	0.05	2.5Y7/3	2.5Y5/3
310	5.30	0.27	0.05	2.5Y7/6	2.5Y5/4
330	5.30	0.23	0.05	2.5Y7/6 & 5YR5/8	2.5Y5/6 & 5YR3/4
350	5.40	0.24	0.05	2.5Y7/6	2.5Y5/4
370	5.00	0.25	0.05	2.5Y7/6	2.5Y5/4
390	5.35	0.26	0.05	2.5Y7/4	2.5Y5/4
410	5.25	0.29	0.04	2.5Y7/4	2.5Y5/4
430	5.40	0.24	0.04	2.5Y7/3	2.5Y5/3
450	5.30	0.23	0.04	2.5Y7/3	2.5Y5/3
470	5.45	0.13	0.02	2.5Y7/3 & 7.5YR6/8	2.5Y5/3 & 5YR4/6

Core: **UD1**	Date Collected: **26-Nov-96**	UTM Zone 10: **402900 E 4831310 N**		Elevation (m): **37**	
Sample Depth	*pH*	*Mean size (mm)*	*St Dev (mm)*	*Dry Color*	*Moist color*
0	5.48	litter and humus			
5	4.95	0.18	0.03	litter and humus	
15	4.28	0.17	0.03	10YR7/1	10YR4/1
25	4.28	0.16	0.03	10YR7/1	10YR4/1
35	4.48	0.16	0.04	10YR7/2	10YR5/2
50	4.80	0.17	0.04	10YR7/2	10YR5/2
70	5.40	0.17	0.04	2.5Y7/4	2.5Y5/4
90	5.85	0.20	0.05	2.5Y7/4	2.5Y5/4
110	6.00	0.17	0.04	2.5Y7/3	2.5Y5/3
130	6.18	0.18	0.05	2.5Y7/3	2.5Y5/3
150	5.83	0.16	0.04	2.5Y7/3	2.5Y5/3
170	5.83	0.15	0.04	2.5Y7/2	2.5Y5/3
190	5.95	0.18	0.05	2.5Y7/2	2.5Y5/3
230	5.85	0.22	0.05	2.5Y7/2	2.5Y5/3
250	5.53	0.22	0.05	2.5Y7/2	2.5Y5/3
270	5.45	0.22	0.06	2.5Y7/2	2.5Y5/3
290	5.90	0.26	0.07	2.5Y7/2	2.5Y5/3
310	6.00	0.19	0.04	2.5Y7/2	2.5Y5/3
330	5.98	0.22	0.06	2.5Y7/2	2.5Y5/3
350	5.98	0.21	0.05	2.5Y7/2	2.5Y5/3
370	5.55	0.23	0.06	2.5Y7/2	2.5Y5/3
390	6.15	0.21	0.05	2.5Y7/2	2.5Y5/3
410	5.78	0.21	0.06	2.5Y7/2	2.5Y5/3
423	5.38	0.18	0.04	2.5Y7/3	2.5Y5/3
433	5.55	0.20	0.06	2.5Y7/3	2.5Y5/3
450	5.48	0.23	0.07	2.5Y7/2	2.5Y5/3
470	5.55	0.20	0.06	2.5Y7/2	2.5Y5/3
490	5.70	0.19	0.05	2.5Y7/2	2.5Y5/3
510	5.85	0.20	0.06	2.5Y7/2	2.5Y5/3
530	6.00	0.20	0.05	2.5Y7/2	2.5Y5/3
550	6.00	0.21	0.07	2.5Y7/2	2.5Y5/3
570	5.90	0.20	0.05	2.5Y7/2	2.5Y5/3
590	6.05	0.21	0.06	2.5Y7/2	2.5Y5/3
610	5.10	0.20	0.06	2.5Y7/2	2.5Y5/3
650	5.50	0.19	0.05	2.5Y7/2	2.5Y5/3

Core: **SW2**	Date Collected: **23-Nov-96**	UTM Zone 10: **400860 E 4811710 N**		Elevation (m): **18**	
Sample Depth	*pH*	*Mean size (mm)*	*St Dev (mm)*	*Dry Color*	*Moist color*
20	4.60	0.10	0.02	10YR5/4	10YR3/4
40	5.10	0.27	0.06	2.5Y7/4	2.5Y5/4
70	5.20	0.27	0.06	2.5Y7/4	2.5Y5/4
110	5.15	0.25	0.06	2.5Y7/4	2.5Y5/4
150	5.05	0.22	0.06	2.5Y7/4	2.5Y5/4
200	5.20	0.25	0.04	2.5Y7/4	2.5Y5/4

Appendix B: GIS azimuth data

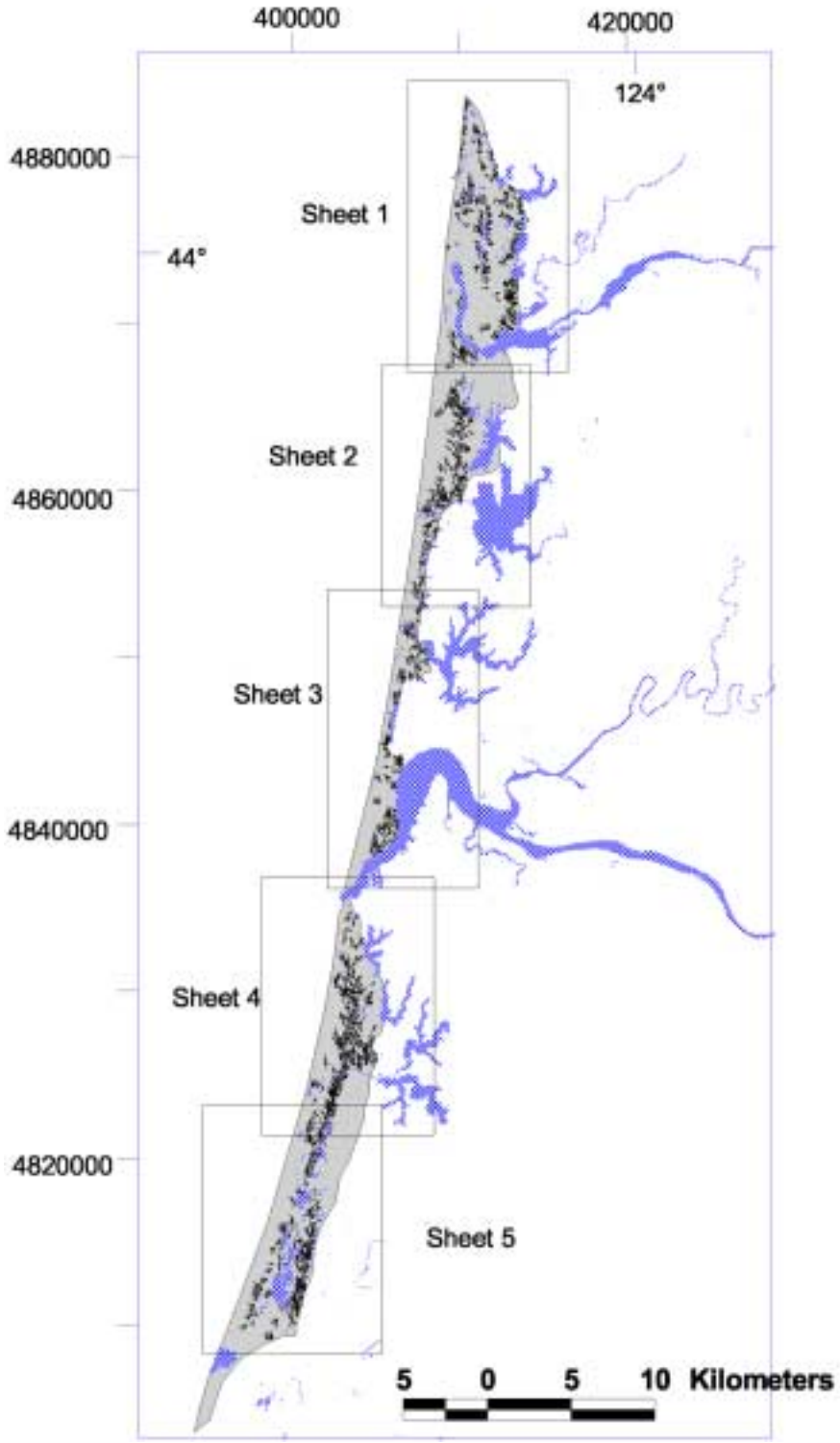

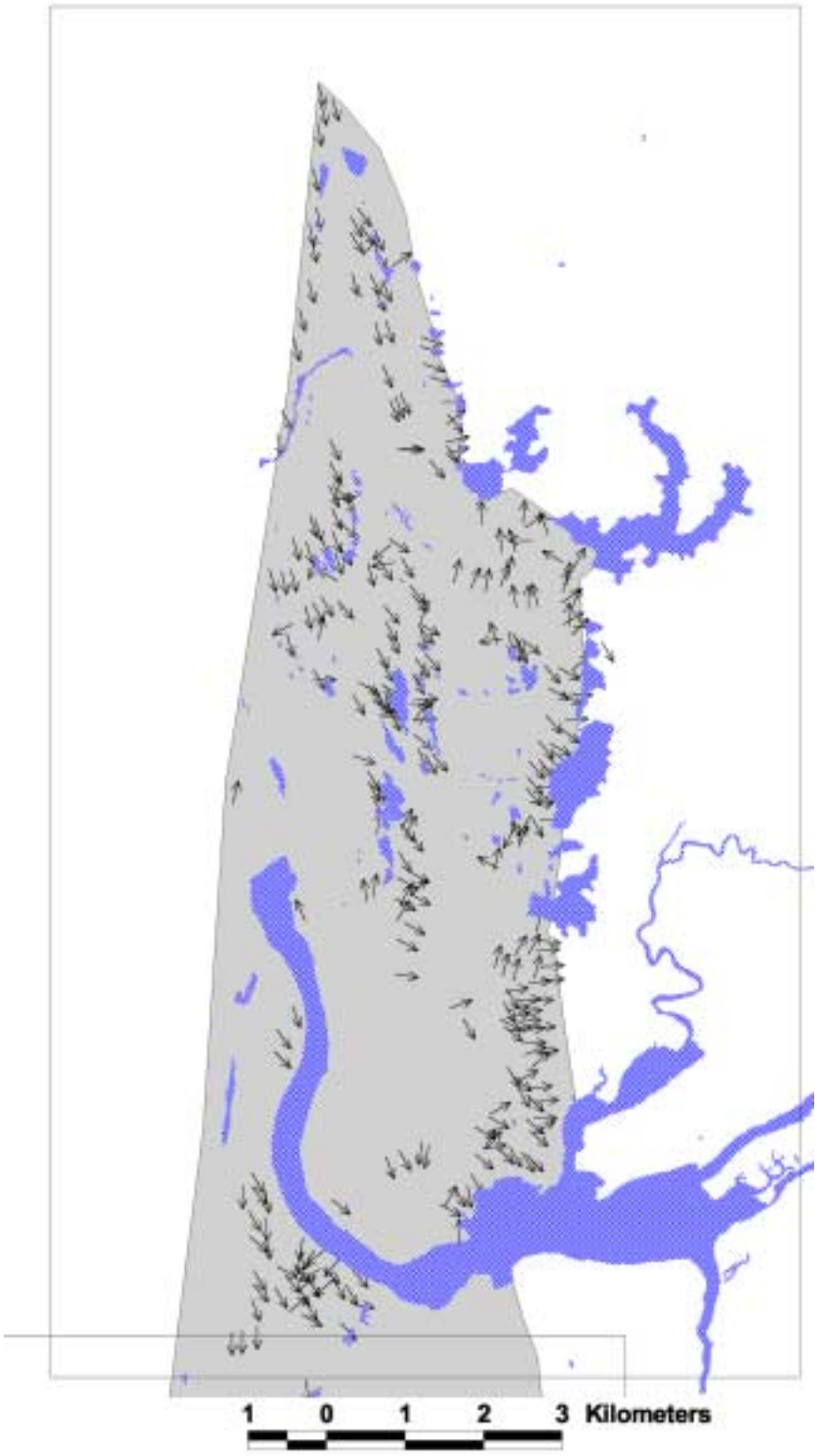

Sheet 1

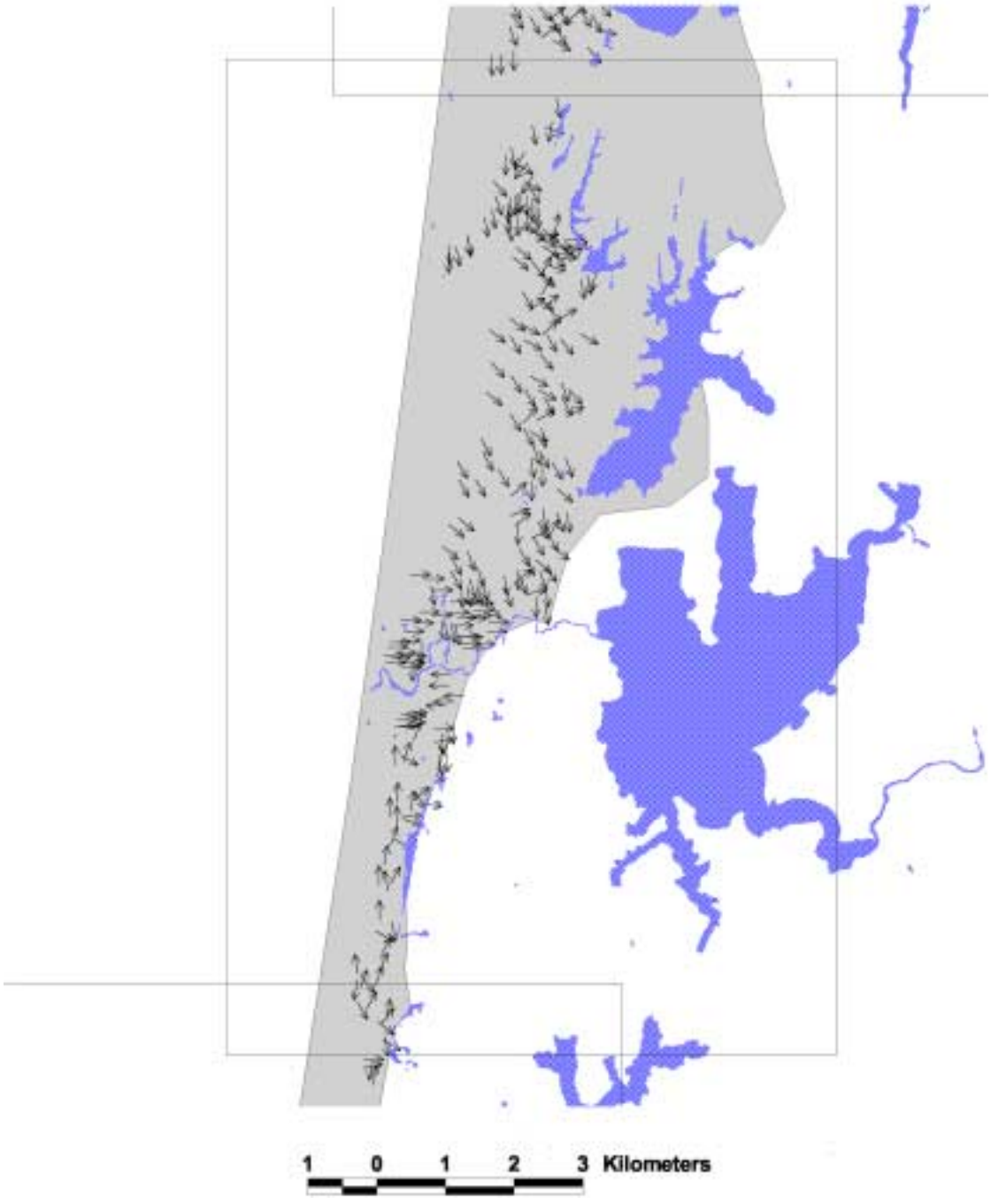

Sheet 2

Sheet 3

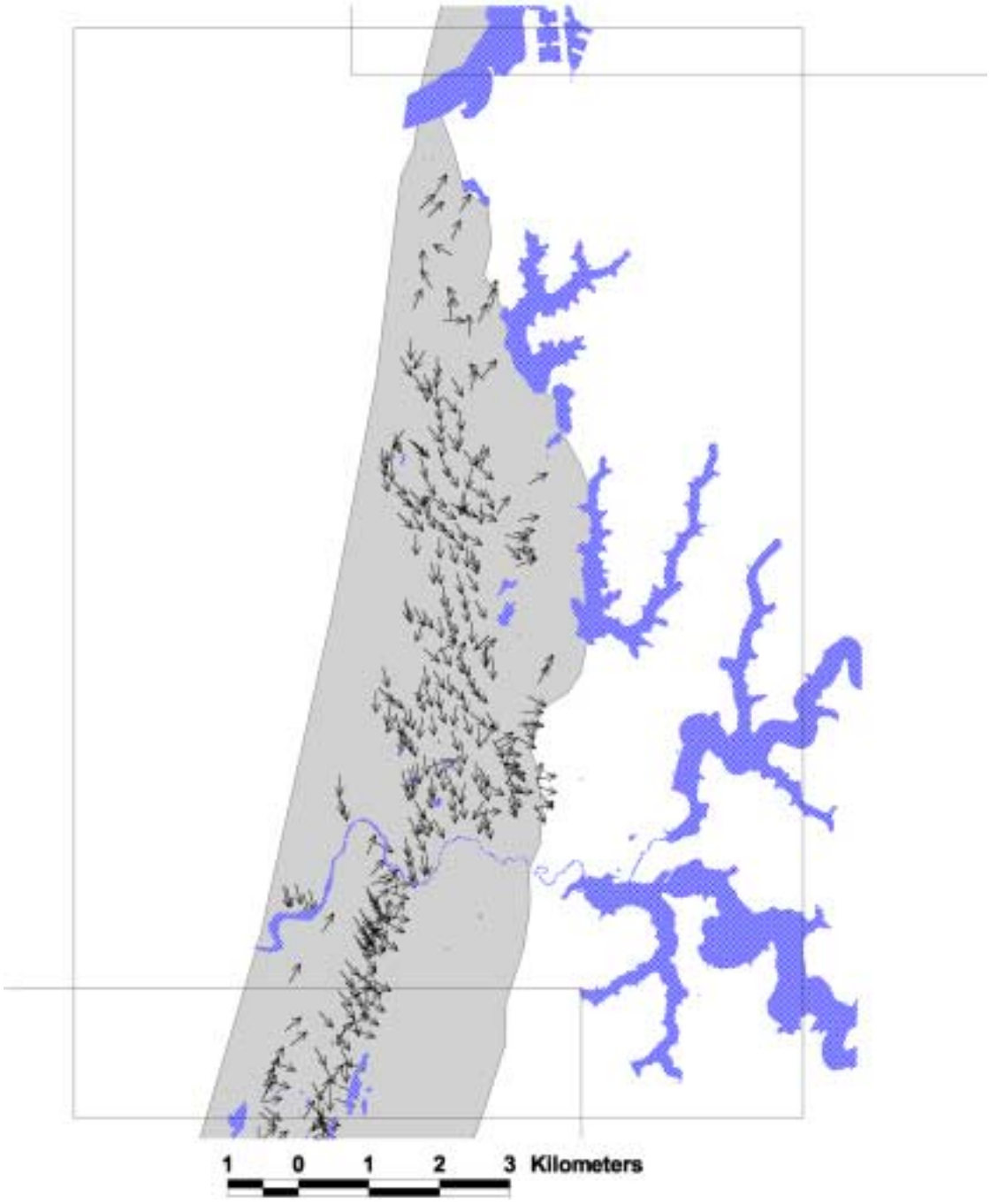

Sheet 4

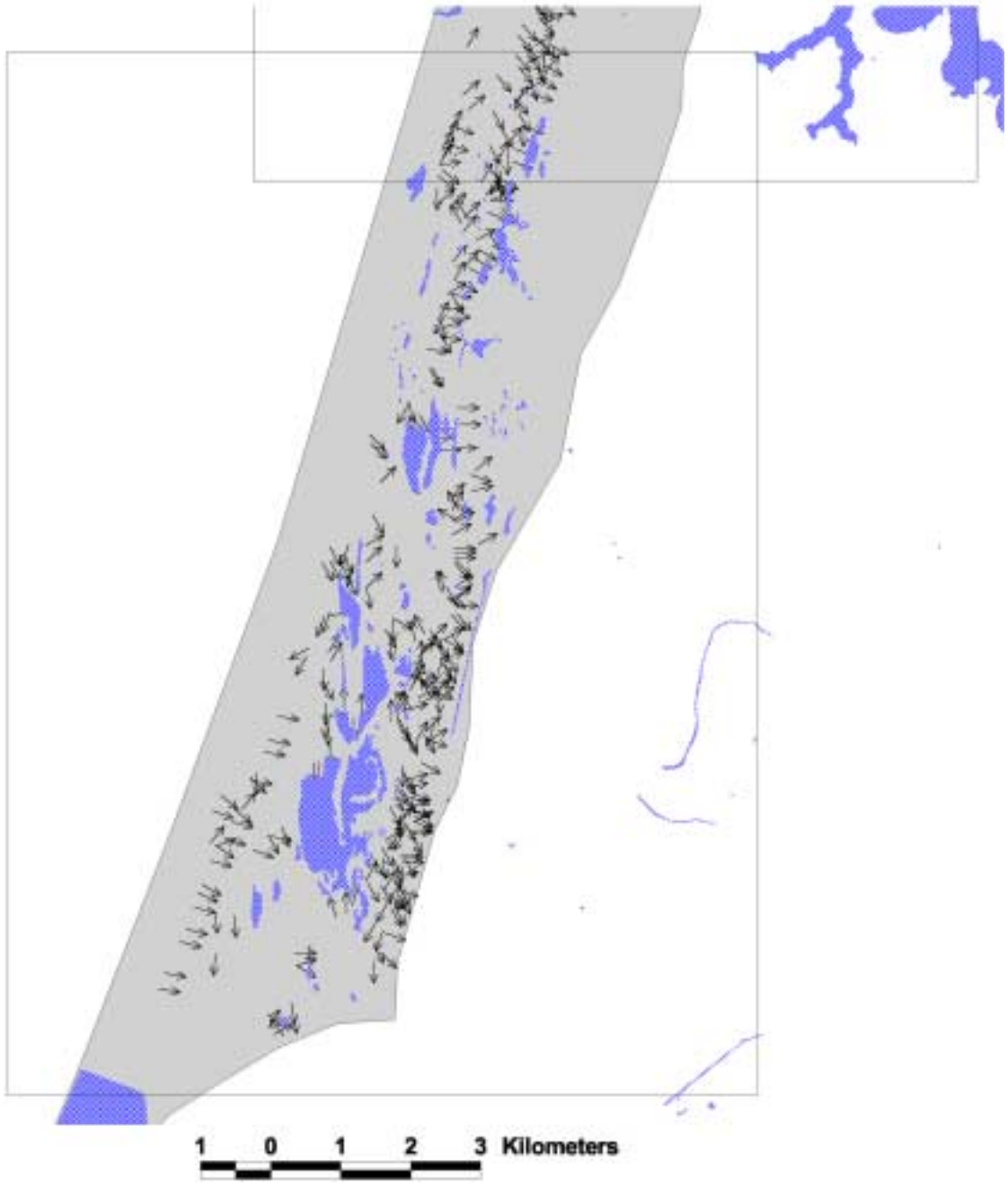

Sheet 5

Appendix C: Vibracore and solid stem auger logs and gradations

Vibracore (with grain size analyses) and solid stem auger stratigraphic columns

Core	Geographic position	Northing (m)	Easting (m)	Mean grain size top (mm)	Mean grain size bottom (mm)
SD1	Immediately behind foredune	4862442	407327	0.1223	0.1472
SD2	At the eastern edge of vegetated deflation plain	4861097	408360	0.1246	0.1220
SD3	At the mid-section of the deflation plane	4863749	408510	0.1189	0.1251
GP1	Near the front of the deflation plane	4867450	408650	0.1335	0.2493
GP2	Neat the rear of the deflation plane	4867450	408650	0.1225	0.1232

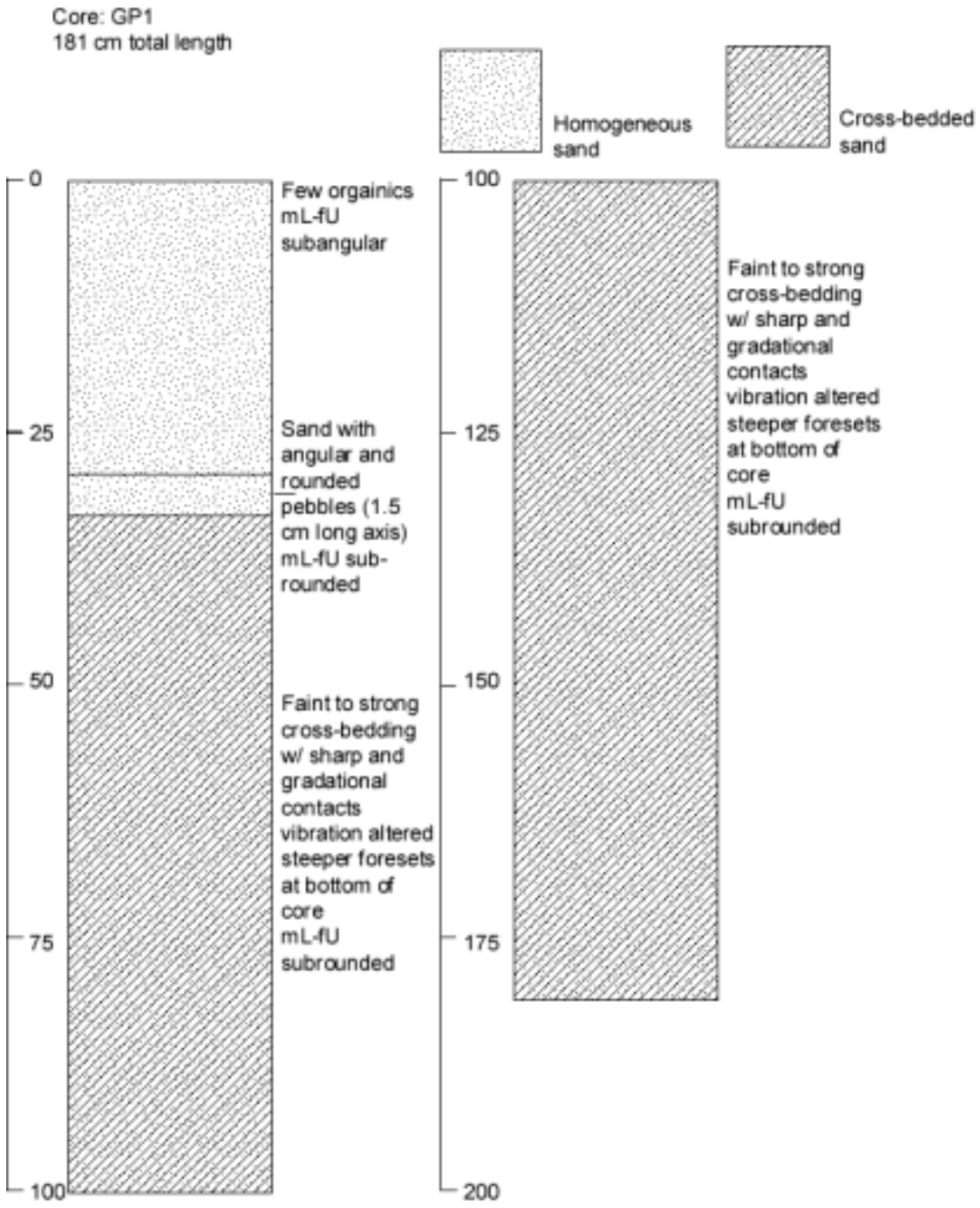
Core: GP1
181 cm total length
Homogeneous sand
Cross-bedded sand
0
25
50
75
100
Few orgainics mL-fU subangular
Sand with angular and rounded pebbles (1.5 cm long axis) mL-fU sub-rounded
Faint to strong cross-bedding w/ sharp and gradational contacts vibration altered steeper foresets at bottom of core mL-fU subrounded
100
125
150
175
200
Faint to strong cross-bedding w/ sharp and gradational contacts vibration altered steeper foresets at bottom of core mL-fU subrounded

Vibracore

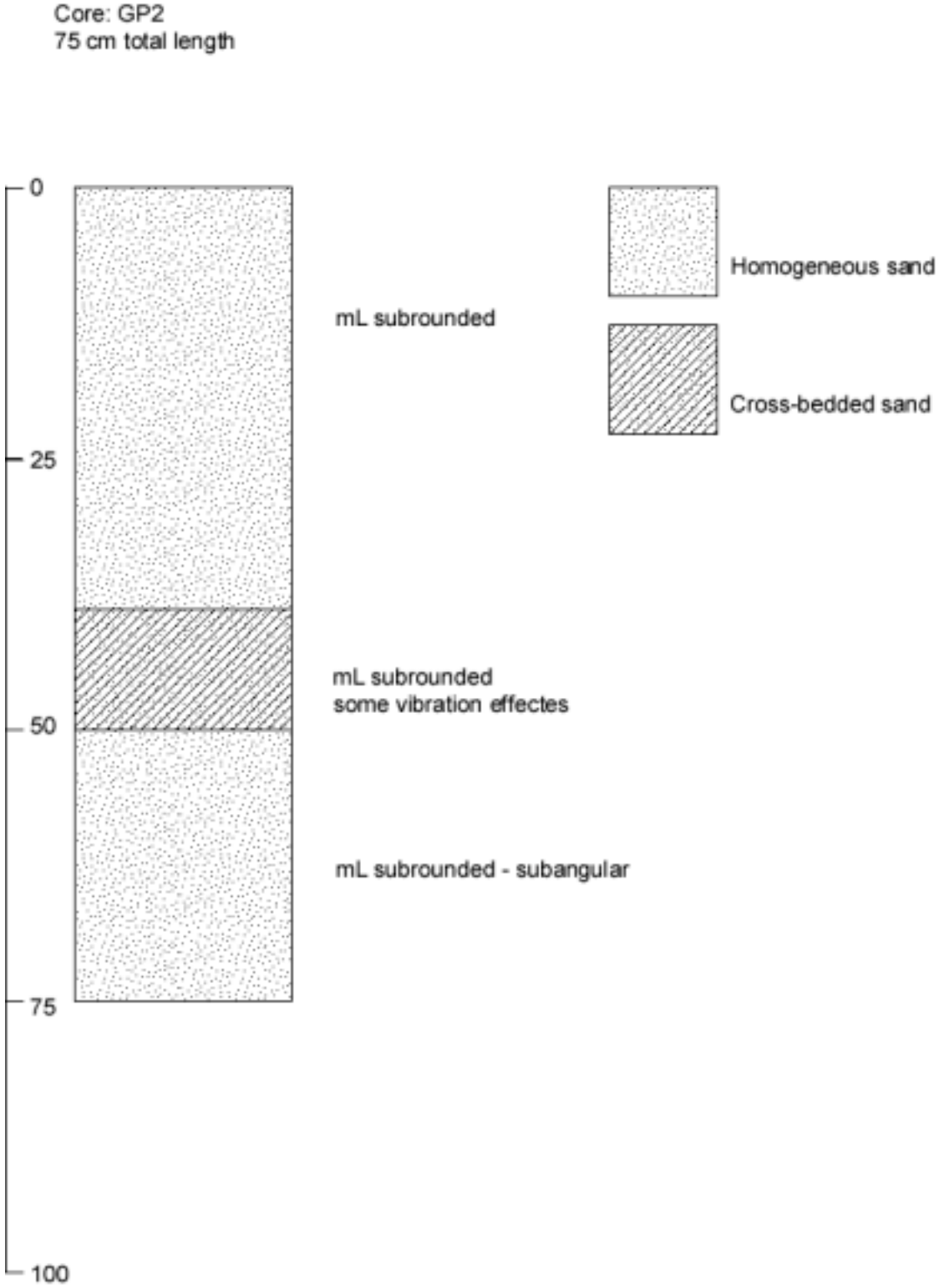
Core: GP2
75 cm total length
0
25
50
75
100
mL subrounded
mL subrounded
some vibration effectes
mL subrounded - subangular
Homogeneous sand
Cross-bedded sand
Vibracore

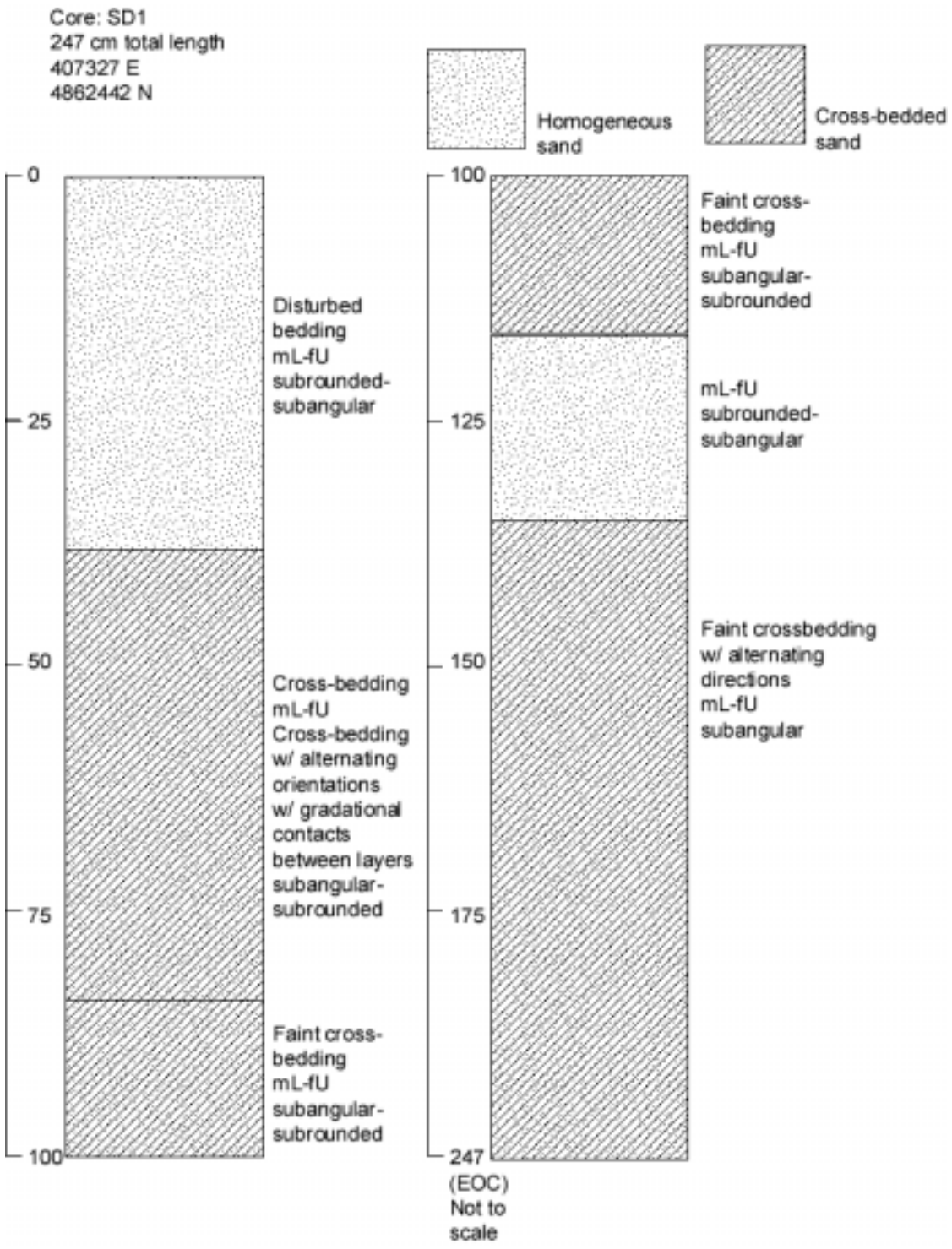
Core: SD1
247 cm total length
407327 E
4862442 N
Homogeneous sand
Cross-bedded sand
0
25
50
75
100
Disturbed bedding mL-fU subrounded-subangular
Cross-bedding mL-fU Cross-bedding w/ alternating orientations w/ gradational contacts between layers subangular-subrounded
Faint cross-bedding mL-fU subangular-subrounded
100
125
150
175
247
(EOC)
Not to scale
Faint cross-bedding mL-fU subangular-subrounded
mL-fU subrounded-subangular
Faint crossbedding w/ alternating directions mL-fU subangular

Vibracore

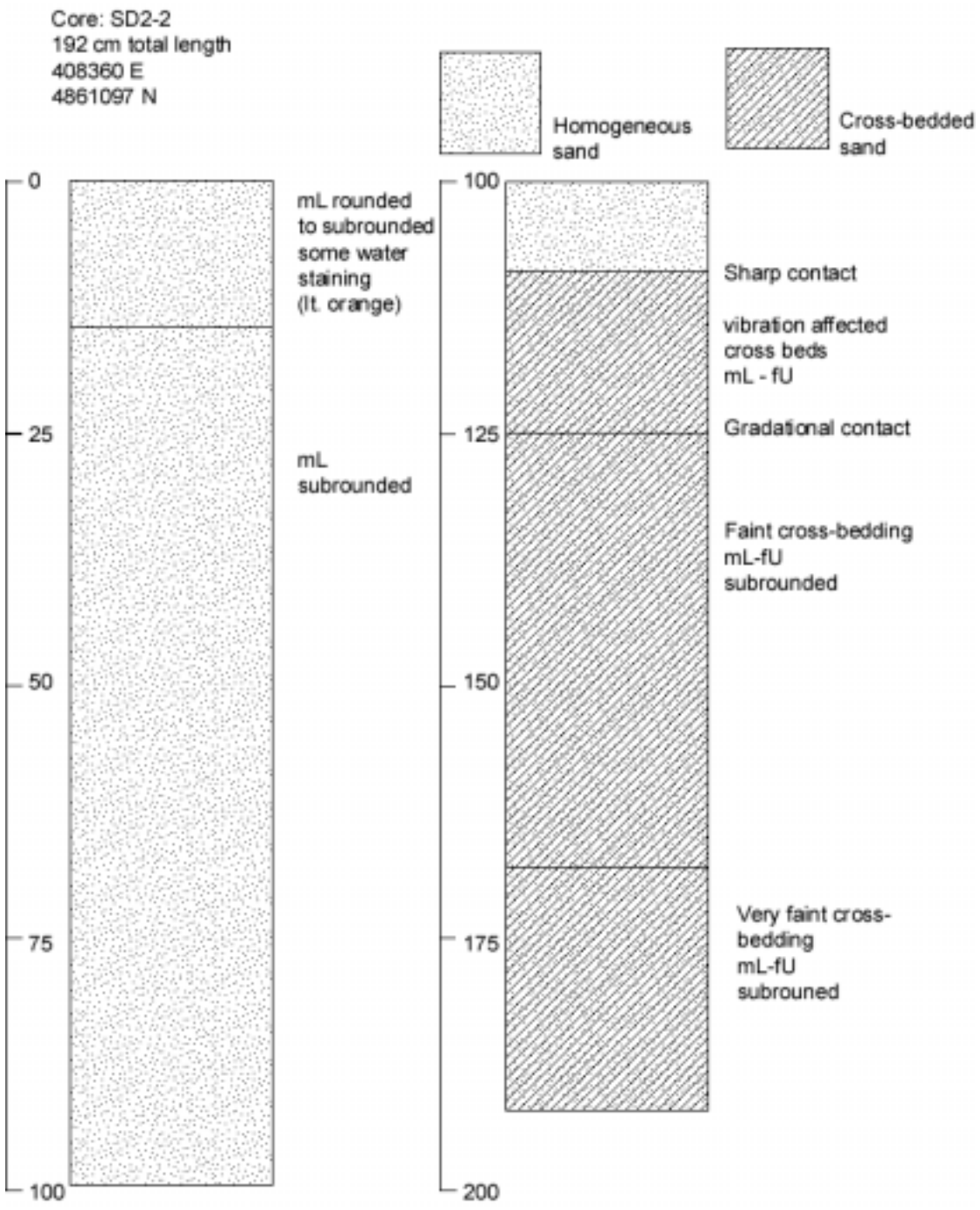
Core: SD2-2
192 cm total length
408360 E
4861097 N
Homogeneous sand
Cross-bedded sand
0
25
50
75
100
mL rounded to subrounded some water staining (lt. orange)
mL subrounded
100
125
150
175
200
Sharp contact
vibration affected cross beds mL - fU
Gradational contact
Faint cross-bedding mL-fU subrounded
Very faint cross-bedding mL-fU subrouned

Vibracore

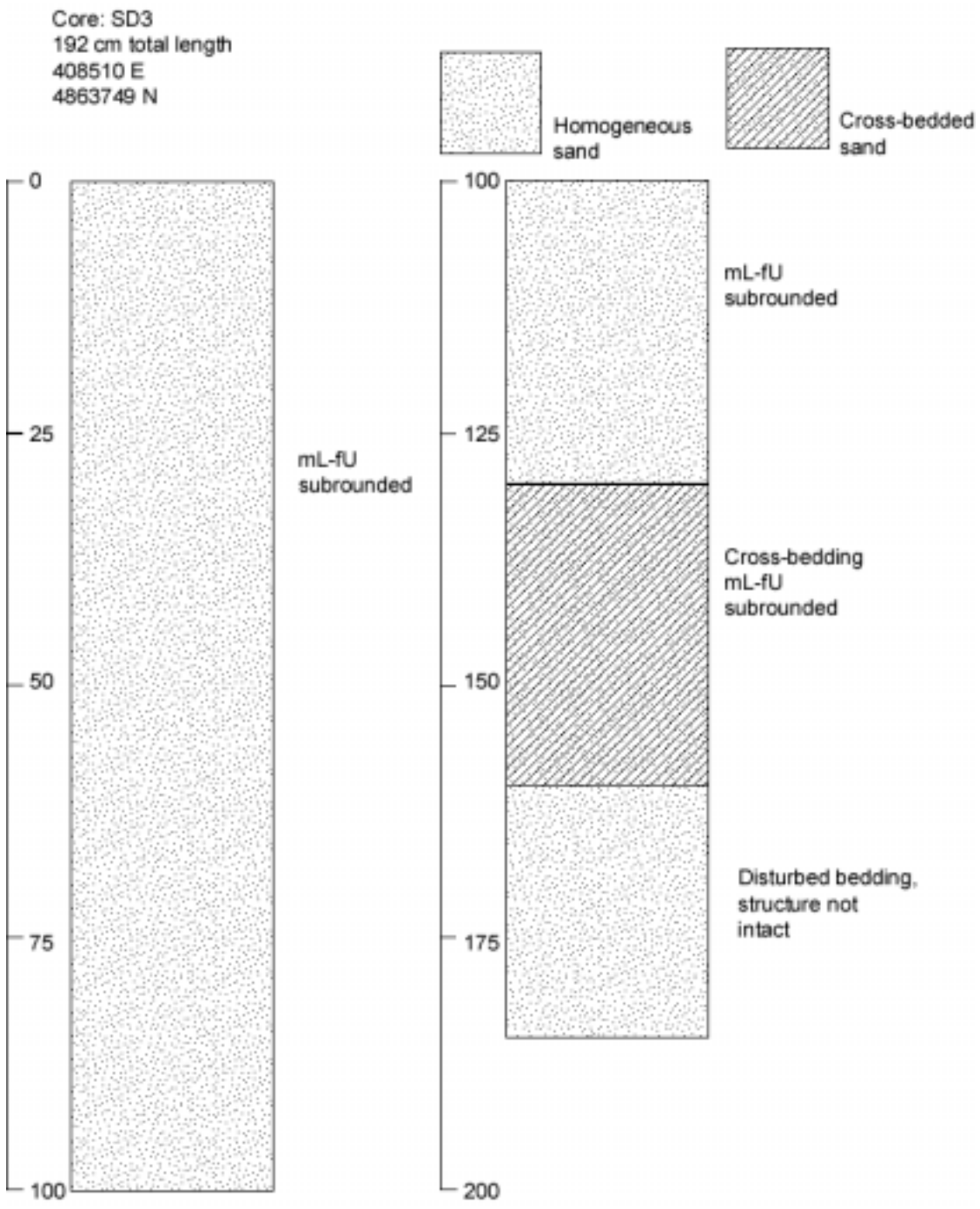
Core: SD3
192 cm total length
408510 E
4863749 N
Homogeneous sand
Cross-bedded sand
0
25
50
75
100
mL-fU subrounded
100
125
150
175
200
mL-fU subrounded
Cross-bedding mL-fU subrounded
Disturbed bedding, structure not intact

Vibracore

Core: GP-3a and GP-3b
Location: 4867418 N 409357 E elevation (m): 10
Drilling Method: Geoprobe 0-8.2 m depth, 4" Solid stem auger 8.2-10.7 m depth

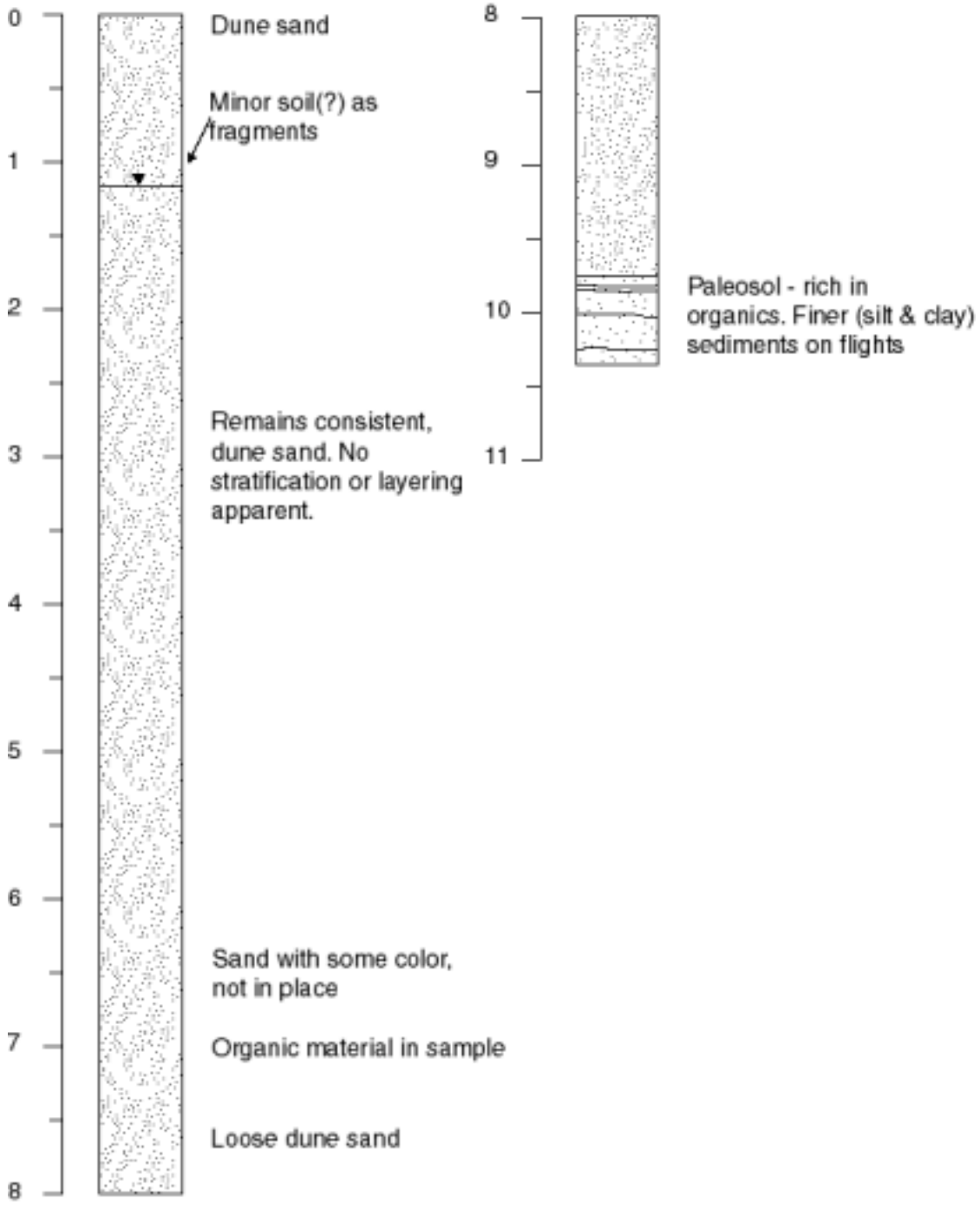

Core: GP-4
Location: 4867576 N 408459 E elevation (m): 1
Drilling Method: 4" Solid stem auger

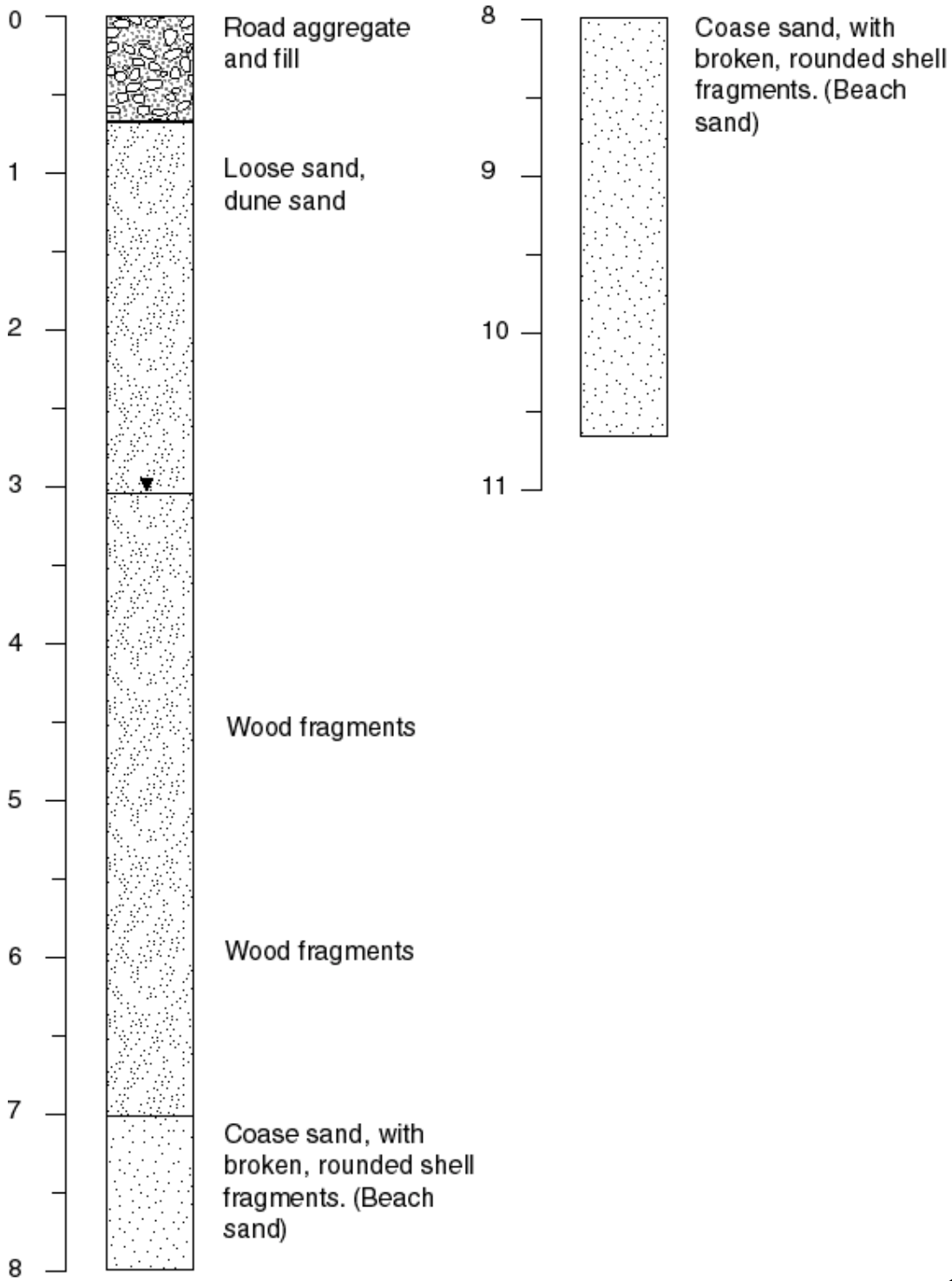

Core: UD-2
Location: 4831802 N 402328 E elevation (m): 3
Drilling Method: 4" Solid stem auger

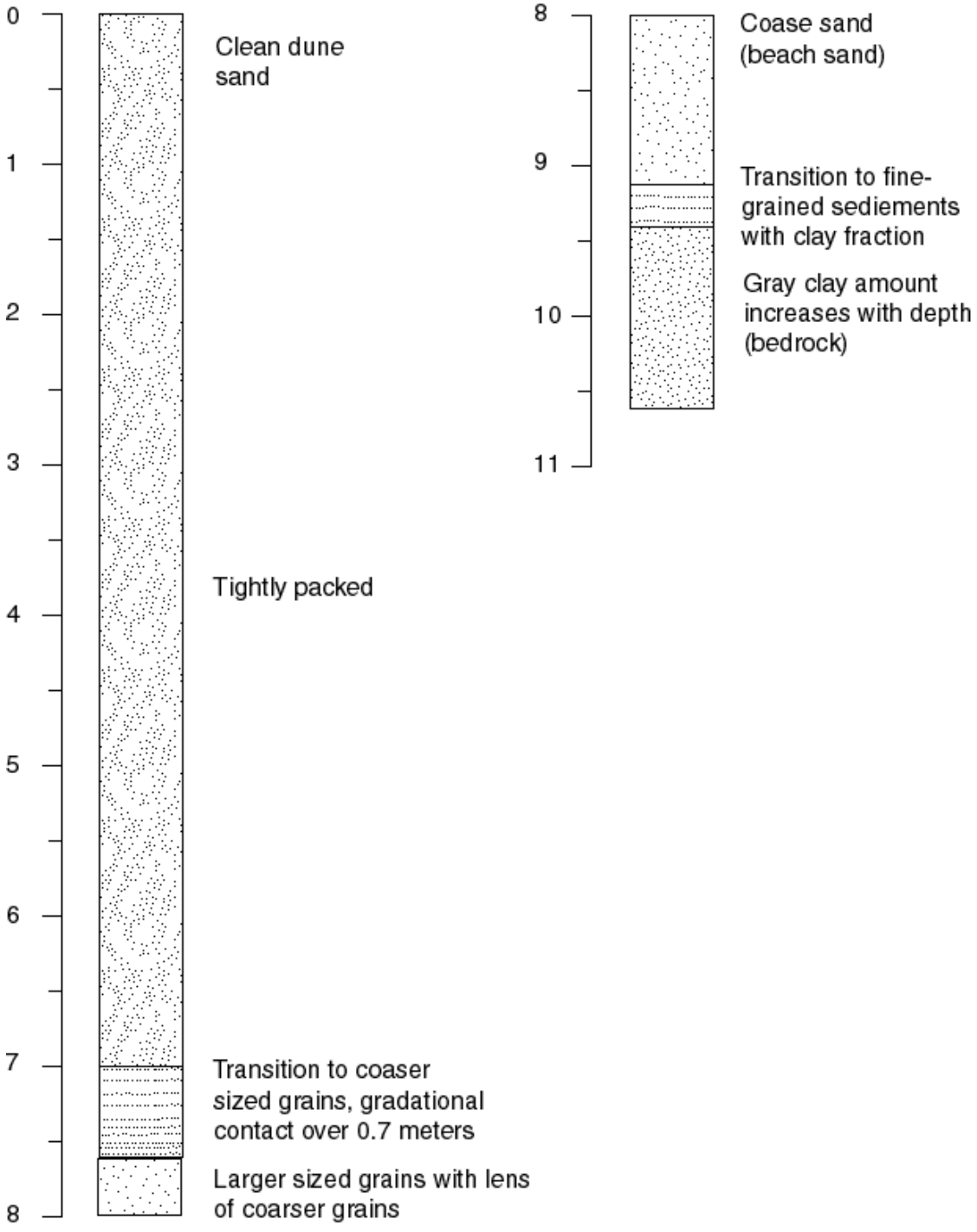

Appendix D: Well logs and interpretive stratigraphic columns

State well number	Address	Easting	Northing	Elevation (m)	Depth of sand (m)	Elevation of contact (m)
LANE 52262	90241 Hwy 101, Florence	411511	4881791	21.4	0.0	21.4

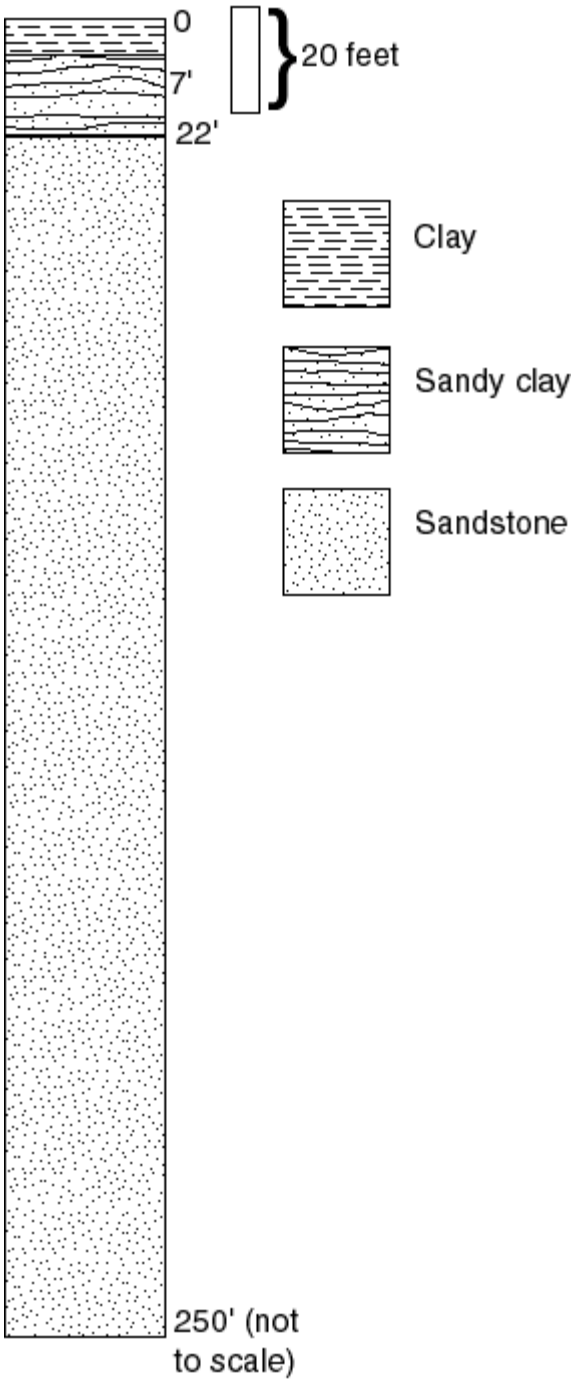

State well number	Address	Easting	Northing	Elevation (m)	Depth of sand (m)	Elevation of contact (m)
LANE 019232	**Siuslaw W. 30th St., Florence**	**411364**	**4871404**	**20.6**	**37.8**	**-17.2**

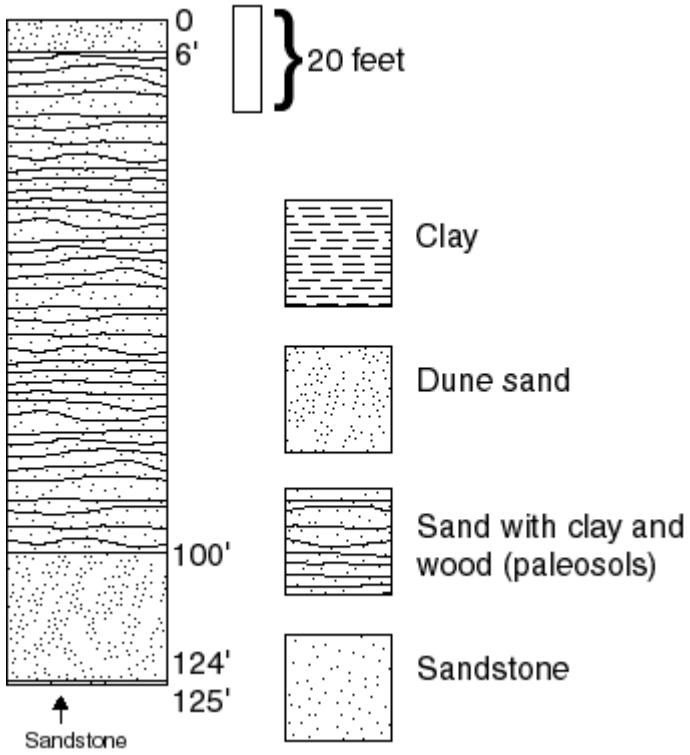

State well number	Address	Easting	Northing	Elevation (m)	Depth of sand (m)	Elevation of contact (m)
LANE 5526	City of Florence well field, 28th and Willow	412496	4871024	14.4	41.7	-27.3

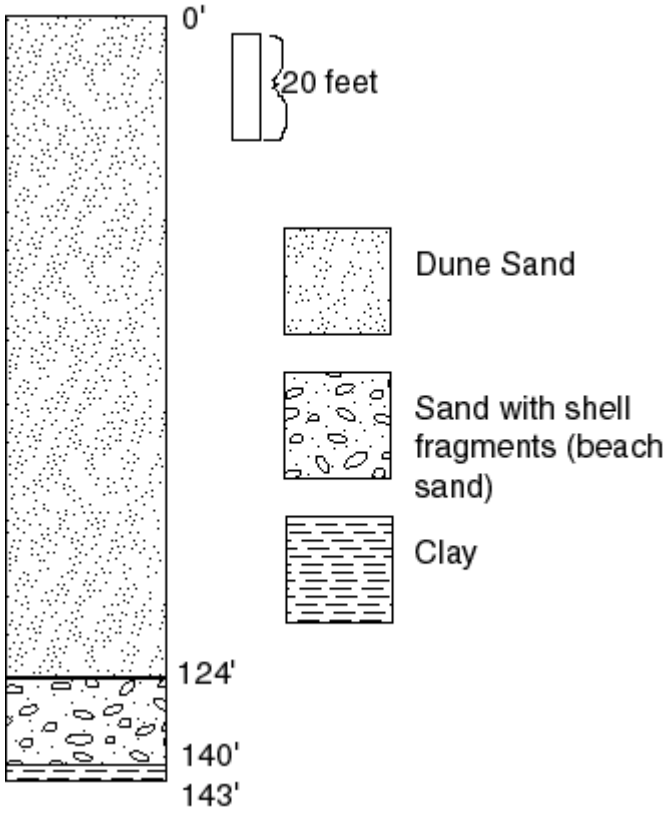

State well number	Address	Easting	Northing	Elevation (m)	Depth of sand (m)	Elevation of contact (m)
LANE 2384	85339 Glenada Rd, Florence	412224	4867010	59.4	28.3	31.1

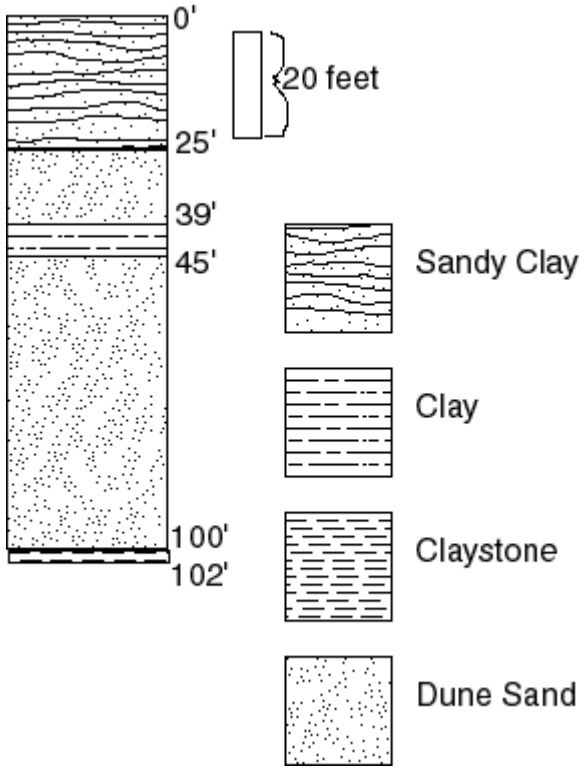

State well number	Address	Easting	Northing	Elevation (m)	Depth of sand (m)	Elevation of contact (m)
LANE 2393	05285 Harvard, Florence	411942	4866851	51.1	29.0	22.2

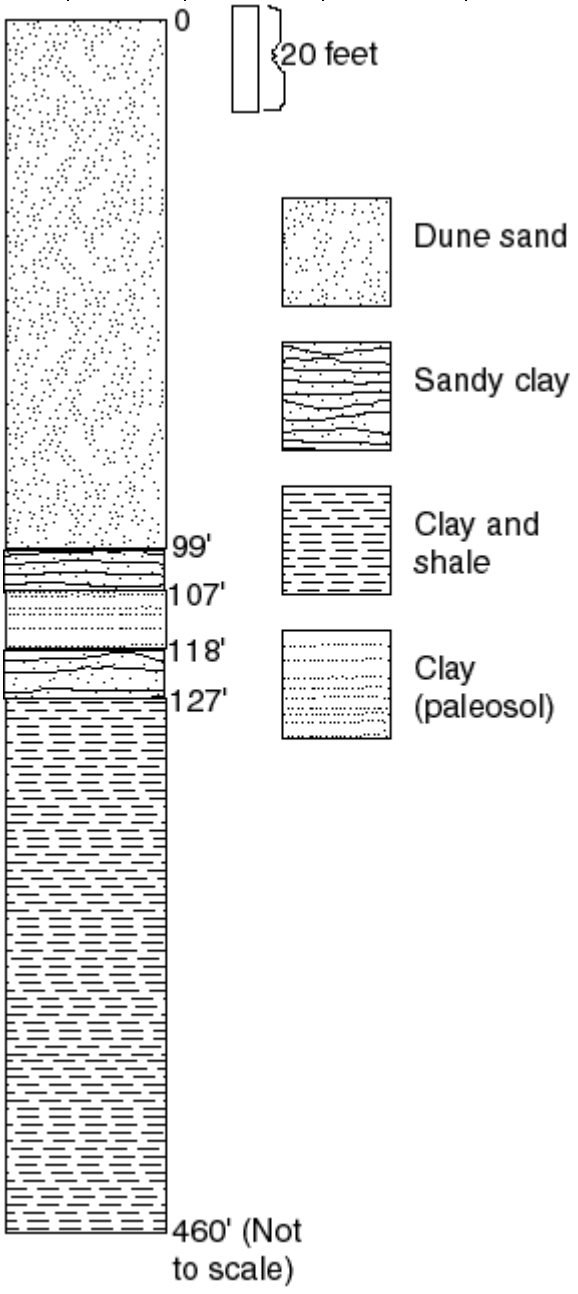

State well number	Address	Easting	Northing	Elevation (m)	Depth of sand (m)	Elevation of contact (m)
LANE 021565	83627 Clear Lake Road, Florence	412120	4861750	37.8	12.2	25.6

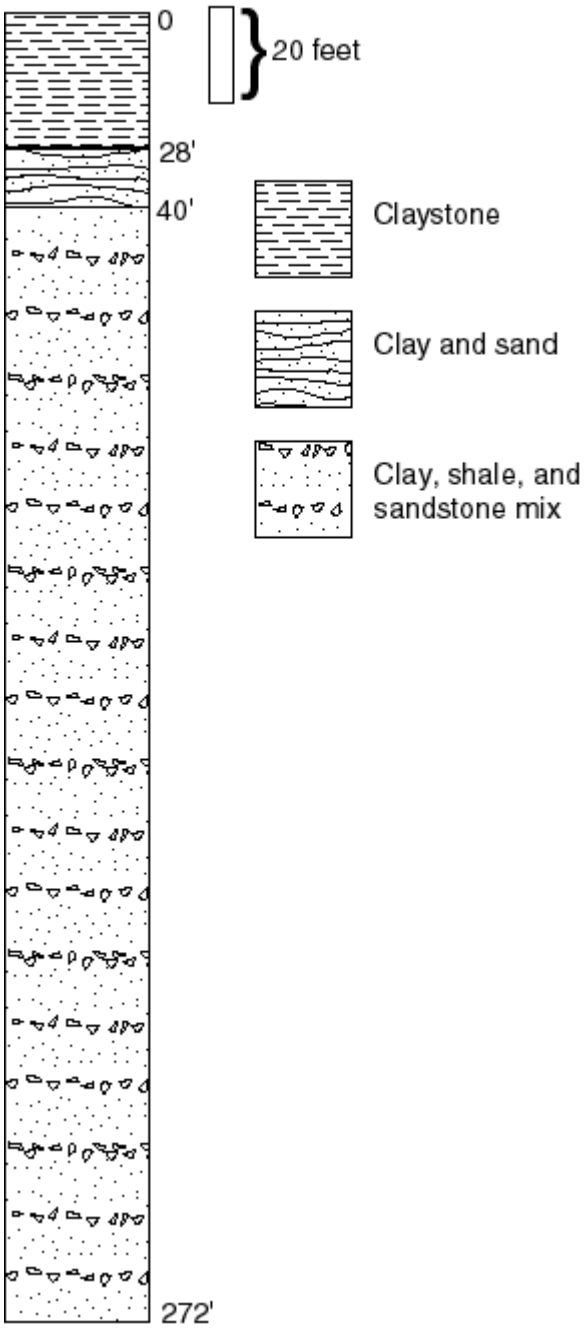

State well number	Address	Easting	Northing	Elevation (m)	Depth of sand (m)	Elevation of contact (m)
DOUG 2026	Oregon Dunes Overlook well	407589	4854029	41.2	48.2	-6.9

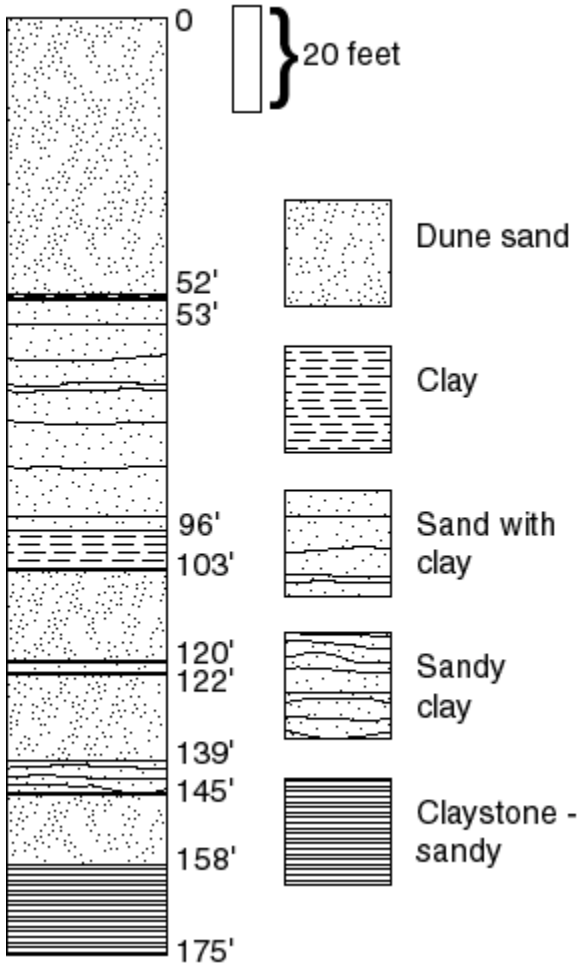

State well number	Address	Easting	Northing	Elevation (m)	Depth of sand (m)	Elevation of contact (m)
DOUG 2029	Tahkenitch Lake Campground	407647	4849686	10.9	12.8	-1.9

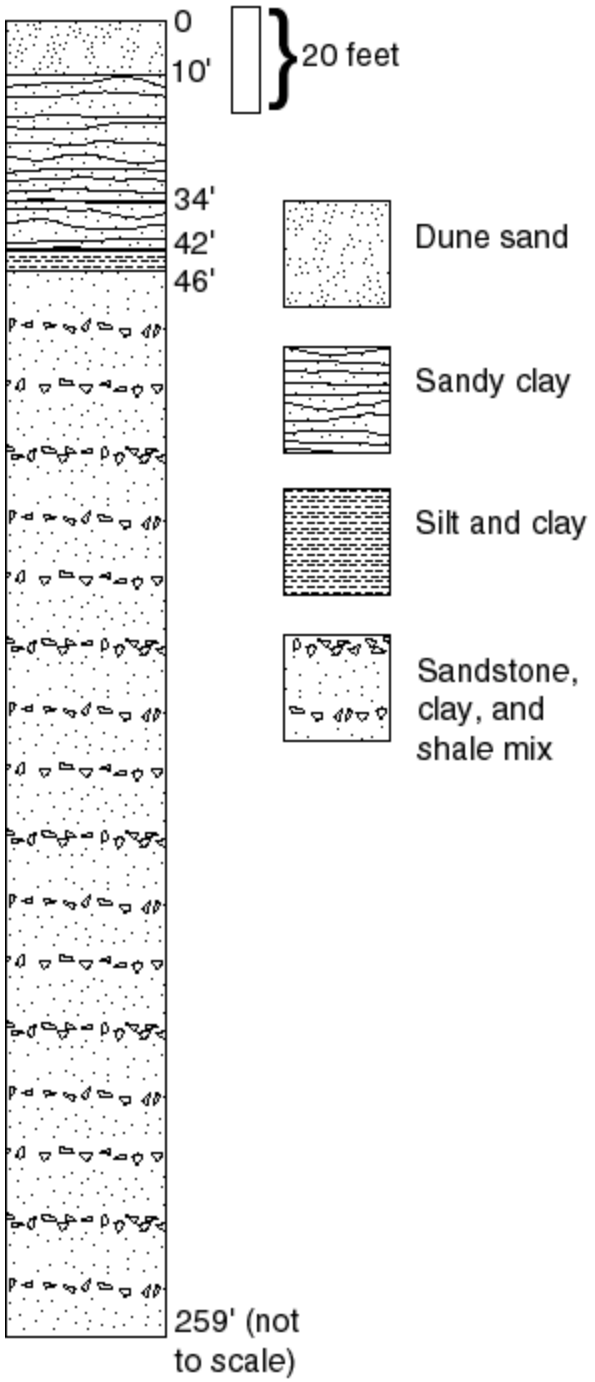

State well number	Address	Easting	Northing	Elevation (m)	Depth of sand (m)	Elevation of contact (m)
DOUG 1703	598½ Evergreen, Reedsport	408585	4839750	16.1	0.0	16.1

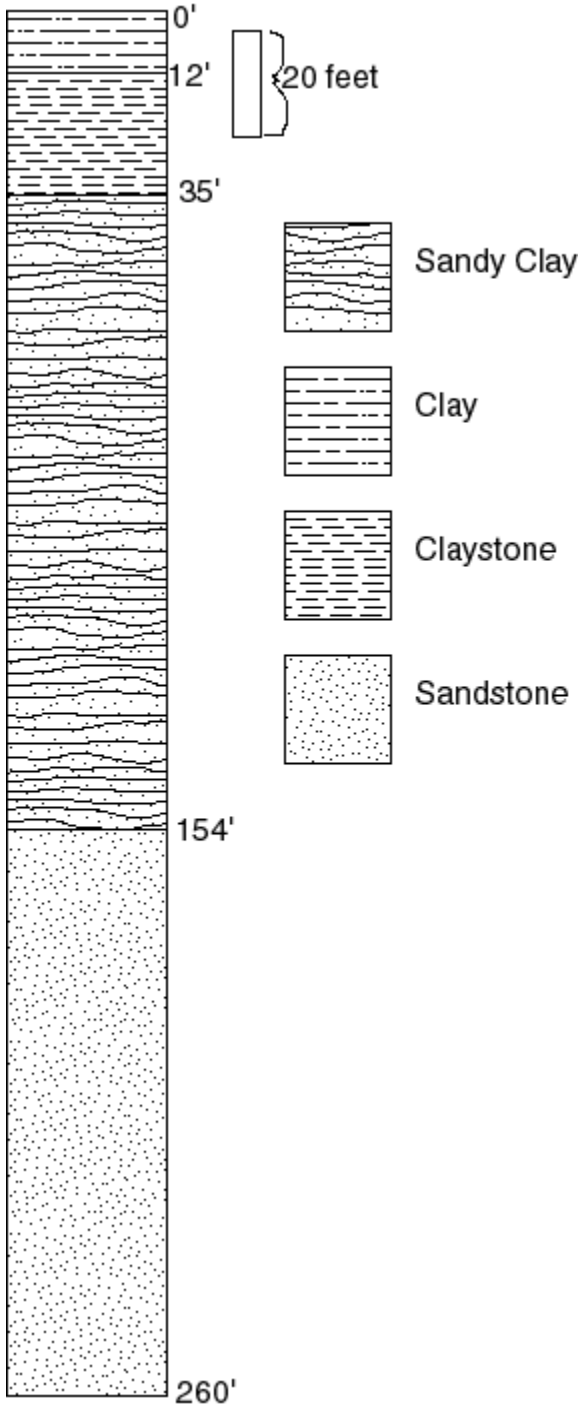

State well number	Address	Easting	Northing	Elevation (m)	Depth of sand (m)	Elevation of contact (m)
DOUG 10060	12912 Wildwood Dr., N. Bend	404642	4830770	82.9	29.0	54.0

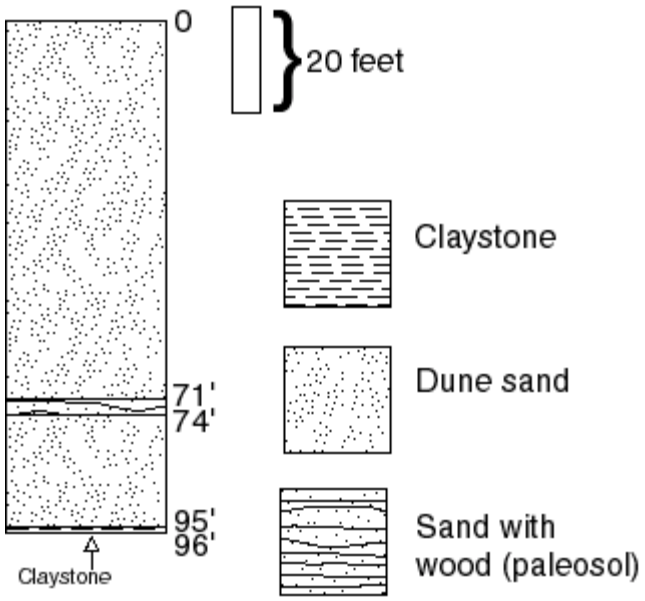

State well number	Address	Easting	Northing	Elevation (m)	Depth of sand (m)	Elevation of contact (m)
DOUG 2979	12830 Wildwood Dr. N. Bend	404573	4830622	73.9	0.0	73.9

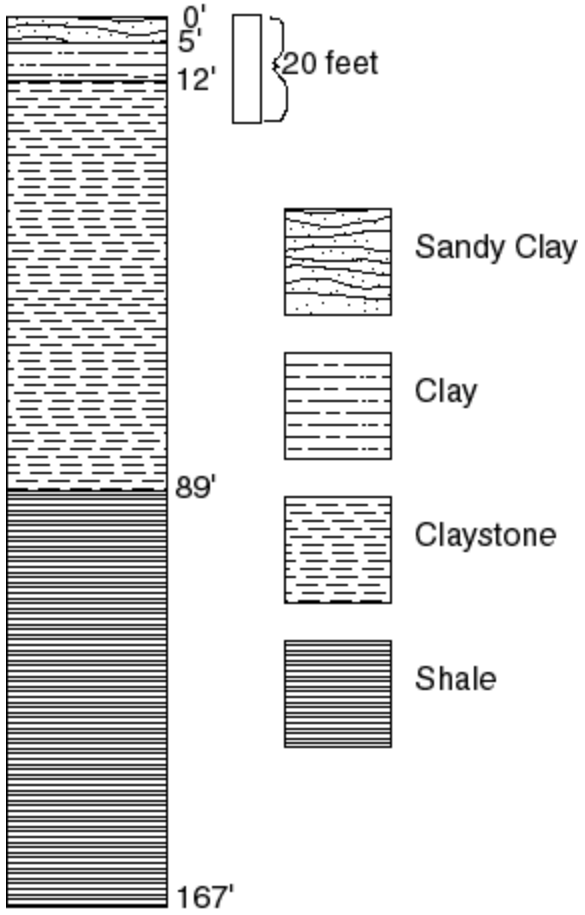

State well number	Address	Easting	Northing	Elevation (m)	Depth of sand (m)	Elevation of contact (m)
DOUG 50103	12671 Wildwood Dr. N. Bend	404661	4830354	66.2	4.6	61.7

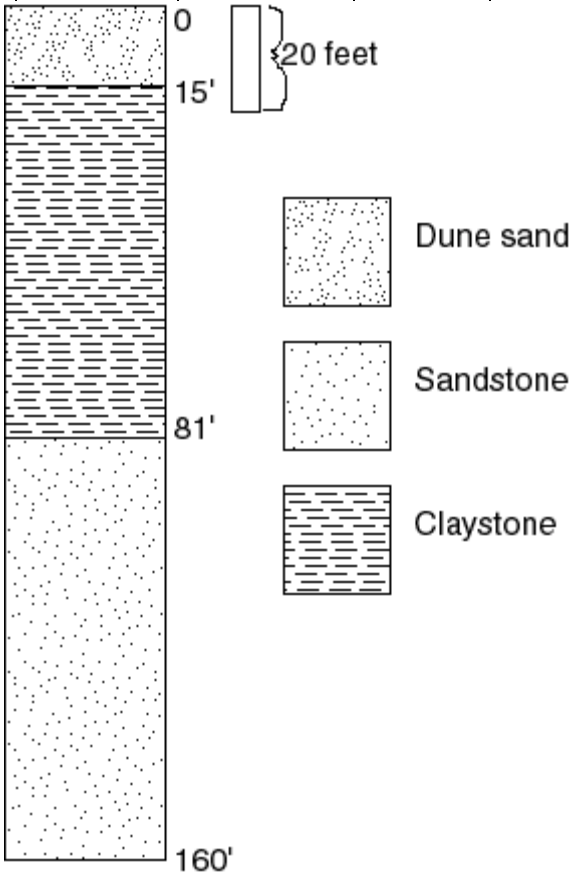

State well number	Address	Easting	Northing	Elevation (m)	Depth of sand (m)	Elevation of contact (m)
DOUG 50103	12671 Wildwood Dr. N. Bend	404661	4830354	66.2	4.6	61.7

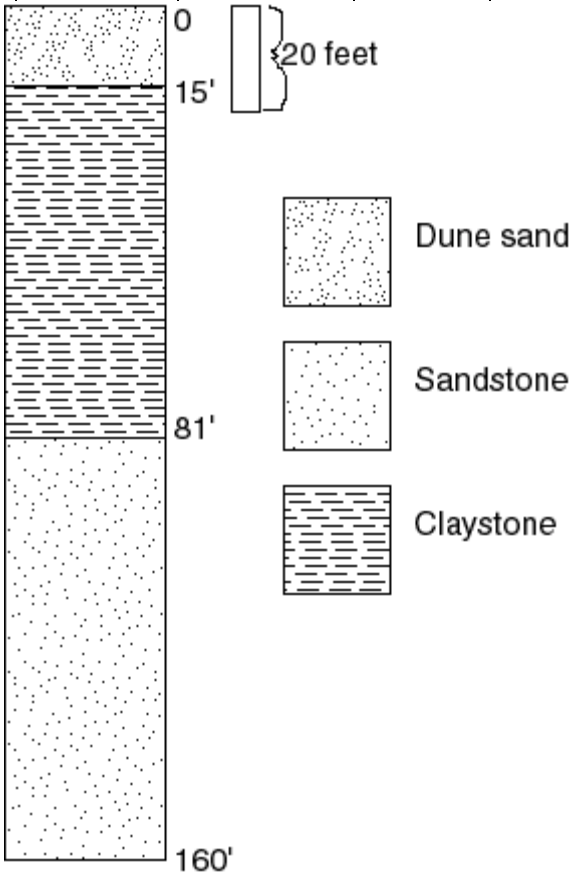

State well number	Address	Easting	Northing	Elevation (m)	Depth of sand (m)	Elevation of contact (m)
COOS 1438	623 Clifton Ct. N. Bend	403046	4824001	45.0	2.4	42.6

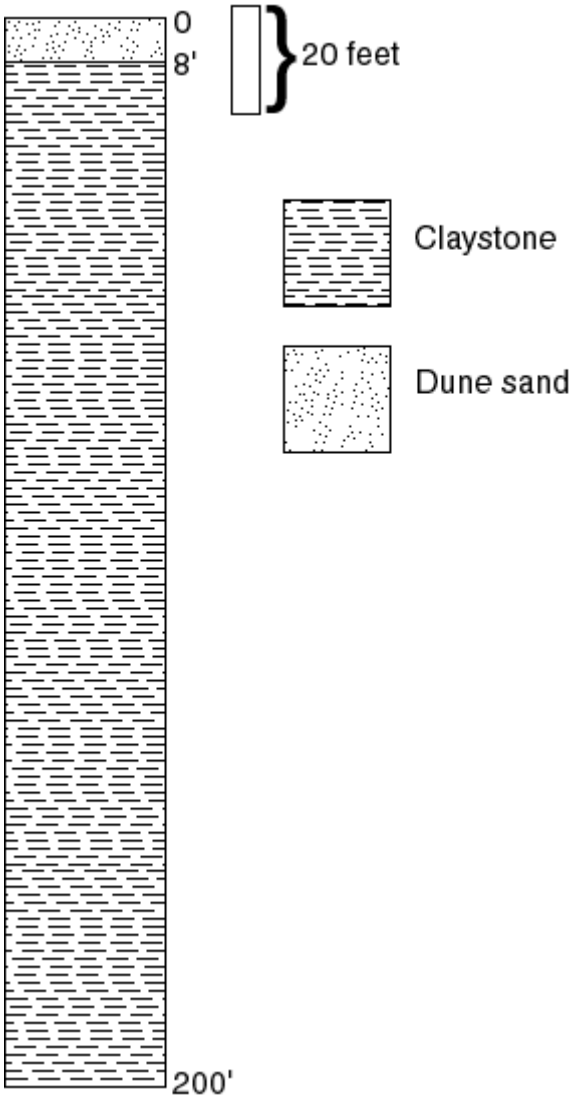

State well number	Address	Easting	Northing	Elevation (m)	Depth of sand (m)	Elevation of contact (m)
COOS 237	7791 Wildwood Rd. N Bend	402488	4822270	36.8	>29.0	<7.6

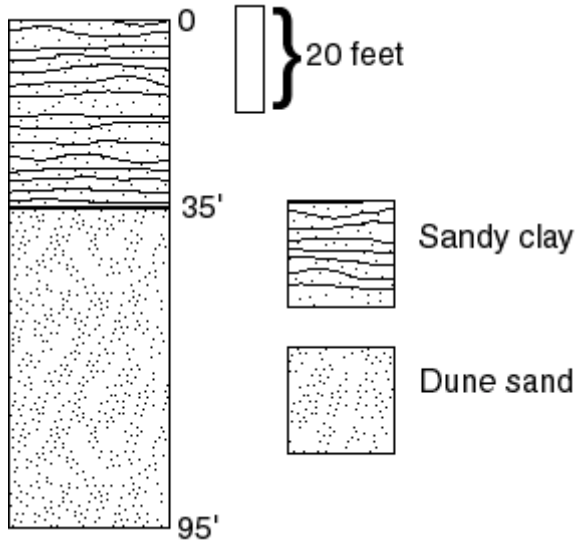

State well number	Address	Easting	Northing	Elevation (m)	Depth of sand (m)	Elevation of contact (m)
COOS 50069	7723 Wildwood Dr. N. Bend	402465	4822211	36.5	0.0	36.3

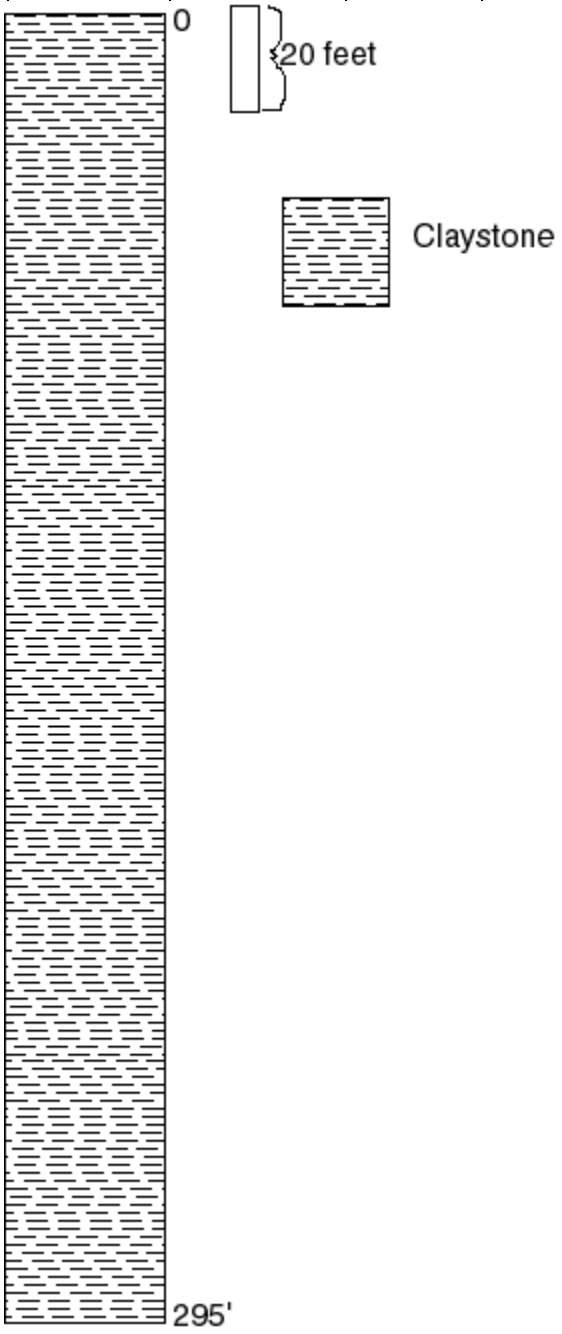

State well number	Address	Easting	Northing	Elevation (m)	Depth of sand (m)	Elevation of contact (m)
COOS 1004	7400 Wildwood Dr. N. Bend	402629	4821573	79.2	0.6	78.6

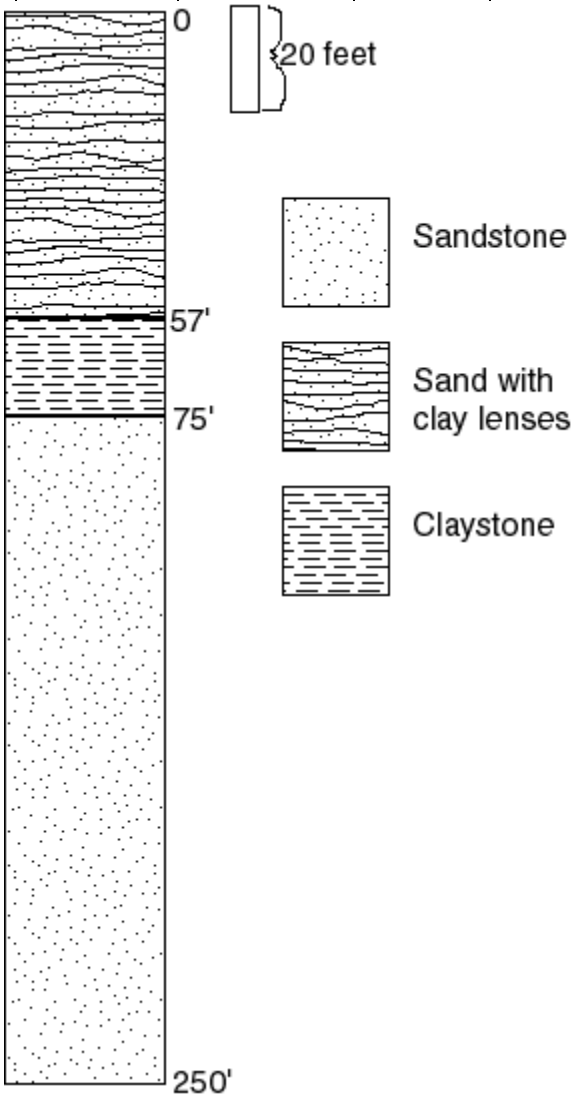

State well number	Address	Easting	Northing	Elevation (m)	Depth of sand (m)	Elevation of contact (m)
COOS 4641	723 Stage Rd. N. Bend	402735	4819699	94.2	3.7	90.5

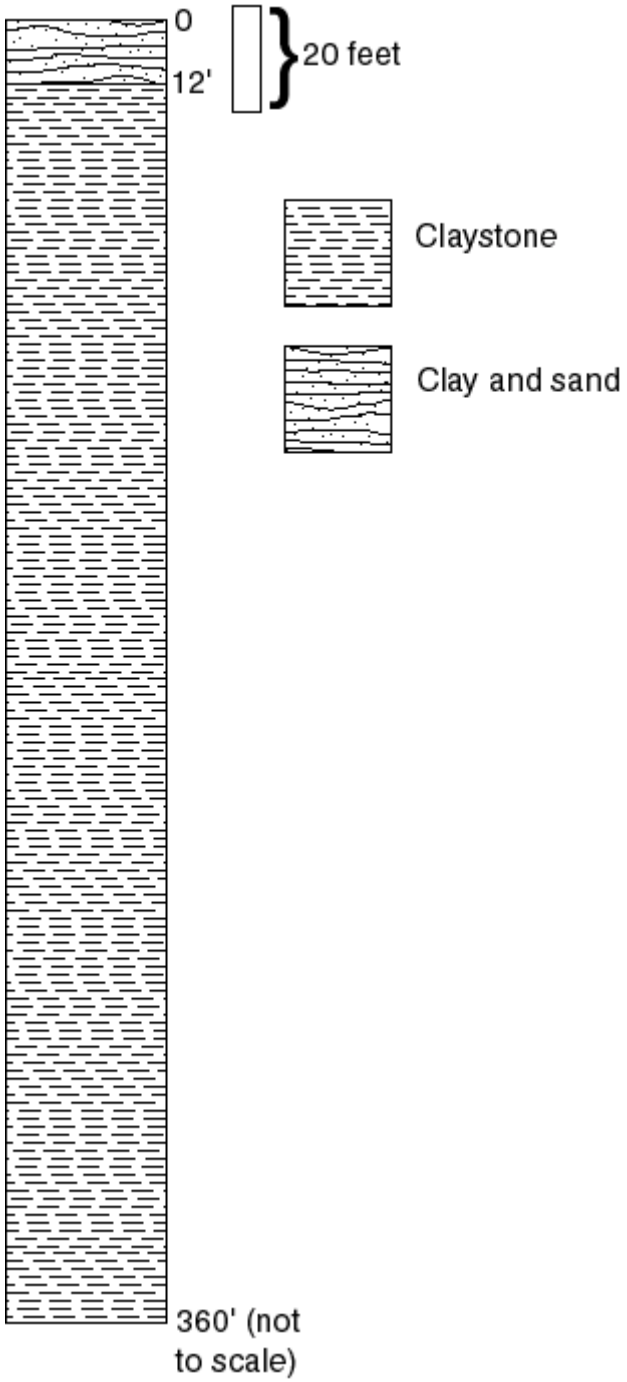

State well number	Address	Easting	Northing	Elevation (m)	Depth of sand (m)	Elevation of contact (m)
COOS 1480	228 Circle Dr. N. Bend	401348	4819666	31.6	>15.8	<15.5

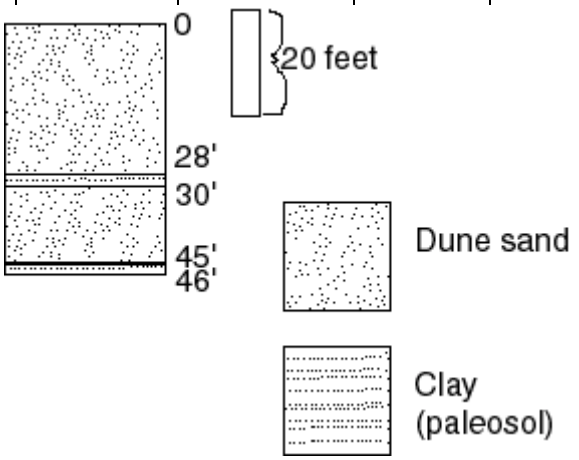

State well number	Address	Easting	Northing	Elevation (m)	Depth of sand (m)	Elevation of contact (m)
COOS 942	4401 Charlotte Ln. N. Bend	401236	4817657	32.4	31.1	1.2

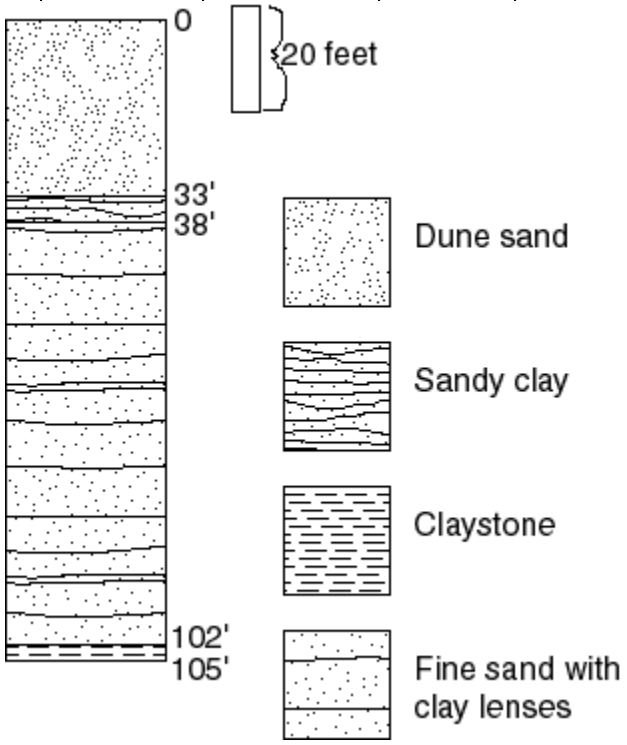

State well number	Address	Easting	Northing	Elevation (m)	Depth of sand (m)	Elevation of contact (m)
COOS 50990	4377 Wildwood Dr. N. Bend	401768	4817150	9.9	>9.9	0

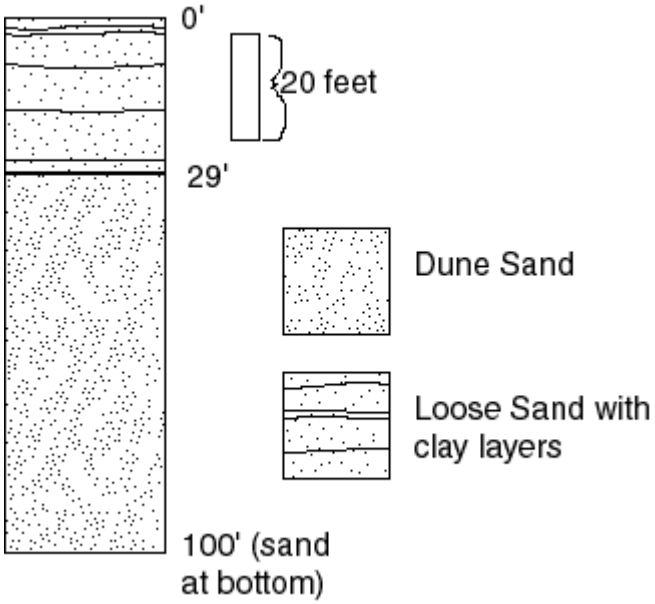

State well number	Address	Easting	Northing	Elevation (m)	Depth of sand (m)	Elevation of contact (m)
COOS 614	Wildmare CG, FS southern dune area Well field well #48	397860	4811415	none	7.6	none

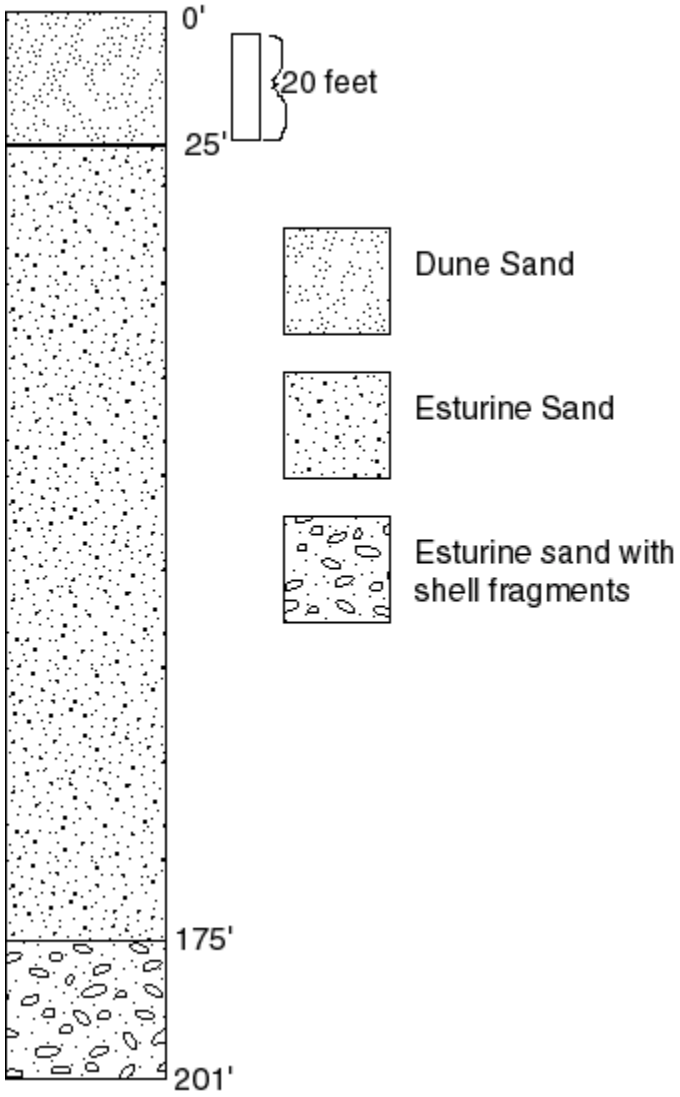

Appendix E: X-Ray diffraction patterns

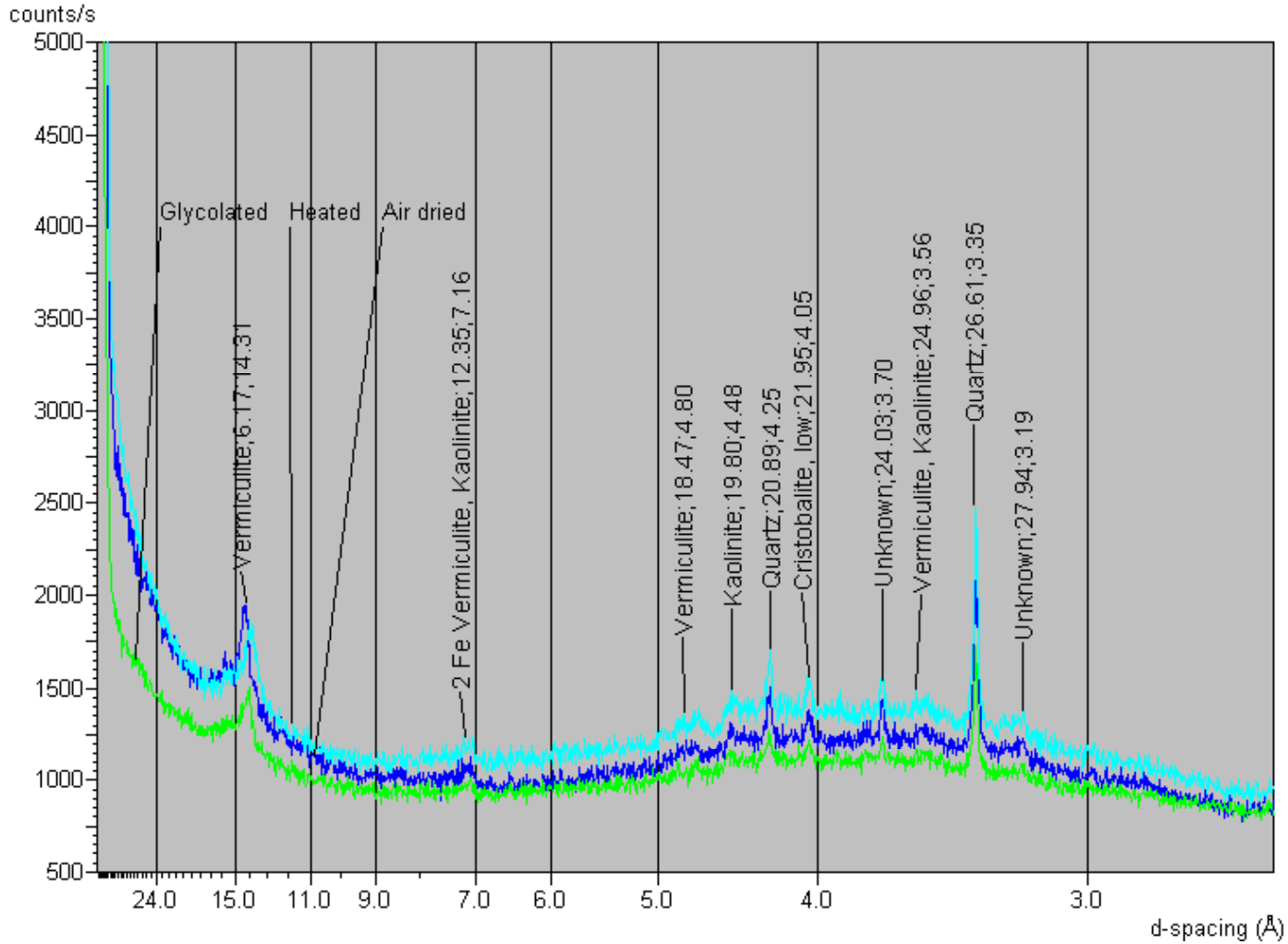

Core: **SP1** UTM Coordinates: **4844150 N 406080 E** Depth: **150 cm**

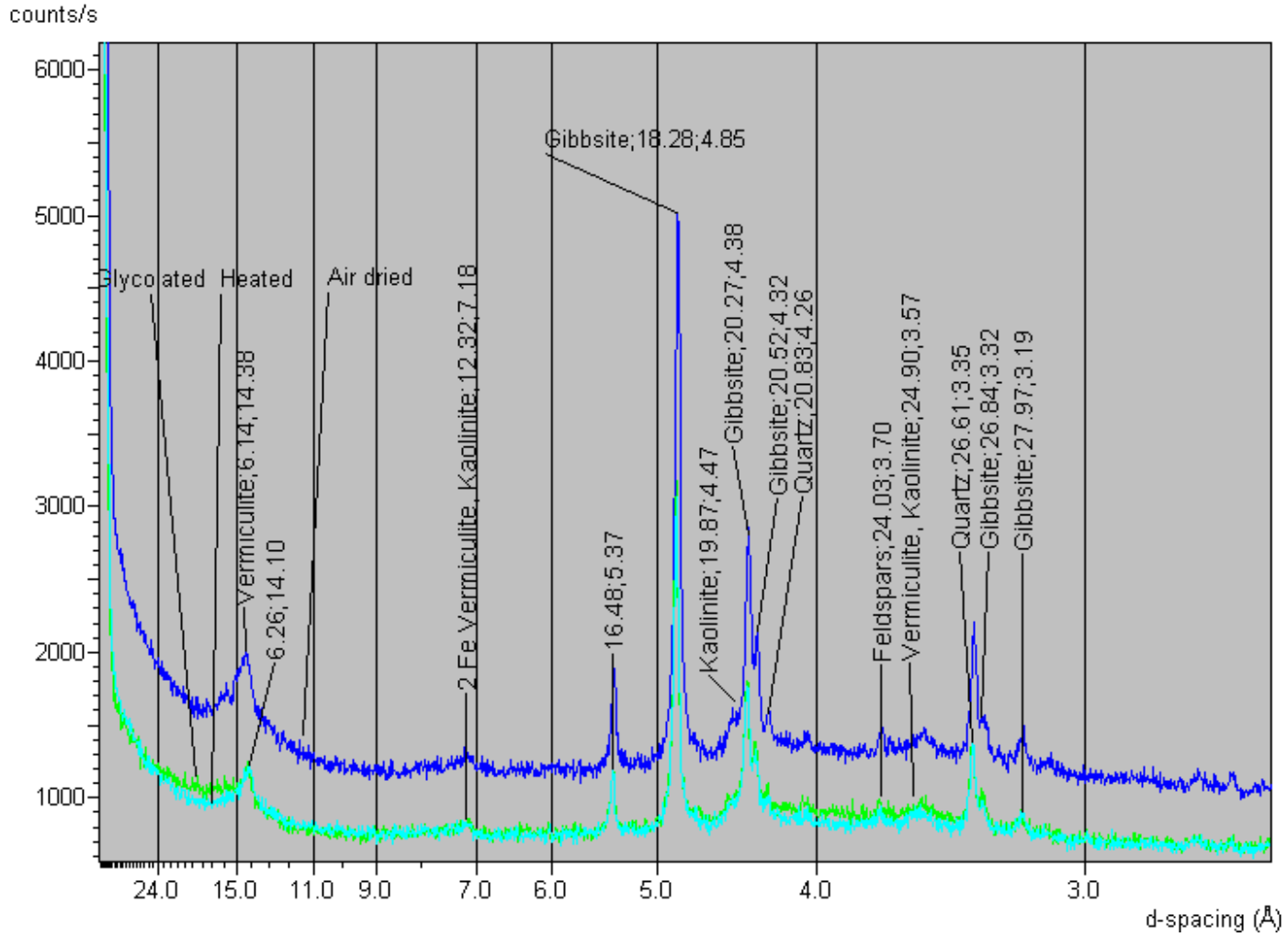

Core: **JN1** UTM Coordinates: **4800020 N 396390 E** Depth: **80 cm**

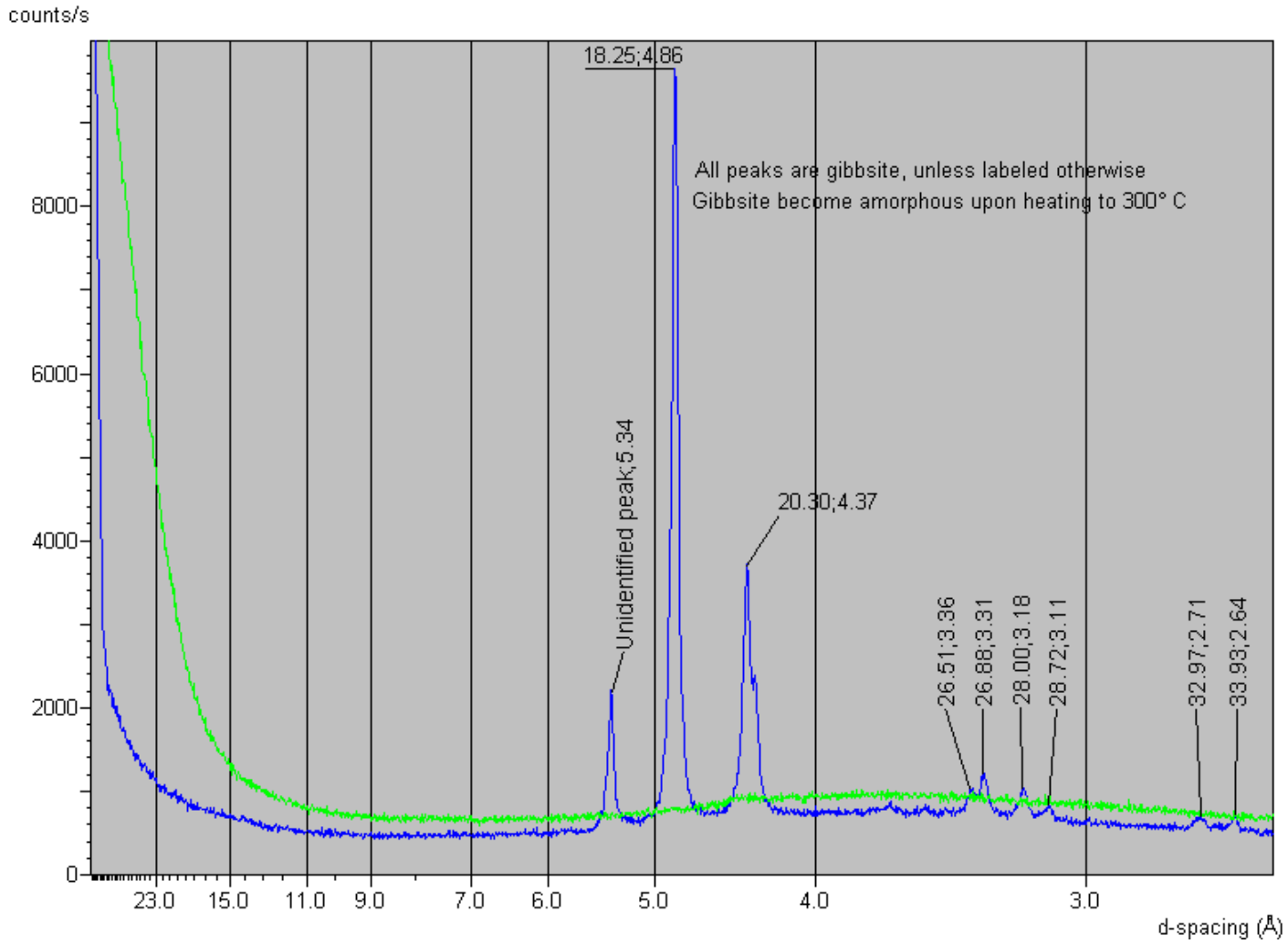

Core: **ME1**, White nodules UTM Coordinates: **4877280 N 414120 E** Depth: **~300 cm**

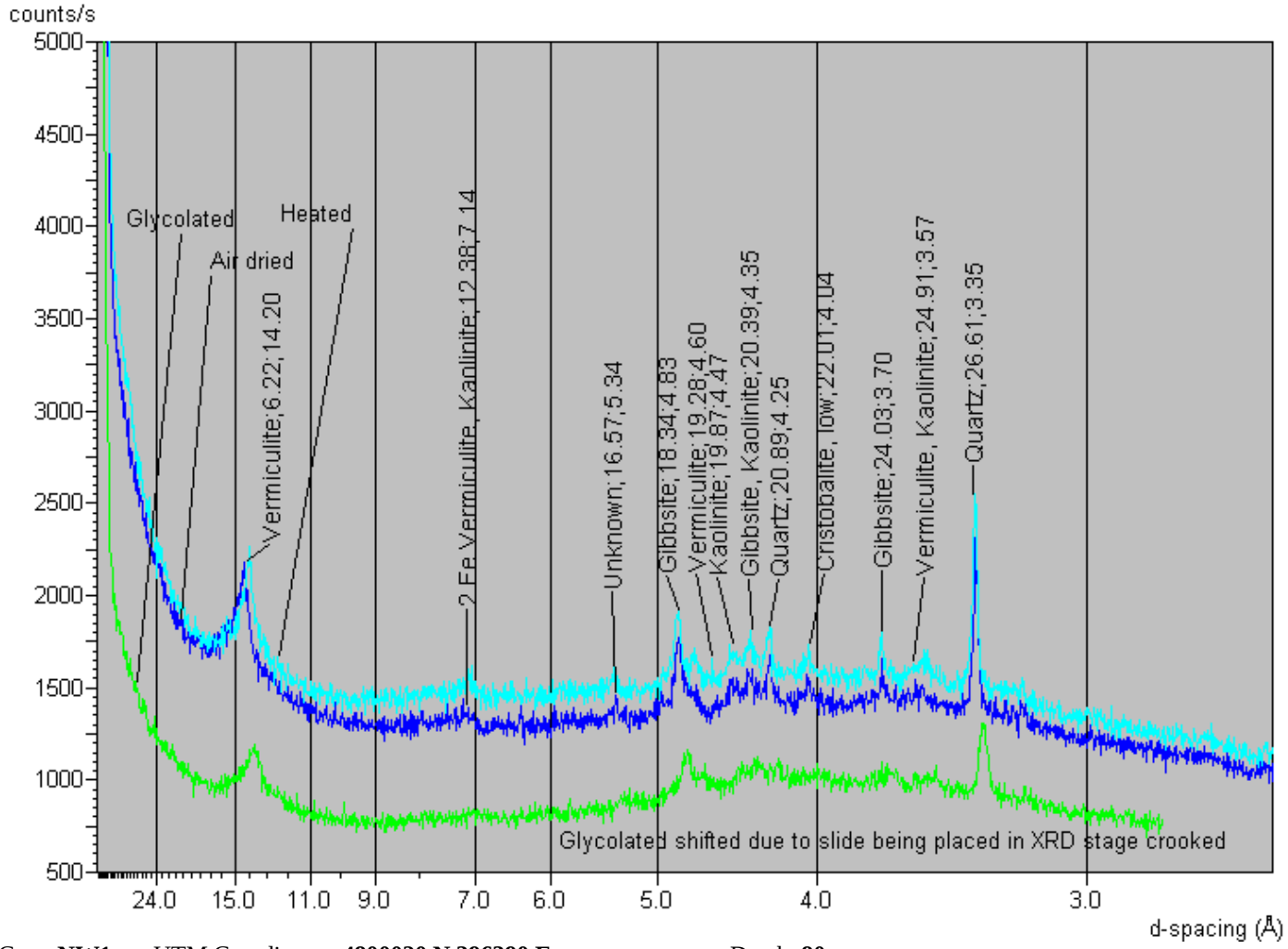

Core: **NW1** UTM Coordinates: **4800020 N 396390 E** Depth: **80 cm**

Appendix F: Microprobe images and raw chemical analyses

Graphic file name is in the lower left hand corner, along with the scale. Labels are where the chemical analyses were taken.

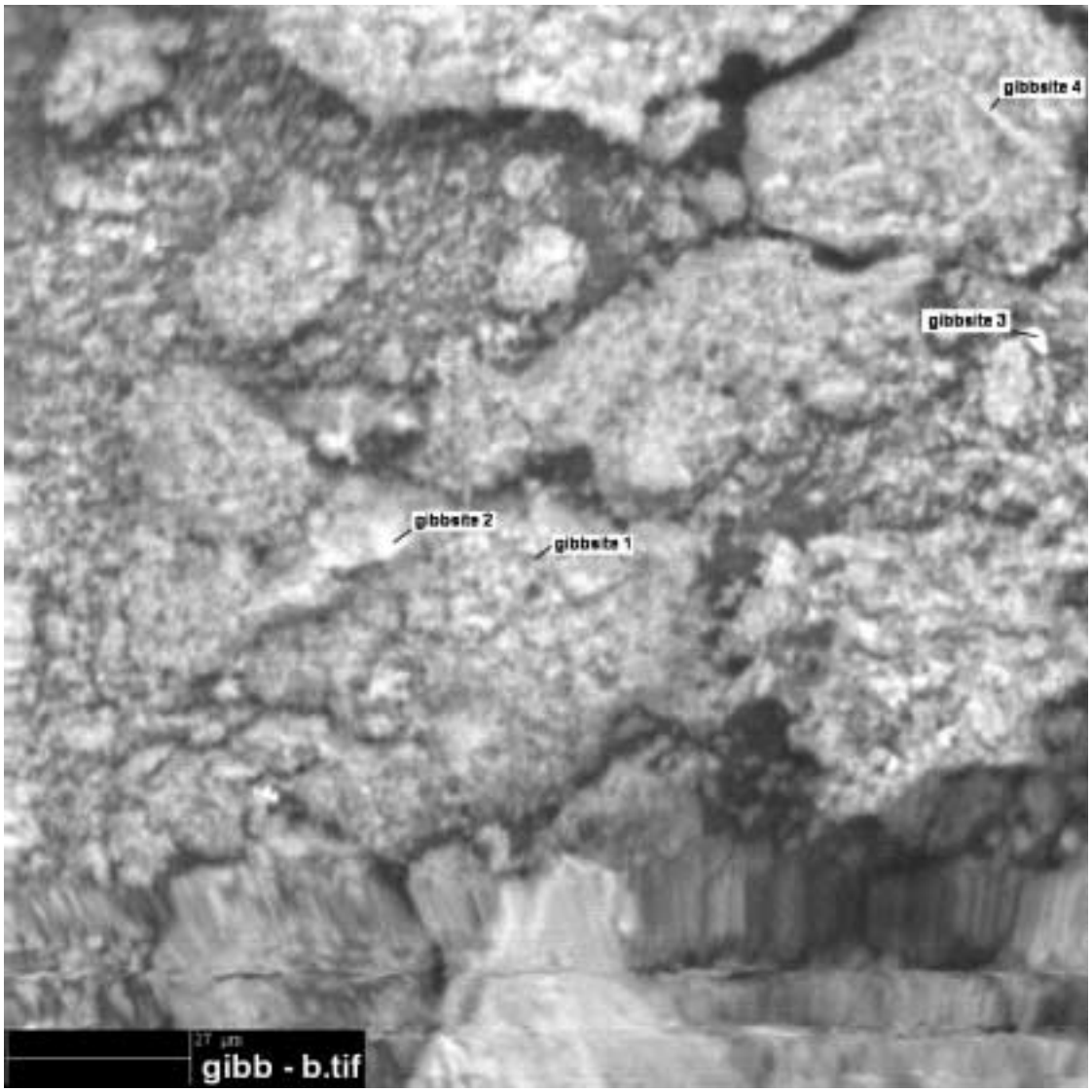

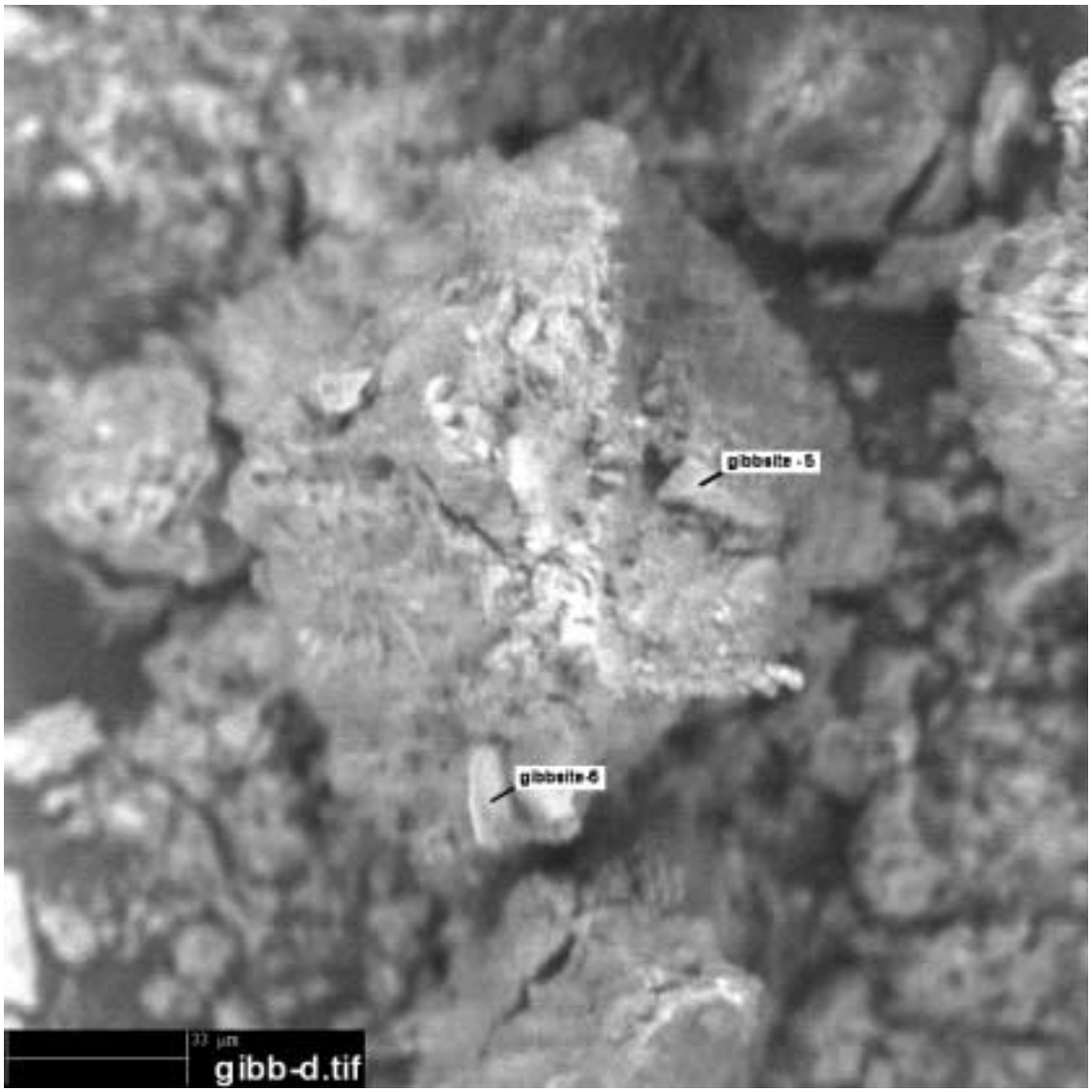
gibbsite -5
gibbsite-6
23 µm
gibb-d.tif

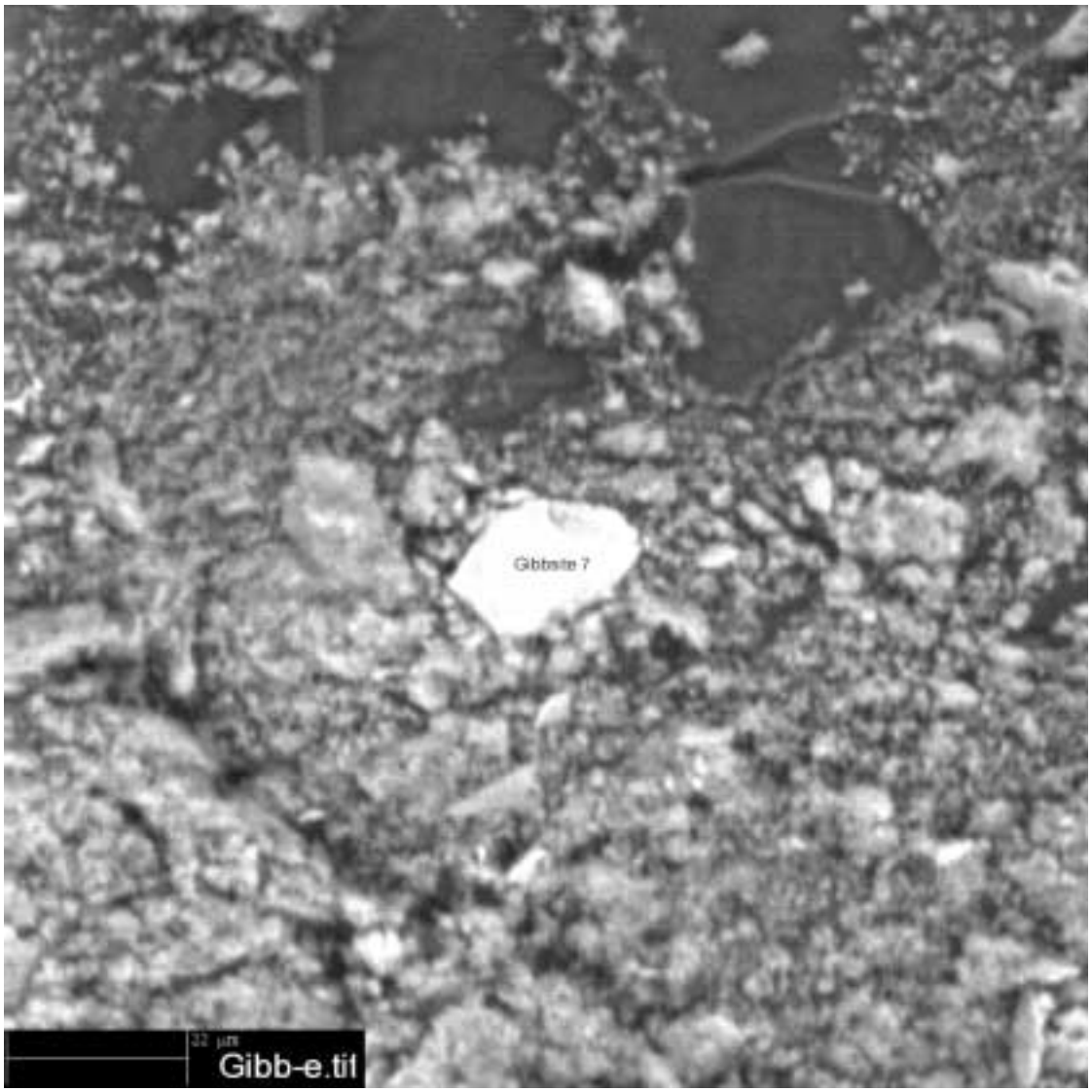
Gibbsite 7
22 µm
Gibb-e.tif

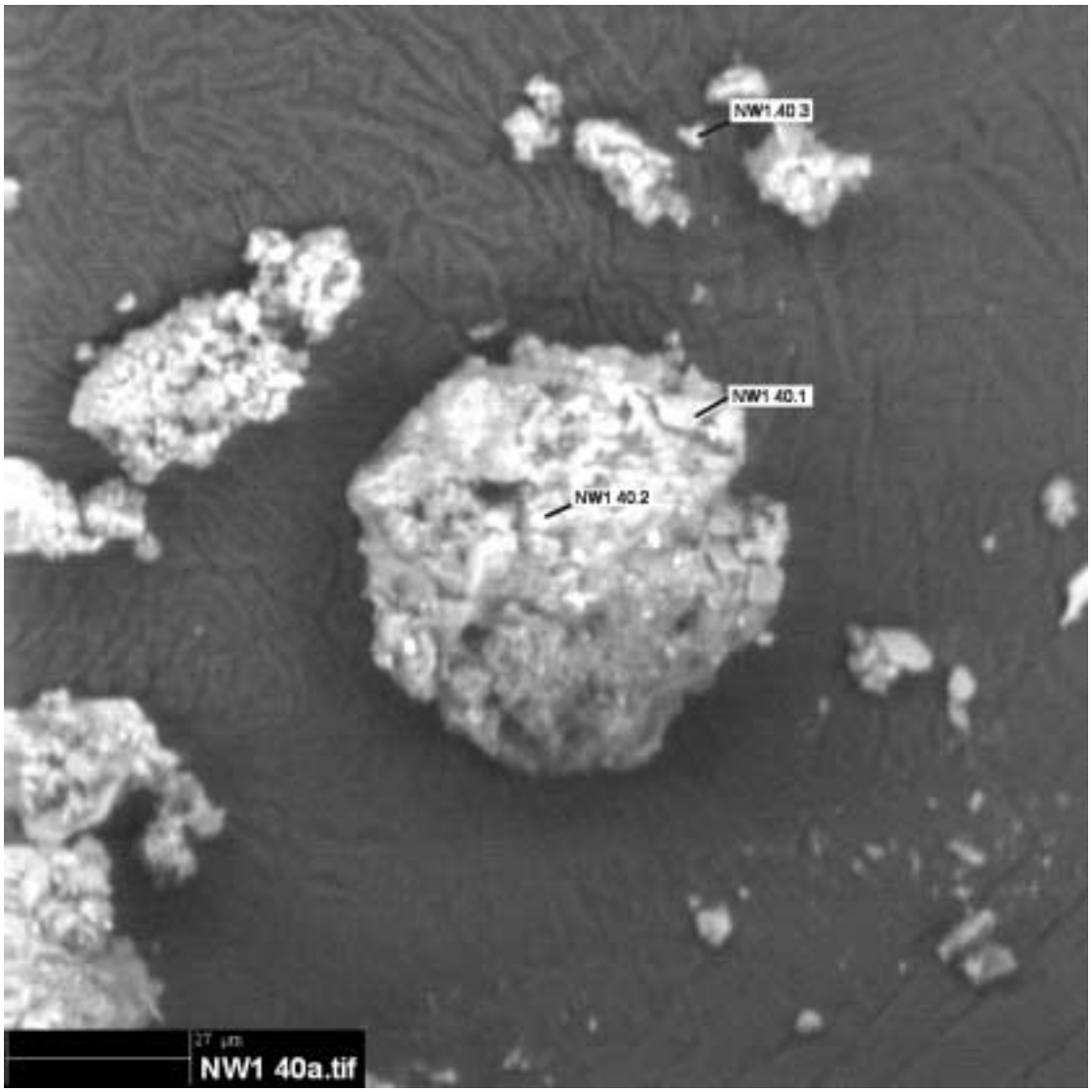
NW1 40.3
NW1 40.1
NW1 40.2
27 µm
NW1 40a.tif

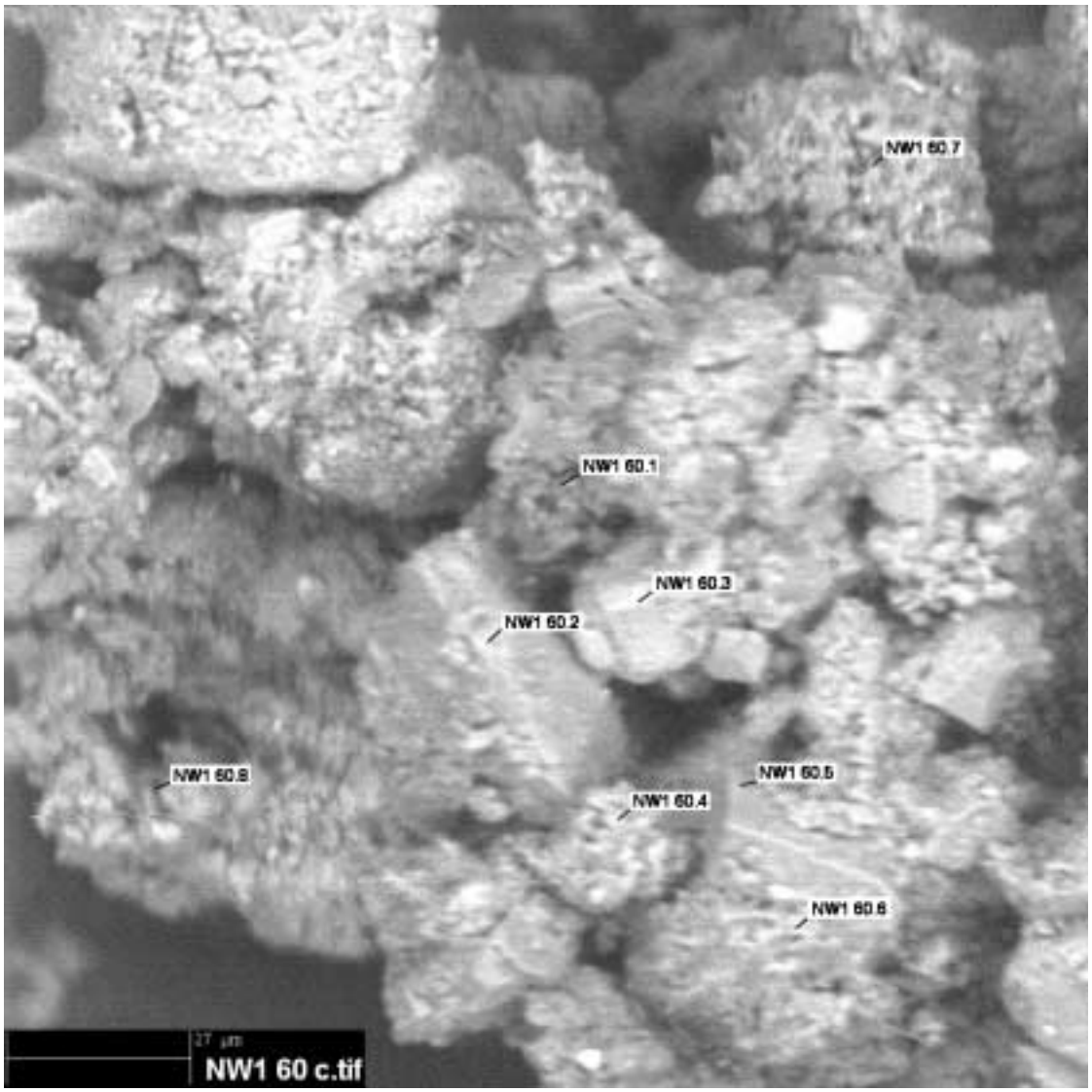
NW1 60.7
NW1 60.1
NW1 60.3
NW1 60.2
NW1 60.8
NW1 60.5
NW1 60.4
NW1 60.6
27 µm
NW1 60 c.tif

Raw data

Label	Na	Mg	Al	Si	P	S	Cl	K	Ca	Ti	Cr	Mn	Fe	SUM
NW1.60cm.1	0.02	0.01	15.95	40.81	0.00	0.01	0.01	0.07	0.04	0.42	0.00	0.00	4.58	61.93
NW1.60cm.2	0.06	0.13	5.01	38.47	0.05	0.18	0.05	0.12	0.27	0.18	0.00	0.00	2.94	47.45
NW1.60cm.3	0.07	0.22	20.33	26.30	0.26	0.12	0.05	0.13	9.84	0.24	0.01	0.05	5.49	63.10
NW1.60cm.4	0.17	1.49	18.86	32.08	0.11	0.25	0.07	0.89	0.02	0.73	0.00	0.03	6.38	61.07
NW1.60cm.5	0.08	0.06	7.33	50.72	0.09	0.11	0.04	0.05	0.01	0.67	0.00	0.02	2.32	61.50
NW1.60cm.6	1.80	0.15	14.85	41.80	0.08	0.18	0.06	0.53	0.04	0.53	0.00	0.00	3.41	63.43
NW1.60cm.7	0.43	0.39	0.55	0.80	0.09	0.13	0.04	1.96	0.22	0.69	0.00	0.01	6.46	11.77
NW1.60cm.8	0.05	0.01	24.79	34.52	0.02	0.00	0.00	0.00	0.02	0.10	0.01	0.01	5.75	65.26
Gibbsite.1	0.00	0.12	53.82	2.75	0.11	0.07	0.02	0.01	0.04	0.05	0.00	0.00	0.57	57.55
Gibbsite.2	0.00	0.04	54.51	2.37	0.12	0.04	0.03	0.02	0.02	0.07	0.05	0.00	0.36	57.63
Gibbsite.3	0.03	0.16	48.81	8.18	0.06	0.02	0.01	0.20	0.03	1.30	0.03	0.04	8.74	67.61
Gibbsite.4	0.00	0.04	76.21	2.85	0.06	0.05	0.01	0.03	0.01	0.03	0.01	0.04	0.53	79.86
Gibbsite.5	0.00	0.22	7.15	0.43	0.00	0.01	0.01	0.07	0.02	0.08	0.02	0.00	0.56	8.57
Gibbsite.6	0.00	6.52	37.25	15.59	0.00	0.01	0.00	0.03	0.03	0.60	0.05	0.02	14.99	75.10
Gibbsite.7	0.03	11.44	19.79	29.53	0.03	0.04	0.05	0.29	0.16	2.60	0.07	0.15	12.85	77.03
NW1.40cm.1	0.13	0.20	5.26	51.46	0.06	0.07	0.06	0.19	0.04	0.85	0.01	0.04	5.20	63.57
NW1.40cm.2	2.72	0.13	24.14	52.43	0.04	0.04	0.05	0.22	2.02	0.48	0.02	0.00	5.82	88.13
NW1.40cm.3	0.03	0.00	0.58	0.73	0.02	0.00	0.01	0.00	0.00	0.02	0.00	0.00	0.13	1.50

Normalized data

Label	Na	Mg	Al	Si	P	S	Cl	K	Ca	Ti	Cr	Mn	Fe
NW1.60cm.1	0.02	0.01	25.76	65.91	0.00	0.02	0.02	0.12	0.07	0.68	0.00	0.00	7.39
NW1.60cm.2	0.12	0.28	10.55	81.07	0.10	0.38	0.11	0.24	0.57	0.38	0.00	0.00	6.19
NW1.60cm.3	0.10	0.35	32.22	41.68	0.41	0.19	0.08	0.21	15.59	0.37	0.01	0.07	8.70
NW1.60cm.4	0.28	2.45	30.88	52.53	0.18	0.40	0.11	1.45	0.03	1.20	0.00	0.05	10.44
NW1.60cm.5	0.13	0.10	11.92	82.47	0.14	0.19	0.07	0.07	0.02	1.08	0.01	0.04	3.77
NW1.60cm.6	2.84	0.24	23.41	65.90	0.13	0.28	0.09	0.84	0.06	0.84	0.00	0.01	5.38
NW1.60cm.7	3.64	3.31	4.65	6.80	0.78	1.12	0.32	16.62	1.86	5.90	0.00	0.07	54.92
NW1.60cm.8	0.07	0.02	37.98	52.89	0.02	0.00	0.00	0.00	0.02	0.15	0.02	0.01	8.81
Gibbsite.1	0.00	0.20	93.52	4.78	0.18	0.12	0.03	0.03	0.07	0.08	0.00	0.00	0.99
Gibbsite.2	0.01	0.06	94.59	4.11	0.20	0.07	0.05	0.03	0.04	0.12	0.08	0.00	0.63
Gibbsite.3	0.04	0.24	72.20	12.10	0.08	0.04	0.02	0.29	0.05	1.93	0.05	0.06	12.92
Gibbsite.4	0.00	0.06	95.43	3.56	0.08	0.06	0.01	0.03	0.01	0.04	0.02	0.05	0.67
Gibbsite.5	0.04	2.54	83.49	5.04	0.00	0.09	0.11	0.83	0.24	0.90	0.19	0.04	6.50
Gibbsite.6	0.01	8.68	49.60	20.76	0.00	0.01	0.00	0.05	0.04	0.80	0.06	0.03	19.96
Gibbsite.7	0.03	14.85	25.69	38.34	0.04	0.06	0.06	0.38	0.21	3.38	0.09	0.20	16.68
NW1.40cm.1	0.20	0.32	8.28	80.95	0.09	0.10	0.09	0.30	0.06	1.34	0.02	0.06	8.18
NW1.40cm.2	3.09	0.15	27.40	59.49	0.05	0.05	0.06	0.25	2.29	0.55	0.02	0.00	6.60
NW1.40cm.3	1.68	0.02	38.63	48.21	1.00	0.01	0.67	0.01	0.01	1.26	0.01	0.01	8.47

Appendix G: Soil development indices

Index values, raw:

Core	Rubification	Buntley-Westin	Maximum grain size decrease (mm)
JN1	90	32	0.14
HB1	40	8	0.03
NA1	10	6	0.01
NA2	20	8	0.03
NA4	40	12	0.04
GO1	60	18	0.17
EM1	120	24	0.26
NA3	70	18	0.08
RD1	10	18	0.16
NB2	30	12	0.19
LL1	55	18	0.09
UL1	50	15	0.18
HB2	0	4	0.03
CL1	20	12	0.12
VG1	50	18	0.10
VG2	50	12	0.05
MS1	53.3	10	0.03
SP1	60	18	0.14
MA1	80	18	0.24
RO1	20	12	0.14
LK1	35	8	0.08
LK2	30	8	0.04
SH1	35	16	0.15
PA1	20	12	0.13
SC1	20	12	0.22
SW1	40	24	0.15
SW2	20	24	0.17
NW1	50	12	0.17
HS1	50	12	0.13
ME1	60	18	0.19
UD1	30	8	0.09

Index values, normalized

Core	Rubification	Buntley-Westin	Maximum grain size decrease (mm)
JN1	0.75	1.00	0.55
HB1	0.33	0.25	0.12
NA1	0.08	0.19	0.05
NA2	0.17	0.25	0.11
NA4	0.33	0.38	0.15
GO1	0.50	0.56	0.67
EM1	1.00	0.75	1.00
NA3	0.58	0.56	0.32
RD1	0.08	0.56	0.62
NB2	0.25	0.38	0.74
LL1	0.46	0.56	0.34
UL1	0.42	0.47	0.68
HB2	0.00	0.13	0.11
CL1	0.17	0.38	0.46
VG1	0.42	0.56	0.40
VG2	0.42	0.38	0.20
MS1	0.44	0.31	0.11
SP1	0.50	0.56	0.53
MA1	0.67	0.56	0.94
RO1	0.17	0.38	0.53
LK1	0.29	0.25	0.30
LK2	0.25	0.25	0.17
SH1	0.29	0.50	0.59
PA1	0.17	0.38	0.52
SC1	0.17	0.38	0.84
SW1	0.33	0.75	0.59
SW2	0.17	0.75	0.66
ME1	0.50	0.56	0.74
UD1	0.25	0.25	0.35

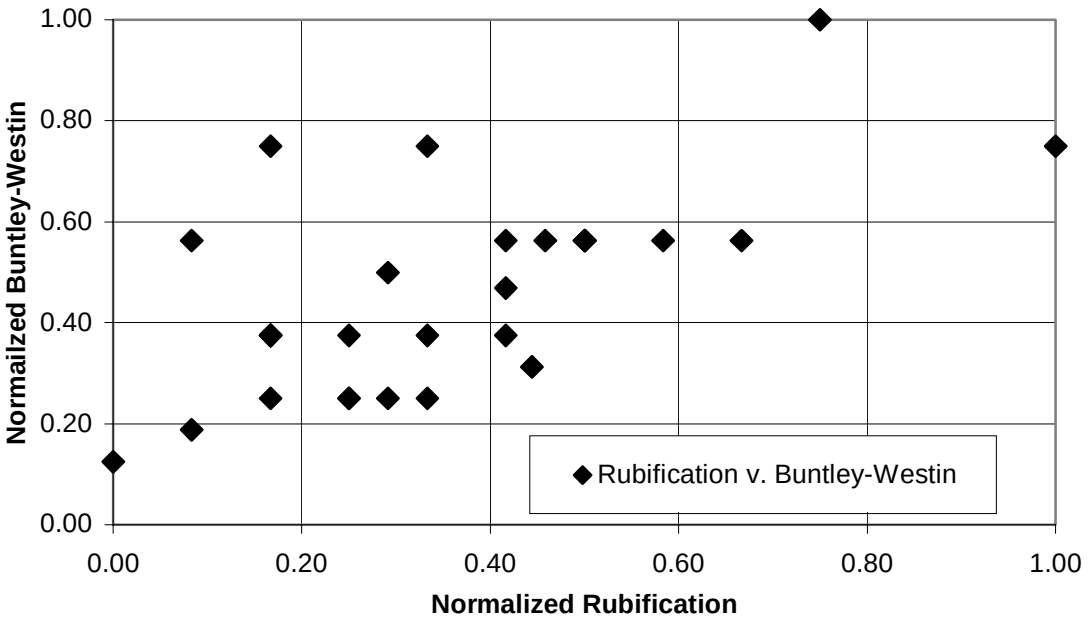
1.00
0.80
0.60
0.40
0.20
0.00
Normailzed Buntley-Westin
0.00
0.20
0.40
0.60
0.80
1.00
Normalized Rubification
Rubification v. Buntley-Westin

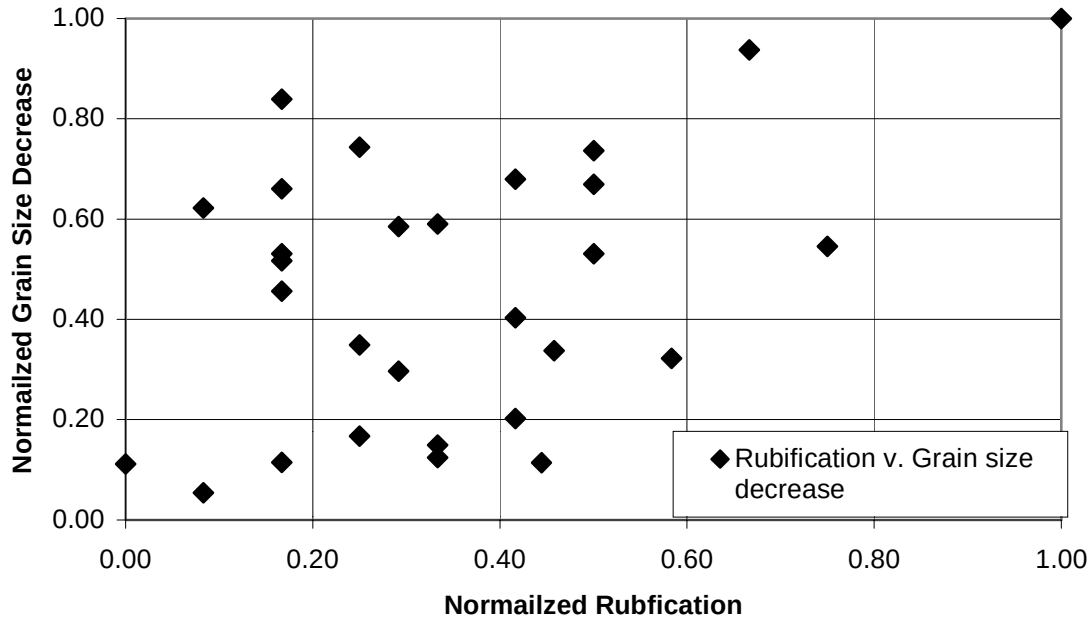
1.00
0.80
0.60
0.40
0.20
0.00
Normailzed Grain Size Decrease
0.00
0.20
0.40
0.60
0.80
1.00
Normailzed Rubfication
Rubification v. Grain size decrease

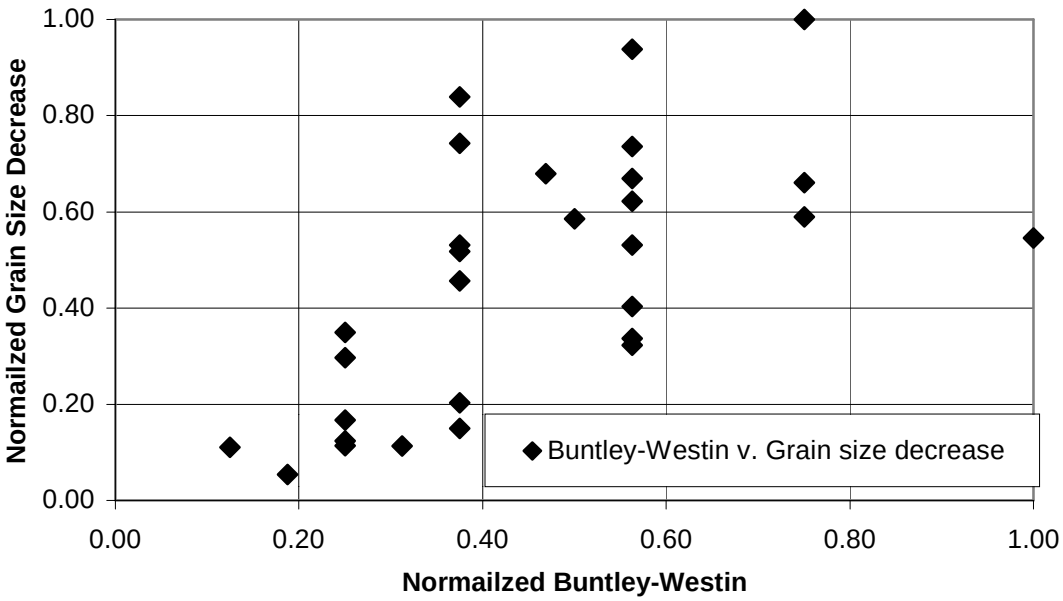
1.00
0.80
0.60
0.40
0.20
0.00
Normailzed Grain Size Decrease
0.00
0.20
0.40
0.60
0.80
1.00
Normailzed Buntley-Westin
Buntley-Westin v. Grain size decrease

Appendix H: Detailed Thermoluminesence Results

Sample site	SD1	SD201	RD1	ME1
Reference number	W2773	W2774	W2775	W2776
Plateau Region (°C)	275-425	300-475	300-500	300-500
Analysis Temp. (°C)	375	375	375	375
Palaeodose (Grays)	6.0 ± 0.5	2.6 ± 0.5	55.7 ± 6.0	116 ± 5
K Content (% by AES)	1.400 ± 0.005	1.300 ± 0.005	1.200 ± 0.005	1.300 ± 0.005
Rb Content (ppm assumed)	100 ± 25	100 ± 25	100 ± 25	100 ± 25
Moisture content (% by weight)	10 ± 3	10 ± 3	8.9 ± 3	22.7 ± 3
Specific Activity (Bq/kg U+Th)	32.4 ± 0.9	17.8 ± 0.6	19.9 ± 0.6	27.1 ± 0.9
Cosmic Contribution (μGy/yr assumed)	138 ± 25	141 ± 25	150 ± 25	126 ± 25
Annual Radiation Dose (μGy/yr)	2086 ± 26	1723 ± 24	1693 ± 25	1660 ± 23
TL age (ka)	2.9 ± 0.3	1.5 ± 0.3	32.9 ± 3.6	70.1 ± 3.0

Sample site	WW1	NW1	CG1	HS1
Reference number	W2327	W2328	W2329	W2330
Plateau Region (°C)	200-300	325-500	200-450	300-400
Analysis Temp. (°C)	375	374	375	375
Palaeodose (Grays)	12.0 ± 1.1	85.2 ± 10.7	48.1 ± 6.0	53.9 ± 10.4
K Content (% by AES)	1.700 ± 0.005	1.500 ± 0.005	1.450 ± 0.005	1.300 ± 0.005
Rb Content (ppm assumed)	100 ± 25	100 ± 25	100 ± 25	100 ± 25
Moisture content (% by weight)	4.7 ± 3	2.9 ± 3	17.6 ± 3	18.9 ± 3
Specific Activity (Bq/kg U+Th)	34.5 ± 1.0	28.4 ± 0.9	30.5 ± 0.9	28.9 ± 0.9
Cosmic Contribution (μGy/yr assumed)	150 ± 50	150 ± 50	150 ± 50	150 ± 50
Annual Radiation Dose (μGy/yr)	2570 ± 50	2290 ± 50	1954 ± 43	1770 ± 43
TL age (ka)	4.7 ± 0.4	37.2 ± 4.8	24.6 ± 3.1	30.5 ± 5.9

Sample site	TI1-2
Reference number	W2331

Plateau Region (°C)	300-500
Analysis Temp. (°C)	375
Palaeodose (Grays)	69.9 ± 17.6
K Content (% by AES)	1.350 ± 0.005
Rb Content (ppm assumed)	100 ± 25
Moisture content (% by weight)	3.9 ± 3
Specific Activity (Bq/kg U+Th)	30.9 ± 1.0
Cosmic Contribution (μGy/yr assumed)	150 ± 50
Annual Radiation Dose (μGy/yr)	2158 ± 50
TL age (ka)	32.4 ± 8.2